Ministère de l'Enseignement Supérieur et de la Recherche Scientifique

Université Hassiba Benbouali de Chlef

Faculté Technologie

Département d'electrotechnique

THÈSE

Présentée pour l'obtention du diplôme de

DOCTORAT LMD

Filière : Electrotechnique

Spécialité : Réseaux Electriques

Par

ZAKARIA REGUIEG

Thème :

Contribution a la commande d'un système hybride de production d'énergie électrique renouvelable alimentant un filtre actif de puissance avec management intelligent de l'énergie électrique

"Contribution to the Control of a Hybrid Renewable Energy Generation System Supplying an Active Power Filter with Intelligent Energy Management"

Soutenue le **09/04/2026**, devant le jury composé de :

Dr. TEBANI Hocine	MCA	Université de Chlef	Président
Dr. BOUYAKOUB Ismail	MCA	Université de Chlef	Directeur de thèse
Pr. HELAIMI M'hamed	Prof	Université de Chlef	Examinateur
Dr. MELLAH Hacene	MCA	Université de Bouira	Examinateur
Dr. MAAFA Amar	MCA	Université de Bouira	Examinateur
Dr. MEHEDI Fayçal	MCA	Université de Chlef	Co- directeur de thèse
Pr. TALEB Rachid	Prof	Université de Chlef	Invité

First of all, I would like to thank God the Almighty and merciful, who gave me the strength and the patience to accomplish this modest work.

*A thought to my **« Dear parents »,** who gave themselves body and soul so that I could complete this thesis in good condition, I wanted to express my deep gratitude to you for all the unconditional support you have given me throughout my doctoral journey. Your love, your encouragement, and the sacrifices you made so that I could succeed are priceless.*

***« Mom »,** your caring presence, your words of encouragement and your dedication have been constant sources of inspiration for me. You have been my rock, my confidante, and my source of inspiration. It's because of you that I was able to persevere through difficult times. Your support has been the driving force behind my determination, and I could not have achieved this doctorate without you by my side. You showed me the importance of perseverance, love and sacrifice. Thank you from the bottom of my heart for everything you have done for me.*

*Secondly, I would like to express my deep gratitude to my supervisor **« Mr. Ismail BOUYAKOUB »,** who played an essential role in the success of my doctoral journey. His wise advice, dedication and unwavering support were key elements in my success. Thanks to your expertise, your patience and your ability to inspire me, I was able to progress, learn and grow throughout this academic adventure. Your mentorship has been invaluable, and I am grateful to you for sharing your expertise and time to help me achieve my goals. Your contribution to my academic success cannot be overstated, and I am honored to have had the opportunity to work under your guidance. Thank you for everything you have done for me.*

*I want to express my sincere gratitude to my co-supervisor, **« Mr. Fayçal MEHEDI»,** for broadening my knowledge and helping me during my work. I also want to use this occasion to express my gratitude to you for your crucial support during my PhD studies. I want to convey my sincere gratitude for your dedication, knowledge, and support in your capacity as co-supervisor, which was crucial to the success of my research.*

*I would like to express my sincere gratitude to **Professor TEBANI Hocine**, President of the jury, for his availability and for providing the necessary administrative support since the beginning of my PhD studies.*

*I am deeply grateful to Professor **HELAIMI M'Hamed** from the University of Chlef, and to **Dr. MELLAH Hacene** and **Dr. MAAFA Amar** from the University of Bouira, for the honor of serving as examiners of my thesis. Their participation as jury members is greatly appreciated, and I sincerely thank them for their valuable time, expertise, and careful evaluation of my work.*

*I would also like to extend my thanks to **Professor TALEB Rachid**, invited guest, for his presence and support.*

Finally, I would like to thank all my teachers and colleagues at Hassiba Benbouali University of Chlef for their continuous encouragement and support throughout the development of this work.

*I will not forget my brother and sister **«Abdellah - Ikram»** and my best friend « **Abdenour»**, and my newborn nephew **«Abderrahmane»** your presence, your unconditional support and your precious fraternity and friendship were a beacon in the difficult moments of my doctoral journey. You followed every step of this adventure alongside me, providing your help, your listening and your encouragement. Thank you for everything.*

In memory of my grandparents,

To my parents,

To my brothers,

To my friends

To all my dear ones,

To all those who have contributed directly or indirectly to the completion of this thesis.

Abstract

The increasing global demand for clean and sustainable energy has driven the widespread integration of renewable energy sources (RES), particularly photovoltaic (PV) and wind systems, into modern power grids. However, the inherent intermittency of these sources, coupled with the presence of nonlinear loads and the variability of power demand, poses significant challenges to power quality (PQ) and system stability. This thesis presents a comprehensive framework for the design, control, and management of a hybrid PV–wind microgrid that ensures efficient energy utilization and enhanced PQ under dynamic operating conditions. An intelligent energy management system (EMS) is developed to coordinate the energy flow between renewable sources, battery energy storage, and the grid, considering load requirements and system constraints. Advanced artificial intelligence-based Maximum Power Point Tracking (MPPT) techniques are proposed to optimize energy harvesting from RESs in real time. Additionally, series, shunt, and hybrid active power filters are integrated to mitigate harmonic distortions, voltage fluctuations, and waveform unbalance. The proposed system is modeled and validated through simulation studies under various scenarios, including nonlinear loads and grid disturbances. The results demonstrate significant improvements in total harmonic distortion (THD), voltage regulation, energy efficiency, and system reliability, making the framework a robust and scalable solution for next-generation smart and resilient power networks.

Résumé

La demande croissante en énergie propre et durable a conduit à une intégration massive des sources d'énergie renouvelable (SER), notamment les systèmes photovoltaïques (PV) et éoliens, dans les réseaux électriques modernes. Toutefois, l'intermittence inhérente à ces sources, la variabilité de la demande énergétique, ainsi que la présence de charges non linéaires posent d'importants défis en matière de qualité de l'énergie (PQ) et de stabilité du système. Cette thèse propose un cadre global pour la conception, le contrôle et la gestion d'un micro-réseau hybride PV–éolien, assurant une utilisation optimale de l'énergie et une amélioration significative de la qualité de l'alimentation électrique dans des conditions de fonctionnement dynamiques. Un système intelligent de gestion de l'énergie (EMS) est développé pour coordonner les flux énergétiques entre les sources renouvelables, le stockage par batterie et le réseau électrique, tout en tenant compte des exigences de charge et des contraintes du système. Des techniques de poursuite du point de puissance maximale (MPPT) basées sur l'intelligence artificielle sont mises en œuvre pour maximiser l'extraction d'énergie en temps réel. En parallèle, des filtres actifs (série, parallèle et hybrides) sont intégrés afin d'atténuer les distorsions harmoniques, les variations de tension et les déséquilibres des formes d'onde. Le système proposé est modélisé et validé par des études de simulation dans divers scénarios, incluant des charges non linéaires et des perturbations du réseau. Les résultats obtenus montrent une nette amélioration en termes de distorsion harmonique totale (THD), de régulation de tension, d'efficacité énergétique et de fiabilité du système, faisant de cette approche une solution robuste et évolutive pour les réseaux électriques intelligents de nouvelle génération.

الملخص

أدّى التزايد المستمر في الطلب العالمي على الطاقة النظيفة والمستدامة إلى التوسع الكبير في دمج مصادر الطاقة المتجددة، ولاسيما الأنظمة الكهروضوئية وطاقة الرياح، ضمن الشبكات الكهربائية الحديثة .غير أنّ الطبيعة المتقطعة لهذه المصادر، إلى جانب تغيّر الطلب على الطاقة ووجود الأحمال غير الخطية، تفرض تحديات كبيرة تتعلق بجودة الطاقة واستقرار النظام الكهربائي .تقدّم هذه الأطروحة إطارًا شاملاً لتصميم وتحكم وإدارة شبكة كهربائية هجينة تعتمد على الطاقة الشمسية وطاقة الرياح، بما يضمن الاستخدام الأمثل للطاقة وتحسين جودة التغذية الكهربائية في ظروف تشغيل ديناميكية .وقد تم تطوير نظام ذكي لإدارة الطاقة بهدف تنسيق تدفق الطاقة بين مصادر الطاقة المتجددة، ووحدات تخزين البطاريات، والشبكة الكهربائية، مع مراعاة متطلبات الأحمال وقيود التشغيل المختلفة .كما تم اقتراح تقنيات متقدمة لتعقب نقطة القدرة العظمى بالاعتماد على الذكاء الاصطناعي، بهدف تعظيم استخلاص الطاقة من المصادر المتجددة في الزمن الحقيقي .بالإضافة إلى ذلك، تم دمج مرشحات قدرة فعالة من النوع التسلسلي والتفرعي والهجين للحد من التشوهات التوافقية، وتقلبات الجهد، وعدم توازن الإشارات الكهربائية .وقد تمت نمذجة النظام المقترح والتحقق من أدائه من خلال دراسات محاكاة تحت سيناريوهات تشغيل متعددة شملت الأحمال غير الخطية واضطرابات الشبكة الكهربائية .وأظهرت النتائج تحسنًا ملحوظًا في تقليل التشوه التوافقي الكلي، وتحسين تنظيم الجهد، ورفع كفاءة الطاقة، وتعزيز موثوقية النظام، مما يجعل الإطار المقترح حلاً فعالًا وقابلاً للتطوير لتطبيقات الشبكات الكهربائية الذكية والمرنة المستقبلية

reguiegzakaria10@gmail.com +213541126997

Table of contents

Table of contents

Table of contents

List of figures

List of figures

List of figures

List of tables

List of abbreviations

RESs	renewable energy sources
PV	Photovoltaic
WTs	wind turbines
PQ	power quality
MPPT	Maximum Power Point Tracking
THD	total harmonic distortion
EMSs	energy management systems
APF	active power filters
HAPFs	hybrid active filters
AC	alternating current
DGS	distributed generation systems
pu	per unit
RMS	root mean square
WRIG	induction generators
PMSG	permanent magnetic synchronous generators
PCC	Point of Common Coupling
LVC	Load Voltage Control
SVC	Source Voltage Control
UVTG	Unit Vector Template Generation
p–q	Method of Real and Imaginary Instantaneous Power
SRF	Synchronous Reference Frame
DCC	Direct Current Control
PDC	Pre-sag/dip compensation
IPC	In-phase Compensation
PLL	Phase-Locked Loop
PWM	pulse-width modulation
IGBT	Insulated Gate Bipolar Transistor
VSI	Voltage Source Inverter
PI	Proportional-Integral
Pdc	direct current power
UPQC	Unified Power Quality Conditioner
BESS	battery energy storage systems
P&O	Perturb and Observe
E-P&O	Enhanced Perturb and Observe
ANN	Artificial Neural Networks
INC	Incremental Conductance
FLC	Fuzzy Logic Control
HRES	Hybrid renewable energy systems
NL	nonlinear loads
LL	linear load
SOC	State of Charge
RB-EMS	Rule-Based Energy Management System
DERs	distributed energy resources
MG	microgrid
ESS	Energy Storage System
SOH	state of health

General Introduction

1. General introduction

Over the past century, the global energy sector has been predominantly powered by conventional energy sources, including coal, oil, and natural gas. In regions where the electrical grid remains underdeveloped or entirely absent, energy access is often secured through the intensive use of diesel generators and other fossil-fuel-based systems. While such solutions provide a short-term response to local energy needs, they are inherently unsustainable and contribute significantly to environmental degradation and climate change due to elevated carbon dioxide (CO_2) emissions and pollutant release.

According to the International Energy Agency (IEA), global CO_2 emissions from fuel combustion reached approximately 33.8 billion metric tons in 2022, underscoring the continued dependence on carbon-intensive fuels and highlighting the urgent necessity for a transition to low-emission, renewable energy alternatives. Despite various international efforts aimed at decarbonization, fossil fuels continue to dominate the global energy mix. In 2020, energy consumption was primarily derived from oil (31.2%), coal (27.2%), and natural gas (24.7%), while renewable energy sources (RESs) accounted for only 5.7% of the total energy supply [1–3]. These statistics not only emphasize the ongoing reliance on finite, high-emission energy sources but also point to the limited global penetration of clean energy technologies.

RESs are central to the pursuit of sustainable development, as they enable clean energy generation and substantially reduce greenhouse gas (GHG) emissions. Among the most mature and widely implemented RES technologies, photovoltaic (PV) systems and wind turbines (WTs) have demonstrated a significant capacity to offset emissions associated with conventional fossil-based electricity production. Their integration into modern power systems contributes to mitigating the environmental impact of electricity generation, supporting the global transition toward a low-carbon, resilient, and sustainable energy future [4].

By the end of 2020, the total installed capacity of RESs worldwide exceeded 750 gigawatts (GW), reflecting a marked acceleration in the global deployment of renewable technologies. However, despite their environmental benefits, RESs such as solar and wind remain inherently intermittent and variable, which introduces operational challenges related to power quality (PQ) and grid stability, particularly in networks with high renewable integration [1].

2. Research problem

2.1. Wind energy conversion systems (WECS)

Despite the continuous advancement in wind energy technologies, Wind Energy Conversion Systems (WECS) still face significant operational and structural challenges that impact their overall efficiency, reliability, and economic viability. One of the most critical issues is the intermittent and stochastic nature of wind speed, which leads to non-uniform and fluctuating power output. These fluctuations not only complicate the integration of wind energy into the grid, but also challenge the design of control systems, which must adapt dynamically to maintain voltage and frequency stability.

From a mechanical perspective, the variable aerodynamic loading on turbine blades results in cyclic stresses on critical components such as the drive shaft, gearbox, and blade root. Over time, these loads cause mechanical fatigue and structural degradation, necessitating frequent maintenance and potentially leading to early component failure. Furthermore, the power

electronic converters used in modern WECS (e.g., back-to-back converters in variable-speed systems) may introduce harmonic distortions and electromagnetic interference, thereby affecting PQ and complicating grid compliance, especially in weak or isolated networks [5].

2.2 Photovoltaic (PV) systems

PV systems, although widely adopted for their simplicity and environmental benefits, are inherently sensitive to environmental conditions. The power output of PV modules is highly dependent on solar irradiance and ambient temperature, which vary significantly across time (e.g., diurnal cycles, cloudy days, and seasonal changes). These variations result in a non-continuous and unpredictable energy supply, posing a major challenge for stable and reliable energy management, particularly in stand-alone or weakly interconnected systems [6].

Another crucial issue is the performance of Maximum Power Point Tracking (MPPT) algorithms, which must rapidly and accurately respond to changing irradiance conditions to maximize energy harvest. Under partial shading conditions or rapidly fluctuating irradiance, conventional MPPT techniques (such as Perturb and Observe or Incremental Conductance) may suffer from slow convergence, power oscillations, or tracking inaccuracies.

Moreover, the use of static power converters (DC/DC boost converters and DC/AC inverters) to condition PV output can inadvertently inject harmonics into the grid, leading to total harmonic distortion (THD) and deterioration of voltage waveform quality. These effects are particularly pronounced when PV systems are connected to low-voltage distribution networks with limited filtering capacity or operate alongside sensitive electronic equipment [6].

2.3. Nonlinear loads

The increasing presence of nonlinear loads such as variable-speed drives, rectifiers, computer power supplies, LED lighting, and consumer electronics in modern electrical systems has become a major concern for PQ. These loads draw non-sinusoidal currents from the supply, even when the source voltage is sinusoidal, leading to current harmonics, voltage distortion, and increased neutral currents in three-phase systems.

These harmonics not only reduce system efficiency but also cause several operational issues, including resonance conditions, overheating of transformers, malfunction of protection devices, and misoperation of sensitive loads. Additionally, harmonic propagation can interfere with communication systems and deteriorate the performance of renewable energy inverters, which are typically designed to operate under clean sinusoidal conditions.

Furthermore, the coexistence of nonlinear loads with RESs, particularly in microgrids or hybrid distributed systems, can exacerbate PQ issues. In such configurations, coordinated control strategies and active filtering mechanisms become essential to maintain system stability, ensure regulatory compliance (e.g., IEEE 519), and preserve load-side PQ.

3. Motivation and objectives of the research

A comprehensive review of the existing literature reveals several critical research gaps and limitations in the integration of RESs with PQ enhancement and energy management systems (EMSs) in modern power systems. One of the primary gaps lies in the segmented treatment of PQ and EMS, where most studies tend to address these domains in isolation, rather than acknowledging their inherent interdependence. This disjointed approach often results in partial

or suboptimal solutions, failing to holistically optimize the performance, reliability, and efficiency of hybrid energy systems.

Moreover, many research efforts underestimate or neglect the impact of harmonics introduced by power electronic interfaces of RESs (e.g., PV inverters, wind converters) on EMS operation. These harmonic distortions, if unaccounted for, can propagate through the network, degrade voltage profiles, distort power flows, and ultimately impair the functionality of energy management strategies. Such oversight leads to higher system losses, voltage instability, and reduced PQ, particularly in low-voltage microgrids and residential environments.

Another pressing concern is the lack of intelligent MPPT algorithms that can respond adaptively to rapid environmental changes and partial shading conditions in PV and wind systems. Traditional MPPT techniques often fail to maintain tracking accuracy under real-world disturbances, leading to reduced energy harvesting and dynamic instabilities in the system.

These identified research gaps form the core motivation for this study, which aims to develop a comprehensive and integrated framework that jointly addresses PQ enhancement and intelligent energy management in hybrid PV–wind microgrids. Special emphasis is placed on the mitigation of harmonic distortions, adaptive MPPT control, and coordinated operation of renewable sources and storage units to ensure reliable, stable, and efficient energy delivery.

3.1 Objectives of the research

Based on the above motivations, the key objectives of this research are defined as follows:

- To design and model a hybrid microgrid system integrating PV, WTs, battery storage, and grid connection, capable of operating under various environmental and load conditions.
- To develop and implement advanced MPPT techniques, particularly using artificial intelligence (e.g., artificial neural networks), for optimal and adaptive power extraction from PV and wind sources under dynamic operating conditions.
- To propose an intelligent energy management strategy (EMS) that ensures optimal coordination of energy flow between RESs, battery storage, and the utility grid, while considering load demands and battery state-of-charge constraints.
- To mitigate PQ issues such as harmonic distortion, voltage sag/swell, and waveform unbalance by integrating power conditioning devices (e.g., active filters) and synchronizing their control with the EMS.
- To evaluate the performance of the proposed system under different operational scenarios, including variable generation, nonlinear loads, and grid disturbances, using simulation tools and relevant performance metrics such as THD, voltage regulation, and system efficiency.

4. Thesis structure

This doctoral thesis is structured into five main chapters, each addressing a key aspect of the integration of renewable energy systems with PQ improvement and intelligent energy management. The chapters are organized as follows:

- **Chapter I – Study of Power Quality Disturbances in Hybrid Renewable Energy Systems under Nonlinear Load Conditions:**
  - This chapter provides an in-depth analysis of common PQ disturbances in renewable-based systems, with a particular focus on the effects of nonlinear loads. It identifies the nature, sources, and impact of harmonics, voltage fluctuations, and waveform distortions in hybrid PV–wind systems.

- **Chapter II – Modeling, Simulation, and Control of Series and Shunt Active Power Filters:**
  - This chapter presents the theoretical foundation, dynamic modeling, and control strategies for series and shunt active power filters (Sereis APF and Shunt APF). It details their role in mitigating harmonics, compensating voltage sags/swells, and enhancing overall PQ in distributed energy systems.

- **Chapter III – Modeling and Integration of Hybrid Renewable Energy Systems into the Grid:**
  - This chapter focuses on the modeling and integration of PV and wind energy systems into the electrical grid. It includes power converter configurations, MPPT algorithms, and grid compliance considerations for stable operation under varying environmental conditions.

- **Chapter IV – Power Quality Enhancement in Grid-Connected Renewable Energy Systems Using Hybrid Active Filters:**
  - This chapter addresses the use of hybrid active filters (HAPFs) for PQ improvement in renewable energy systems. It evaluates their performance in mitigating harmonics, balancing loads, and maintaining voltage quality in grid-connected scenarios, especially in the presence of nonlinear loads.

- **Chapter V – Intelligent Energy Management of a Hybrid Renewable Microgrid:**
  - The final chapter proposes and implements an intelligent energy management system (EMS) for a hybrid microgrid integrating PV, wind, battery storage, and the utility grid. It incorporates AI-based MPPT control, real-time decision strategies, and coordinated operation for efficient energy utilization and PQ assurance

Chapter I:

Study of Power Quality Disturbances in Hybrid Renewable Energy Systems under Nonlinear Load Conditions

I.1 Introduction

The continued reliance on non-RESs has led to significant greenhouse gas emissions, accelerating global warming and environmental degradation. In response, governments and industries worldwide are shifting towards more sustainable and environmentally friendly alternatives, notably RES such as wind and solar energy [7]. These resources are widely recognized for their abundance, availability, and sustainability, and they play a crucial role in reducing dependence on fossil fuels, particularly in isolated or rural areas [8].

However, the large-scale integration of RES into electrical networks introduces new technical challenges. Their intermittent and variable nature, coupled with the non-synchronous behavior of their generation mechanisms, raises concerns related to system stability, power continuity, and grid reliability. Furthermore, the increasing deployment of power electronic converters for RES interfacing exacerbates PQ issues such as voltage sags, swells, flicker, unbalance, and most critically, harmonics [9].

Harmonic distortions arising from both nonlinear loads and the switching actions of converters lead to significant voltage and current waveform deformation, which can degrade system performance and damage sensitive equipment. To address these disturbances, standards such as IEEE 519-2014 have been established, defining acceptable limits for harmonic content in voltage and current waveforms, with THD serving as a key performance indicator [10,11].

In the context of growing RES integration, harmonic mitigation and PQ enhancement have become essential to ensure secure, efficient, and reliable operation of modern power systems. As such, this thesis focuses on the study of PQ disturbances with particular emphasis on harmonics in hybrid renewable energy systems, and investigates advanced control strategies for mitigating these issues. Special attention is given to the influence of nonlinear loads, converter technologies, and their interaction with grid-connected PV and wind systems [12].

This chapter provides a comprehensive overview of PQ disturbances in hybrid RES environments, focusing on the impact of nonlinear loads, the propagation of harmonics, and the importance of compliance with harmonic standards.

I.2 Structure of the electrical system

The electrical system encompasses all the resources and mechanisms necessary for generating, transporting, and distributing electricity across a defined geographical area. Predominantly, electricity is produced as alternating current (AC), preferred due to its significant advantages:

- Efficient Transport: AC allows voltage adjustment via transformers, reducing transmission losses.
- Enhanced Generator Design: The multiphase nature of AC facilitates the creation of more efficient generators.
- Simplified Interruption: The zero-crossing of AC makes it easier to interrupt current using circuit breakers.

Currently, fossil fuels such as gas, oil, and coal dominate global electricity production, supplying around 80% of the world's energy needs. Despite growing awareness of their

environmental impact, this dominance is projected to persist until 2030, with coal regaining some prominence.

I.2.1 Transition to renewable energy

RESs like solar, wind, hydropower, biomass, and geothermal—are gaining traction. These resources can be integrated into electric grids or deployed in hybrid systems, offering a pathway to reduce reliance on fossil fuels and promote sustainable energy transitions.

Combating climate change and promoting sustainable energy practices need a transition from traditional fossil fuel-based synchronous generators to inverter-based RES. Biogas, biomass, WT, and PV systems are examples of distributed generation systems (DGS) that provide practical ways to get around the drawbacks of conventional energy production and cut greenhouse gas emissions. Incorporating these RESs enhances energy sustainability and mitigates the effects of climate change. With a global installed capacity of over 750 GW by the end of 2020, RES usage and development have grown significantly [13–15].

Because they provide clean energy and lower greenhouse gas emissions, RES is essential for sustainable development. Two RES that can drastically cut emissions are PV and WTs. The environmental impact of conventional fossil fuel-based power generation may be reduced by including RES technologies like PV systems and WT, supporting international efforts to tackle climate change and advance a more sustainable energy future [4,16]. However, conventional power networks may become unstable due to the erratic nature of wind and PV electricity [17–20]. The optimization of PQ emerges as a crucial issue when alternative sources become more integrated with the traditional system [21,22].

I.3 Power quality

Power quality refers to the ability of an electrical power source to deliver electricity that meets specific standards for voltage and current, ensuring the proper operation of electrical equipment.

I.3.1 Voltage quality

In practical applications, the distributed electrical energy is delivered as a three-phase AC system. The amplitude, frequency, waveform, and symmetry are fundamental parameters for analyzing and evaluating PQ, as illustrated in **Figure I.1**.

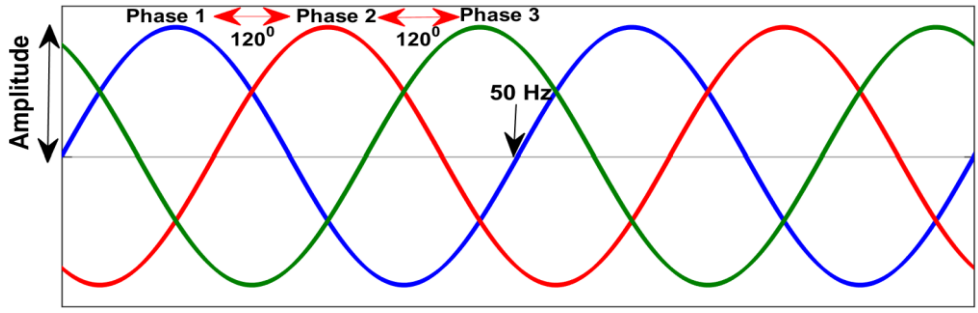

Figure I.1: Fundamental parameters for analyzing voltage quality in a three-phase AC system

A. Voltage magnitude

The voltage magnitude, typically expressed as the root-mean-square (RMS) value, is a critical parameter for PQ [23]. It represents the effective value of the voltage over a period and often constitutes the primary contractual obligation of the energy distributor to its customers.

Ideally, the magnitude of each of the three phases in a balanced three-phase system remains constant and identical. However, various disturbances can induce voltage magnitude variations, thereby degrading PQ.

Based on the severity and duration of these variations, two primary types of disturbances can be identified:

- Transient Events: These disturbances are characterized by abrupt and significant variations in voltage magnitude, which can even lead to complete power interruptions. Common causes include short circuits, switching operations on the grid, and atmospheric phenomena such as lightning strikes. These events can cause irreversible damage to electrical and electronic equipment.
- Long-Term Voltage Variations: These perturbations manifest as slower and less pronounced fluctuations in voltage magnitude, typically within 10% of the nominal value. They are primarily caused by load variations, changes in grid configuration, or voltage regulation issues. Although less dramatic than transient events, these variations can degrade equipment performance and reduce their lifespan.

B. Frequency

In an ideal scenario, the three-phase voltages are sinusoidal waveforms with a constant frequency of 50 Hz or 60 Hz, depending on the regional standard (50 Hz in Algeria). Frequency variations can be caused by:

- Significant generation losses: A substantial decline in power generation can lead to a decrease in system frequency.
- Islanding: When a portion of the grid becomes isolated from the main network, frequency deviations can occur due to imbalances between local generation and load.
- Faults: Short circuits and other grid faults can result in voltage drops, which can subsequently affect system frequency.

However, these frequency variations are generally small (less than 1%) and do not significantly impact the operation of most electrical and electronic equipment.

For interconnected grids, the EN 50160 standard specifies that the fundamental frequency measured over 10 seconds must remain within the range of 50 Hz ± 1% for 99.5% of the year and within ± 4% for 100% of the time. It is important to note that frequency variations can be more pronounced in isolated grids due to limited grid regulation capabilities.

Frequency fluctuations in renewable energy systems arise from the uncontrollable variability of resources and grid disturbances, and significant deviations from standard values, as defined by IEEE Standard 929-2000, may necessitate inverter disconnection from utility lines [24].

C. Waveform

The waveform of the three-phase voltages in a three-phase system should ideally be as close as possible to a perfect sinusoidal shape. However, in the presence of disturbances affecting the waveform, the voltage deviates from its sinusoidal form. It can then generally be represented as a fundamental wave at 50 Hz, combined with waves at higher or lower frequencies, commonly referred to as harmonics. Additionally, the voltage may include non-periodic, steady signals, which are referred to as noise.

D. Symmetry

The symmetry of a three-phase system is defined by the equality of the magnitudes of the three voltages and the uniformity of their relative phase angles. Any deviation from this symmetry is commonly referred to as imbalance.

I.3.2 Current quality

The quality of current refers to deviations from its ideal form and is characterized by the same four parameters as voltage: amplitude, frequency, waveform, and symmetry. Ideally, the three currents maintain constant amplitude and frequency, are phase-shifted by 120° relative to one another, and exhibit a purely sinusoidal waveform.

The term "current quality" is rarely used, as it is closely tied to voltage quality and the nature of the connected loads. For this reason, "power quality" is often simplified to "voltage quality." This assumption will be adopted throughout this document, where the term "power quality" will exclusively refer to voltage quality.

I.4 Classification of electrical disturbances

Based on the parameters characterizing voltage, as outlined in the previous section, electrical disturbances can be classified into four main categories:

- Amplitude variations: These include voltage sags, short interruptions, overvoltages, and flicker.
- Frequency fluctuations: Deviations from the fundamental frequency.
- Waveform distortions: Such as harmonics, inter-harmonics, and noise.
- Phase system asymmetry: Commonly referred to as imbalance.

Another classification approach categorizes electrical disturbances based on their duration [25]:

- Transient disturbances:

Transient disturbances last less than half of a fundamental cycle. They are primarily caused by switching operations in transmission and distribution networks or natural phenomena such as lightning.

- Short-duration disturbances:

These include voltage sags, short interruptions, and overvoltages, which are typically caused by short circuits. They are characterized by significant amplitude variations and can have detrimental and costly effects on electrical equipment.

- Sustained disturbances:

This category includes harmonics, noise, imbalances, and variations in voltage and frequency. Sustained disturbances are generally caused by the presence of nonlinear and fluctuating loads in the power grid. They are characterized by minor amplitude variations and can lead to overheating, additional energy losses, premature aging of electrical equipment, and malfunctions in certain control and monitoring devices. Electrical disturbances can also be broadly classified into two types based on their origins and impacts. Significant voltage disturbances are usually expressed in per unit (pu), while minor amplitude variations are represented as percentages (%).

Table I.1 Electrical disturbances

Duration	Disturbance Type	Amplitude	Origin	Consequences
< 10 ms	Transients	-	Switching of devices, capacitor connections, circuit operations	Disruptions, equipment malfunctions
10 ms – 1 min	Voltage Sag	0.1 – 0.9 pu	Short circuits, large motor startups, transformer saturation	Equipment shutdowns, production losses
	Brief Interruptions	< 0.1 pu	Short circuits	Equipment shutdowns, production losses
	Overvoltages	1.1 – 1.8 pu	Short circuits, disconnection of large loads	Equipment failures, safety risks for personnel and devices
	Unbalance		Asymmetric or single-phase loads	Overheating of rotating machines, vibrations
	Rapid Voltage Fluctuations (Flicker)	0.1 – 7%	Fluctuating loads (arc furnaces, frequently starting motors, welders, wind turbines)	Light flickering

Steady-State	Harmonics	0 – 20%	Non-linear loads (power electronics, arc discharges)	Overheating, aging, additional losses, operational disturbances
	Interharmonics	0 – 2%	Non-linear and fluctuating loads (arc furnaces, welders, wind turbines)	Light flickering
	Noise	0 – 1%	Arc furnaces, non-linear loads	Overheating, losses, aging
	Frequency Variations	-	Imbalance between production and consumption	Malfunctions of electrical equipment

I.4.1 Voltage sags and short interruptions

Voltage sags and short interruptions are major causes of electrical equipment malfunctions. By definition, a voltage sag refers to a drop in voltage ranging from 10% to 90% of its nominal value, lasting between 10 ms and 1 minute [26]. A short interruption, on the other hand, represents a voltage drop exceeding 90% of the nominal value within the same duration range. Voltage sags are among the most detrimental electrical disturbances due to their high frequency of occurrence and the sensitivity of many industrial devices to such disruptions. While short interruptions can have more severe consequences, particularly during recovery, they are much less frequent. **Figure I.2** illustrates the distinction between a voltage sag and a short interruption.

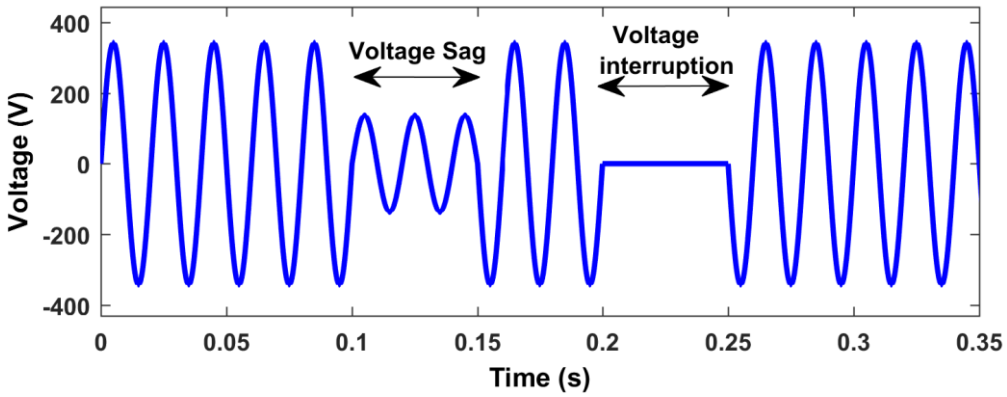

Figure I.2 Voltage Sag and Short Interruption

Characteristics of voltage sags and short interruptions

- Short circuits:

Short circuits are the primary source of voltage sags and short interruptions. They cause abrupt changes in voltage amplitude, leading to sags that are typically rectangular in shape over time. Short circuits may affect one, two, or all three phases, often introducing additional phase shifts.

- High-Power motor startups:

The startup of high-power motors (primarily asynchronous motors) can also induce voltage sags. At startup, the current drawn by these motors is 5 to 6 times their nominal current, gradually decreasing as the machine approaches its nominal speed. This high inrush current results in a voltage drop that diminishes as the current stabilizes (**Figure I.2**). Such sags typically last from a few seconds to several tens of seconds and impact all three phases simultaneously.

- Transformer saturation and network changes:

Voltage sags may also result from transformer saturation or changes in the network structure. However, these phenomena rarely lead to significant voltage drops.

I.4.2 Overvoltages and overcurrents

Overvoltages refer to increases in voltage amplitude ranging from 1.1 p.u. to 1.8 p.u. Although less frequent than voltage sags, overvoltages are often associated with faults such as short circuits in isolated neutral systems, which can simultaneously cause voltage sags and overvoltages. **Figure I.3** provides an example of an overvoltage occurrence.

In the case of a single-phase short circuit in an isolated neutral system, the two unaffected phases may experience voltage levels of up to 1.73 p.u, equivalent to the line-to-line voltage [27]. For a two-phase short circuit, the unaffected phase may be subjected to an overvoltage of up to 1.5 p.u.

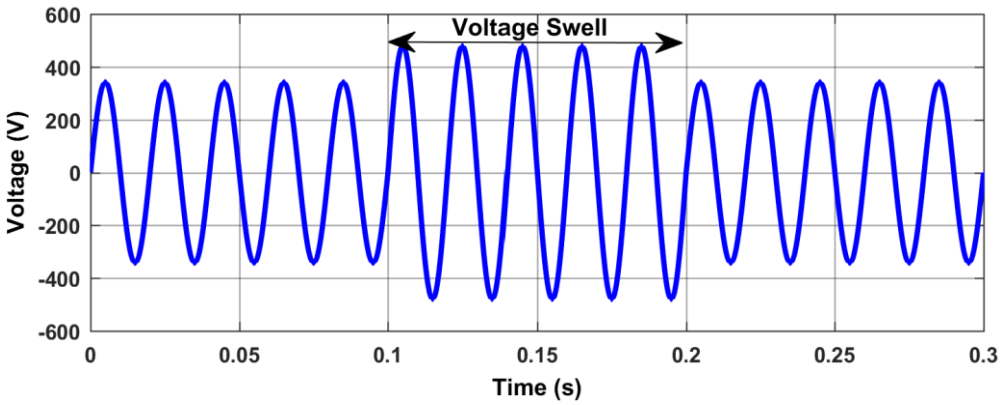

Figure I.3 Example of an overvoltage

Overvoltages may also arise from atmospheric phenomena such as lightning, the disconnection of large loads, faulty voltage regulators, ferroresonance, or switching operations within the network. These types of overvoltages are typically brief in duration and are often classified as transient events.

I.4.3 Voltage variations

The switching on or off of electrical equipment and the operation of certain variable-power loads lead to voltage variations, as illustrated in **Figure I.4**. These variations manifest in two primary forms:

- Slow voltage variations

Slow variations occur over intervals longer than a few seconds. These are primarily caused by the connection and disconnection of loads. Generally, they do not exceed ±10% of the nominal voltage and are not harmful to most electrical equipment.

- Rapid voltage variations

Rapid variations result in a spectral frequency composition within the 0.5 to 25 Hz range. These are caused by loads with rapidly fluctuating power consumption, such as arc furnaces, welding machines, motors with pulsating torque, or motors with frequent starts.

These rapid fluctuations are particularly noticeable in the luminous flux of lamps, causing a flickering effect known as flicker, which is highly unpleasant for consumers.

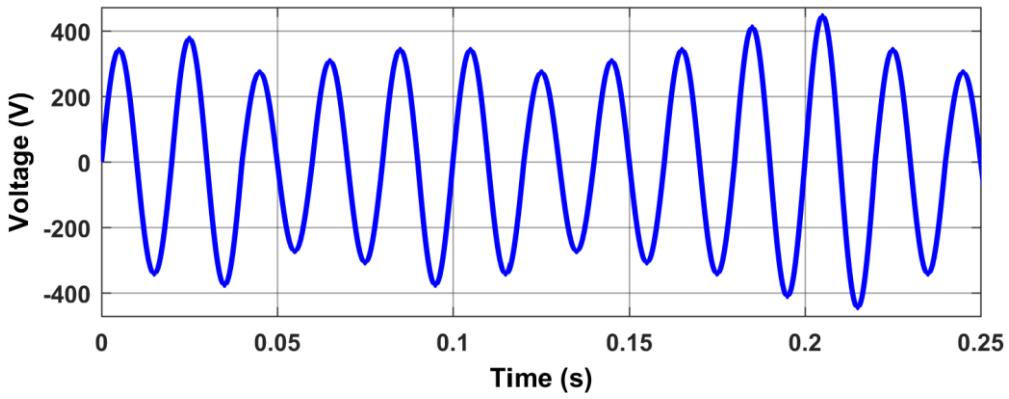

Figure I.4 Example of voltage variations

I.4.4 Imbalance

A three-phase system is considered balanced when three quantities of the same nature and frequency have equal amplitudes and are phase-shifted by ±120°. If these conditions of phase and amplitude are not met, the system is classified as unbalanced.

Imbalances typically arise from single-phase loads, as the currents drawn on the three phases exhibit differences in amplitude and/or phase, leading to an imbalance in the three-phase voltages. Voltage imbalance can also result from asymmetrical three-phase loads.

- Amplitude Imbalance: Occurs when the root mean square (RMS) values of the three-phase voltages are not equal.
- Phase Imbalance: Happens when the phase angle between successive phases deviates from 120°, as illustrated in **Figure I.5**.

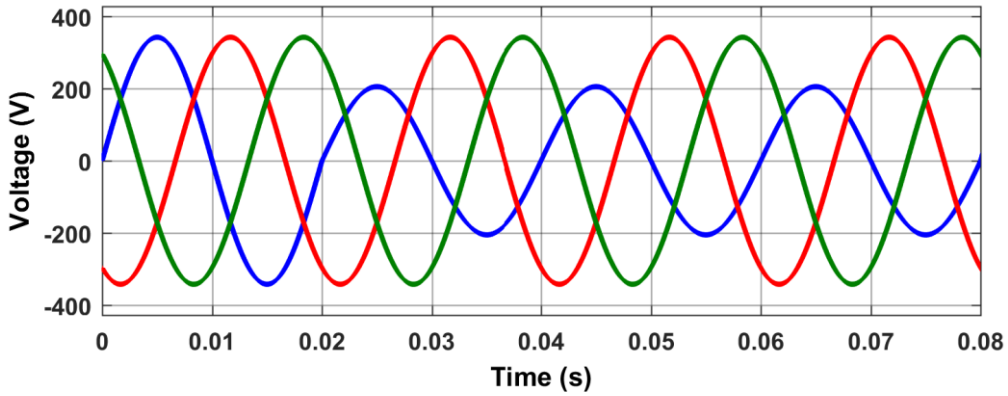

Figure I.5 Example of amplitude and phase imbalance

The level of imbalance is influenced by the power and location of the disturbing loads, as well as the short-circuit power of the upstream network. Network meshing, which increases short-circuit power, helps reduce the degree of imbalance.

Voltage imbalances generate negative-sequence current components, which cause parasitic braking torques and overheating in AC motors. They can also disrupt the operation of phase-controlled thyristor devices.

I.4.5 Harmonics

The sinusoidal components of a signal with frequencies that are multiples of its fundamental frequency are called harmonics, as shown in **Figure I.6**. The primary sources of harmonics in electrical systems include devices with switching elements (such as static converters) and devices with nonlinear voltage-current characteristics (e.g., arc furnaces, saturated inductances, transformers, rotating machines, etc.).

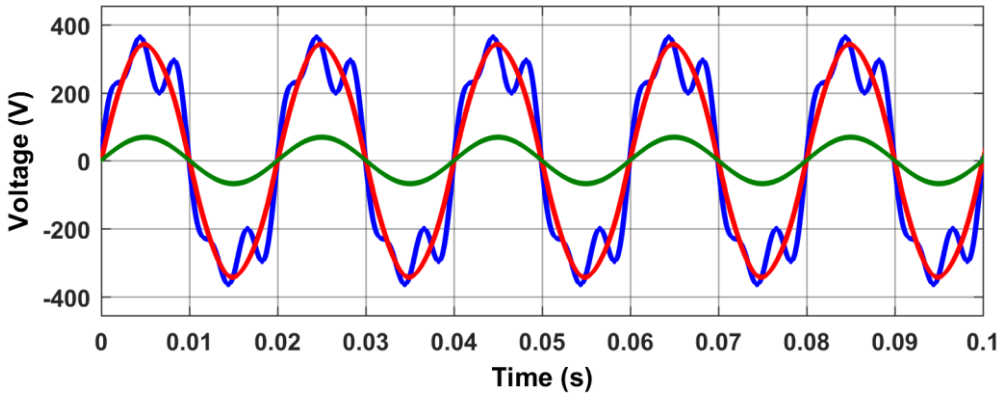

Figure I.6 Harmonics as sinusoidal components of a signal with multiple frequencies

I.5 Impact of RES on power quality (source side)

Power quality is one of the primary problems that arises when RES like solar and wind energy (WE) are incorporated into the system [9,10,28]. A range of power electronic converters are needed for the integration, and these converters affect the power system and lower PQ by producing harmonics in the voltage and current [29–32].

As shown in the literature references [33,34], different writers have also recorded a variety of techniques used to identify and classify distinct PQ experiences. Weaker and smaller MGs frequently have PQ anomalies like as voltage sags and swells. While voltage sags are commonly observed in grid-tied mode, voltage distortion and imbalance are more likely to occur in islanded operation [35].

RES or variations in load cause PQ problems, which include voltage sag, swell, dips, harmonics, three-phase failures, and voltage imbalance [36]. Although these problems are well known in traditional centralized power systems, their prevalence increases as RES use rises [37].

I.5.1 Harmonic challenges in renewable energy systems

A. Influence of PV and Wind inverters on power quality

In PV solar power systems, which produce DC electricity, DC/AC inverters are crucial parts. To transform the DC energy generated by solar panels into AC electricity, these inverters are required. The need for converting DC energy to AC in solar power systems is met in large part by inverters, which are well-known for their dependability, affordability, simplicity, and efficiency [38]. Wind power plants also employ inverters to transform power. Despite their widespread use and usefulness, inverters' primary drawback is that they produce unwanted harmonics. Unwanted energy is produced by these harmonics. Because they are similar to the system frequency, low order harmonics produced by the inverter pose a threat to the system [39]. When contrasted to the fundamental component of the system, these harmonics can have significant amplitudes. The efficiency of renewable energy systems is challenged by the existence of system harmonics [40]. According to [41], these harmonics cause a number of detrimental consequences on the system, including increased switching losses in inverters, variations in the speed of rotating machinery, torque issues, vibrations, and mechanical fatigue.

B. Effect of wind energy converters on grid integration quality

Wind conditions and related transients cause the AC generators of WTs to rotate at different speeds. Power converters, which are found in many power electronic devices in wind farms, are the main source of harmonics, even though individual AC generators are less likely to produce harmonic disturbances than power electronics components [40]. They are essential to the smooth integration of WTs varying output into the electrical grid. Due to power electronics components that work on the switching principle, these converters make it easier to modify speeds and power output to desired levels. It's important to remember, nevertheless, that these components are the main generators of harmonics in the system [42]. Variable speed wind turbine generator (WTG) systems are composed of many components, but one of the most crucial is the WTG step-up transformer. This transformer has a lot of parts, such as squirrel cage induction generators (SCIG), capacitors, soft starters, wound rotor induction generators (WRIG) with soft starting capabilities, and permanent magnetic synchronous generators (PMSG).

I.6 Impact of nonlinear loads on power quality (load side)

NL and switched devices, which make up around 40% of the utility load, are the source of harmonics [43]. Interest in power system harmonics has increased as a result of the expanding use of NL in power systems. Although NL uses a sinusoidal power source, they produce harmonic currents that could cause insulation damage and overheating. Within the system, harmonic resonance presents serious difficulties. Thus, power system modeling and analysis are essential for recognizing and resolving these problems [44]. A sense of quality has historically been linked to the supply of electricity, but this quality is greatly reduced by the growing use of power electronics devices such as converters, variable speed drives, and switching power supplies in electrical networks. This contamination in power networks was caused by harmonic voltages and currents. Undoubtedly, these non-linear loads require the grid to supply a non-sinusoidal current with a significant harmonic component. Furthermore, they use reactive power, which has a direct impact on the non-sinusoidal shape of the voltage and current waves. High harmonic levels can cause a variety of sensitive devices connected to the common point of connection, such as computers, medical equipment, programmable logic controllers (PLCs), and rotating machinery, to malfunction. Harmonic currents flow through the electric grid's impedances. Furthermore, network safeguards might not perform as intended, and electrical grid elements like cables and transformers might age more quickly. Reducing these conspicuous harmonics below the THD limitations outlined in the IEEE International Harmonic Standard which is mandatory for both suppliers and industrial customers is crucial to addressing these problems.

Table I.2 illustrates various PQ problems observed in hybrid renewable energy systems, including PV and WT technologies, when integrated with the grid. It also highlights the applicability of these issues in an AC microgrid environment.

Table I.2 Power quality problems in a hybrid renewable energy system (PV and Wind) integrated with the grid [31].

Power quality phenomenon	PV	WT	Applicable in hybrid renewable system
Transients			
Impulsive		✓	✓
Oscillatory		✓	✓
Short-duration RMS variation			
Voltage Sag		✓	✓
Voltage Swell		✓	✓
Short Interruption			✓
Long-duration RMS variation			
Undervoltage		✓	✓
Overvoltage		✓	✓
Sustained Interruption	✓	✓	✓
Unbalance			
Voltage	✓		✓

Current			✓
Waveform distortion			
DC Offset			✓
Harmonics	✓	✓	✓
Interharmonics			✓
Noise			✓
Notching			✓
Voltage fluctuation	✓	✓	✓
Power frequency variations			✓

Figure I.7 provides a schematic representation of harmonic generation and propagation mechanisms in a grid-connected hybrid renewable energy system comprising PV and wind energy sources. The figure highlights the influence of intermittent renewable generation, characterized by variable solar irradiance and fluctuating wind speed, on the electrical PQ.

To enable synchronization with the grid and ensure power adaptability, both PV and wind energy systems rely heavily on static power converters (AC/DC, DC/DC, DC/AC). These converters, essential for voltage regulation and interfacing, are also the primary sources of harmonic distortion due to their high-frequency switching operations.

The integration of these energy sources into the grid occurs via transformers and connection points, particularly the Point of Common Coupling (PCC), where voltage and current distortions become apparent. This distortion is illustrated through the waveforms of V_{PCC} and I_{PCC}, reflecting harmonic-rich signals.

Furthermore, the presence of nonlinear loads on the grid side intensifies harmonic content, leading to increased THD. This degradation in PQ adversely impacts sensitive equipment, disrupts protection systems, accelerates component aging, and introduces resonances within the network. Therefore, understanding and mitigating harmonic disturbances in renewable-rich systems is critical to maintaining power system stability and compliance with grid codes.

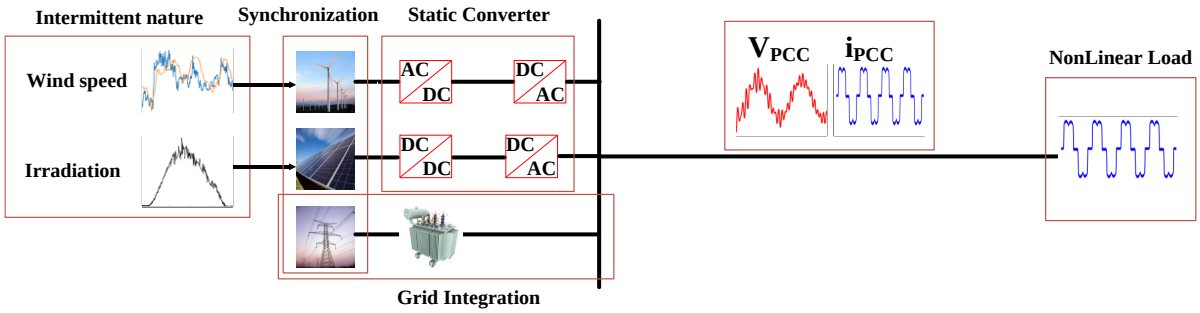

Figure I.7 Harmonic disturbance propagation in grid-connected renewable energy systems

I.7 Solutions for reducing pollution in electrical networks

To ensure good electrical PQ, the first step is to address disturbed signals caused by nonlinear loads through proposed solutions, which include both traditional and modern approaches [45].

I.7.1 Traditional solutions

These techniques should be known by all electricians. They provide easy and quick solutions for certain localized disturbances and use passive components such as inductors, capacitors, and transformers.

A. Intervention on the installation structure

It is advisable to supply a major polluter with a separate transformer to isolate it from a sensitive receiver. In the case of a medium polluter, it is preferable to use separate cables instead of connecting them in parallel. A star distribution allows for decoupling through natural and/or additional impedances.

B. Oversizing or downgrading the electrical installation

Oversizing the equipment is generally used to ensure it can withstand harmonic overloads. This solution does not directly affect the harmonics, which remain unaddressed by the user. With this approach, problems related to harmonic pollution are resolved only for a limited time.

Downgrading the distribution equipment exposed to harmonics is employed in the case of existing installations. However, this method leads to additional production costs and does not take full advantage of the installation's actual potential.

C. Strengthening the short-circuit power

Reducing the total impedance upstream of the nonlinear load helps to lower the voltage created by the current harmonics, thus decreasing the harmonic distortion rate at the connection point. However, the harmonic currents are not attenuated.

D. Rebalancing the electric grid currents

This solution distributes the loads evenly across the three phases. In fact, poorly distributed single-phase and two-phase loads generate unbalanced currents in low-voltage electrical networks.

E. Passive filtering

The principle of passive filtering involves inserting one or more circuits upstream of the load, tuned to the harmonics to be rejected. To filter current at a specific frequency, a series resonant filter is placed in parallel with the network. However, this type of filter is highly selective. To attenuate a wide frequency range, a second-order passive damped filter, is preferable. The design of these filters depends on the harmonics to be eliminated, the required performance, the network structure, and the nature of the receivers. Generally, this technique makes it easier to reject higher-order harmonics than lower-order ones. Despite its widespread use in industry, this simple device has some drawbacks [46]:

- A deep understanding of the electrical network configuration is required.
- Variations in the network impedance can degrade filter performance.

- The network may form a resonant system with the filter, and frequencies near the resonance frequency will be amplified.
- Bulky equipment.
- Inadaptability and loss of efficiency when the characteristics of the electrical network change.

I.7.2 Modern solutions

Two main reasons led to the development of a new and efficient filtering structure known as the active filter. The first factor is the inherent limitations of traditional power quality mitigation solutions, which no longer meet the evolving demands of loads and electrical networks. The second reason is the emergence of new semiconductor components, such as GTO thyristors and IGBT transistors. The purpose of these filters is to generate either harmonic currents or voltages in order to compensate for disturbances that degrade the performance of electrical equipment and installations.

Four possible topologies of active filters are as follows:

- Shunt Active Power Filter (APF): Designed to compensate for current disturbances such as harmonics, imbalances, and reactive power, as shown in **Figure I.8.**

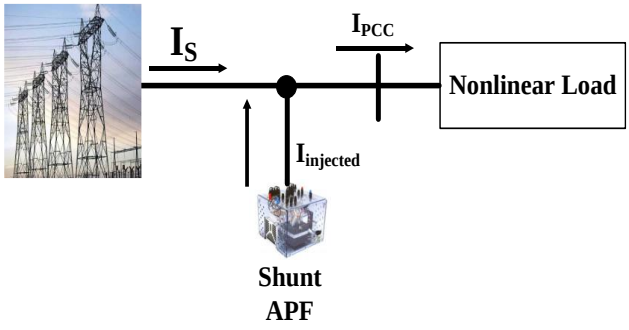

Figure I.8 Shunt active filter

- Series Active Power Filter (APF): Designed to compensate for voltage disturbances such as harmonics, imbalances, and voltage sags, as shown in **Figure I.9.**

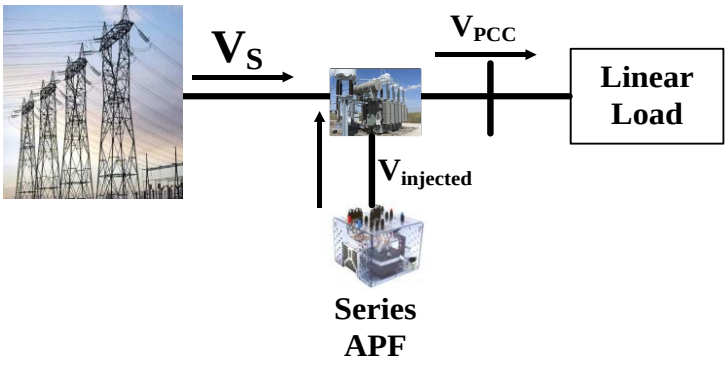

Figure I.9 Series active filter

- Series-Parallel Combination: A universal solution to compensate for both current and voltage disturbances.
- Hybrid Active-Passive Combination: These structures are designed to optimize the performance/cost ratio.

I.8 Conclusion

This chapter presented a comprehensive study of PQ disturbances in hybrid renewable energy systems, particularly under nonlinear load conditions. As the global energy transition accelerates toward sustainable sources like PV and wind energy, the integration of these resources into electrical grids introduces new challenges related to voltage and current quality. While RES offer significant environmental and economic benefits, their inherently intermittent nature and dependence on power electronic converters contribute to a range of PQ issues, including harmonics, voltage sags/swells, unbalance, and transients.

The classification of electrical disturbances was reviewed, emphasizing the mechanisms by which RES and nonlinear loads degrade PQ. The chapter discussed the impact of source-side components, such as PV and wind inverters, and load-side contributors, particularly nonlinear devices that draw non-sinusoidal currents. It was shown that the interaction of these elements leads to waveform distortions and increased THD, affecting grid stability, equipment lifespan, and energy efficiency.

To address these challenges, both conventional and modern solutions were explored. Traditional methods such as passive filtering, grid reinforcement, and load balancing provide partial mitigation. However, with the increasing penetration of power electronics and distributed generation, advanced mitigation strategies—such as active filtering and intelligent control—have become essential for ensuring compliance with standards like IEEE 519-2014 and maintaining overall grid reliability.

In conclusion, ensuring high PQ in hybrid RES environments demands not only accurate modeling and analysis of disturbances but also the deployment of robust control and filtering strategies. This chapter lays the foundational understanding necessary for the subsequent development and simulation of effective solutions, which will be addressed in the following chapters.

Chapter II:

Modeling, Simulation, and Control of Series and Shunt Active Power Filters

II.1 Introduction

With the increasing penetration of nonlinear loads and RES into modern power systems, maintaining high PQ has become a major challenge. Issues such as voltage distortions, harmonic currents, voltage sags/swells, and reactive power imbalances compromise the reliability and efficiency of electrical networks. To address these challenges, APFs both series and shunt configurations—have been widely adopted due to their real-time compensation capabilities and adaptability to varying operating conditions.

This chapter focuses on the modeling, simulation, and performance evaluation of both Series APF and Shunt APF. The aim is to assess and compare multiple control strategies applied to each filter type in order to determine the most robust and efficient method for mitigating PQ disturbances.

For the Series APF, three control strategies are investigated:

- Load Voltage Control (LVC),
- Source Voltage Control (SVC), and
- Unit Vector Template Generation (UVTG).

These are designed to improve voltage quality at the PCC, particularly during sags, swells, and harmonic distortion events.

For the Shunt APF, three classical control methods are evaluated:

- Instantaneous Active and Reactive Power Theory (p–q theory)
- Synchronous Reference Frame (SRF) Method, and
- Direct Current Control (DCC).

These aim to enhance current quality, reduce THD, and correct the power factor.

Each control strategy is modelled and simulated using MATLAB/Simulink under identical system conditions, including the presence of nonlinear loads and typical grid disturbances. The performance of each technique is then compared based on key metrics, such as:

- THD reduction,
- dynamic response speed,
- control robustness, and
- stability under transient conditions.

By performing a detailed comparative analysis, this chapter identifies the most effective control techniques for each APF type, providing valuable insight into their suitability for hybrid renewable energy systems where PQ is critical.

II.2 Principle of operation of a series active power filter with voltage structure

The series APF is a solution designed to protect sensitive loads from voltage disturbances in the electrical grid. It is positioned between the disturbed grid and the load to be protected via a voltage injection transformer. The basic schematic of a series APF is shown in **Figure II.1**. It primarily consists of two blocks: one for power and the other for control. The power block typically includes a three-phase voltage converter, either two-level or three-level (NPC), a DC

voltage supply system, an output filter, and three single-phase voltage injection transformers. The control block is responsible for identifying the disturbing voltages and controlling the injected voltages into the grid.

The series APF maintains the desired load voltage magnitude (V_L) by compensating by injecting a correction voltage (V_i) through an injection transformer when the source voltage (V_S) fluctuates, either sagging or swelling. The equation describes the relationship regulating this process:

$$V_i = V_L + V_S \quad \text{(II-1)}$$

Where (V_S) is the changed source voltage during these disturbances. By ensuring that sensitive loads get steady voltage levels, this device protects them against power distribution system voltage anomalies.

Table II-1 provides a comprehensive overview of the roles of each component within the Series APF. These components collectively ensure effective voltage regulation, harmonic mitigation, and stability for sensitive loads under various power disturbances.

Table II-1 Roles of series active power filter (APF) components in voltage regulation

Component	Role
Series transformer	Couples the VSI with the power distribution system. Injects compensating voltage via the primary winding and interfaces with the load and distribution network through the secondary winding to mitigate voltage sags, swells, and disturbances.
Voltage Source Inverter (VSI)	Generates compensating voltage using IGBT switches. Controls the output voltage (V_{inv}) by adjusting switching states, minimizing losses, and ensuring efficient operation to stabilize the voltage under disturbances, (For instance, activating switches **S1** and **S4** while deactivating **S2** and **S3** produces a positive DC voltage (V_{inv}=+Vdc), and reversing this configuration outputs a negative DC voltage.)
Energy storage unit	Supplies active and reactive power during voltage sags or swells. Uses technologies like batteries, flywheels, or capacitors to maintain stable voltage supply for sensitive loads.
Filter (LC)	Eliminates harmonics caused by VSI switching. The capacitor (Cs) and inductor (Ls) are tuned to reduce harmonic distortions, ensuring a clean and stable output voltage to protect sensitive loads.
Control unit	Detects voltage disturbances in real time and implements switching strategies for the VSI. Ensures consistent and stable voltage supply to sensitive loads by dynamically compensating for sags, swells, and other disturbances.

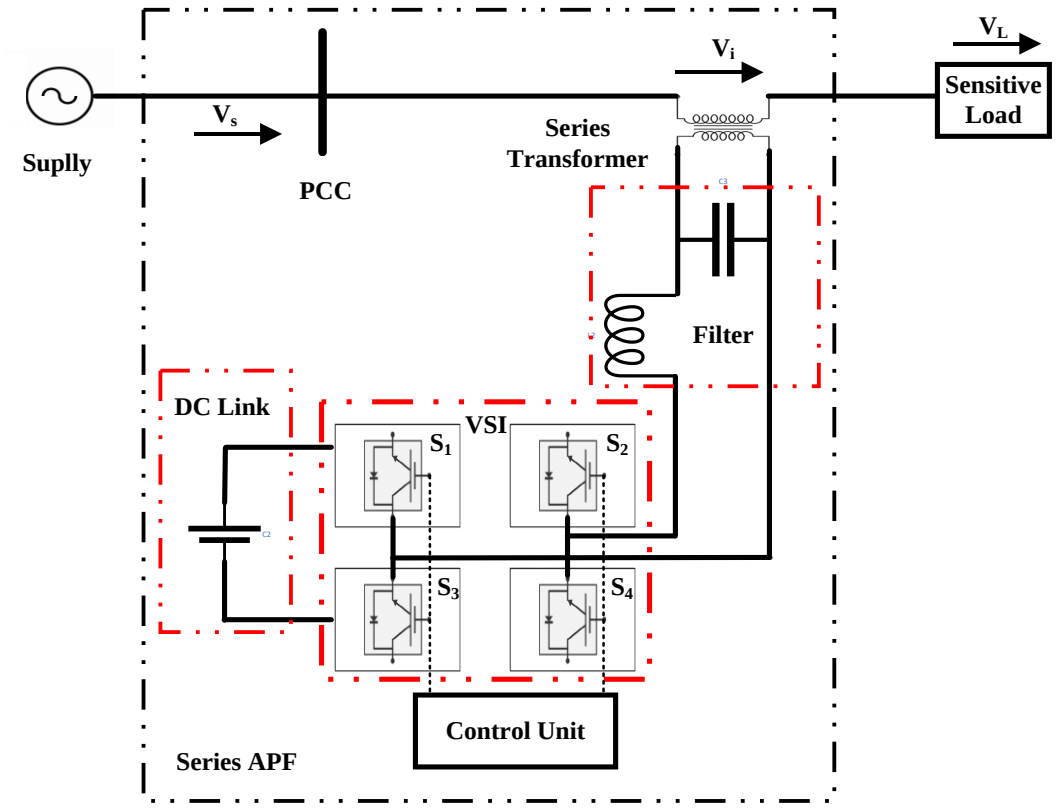

Figure II.1 Series APF configuration

II.2.1 Mode of series APF

The Series APF operates primarily to inject a dynamically regulated voltage into the transport voltage system via a booster transformer, effectively mitigating voltage sags and other disturbances. It functions in three modes [47]:

- protection mode: where it disconnects from the system during overcurrent conditions using bypass switches; (**Figure II.2**).
- standby mode: where it maintains a low voltage state without semiconductor activity; (**Figure II.3**).
- injection mode: where it actively compensates for voltage fluctuations by injecting a corrective voltage based on real-time assessments of the source voltage.

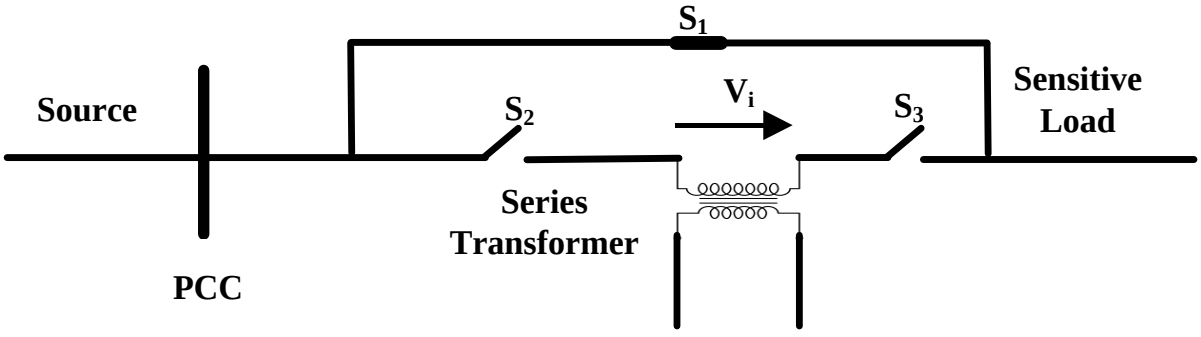

Figure II.2 Protection mode

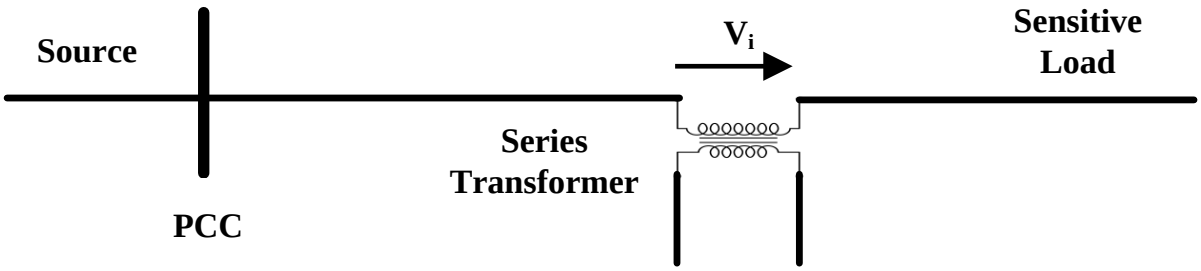

Figure II.3 Standby mode

II.2.2 Compensation strategies

Different techniques are used to address voltage problems in electrical systems as part of compensation schemes for a Series APF. Depending on the load conditions, voltage sag type, and Series APF power rating, the Series APF provides voltage support when operating in injection mode. The system is stabilized by three primary methods [48].

A. Pre-sag/dip compensation (PDC) technique

An electrical load's voltage and phase angle can be restored to their pre-sag (sag) levels using the Pre-sag/dip compensation (PDC) approach. This technique aids in correcting sudden phase angle changes, but it needs additional power from a DC link capacitor. Because the Series APF requires more active power during a positive phase leap than during a negative one, its performance may suffer.

In order to correct for voltage sags in the electrical system, a Series APF modifies the voltage it delivers, as shown in **Figure II.4**. While Equation (II-2) establishes the phase angle of that voltage, Equation (II-3) computes the size of the voltage that the Series APF must inject.

$$V_{Series\ APF} = \sqrt{2(V_L^2 + V_S'^2) - 2V_L V_S' \cos\phi} \quad \text{(II-2)}$$

$$\angle V_{Series\ APF} = \tan^{-1}\left(\frac{V_L \sin\theta_L - V_S' \sin(\theta_L - \phi)}{V_S' \cos(\theta_L - \phi) - V_L \cos(\theta_L)}\right) \quad \text{(II-3)}$$

" ϕ " stands for the phase jump, which is a shift in the electrical grid's voltage angle brought on by a voltage sag, or brief voltage decrease. V_S' is the voltage level of the supply after it has sagged, whereas V_L represents the load voltage before to the sag.

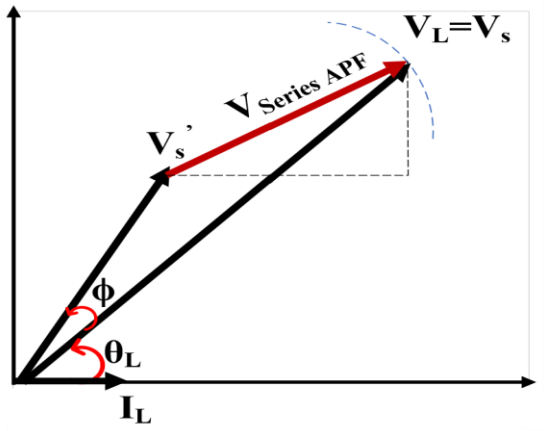

Figure II.4 Phasor representation of various compensation methods (a) Pre-sag compensation method

B. In-phase compensation (IPC) method

A Series APF is used in the In-phase Compensation (IPC) technique to assist stabilize the current drooping supply voltage by adding a small quantity of voltage. This technique seeks to align the voltage's magnitude and phase with the sagging supply, but it has a drawback in that it is unable to rectify sudden phase shifts, or phase jumps as shown in **Figure II.5**. Equations (II-4) and (II-5) define the precise values for the voltage magnitude and angle that the Series APF injects, respectively.

$$V_{Series\ APF} = V_i = \sqrt{2}(V_L - V_S') \quad \text{(II-4)}$$

$$\angle V_{Series\ APF} = \theta_L \quad \text{(II-5)}$$

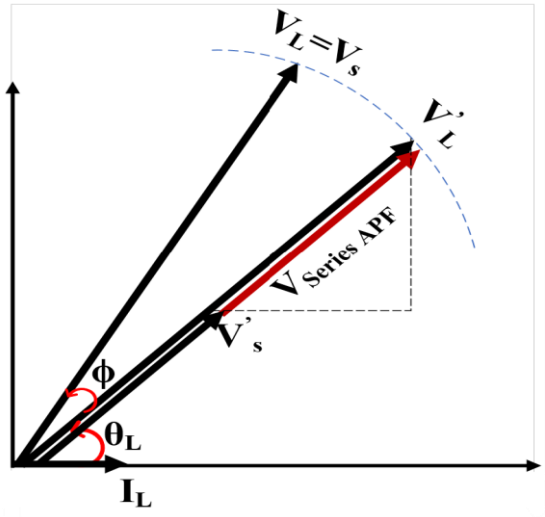

Figure II.5 In phase compensation method

C. Energy optimization method

When dealing with large voltage sags, or dips in voltage levels, the Energy Optimization Method is intended to improve the efficacy of the quadrature injection strategy. This technique helps maintain the voltage by injecting a certain amount of active power through the Series

APF. The given equations may be used to calculate the voltage magnitude and angle that the Series APF must inject, ensuring that the system functions well during these voltage disruptions. To guarantee that the system functions well during these voltage fluctuations, the equations supplied may be used to estimate the voltage magnitude and angle that the Series APF needs to inject.

$$V_{Series\ APF} = \sqrt{2(V_L^2 + V_S'^2) - 2V_L V_S' \cos\theta_L} \text{ (II-6)}$$

$$\angle V_{Series\ APF} = \tan^{-1}\left(\frac{V_L \sin\theta_L}{V_L' \cos(\theta_L) - V_S \cos(\theta_L)}\right) \text{ (II-7)}$$

In this thesis, the pre-sag/dip compensation technique is adopted for the Series Active Power Filter, as it enables the restoration of the load voltage to its pre-disturbance magnitude and phase under various power quality disturbances, including voltage sags, swells, and short-circuit conditions.

II.2.3 Control strategies for a series active power filter with voltage structure

To identify the disturbing voltages of the direct fundamental component of the electrical grid voltage, several methods have been studied [43,44]. These include methods based on the calculation of symmetrical components, methods based on the calculation of disturbances in the (d,q) reference frame, and methods using a system based on a Phase-Locked Loop (PLL) [51,52]. In this section, we will describe the main methods used to identify the compensation voltages necessary for the proper functioning of a series APF.

A. Load voltage control

Through the use of a closed-loop control technique in [53], the controller plays a crucial part in preserving voltage stability and quality. This method enables the Series APF controller to provide suitable pulse-width modulation (PWM) signals for the Insulated Gate Bipolar Transistor (IGBT) within the VSI and track voltage variations in real-time. The VSI, which is controlled by pulse width modulation (PWM), is triggered to rectify any voltage imbalance that arises in the power supply. A Proportional-Integral (PI) controller generates the required control signals for the VSI by processing the differences between the reference and real voltage signals to guarantee accurate voltage regulation [54].

To enable efficient regulation of voltage disturbances in power systems, the three-phase ABC coordinate system is transformed to the dq0 reference frame, as shown in **Figure II.6**. The ABC coordinate system may be changed into the dq0 system using the equations above:

$$V_d = \frac{2}{3}\left[V_a \sin wt + V_b \sin\left(wt - \frac{2\pi}{3}\right) + V_c \sin\left(wt + \frac{2\pi}{3}\right)\right] \text{ (II-8)}$$

$$V_q = \frac{2}{3}\left[V_a \cos wt + V_b \cos\left(wt - \frac{2\pi}{3}\right) + V_c \cos\left(wt + \frac{2\pi}{3}\right)\right] \text{ (II-9)}$$

$$V_0 = \frac{1}{3}[V_a + V_b + V_b] \text{ (II-10)}$$

The voltage signals are converted from the three-phase ABC system into a two-axis representation using the dq coordinate system, which makes disturbance detection and control

simpler. By comparing the actual dq voltage values to their reference values, the disturbances in the dq coordinates are computed, allowing for accurate voltage output modifications. A phase-locked loop (PLL), which guarantees synchronization and stability in the control process and permits efficient voltage regulation in response to variations, is also used to monitor the system frequency.

The Series APF's PI controller gets its input from the difference between the actual and reference values of the dq voltage, as shown by the following equations:

$error_d(t) = V_{dref} - V_d$ (II-11)

$error_q(t) = V_{qref} - V_q$ (II-12)

The error signals, namely the differences between the reference voltages (V_{dref} and V_{qref}) and the actual measured voltages (V_d and V_q), are used as inputs by the proportional-integral (PI) controllers for the direct (d) and quadrature (q) axes. In order for the PI controllers to properly modify the output and guarantee that the Series APF can react precisely to voltage changes in the power supply, these error signals designated as $error_d$ and $error_q$ are essential. The PI controllers interpret these error signals to produce control actions, which are then converted back into the ABC coordinate system for VSI pulse-width modulation (PWM) control.

The Series APF control circuit designed for Load Voltage Control (LVC) is illustrated in **Figure II.6**. This control strategy employs a Proportional-Integral (PI) regulator to maintain the load voltage at the desired reference level, particularly during transient grid conditions such as voltage sags, swells, and unbalanced faults.

The performance of this control approach under various disturbances is demonstrated in **Figure II.7**, which presents the waveforms of the source voltage, load voltage, and the voltage injected by the Series APF during (a) a voltage sag, (b) a voltage swell, (c) a voltage unbalance, and (d) a short-circuit event.

Furthermore, the effectiveness of the Load Voltage Control in improving PQ is evaluated in **Figure II.8**, which shows the THD of the load voltage under the same four fault scenarios. The THD values clearly highlight the controller's ability to mitigate harmonic distortions and stabilize the load voltage across a range of grid disturbances.

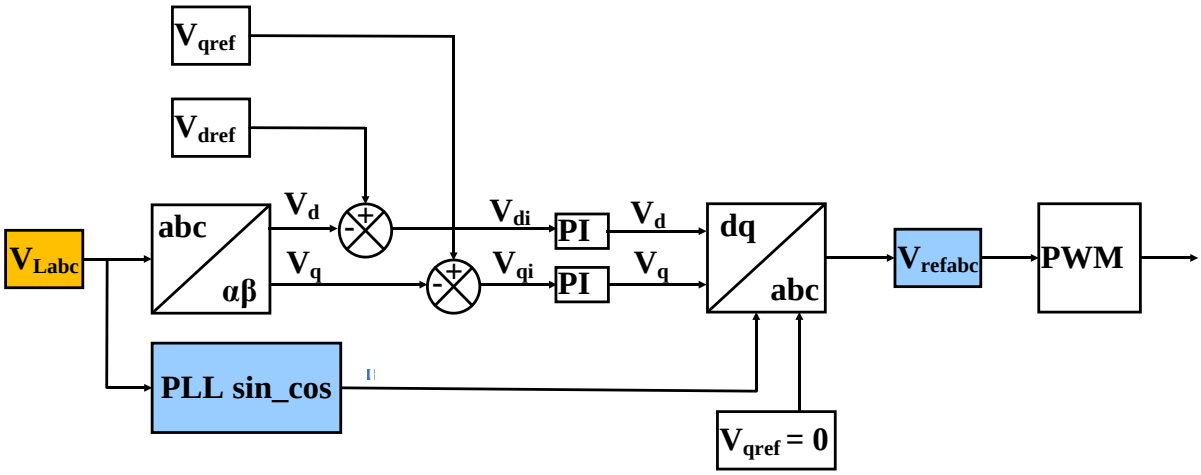

Figure II.6 Load voltage control

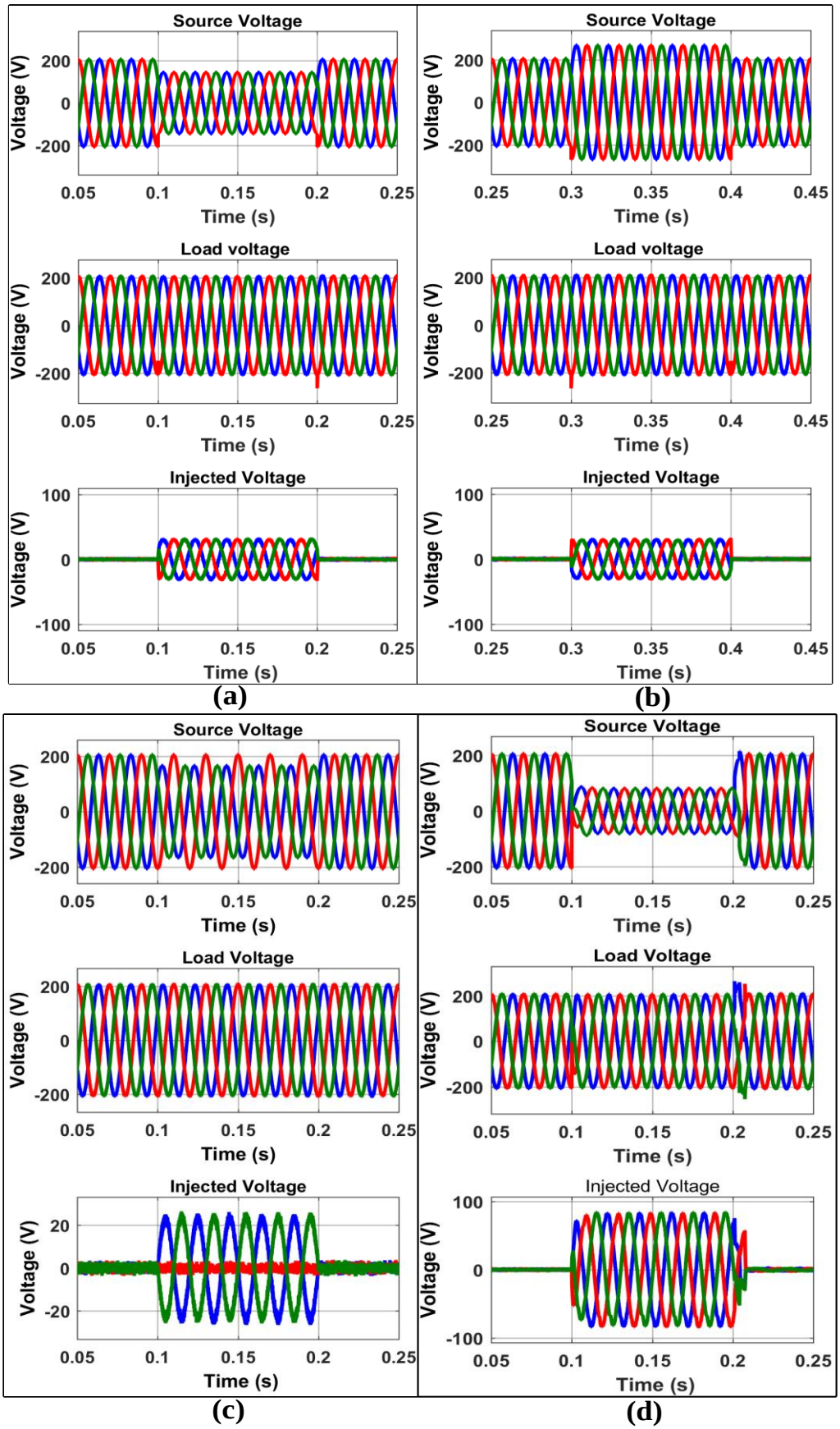

Figure II.7 Source, load and injected voltage for the first control during (a) voltage sag, (b) voltage swell, (c) voltage unbalanced, (d) short circuit

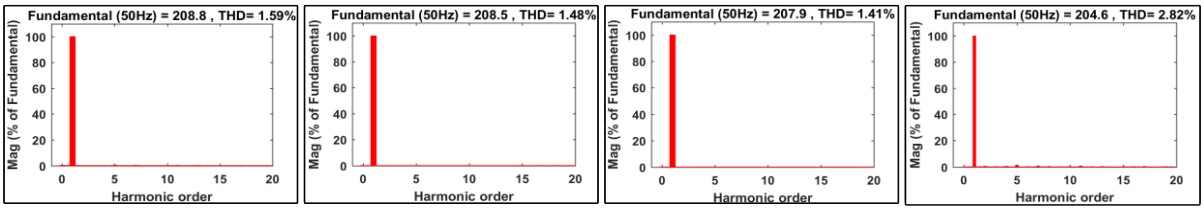

(a) **(b)** **(c)** **(d)**

Figure II.8 THD of load voltage during (a) voltage sag, (b) voltage swell, (c) voltage unbalanced, (d) short circuit

B. Source Voltage Control (SVC)

A control circuit design that uses a reference voltage produced by combining the source voltage and system frequency to provide a without distortion, balanced three-phase output. An essential part of the Series APF system is the three-phase full-bridge inverter, which produces the AC voltage that is sent into the distribution network through a transformer. In order to maintain balanced three-phase output, each leg of the inverter uses complimentary switching signals to provide voltages for specific phases with a 120° phase shift. By comparing the load voltage with a reference voltage and producing switching signals based on the error signal that travels through a specified hysteresis band, the hysteresis controller plays a crucial role in enabling dynamic adjustment of the injected voltage to effectively mitigate voltage sags and swells. This method reduces harmonic distortion, keeps the output voltage steady during cycles, and eliminates the need for extra parts, all of which increase the system's efficiency.

The detailed structure of the SVC control circuit is illustrated in **Figure II.9**. Its performance under various disturbance conditions—namely voltage sag, swell, unbalance, and short circuit—is shown in **Figure II.10**, where the source voltage, load voltage, and injected compensating voltage are presented for each case. The system's harmonic suppression capability is further validated in **Figure II.11**, which shows the THD of the load voltage across the same disturbance scenarios. These results confirm the controller's effectiveness in delivering high-quality voltage and maintaining grid stability under fault conditions.

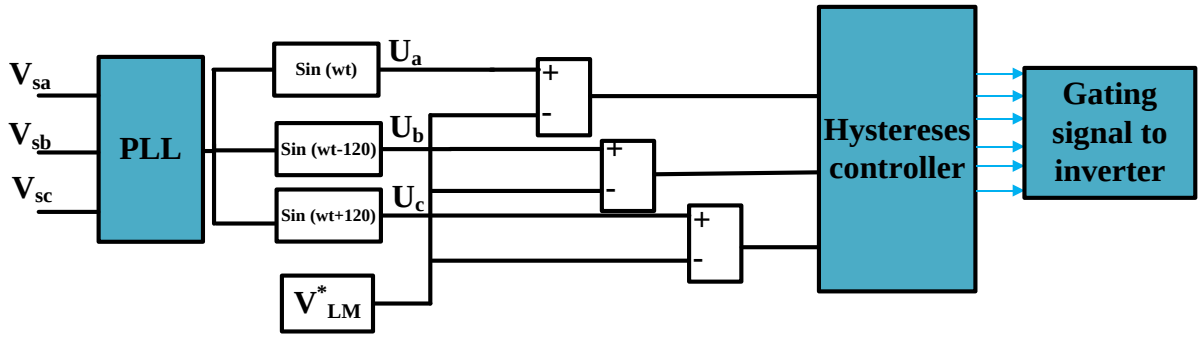

Figure II.9 Source voltage control

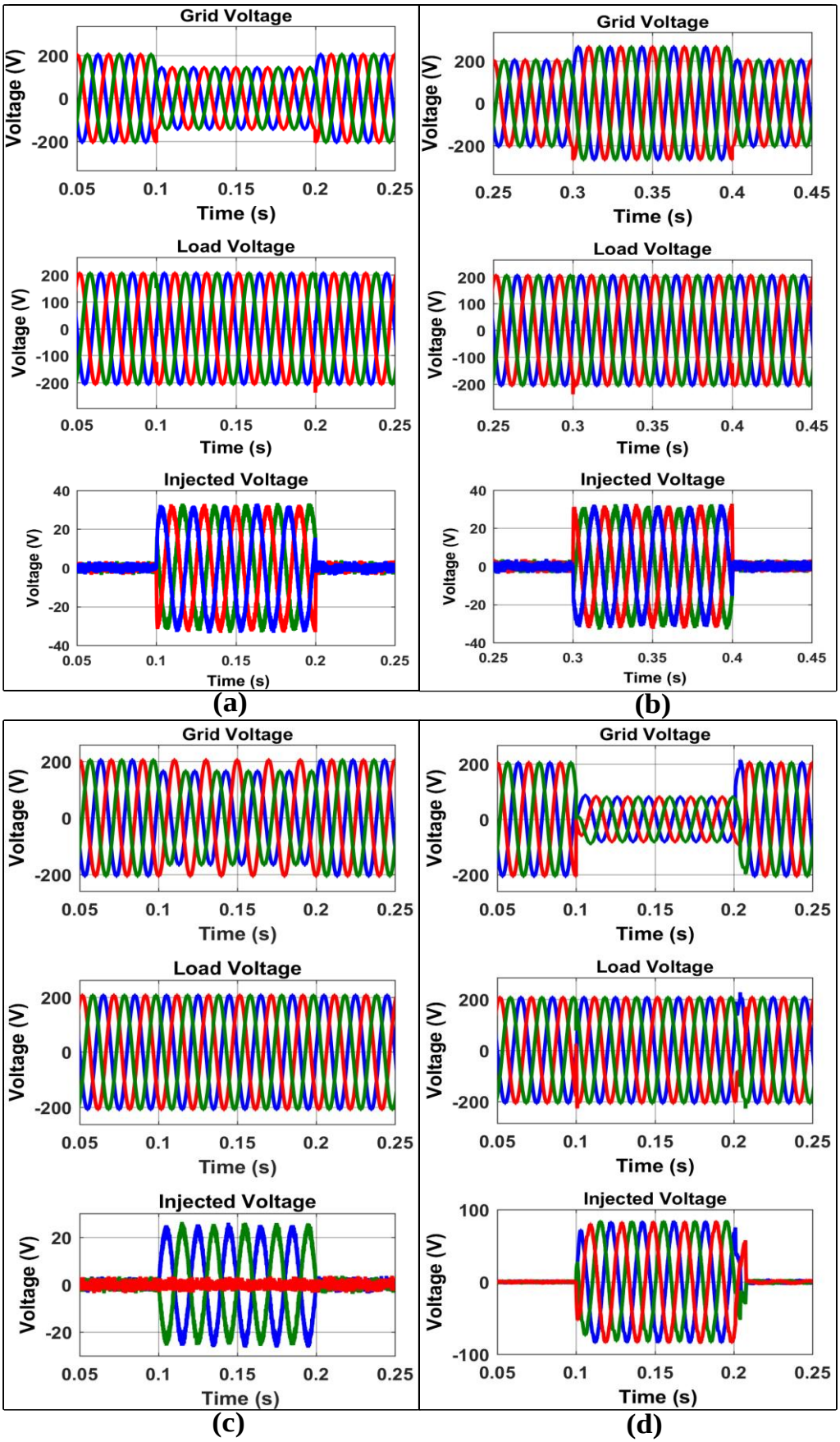

Figure II.10 Source, load and injected voltage for the Second control during (a) voltage sag, (b) voltage swell, (c) voltage unbalanced, (d) short circuit

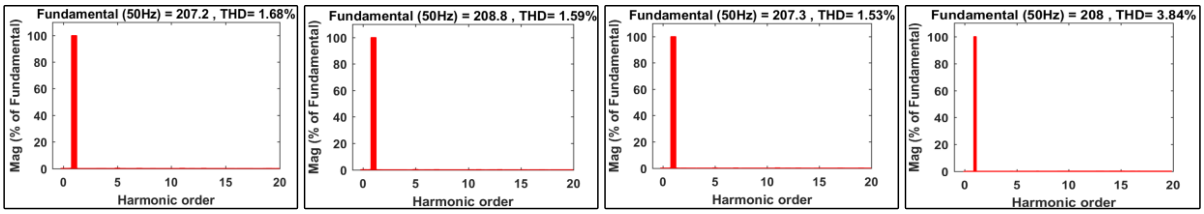

(a) **(b)** **(c)** **(d)**

Figure II.11 THD of load voltage during (a) voltage sag, (b) voltage swell, (c) voltage unbalanced, (d) short circuit

C. Unit Vector Template Generation (UVTG) algorithm

By synchronizing with supply voltage and producing accurate switching signals, the algorithm plays a critical role in managing series APF inside power systems, guaranteeing free of distortion load voltages [55]. The steps of the algorithm, which are depicted in a flowchart, improve APFs' efficacy and efficiency in preserving PQ. The flowchart describing the control algorithm for the series APF utilized as shown in **Figure II.12**. The comprehensive control algorithm used for the series APF is depicted in **Figure II.13**, which also shows the decision-making procedure for harmonic mitigation and voltage regulation.

The supply's phase voltages are:

$V_a = sin(wt)$ (II-13)

$V_b = sin(wt - 120)$ (II-14)

$V_c = sin(wt + 120)$ (II-15)

Furthermore, the reference load voltage may be written as follows:

$V^*_{Labc} = V^*_{Lm} * V_{abc}$ (II-16)

V_{Lm}: Magnitude (reference amplitude) of the load voltage.

V_{abc}: Unit load voltage vector in the abc reference frame

The effectiveness of the UVTG-based Series APF control under various voltage disturbance scenarios is presented in **Figure II.14**, which shows the source voltage, load voltage, and injected voltage during (a) voltage sag, (b) voltage swell, (c) voltage unbalanced, and (d) short-circuit events.

To evaluate the harmonic mitigation performance, **Figure II.15** presents the THD of the load voltage under the same disturbance conditions. These results demonstrate that the UVTG algorithm achieves excellent performance in maintaining voltage quality, with fast dynamic response and high accuracy in harmonic suppression.

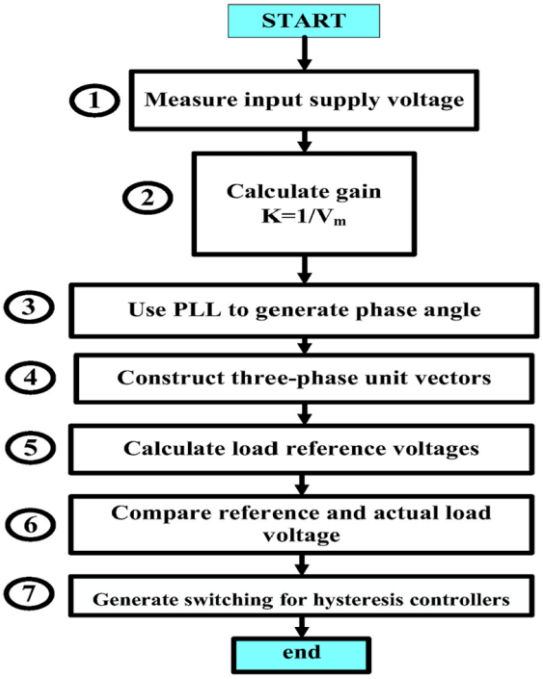

Figure II.12 Algorithm flowchart for the third control

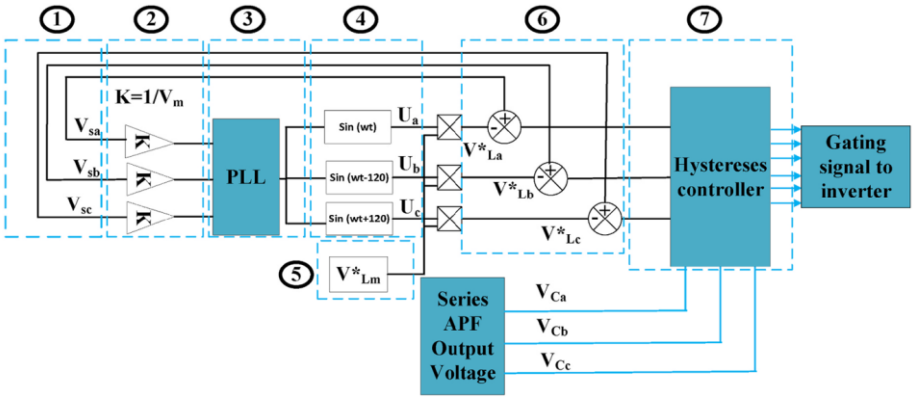

Figure II.13 Algorithm control of the third control

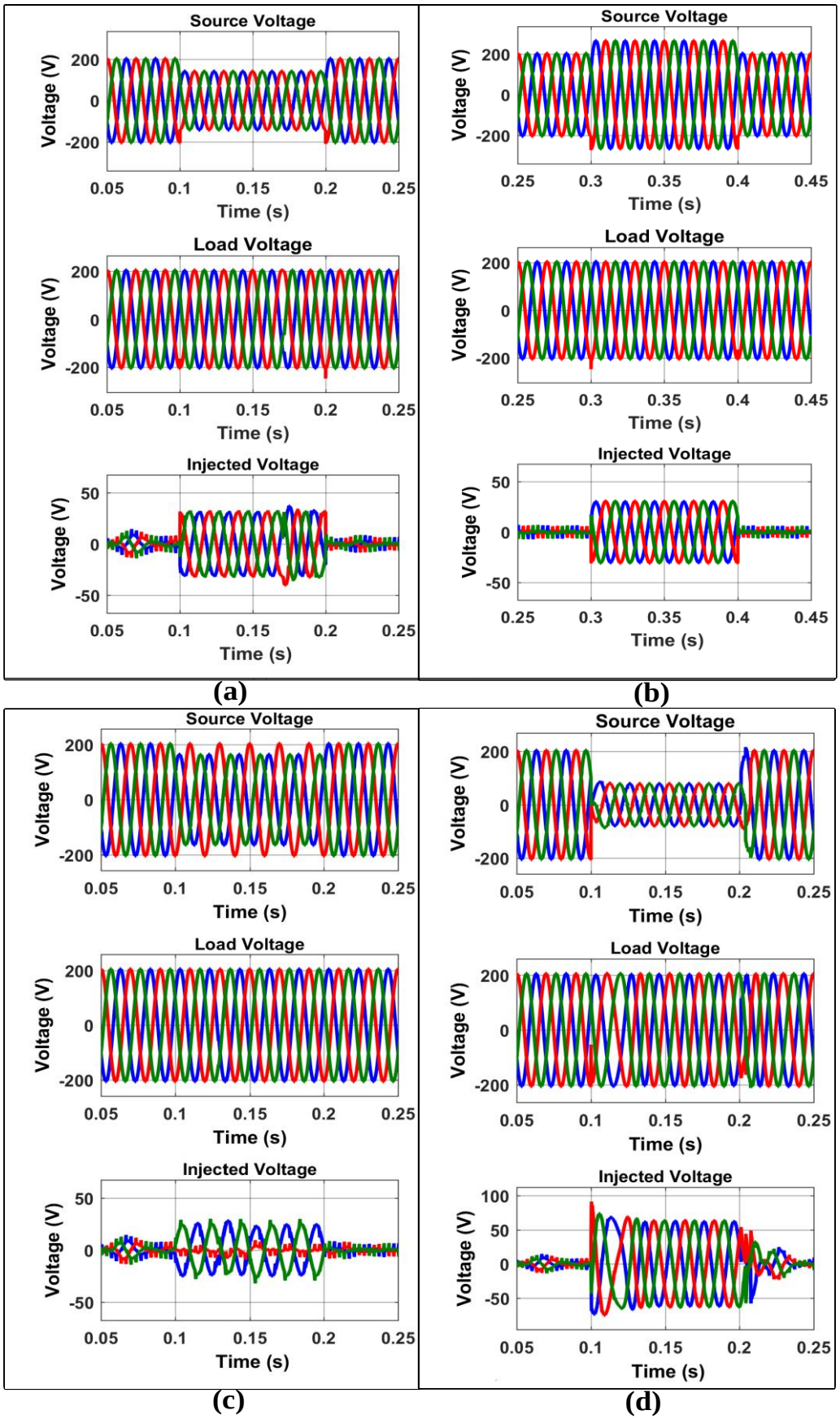

Figure II.14 Source, load and injected voltage for the third control during (a) voltage sag, (b) voltage swell, (c) voltage unbalanced, (d) short circuit

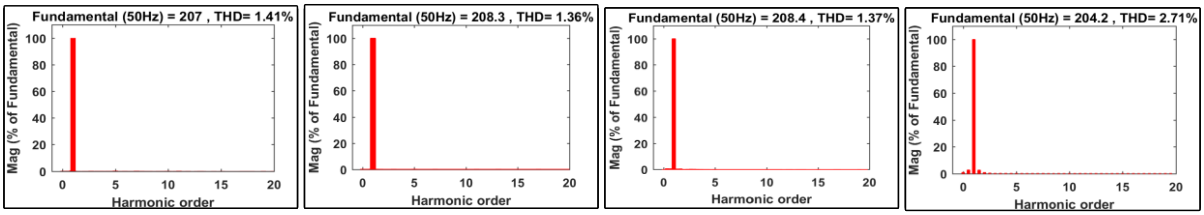

(a) **(b)** **(c)** **(d)**

Figure II.15 THD of load voltage during (a) voltage sag, (b) voltage swell, (c) voltage unbalanced, (d) short circuit

To evaluate the dynamic performance and robustness of the three implemented control strategies for the Series APF, a comparative analysis of the RMS load voltage under different disturbance scenarios is presented in **Figure II.16**. This figure illustrates the system response during (a) voltage sag, (b) voltage swell, (c) voltage unbalance, and (d) short circuit conditions.

The results clearly demonstrate that the third control strategy, based on the UVTG algorithm, exhibits superior performance compared to the Load Voltage Control (LVC) and Source Voltage Control (SVC) methods. Specifically, the UVTG approach shows:

- Faster response time to disturbances,
- Lower peak voltage deviations,
- Improved voltage stability, and
- Robust dynamic behavior under all tested scenarios.

Moreover, in terms of harmonic performance, the UVTG method also achieves the lowest THD of the load voltage, further confirming its effectiveness for high-quality voltage regulation in power systems. These comparative findings validate UVTG as a more robust and efficient control strategy for Series APF applications in environments subject to frequent voltage disturbances and harmonic pollution.

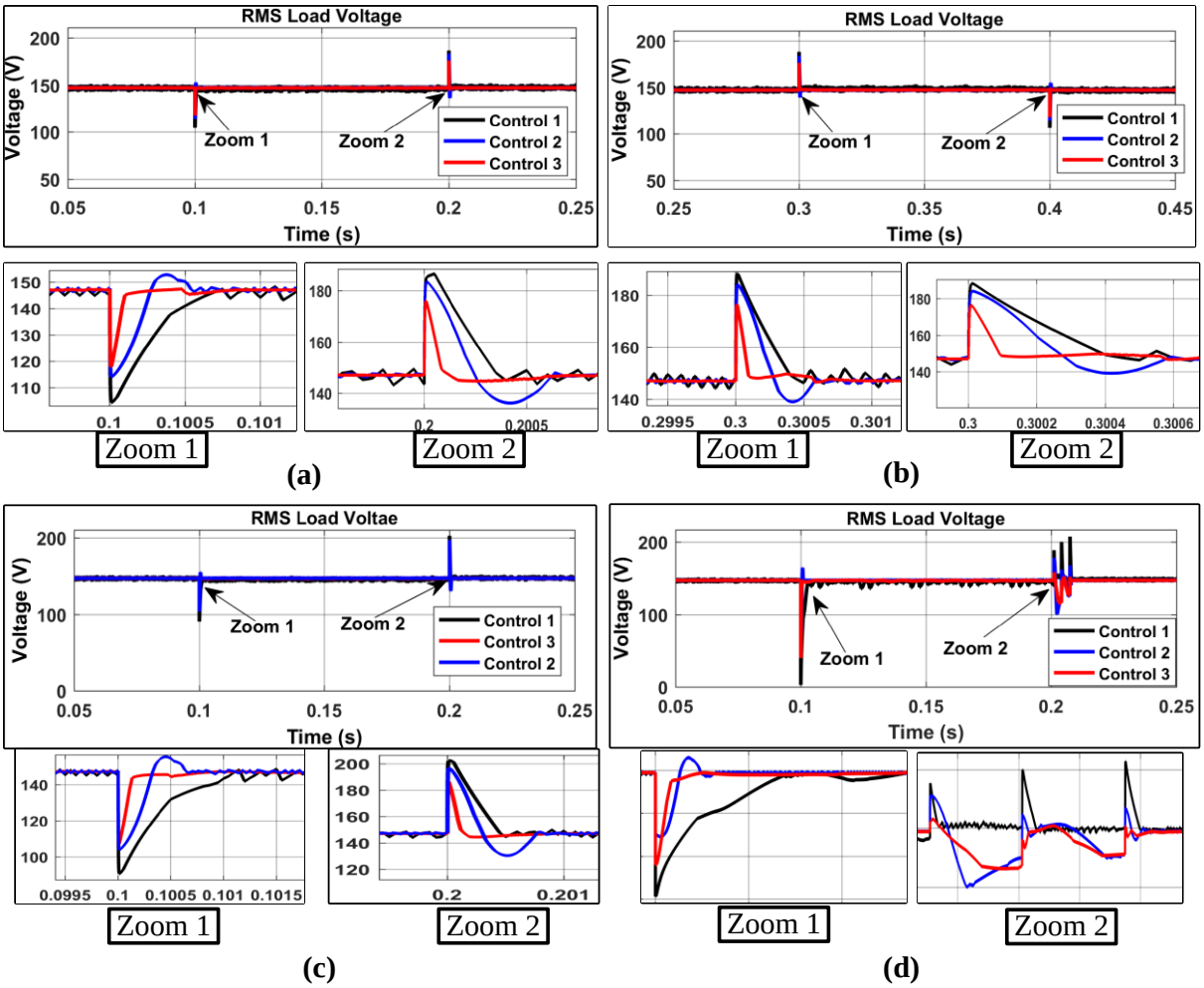

Figure II.16 Comparative analysis of RMS load voltage for series active power filter using three different control strategies under various disturbances: (a) Voltage sag, (b) Voltage swell, (c) Voltage unbalance, and (d) Short circuit.

II.3 Shunt active power filter

The power part and the control part are the two primary parts which make the active filters. The energy storage component, which is inductive for current filters and capacitive for voltage filters, a coupling filter, and an inverter which may handle voltage or current in single or multi-phase configurations and be two-level or multi-level are all used in the power section [56]. In order to reduce distortion in the electrical network, the control section regulates the switching of the inverter's semiconductor devices. It does this by using a variety of control schemes to produce harmonic currents that are opposite in phase but equal in amplitude to those absorbed by the load [57].

The power stage of the shunt APF consists of three primary components, as summarized in **Table II-2**. These include the inverter, energy storage circuit, and output filter. Each component plays a vital role in ensuring harmonic mitigation, voltage stability, and clean sinusoidal current output, contributing to the overall efficiency of the system.

Table II-2 Key Components of a Shunt Active Power Filter

Component	Description	Function
Inverter	Utilizes power switches like GTO thyristors or IGBTs, paired with antiparallel diodes [58].	Converts DC to AC for harmonic compensation and manages reverse currents.
Energy storage	Typically, a capacitive circuit.	Maintains voltage stability and ensures energy balance during operation.
Output filter	Integrated filter connecting the system to the electrical grid.	Reduces high-frequency harmonics from inverter switching and provides a cleaner sinusoidal output.

Electrical systems may have PQ problems as a result of the non-linear (NL) load absorbing a distorting current made up of a fundamental component and its harmonic components [59]. In order to make the source current almost sinusoidal, the active filter's main job is to produce harmonic currents that are equal in amplitude but phase-opposed to those absorbed by the load [49,50].

Table II.3 summarizes the core components involved in the shunt APF control system and their respective functions:

Table II-3 Main functional blocks of the shunt active power filter control system

Component	Description	Function
Harmonic current identification circuit	Uses measurement transformers to monitor network and load voltages and currents.	Identifies harmonic currents for compensation.
Phase-Locked Loop (PLL)	Synchronizes with the network frequency.	Ensures accurate harmonic current compensation and frequency alignment.
DC voltage regulation system	Regulates the energy storage element voltage [61].	Maintains stable operation and energy balance for the inverter.
Current regulation system	Manages the injection of compensating current into the network.	Controls the quality and magnitude of the injected current for harmonic mitigation.
Control strategies (PWM/Hysteresis)	Governs the switching of the inverter system.	Enhances precision in harmonic compensation and improves overall system efficiency.

The detection of crucial voltage and current signals, which supply the data required for system identification variables, initiates the reference signal for harmonic current identification [62]. While current detection usually entails detecting the load currents and source currents, key voltage variables include the source voltage (Vs), the inverter's DC bus voltage (Vdc), and the

reference DC voltage (Vdc_ref). Using hysteresis control, three distinct algorithms DCC, Real and Reactive Power (p-q), and SRF are assessed for a three-phase inverter [63]. Artificial intelligence methods such as neural networks and fuzzy logic are also incorporated to improve algorithm optimization. The performance of the selected identification algorithm is crucial to the efficacy of harmonic current compensation [53,54].

The fundamental concept and structure of the Shunt APF, including signal acquisition, reference generation, and current injection, are illustrated in **Figure II.17**, which presents the principle of shunt active filtering for harmonic mitigation in power systems.

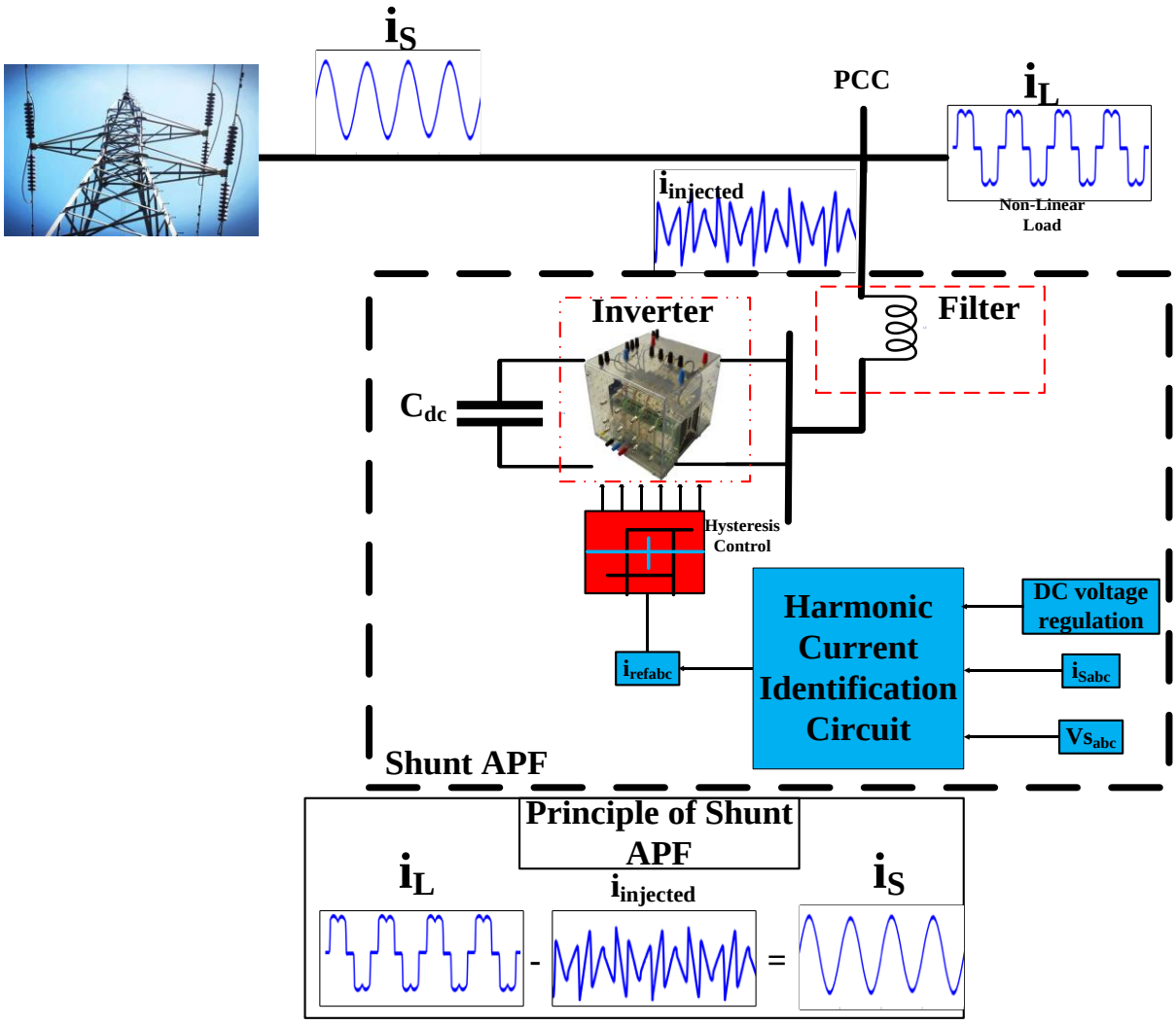

Figure II.17 Principle of a Shunt Active Power Filter (APF) for harmonic mitigation in power systems

II.3.1 Control strategies for a shunt active power filter

Shunt APF rely on effective control strategies to detect and compensate for harmonic currents injected by nonlinear loads. The core objective of these strategies is to generate accurate reference current signals and ensure that the inverter injects compensating currents in real time. Various control methods have been developed, each with specific strengths in terms of dynamic

response, harmonic suppression, and robustness [60,65]. In the following subsections, three widely used control techniques DCC, Instantaneous Power Theory (PQ), and the SRF method are examined and compared based on their effectiveness in improving PQ.

A. Active and Reactive power method (p-q)

The method of real and imaginary powers (p-q) is a widely utilized technique for identifying harmonic currents due to its precision, speed, and ease of implementation in power systems. This method involves:

- Captures three-phase source voltages and load currents.
- Transforms them into a two-phase power reference frame.
- Calculates active and reactive powers.
- Use a low-pass or high-pass filter to separate the active and reactive power components.
- Adjust reactive power to correct the power factor and enhance system performance.
- Adds a direct current power (Pdc) from a DC voltage regulator.
- Transform the reference currents back to the three-phase system using the inverse Concordia transformation.

The initial step in identifying harmonic currents involves transforming the three-phase (abc) currents and voltages into a two-phase (α, β) reference frame, where the axes are orthogonal (in quadrature). This transformation is crucial as it simplifies the analysis of the system by decoupling the harmonic components, allowing for a clearer assessment of the active and reactive power contributions [66].

The three-phase (α,β,0) transformation allows us to express the following relationships in currents and voltages:

$$\begin{bmatrix} V_\alpha \\ V_\beta \end{bmatrix} = \sqrt{\frac{2}{3}} \begin{bmatrix} 1 & -\frac{1}{2} & -\frac{1}{2} \\ 0 & \frac{\sqrt{3}}{2} & -\frac{\sqrt{3}}{2} \end{bmatrix} \begin{bmatrix} V_a \\ V_b \\ V_c \end{bmatrix} \quad \text{(II-18)}$$

$$\begin{bmatrix} i_\alpha \\ i_\beta \end{bmatrix} = \sqrt{\frac{2}{3}} \begin{bmatrix} 1 & -\frac{1}{2} & -\frac{1}{2} \\ 0 & \frac{\sqrt{3}}{2} & -\frac{\sqrt{3}}{2} \end{bmatrix} \begin{bmatrix} i_a \\ i_b \\ i_c \end{bmatrix} \quad \text{(II-19)}$$

a three-wire, three-phase system without a zero-sequence component. The system's currents and voltages are represented by the letters va, vb, and vc in the a-b-c coordinate system, ia, ib, and ic in the a-b-c coordinate system, and v0, vα, and vβ in the 0-α-β coordinate system. The α-β coordinate system may be used to describe the complex sum of active and reactive powers (p-q) as follows:

$P = V_\alpha i_\alpha + V_\beta i_\beta$ (II-20)

$Q = V_\alpha i_\beta - V_\beta i_\alpha$ (II-21)

Where P refers to the active power, Q represents the reactive power

The instantaneous active and reactive power components divide into AC and DC segments when nonlinear loads are present. The DC portion ($\bar{p}$) represents the basic voltage and current

components, which show the power transferred from the source to the load. In the meanwhile, the energy exchanged between the source and the load is shown by the AC part ($\tilde{p}$).

The goal of the method involving real and imaginary powers is to convert the main power component into a continuous form while separating the harmonic components into alternative forms. This allows the alternative components, represented as $\tilde{p}$ and $\tilde{q}$, to be easily extracted from the original power values p and q using low-pass (FPB) or high-pass (FPH) filters.

A high-order low-pass filter is used to extract the average DC component of the instantaneous real power. The fundamental and harmonic components responsible for energy circulation between load phases are identified by the instantaneous reactive power component (Q).

$$p = \bar{p} + \tilde{p} \quad and \quad q = \bar{q} + \tilde{q}$$

Both the total reactive power (Q) and the AC component ($\tilde{p}$) of active power are necessary to generate harmonic reference currents. To compensate for voltage source inverter switching losses and maintain the DC-link voltage, the shunt APF takes a tiny amount of actual power from an external power source or a three-phase AC source. After measuring the AC component, compensatory reference currents are calculated and inversely transformed to the a-b-c coordinates.

$$\begin{bmatrix} i_\alpha \\ i_\beta \end{bmatrix} = \frac{1}{\Delta}\begin{bmatrix} V_\alpha & -V_\beta \\ V_\beta & V_\alpha \end{bmatrix}\begin{bmatrix} \bar{p} \\ 0 \end{bmatrix} + \frac{1}{\Delta}\begin{bmatrix} V_\alpha & -V_\beta \\ V_\beta & V_\alpha \end{bmatrix}\begin{bmatrix} 0 \\ \bar{q} \end{bmatrix} + \frac{1}{\Delta}\begin{bmatrix} V_\alpha & -V_\beta \\ V_\beta & V_\alpha \end{bmatrix}\begin{bmatrix} \tilde{p} \\ \tilde{q} \end{bmatrix} \quad \text{(II-22)}$$

with : $\Delta = V_\alpha^2 + V_\beta^2$ (II-23)

As a result, the relationship will determine the reference current:

$$\begin{bmatrix} i_{ref\,\alpha} \\ i_{ref\,\beta} \end{bmatrix} = \frac{1}{\Delta}\begin{bmatrix} V_\alpha & -V_\beta \\ V_\beta & V_\alpha \end{bmatrix}\begin{bmatrix} \tilde{p} \\ \tilde{q} \end{bmatrix} \quad \text{(II-24)}$$

The inverse transformation can be used to write:

$$\begin{bmatrix} i_{ref\,a} \\ i_{ref\,b} \\ i_{ref\,c} \end{bmatrix} = \sqrt{\frac{2}{3}}\begin{bmatrix} 1 & 0 \\ -\frac{1}{2} & \frac{\sqrt{3}}{2} \\ -\frac{1}{2} & -\frac{\sqrt{3}}{2} \end{bmatrix}\begin{bmatrix} i_{ref\,\alpha} \\ i_{ref\,\beta} \end{bmatrix} \quad \text{(II-25)}$$

Figure II.18 illustrates the process of identifying reference harmonic currents using the real and imaginary power (p-q) method. This method helps to analyze and filter the currents, and the filtered output currents will later be used as a reference for controlling currents that exhibit hysteresis behavior.

The dynamic performance of the Shunt APF controlled by the p–q theory is shown in **Figure II.19**, which presents the waveforms of grid current, load current, injected current, and the DC-link voltage.

Furthermore, **Figure II.20** quantitatively evaluates the harmonic mitigation capability of the Shunt APF using the p–q theory. The THD of the load current before compensation is observed to be 27.54%, indicating a highly distorted waveform due to the nonlinear nature of the load. After compensation, the source current THD is significantly reduced to 1.44%, which complies with the IEEE 519 standard.

Figure II.21 illustrates the waveforms of source voltage and source current before and after activating the shunt APF at t = 0.15 s. Before this instant, the source current (blue) is distorted and exhibits a clear phase shift relative to the source voltage (red). This misalignment indicates the presence of harmonics and reactive power components caused by nonlinear loads.

Once the APF is activated, the source current waveform becomes nearly sinusoidal and perfectly synchronized with the source voltage. The elimination of phase shift confirms a unity power factor, meaning that the active filter has effectively compensated for both harmonic content and reactive power. This synchronization proves the APF's ability to restore PQ and ensure simultaneous voltage-current alignment, a crucial requirement for enhancing system efficiency and reducing losses in power distribution networks.

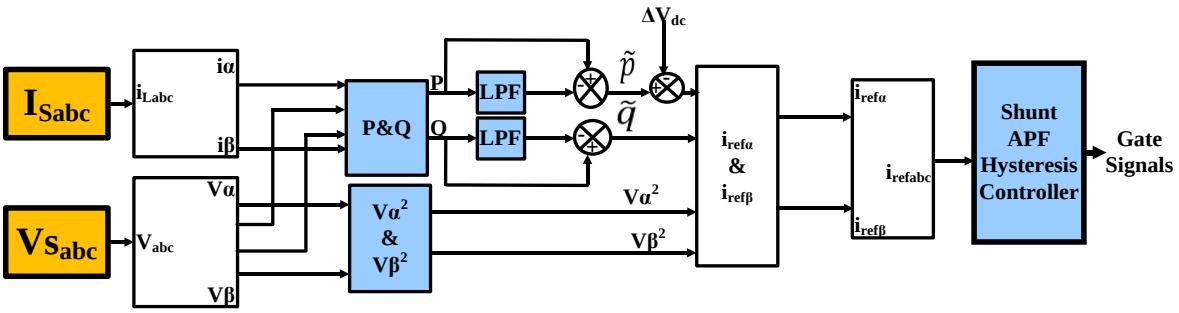

Figure II.18 p-q theory algorithm

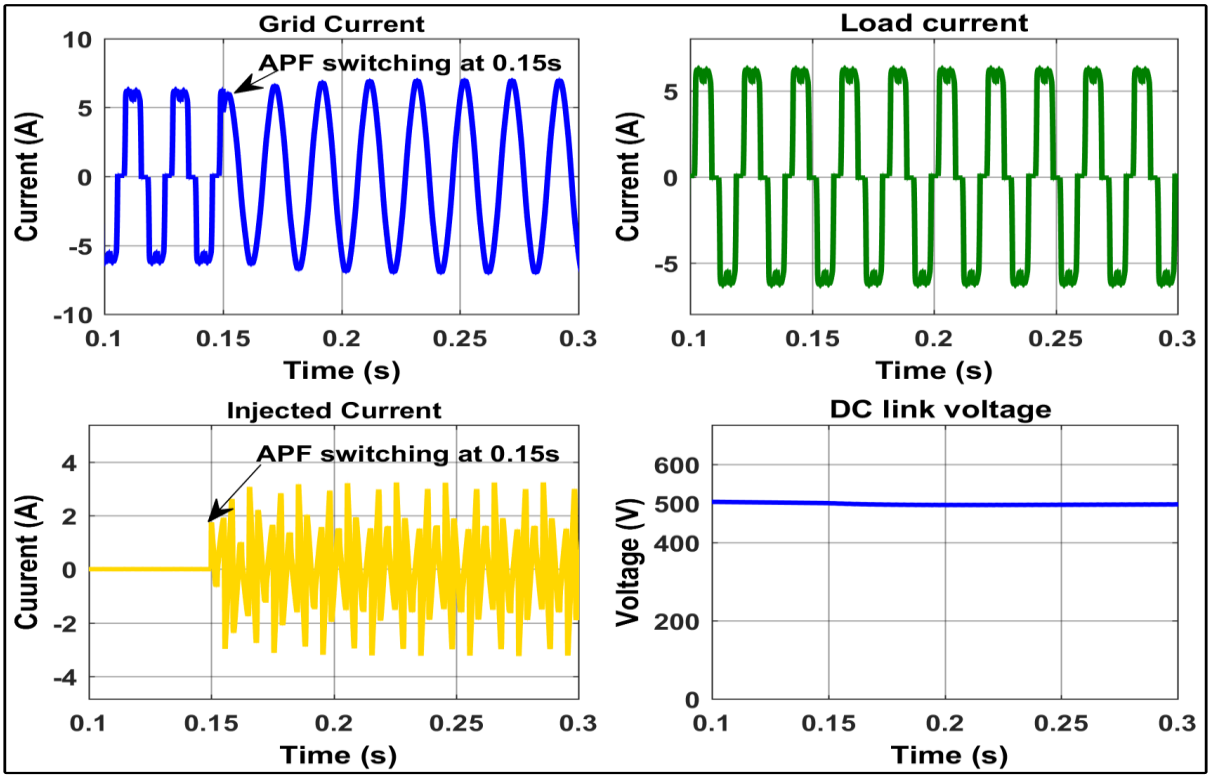

Figure II.19 Performance analysis of shunt active power filter: Grid current, Load current, Injected current, and DC link voltage response using p-q theory

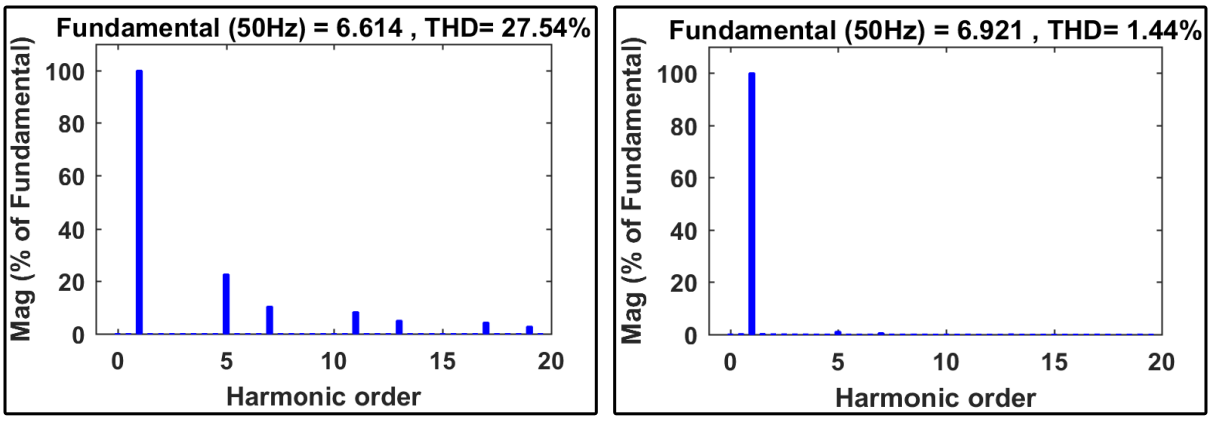

(a) **(b)**

Figure II.20 THD (a) load current, (b) source current

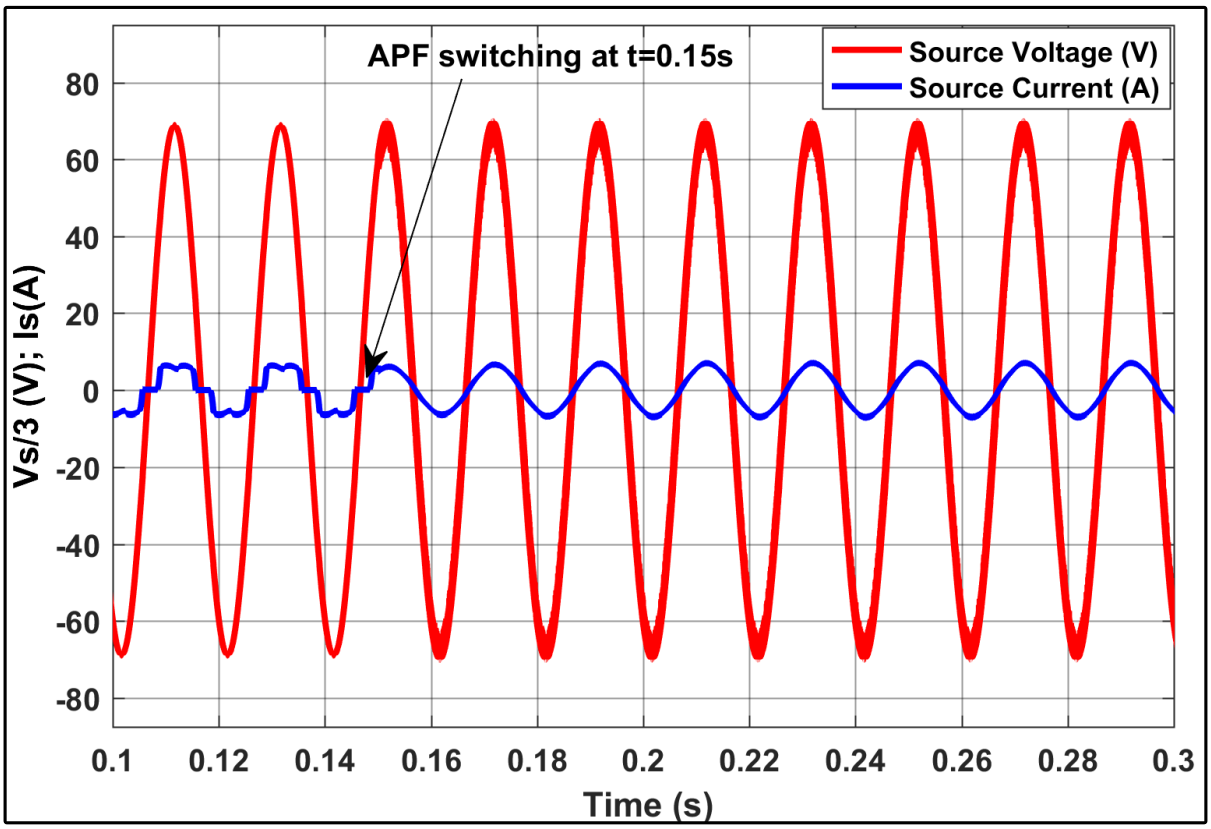

Figure II.21: Source voltage and source current

B. synchronous reference frame (SRF)

The SRF theory is a method used in electrical engineering to analyze and control currents in systems, particularly when dealing with power supplies. One of its main advantages is that it remains unaffected by distortions or imbalances in the source voltage, allowing for more accurate reference currents to be derived directly from the load currents. This insensitivity helps improve the performance and reliability of the compensation process in power systems.

In order to analyze sinusoidal signals that are synchronized with the power network's simple voltages, the signals must be transformed from the (α, β) plane to the (d, q) reference plane. These synchronized signals are generated using a phase-locked loop (PLL), a signal processing method that is frequently employed to preserve a steady phase connection.

The neutral current is the sum of the three currents (ia, ib, ic), so the homopolar current is therefore equal to:

$$i_0 = I_{ca} + I_{cb} + I_{cc} = \frac{1}{\sqrt{3}}(i_{ca} + i_{cb} + i_{cc}) = \frac{1}{\sqrt{3}} i_n \quad \text{(II-26)}$$

The expression of the current id and iq in the reference frame (d, q) is given by:

$$\begin{bmatrix} i_d \\ i_q \end{bmatrix} = \begin{bmatrix} \sin(\theta) & -\cos(\theta) \\ \cos(\theta) & \sin(\theta) \end{bmatrix} \begin{bmatrix} i_\alpha \\ i_\beta \end{bmatrix}$$

(II-28)

Where (θ) represents the angular position of the fundamental voltage of the source estimated by the PLL technique. These components can then be expressed as the sum of a DC component and a harmonic component:

$$\begin{bmatrix} i_d \\ i_q \end{bmatrix} = \begin{bmatrix} \bar{i}_d + & \tilde{i}_d \\ \bar{i}_q + & \tilde{i}_q \end{bmatrix}$$

(II-29)

Where i_d and i_q represent the DC components, and $\tilde{i}_d$ and $\tilde{i}_q$ represent the alternating components.

At this point, we can express the current components along the (α, β) axes as follows:

$$\begin{bmatrix} i_\alpha \\ i_\beta \end{bmatrix} = \begin{bmatrix} \sin(\theta) & -\cos(\theta) \\ \cos(\theta) & \sin(\theta) \end{bmatrix}^{-1} \begin{bmatrix} i_d \\ i_q \end{bmatrix} = \begin{bmatrix} \sin(\theta) & \cos(\theta) \\ -\cos(\theta) & \sin(\theta) \end{bmatrix} \begin{bmatrix} i_d \\ i_q \end{bmatrix}$$

(II-30)

By separating the DC components from the harmonic components, we obtain:

$$\begin{bmatrix} i_\alpha \\ i_\beta \end{bmatrix} = \begin{bmatrix} \sin(\theta) & \cos(\theta) \\ -\cos(\theta) & \sin(\theta) \end{bmatrix} \begin{bmatrix} \bar{i}_d \\ \bar{i}_q \end{bmatrix} + \begin{bmatrix} \sin(\theta) & \cos(\theta) \\ -\cos(\theta) & \sin(\theta) \end{bmatrix} \begin{bmatrix} \tilde{i}_d \\ \tilde{i}_q \end{bmatrix}$$

(II-31)

The expressions for the reference currents are given by:

$$\begin{bmatrix} i_{\alpha_{réf}} \\ i_{\beta_{réf}} \end{bmatrix} = \begin{bmatrix} \sin(\theta) & -\cos(\theta) \\ \cos(\theta) & \sin(\theta) \end{bmatrix}^{-1} \begin{bmatrix} \tilde{i}_d + i_{dc} \\ \tilde{i}_q \end{bmatrix} \text{(II-32)}$$

The reference currents in the three-phase (abc) coordinate system can be expressed as follows:

$$\begin{bmatrix} i_{a_{réf}} \\ i_{b_{réf}} \\ i_{c_{réf}} \end{bmatrix} = \sqrt{\frac{2}{3}} \begin{bmatrix} 1 & 0 \\ -\frac{1}{2} & \frac{\sqrt{3}}{2} \\ -\frac{1}{2} & -\frac{\sqrt{3}}{2} \end{bmatrix} \begin{bmatrix} i_{\alpha_{réf}} \\ i_{\beta_{réf}} \end{bmatrix} \quad \text{(II-33)}$$

Figure II.22 presents the implementation architecture of the SRF algorithm used to generate reference currents for the Shunt APF. This control method transforms the three-phase current signals from the stationary abc frame into the rotating dq0 frame, enabling accurate separation of fundamental and harmonic components. Once the reference current is generated, a hysteresis current controller ensures precise tracking by the inverter.

Figure II.23 displays the performance of the Shunt APF under SRF control, showing the grid current, load current, injected current, and DC link voltage. Prior to t = 0.15 s, the grid current is heavily distorted due to nonlinear loads. Upon activation of the APF at 0.15 s, the injected current effectively cancels the harmonic content, restoring the grid current to a sinusoidal shape and maintaining a stable DC bus voltage—demonstrating the control scheme's effectiveness.

Figure II.24 compares source voltage and source current waveforms. Before t = 0.15 s, the current is distorted and exhibits noticeable phase displacement from the voltage waveform, indicating the presence of harmonics and reactive power. After the APF is activated, the current waveform becomes clean and well-aligned with the voltage, confirming harmonic compensation and unity power factor.

Figure II.25 illustrates the THD levels of both the load current and the source current. The load current exhibits a high THD of 27.44%, confirming the nonlinearity of the connected load. However, the source current THD is drastically reduced to 2.45% after the APF activation, demonstrating the SRF algorithm's robustness and its ability to significantly improve PQ.

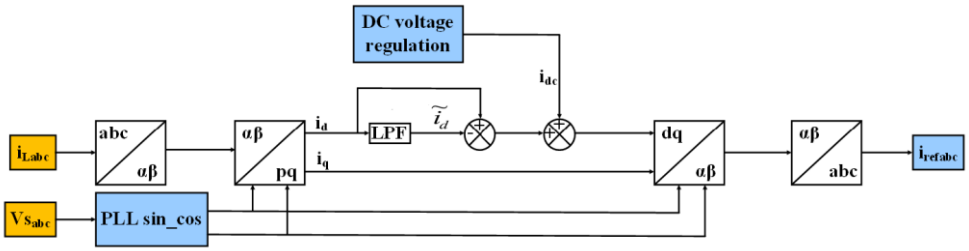

Figure II.22 Implementation of Synchronous Reference Frame (SRF) algorithm

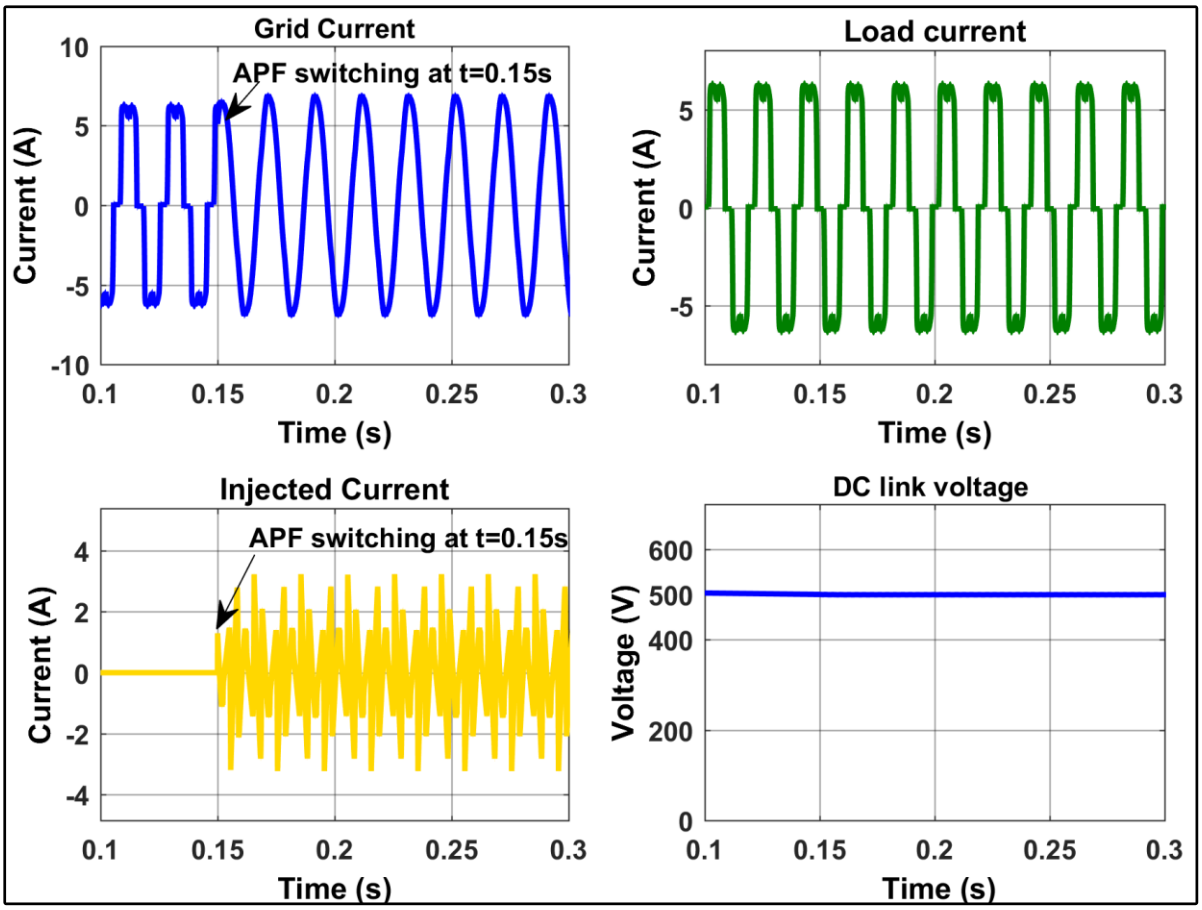

Figure II.23 Performance analysis of shunt active power filter: Grid current, Load current, Injected current, and DC link voltage response

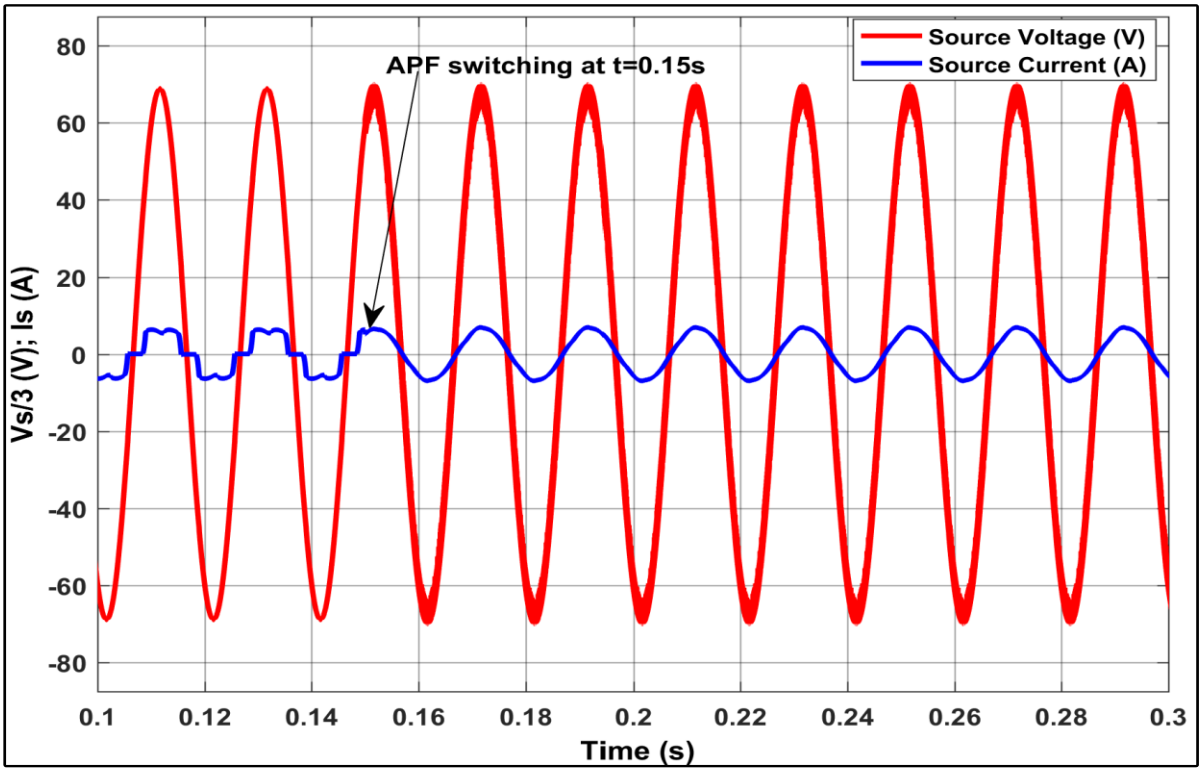

Figure II.24 Source voltage and source current

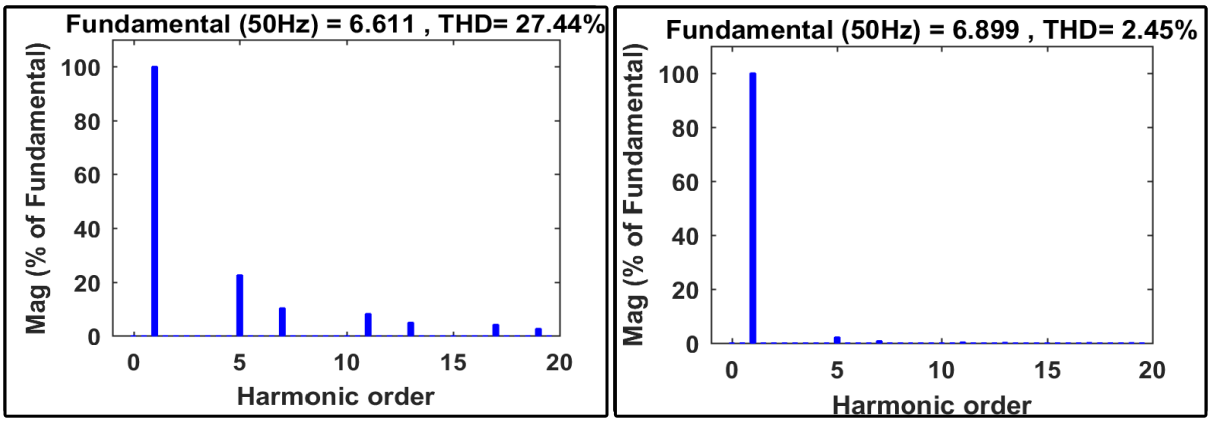

(a) **(b)**

Figure II.25 THD (a) load current, (b) source current

C. Direct Current Control (DCC)

Figure II.26 shows the management of a shunt APF through DCC theory. A reference supply current signal is generated using the DCC approach using DC link voltages, source voltages and load currents. Traditionally, a PI controller calculated the necessary current (I_{dloss}) to control the DC link voltage by comparing it to a set reference value (V_{dc}^{*}) [67].

The identification method uses a simple algorithm to provide high-quality reference currents. A current control algorithm may directly regulate the injected current (i_{inj}) for harmonic mitigation, according to the DCC system [68].

A contemporary control algorithm built on the DCC methodology is displayed in **Figure II.26**. Generally, the DCC technique is used to compare the observed injection current (i_{inj}) with its matching non-sinusoidal reference current (i_{ref}, i_{inj}). By adhering to the properties of the reference current (i_{ref}, i_{inj}), the Shunt APF can precisely recreate the injection current (i_{inj}) with the least amount of current error (e_C) [69]. It is noteworthy that the reference current (i_{ref}, i_{inj}) exhibits non-sinusoidal behavior and mirrors the properties of harmonic currents (i_H) [62–64].

As seen in **Figure II.26**, once the three sinusoidal signals are produced by the PLL technique, the peak current (I_{peak}) is determined by treating the output of the PI regulator in the DC voltage control section. The reference source currents may then be produced by multiplying this peak current, and they are shown by the following equations:

$$\begin{cases} i_{sa}^{*} = i_{sp} \sin wt \\ i_{sb}^{*} = i_{sp} \sin(wt - 120) \\ i_{sc}^{*} = i_{sp} \sin(wt + 120) \end{cases} \quad \text{(II-34)}$$

The hysteresis band current controller is utilized to compare the reference source currents with the actual source currents, enabling compensation for various current-related issues like load-current imbalances, DC-link voltage regulation, current harmonics, reactive power and zero-negative-sequence components [70,71]. This controller plays a crucial role in ensuring the effective operation of the inverter by adjusting the switching signals of the IGBTs based on the comparison between the desired and actual source currents, thereby addressing and mitigating multiple challenges associated with current quality and balance in the system [72].

The IEEE Standard 519-1992, which provides guidelines and restrictions for harmonic voltage and current levels in supply systems. This standard sets the specifications for acceptable levels of harmonics in electrical power systems to ensure the quality and reliability of the power supply. Compliance with these specifications helps in maintaining the stability and efficiency of the electrical grid and equipment connected to it.

Figure II.27 illustrates the performance of the Shunt APF using the DCC algorithm. Before activation (at t=0.15s), the grid current is distorted due to nonlinear load effects. Upon activation, the APF injects the required compensation current, resulting in a significant improvement in the waveform quality of the grid current. The DC link voltage remains stable, indicating efficient energy regulation.

Figure II.28 displays the source voltage and current waveforms. Prior to APF activation, the source current is non-sinusoidal and out of phase with the voltage. After t=0.15s, the source current becomes sinusoidal and in phase with the source voltage, demonstrating both harmonic filtering and power factor correction.

Figure II.29 shows the THD for both load and source currents. The load current THD remains high at 27.44%, highlighting the nonlinear load nature. However, after compensation, the source current THD is significantly reduced to 1.42%, confirming the robustness and effectiveness of the DCC algorithm in mitigating current harmonics.

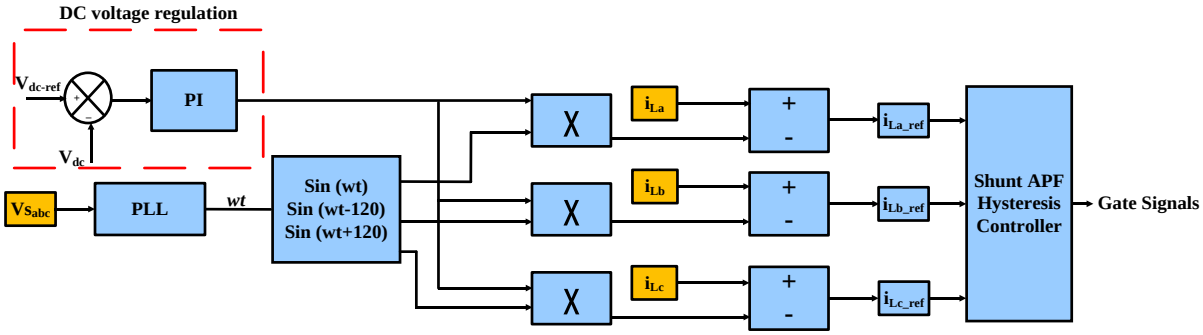

Figure II.26 DCC algorithm.

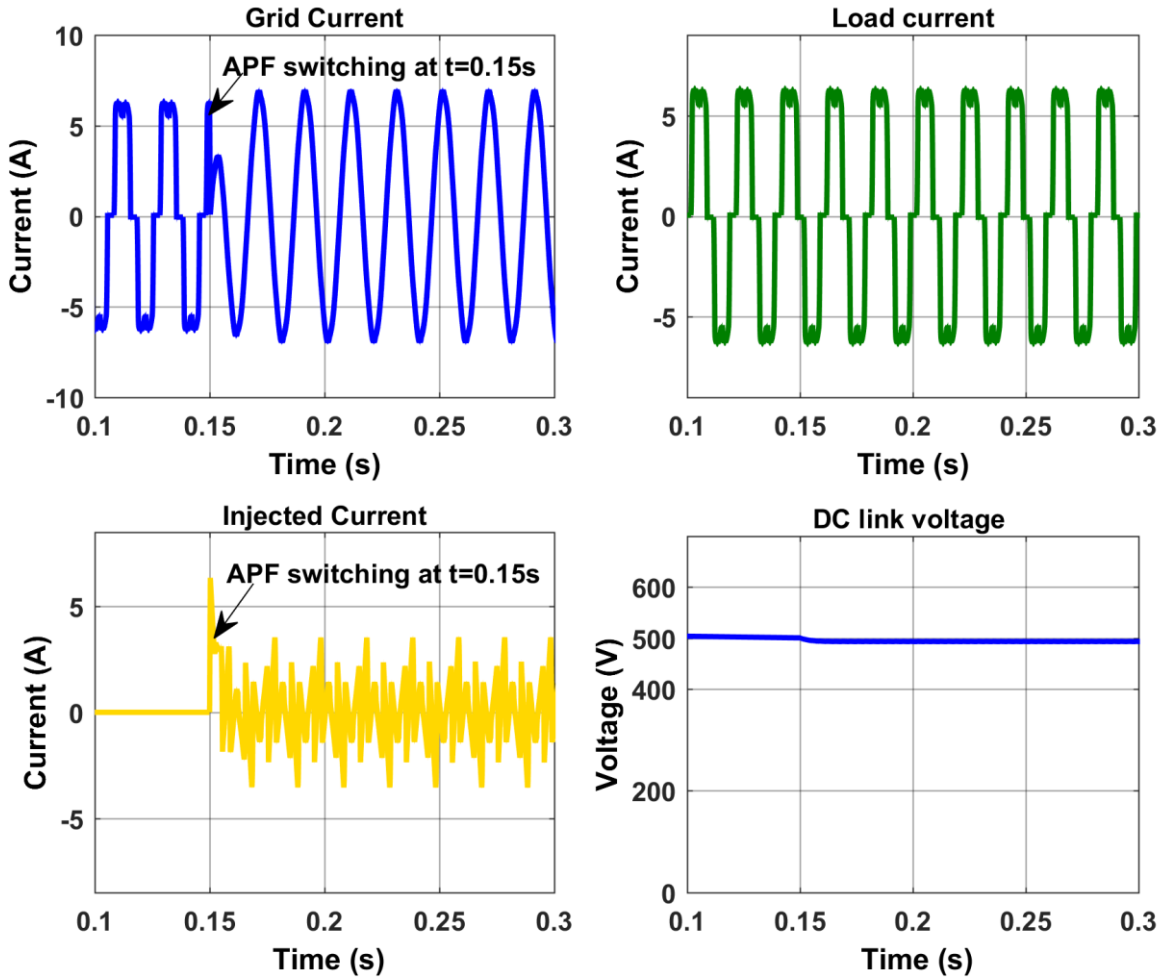

Figure II.27 Performance analysis of shunt active power filter: Grid current, Load current, Injected current, and DC link voltage response

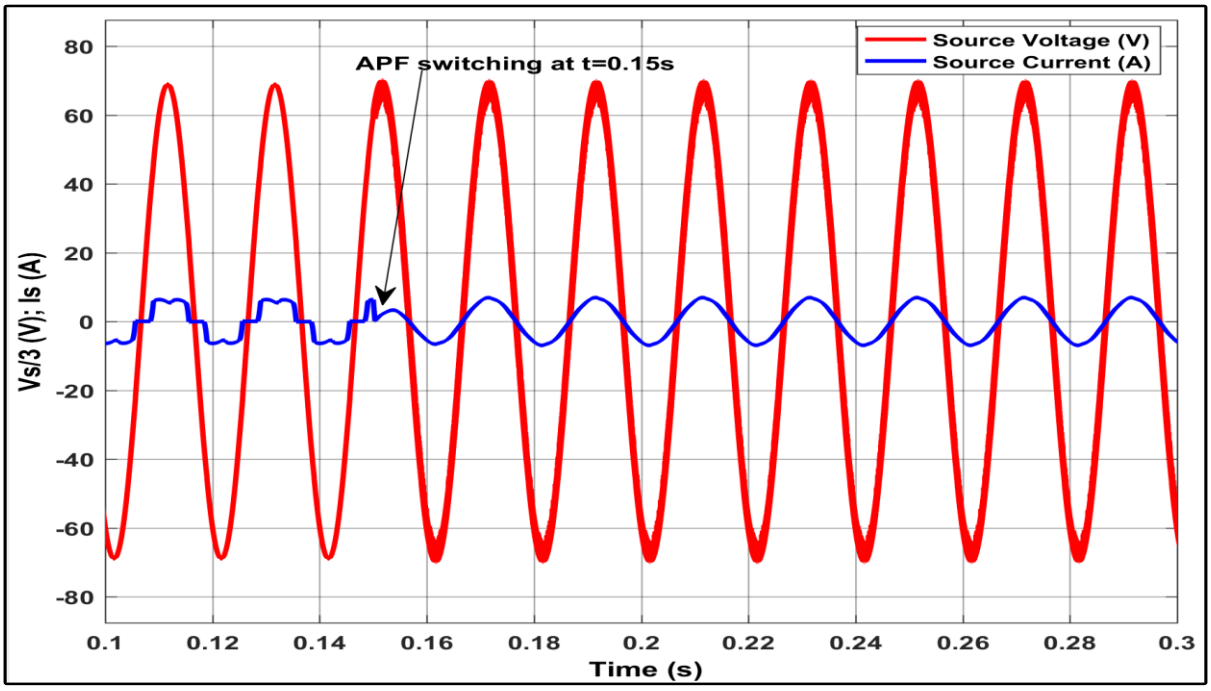

Figure II.28 Source voltage and source current

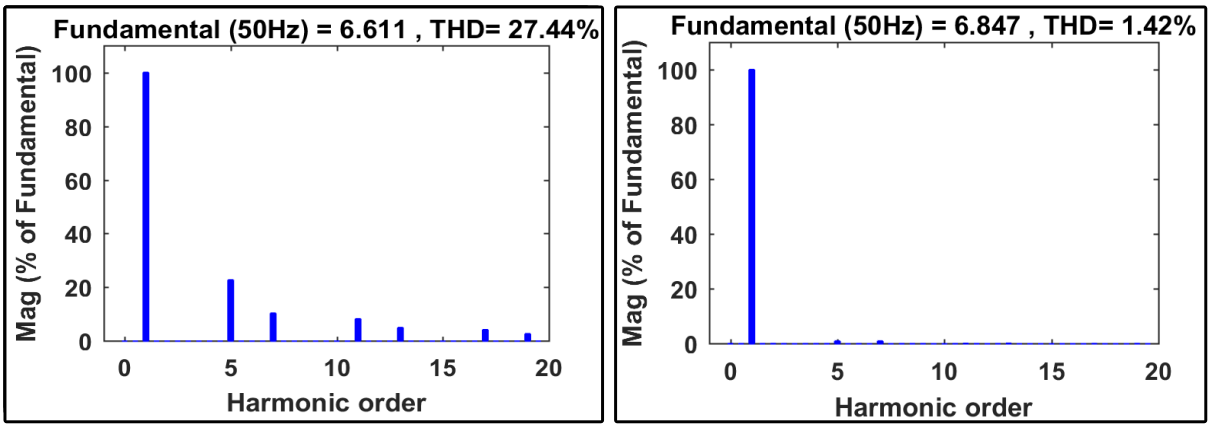

(a) **(b)**

Figure II.29 THD (a) load current, (b) source current

Three control strategies for the Shunt APF: DCC, p-q theory, and SRF were implemented and evaluated under nonlinear load conditions. The DCC method demonstrated excellent performance in minimizing THD in the source current, with a value of 1.42%, outperforming p-q (2.45%) and SRF (slightly higher in some instances). However, DCC's performance relies heavily on the quality of the source voltage signal, making it less robust under distorted or unbalanced source conditions. The p-q method, while simple and effective for harmonic current detection, also suffers from its sensitivity to voltage quality, and is thus not optimal when source voltage is deformed. Conversely, the SRF method provided a balanced compromise between accuracy and robustness. It achieved a lower THD than p-q and maintained stable operation even with distorted or unbalanced source voltages. This independence from the voltage waveform makes SRF particularly advantageous in real-world conditions, where voltage distortions are common.

Strategies for controlling a parallel active filter, which is used to improve the quality of electrical currents by reducing THD. The control system compares the actual output currents from the filter to reference currents calculated using different methods, ensuring that the output matches the desired performance. Two main control methods are highlighted: hysteresis control, which is simple and effective but can lead to variable high-frequency switching, and Pulse Width Modulation (PWM), which is another approach used for managing the inverter's output.

Using a technique known as hysteresis control, or on-off control, we produce six switching pulses for the inverter in this study. The difference (or error) between the reference current and the actual current generated by the inverter is compared using this nonlinear control approach. This approach is easy to build, but because of changing switching frequencies, it may be difficult to manage high-frequency signals. When this error exceeds specific limitations, known as the hysteresis band, a command is delivered to the switches to keep the current within those limits.

Figure II.30 illustrates how hysteresis-based control works in active filtering systems. In this technique, the main control parameter is the width of the hysteresis band (HB), which determines how much the output current can fluctuate around a reference signal. While this method effectively keeps the compensation current within a specific range, a drawback is that

it causes variations in the switching frequency of the inverter's switches within the hysteresis band.

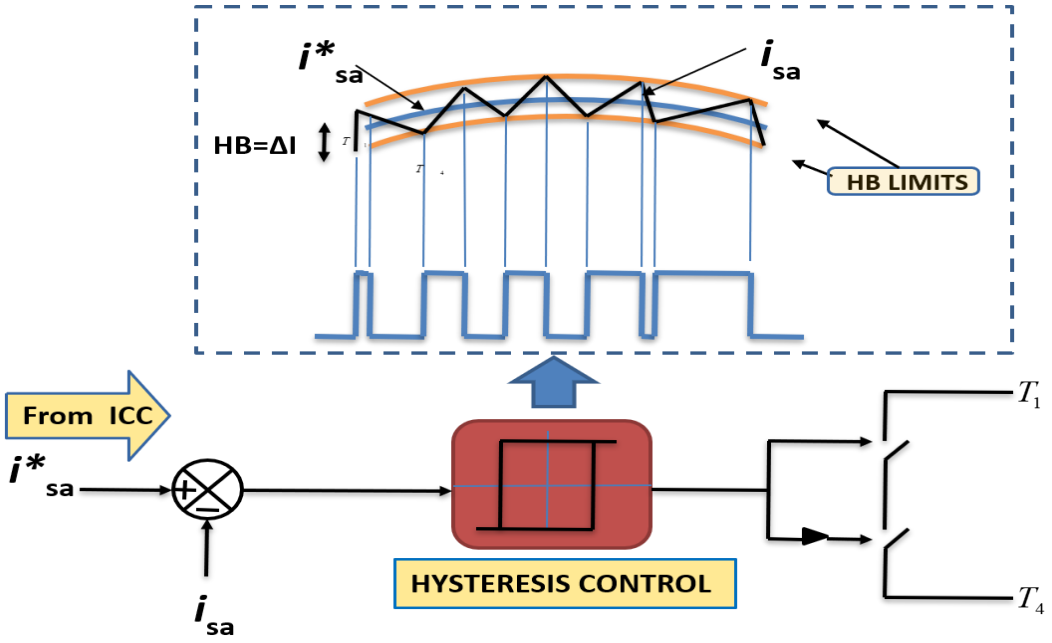

Figure II.30 Principle of hysteresis-based current control [73]

II.4 Conclusion

This chapter presented the modeling, simulation, and comparative evaluation of Series and Shunt APF under different control strategies. For the Series APF, three voltage regulation approaches were implemented: Load Voltage Control, Source Voltage Control, and the UVTG method. Results demonstrated that UVTG offers superior performance in terms of dynamic response, stability, and THD minimization under disturbances such as voltage sags, swells, unbalance, and short circuits.

For the Shunt APF, three harmonic current compensation strategies— p-q theory, DCC, and SRF—were tested. Although DCC achieved the lowest THD, its dependence on source voltage quality limits its reliability under practical conditions. The SRF strategy stood out for its robustness and independence from source-side distortions, making it a suitable choice for dynamic and distorted environments.

In the next chapter, we will proceed with the modeling of the hybrid energy system, which constitutes the source side of the grid. This system integrates PV, wind energy, and battery storage, and reflects real-world scenarios where source-side disturbances emerge due to the variability and intermittency of renewable resources. The aim is to establish a realistic operating environment in which to design and evaluate a Unified Power Quality Conditioner (UPQC) that will ultimately address both source-side and load-side PQ issues.

Chapter III:
Modeling and Integration of Hybrid Renewable Energy Systems into the Grid

III.1 Introduction

The increasing global demand for sustainable energy solutions has led to the widespread adoption of hybrid renewable energy systems (HRES), combining multiple renewable sources such as PV and wind energy, often supported by battery energy storage systems (BESS). These systems offer a promising alternative to conventional fossil-fuel-based generation by ensuring more reliable, resilient, and environmentally friendly electricity production. However, the variable and intermittent nature of renewable sources poses significant challenges in terms of power flow control, grid stability, and PQ.

This chapter focuses on the modeling, control, and integration of a PV-Wind-Battery-based hybrid system into the grid. It begins with a detailed description of the PV system, including the modeling of its electrical characteristics, power electronics interface (DC/DC boost converter), and various MPPT algorithms. A comparative analysis is carried out among techniques such as Incremental Conductance (INC), Perturb and Observe (P&O), Enhanced (E-P&O), and Artificial Neural Networks (ANN), highlighting their effectiveness under dynamic irradiance conditions.

The chapter then proceeds to the wind energy subsystem, presenting the principles of wind energy conversion, turbine modeling, generator dynamics (based on a Permanent Magnet Synchronous Generator - PMSG), and rectification. Multiple MPPT techniques—P&O, Enhanced P&O, ANN, and fuzzy logic—are implemented and tested to ensure optimal extraction of wind energy under fluctuating wind speed profiles.

A BESS is introduced to enhance the system's operational flexibility and to manage the energy flow during surplus or deficit conditions. This storage system plays a key role in compensating for the inherent variability of renewable resources.

The final section integrates the PV, wind, and battery systems into a unified HRES architecture connected to the grid. The performance of this system is analyzed under both linear and nonlinear load conditions, exposing the PQ issues that arise from intermittent RES generation and non-linear loads. The simulation results confirm that voltage distortion, harmonics, and source-load side imbalances are prevalent in such configurations.

III.2 Topology of photovoltaic energy conversion systems

PV energy conversion systems may be classified into two groups based on their topology: grid-connected systems and Standalone systems [1,2].

III.2.1 Standalone system

In order to satisfy the energy needs of customers who are not connected to the electrical grid, autonomous PV systems were created. These systems provide a dependable power source even when solar energy is intermittent since the user may use the energy produced by the solar panels right away or store it in batteries for later use. As seen in the cited **Figure III.1**, the configuration of such systems usually consists of parts like solar panels, charge controllers, batteries, and inverters that work together to enable effective energy conversion and storage [74,76].

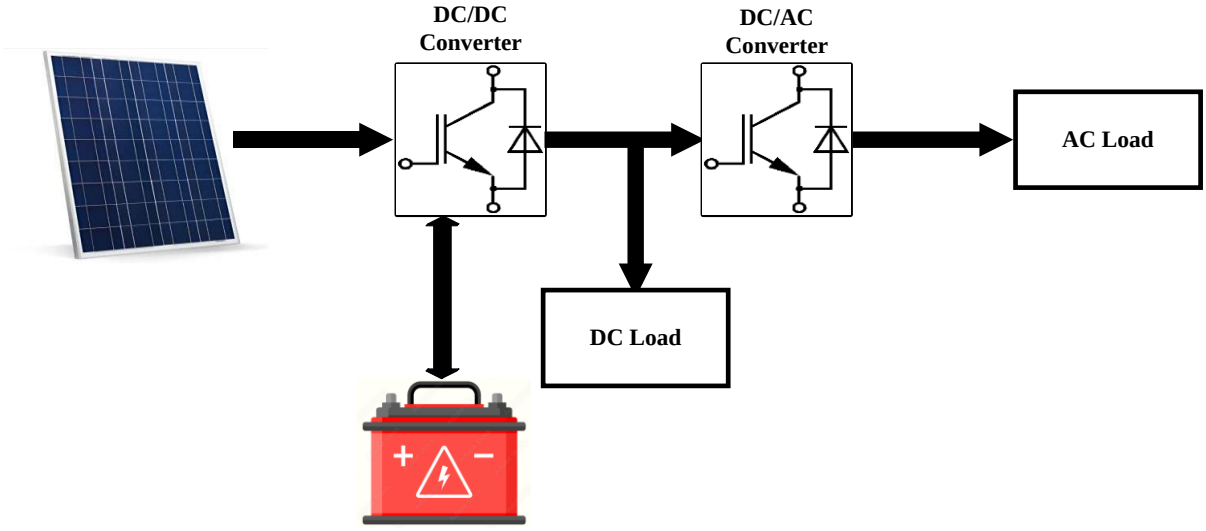

Figure III.1 Structure of a standalone photovoltaic system

III.2.2 Grid-connected system

Grid-connected PV systems, which are designed to inject energy produced by solar panels into the electrical distribution network in AC mode. These systems operate under two primary modes: first, by injecting the total energy produced during designated injection periods that align with production times; second, by allowing for the injection of surplus energy, particularly in residential installations where the energy generated is first consumed on-site, with any excess fed back into the grid, as illustrated in **Figure III.2**.

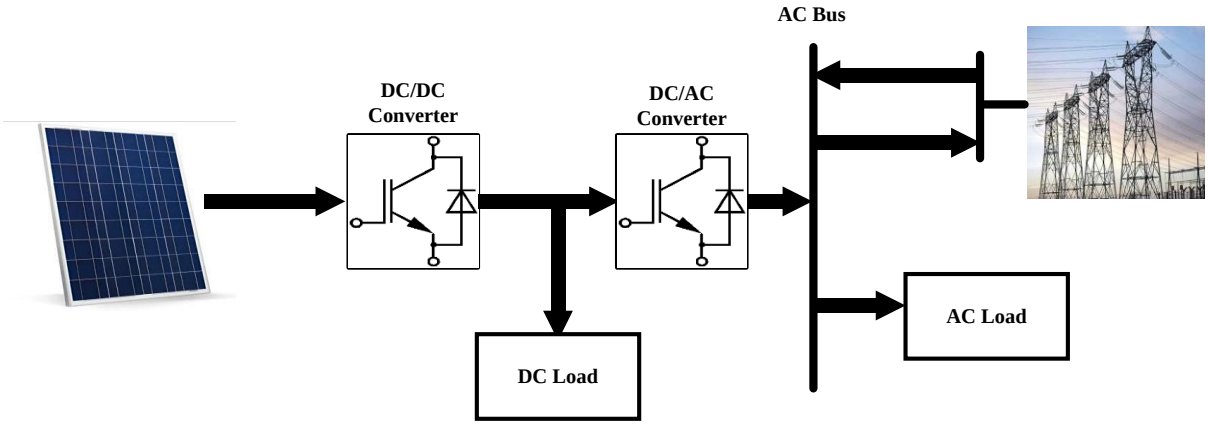

Figure III.2 Structure of a grid-connected photovoltaic system

III.3 Description of the system under study

The PV conversion system under study is a grid-connected system, as illustrated in **Figure III.3**.

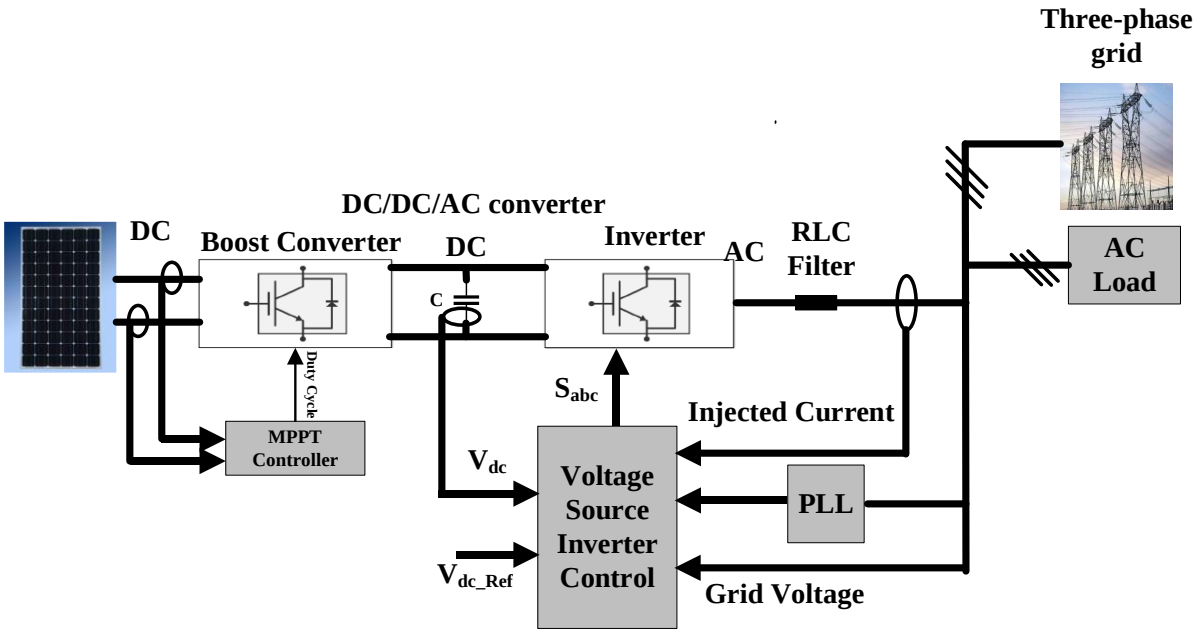

Figure III.3 Architecture of a grid-connected photovoltaic system

In order to guarantee effective energy extraction from solar panels, the system presented comprises of a PV generator coupled to a power conditioning stage that incorporates a DC/DC Boost converter that enhances the MPPT. A regulated three-phase inverter connects this setup to a low-voltage distribution network, allowing produced energy to be sent to a low-consumption building and satisfying its electrical energy requirements. Any extra energy generated over what the building needs is returned to the grid.

III.4 Basics of The PV energy

III.4.1 Overview of the PV system

Solar panels and other components, such as electrical connections and regulation systems, are used in PV systems to transform sunlight into electrical energy. A PV cell's core is composed of semiconductor materials, such as silicon, which are intended to function well in parallel or series configurations. When sunlight hits a solar cell, the semiconductor's electrons separate from their atoms, producing an electric current that may be used to generate electricity [77].

III.4.2 PV system modelling

The process of PV system modelling, the solar cell is modelled as an ideal current source coupled in parallel with a diode, which helps to simulate how the cell would act in real-world scenarios with temperature (T) and sunlight (G), as illustrated in **Figure III.4**.

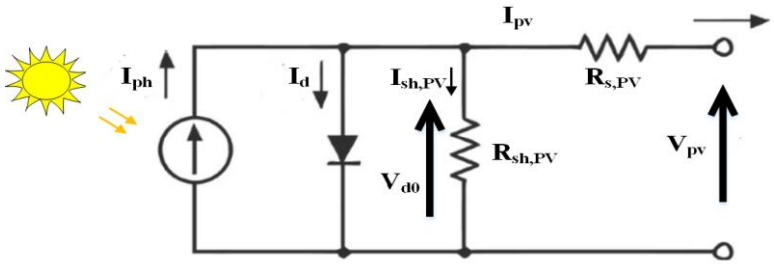

Figure III.4 Schematic representation of a PV Cell's equivalent circuit

One diode may be used to imitate a solar cell as an electrical circuit, where I_{d0} is the average current flowing through the diode and I_{Ph} is the photocurrent produced by the solar module. Certain equations that take into consideration variables like temperature (T), electron charge (q), Boltzmann's constant (K), and diode factor (n) can be used to characterize the solar cell's output current (I_{PV}) and output voltage (V_{PV}), as expressed in the following relations:

$$I_{PV} = I_{Ph} - I_{d0}\left[esp\left(\frac{q}{nKT}\,V_{do}\right) - 1\right] - \left(V_{do}\,\frac{V_{PV}+R_S I_{PV}}{R_{Sh}}\right) \quad \text{(III-1)}$$

$$V_{PV} = V_{d0} - R_s I_{pv} \quad \text{(III-2)}$$

Depending on how much energy the system requires, PV cells can be linked in parallel or series. While connecting cells in parallel raises the current at the same voltage, connecting them in series raises the voltage while maintaining the same current. A photovoltaic generator (GPV) is produced by this configuration, and a solar panel is made up of numerous modules, each of which consists of multiple cells. These cells' efficiencies range from 13–18% for monocrystalline silicon cells to 11–15% for polycrystalline silicon cells and 5-8% for amorphous thin-film cells, , depending on the technology and manufacturing process [78].

III.4.3 Characteristics of the photovoltaic generator

The current-voltage ($I-V$) and power-voltage ($P-V$) curves of a PV panel, which are shown in **Figure III.5**. These curves illustrate key points such as the maximum power output, open-circuit voltage, and short-circuit current, and how they change with varying atmospheric conditions like light intensity and temperature.

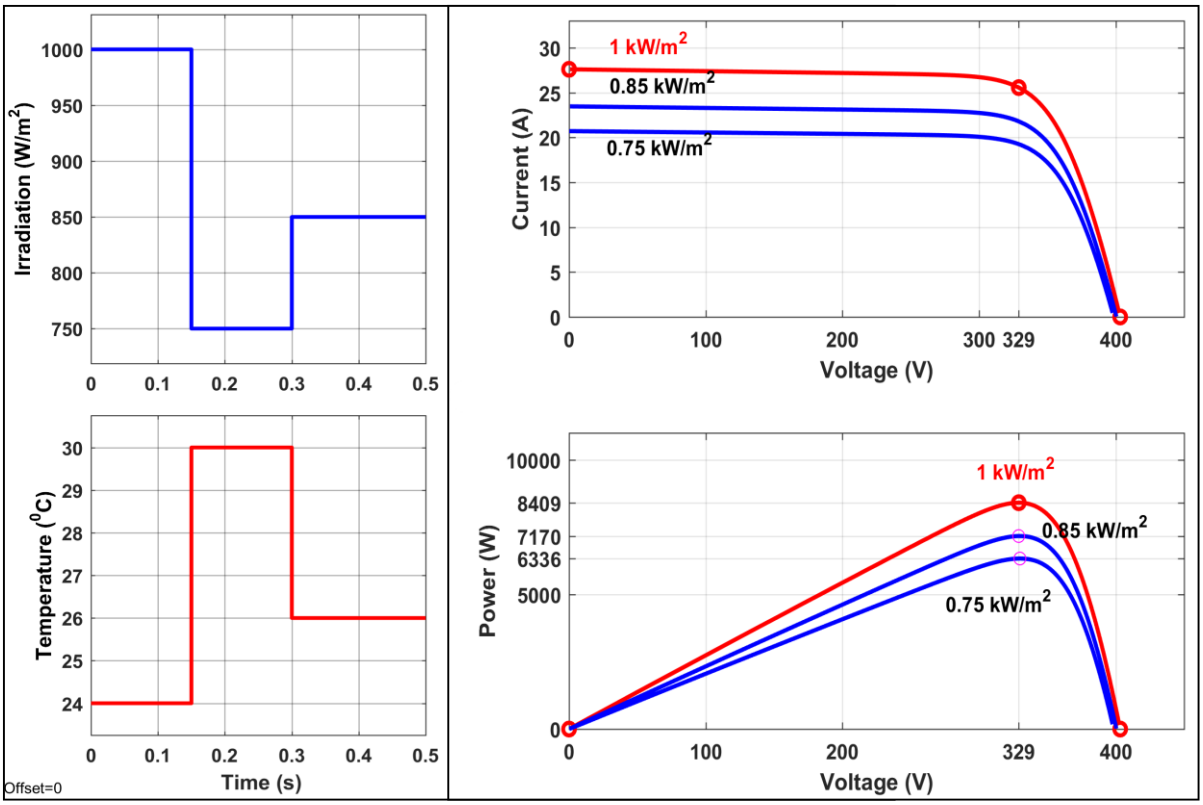

Figure III.5 Photovoltaic characteristics: Iradiation and temperature effects on current-voltage and power-voltage curves

As the illumination increases, the current produced by the panel also increases, leading to more available power. Conversely, when the temperature of the panel rises, the power output decreases significantly, indicating that higher temperatures can negatively impact the efficiency of the PV system.

III.4.4 Modeling of the DC/DC converter (boost converter)

The modeling of a DC/DC converter known as a Boost converter, which is used in PV (solar) energy systems. This converter is placed between the solar panel (PV generator) and the load as illustrated in **Figure III.6**, the device using the energy) to increase the voltage from the solar panel to match the voltage required by the load. Additionally, it helps implement algorithms that ensure the system operates at its maximum power point, optimizing energy efficiency.

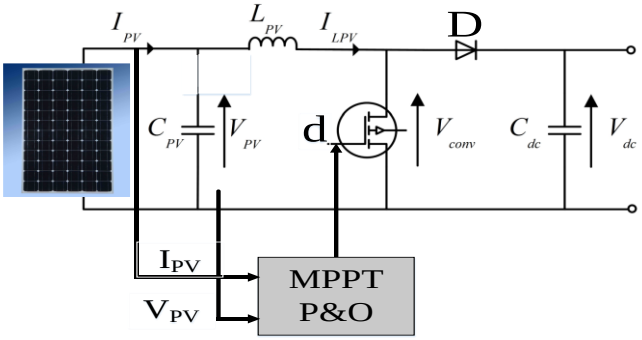

Figure III.6 Circuit of the DC/DC boost converter

The mathematical model mentioned is created by using Kirchhoff's laws, In this context, the model takes into account the operating conditions of the circuit and the state of a switch labeled 'T' [75]. In this context, the model reflects the real operating conditions of the circuit, including the influence of the duty cycle α, which determines the switching activity. The system dynamics are governed by the following differential equations:

$$L_{PV}\frac{dI_{PV}}{dt} = V_{PV} - (1-\alpha)V_{dc} \quad \text{(III-3)}$$

$$C_{PV}\frac{dV_{dc}}{dt} = (1-\alpha)I_{PV} - \frac{V_{dc}}{R} \quad \text{(III-4)}$$

Here, L_{PV} and C_{PV} represent the inductance and capacitance of the system respectively, while R is the equivalent resistive load.

The dynamic equations of the inductor current and the capacitor voltage are rewritten in the state-space form, by defining $x_1 = I_{PV}$ and $x_2 = V_S$ resulting in the standard state-space representation $X = A\dot{X} + BU$ as follows:

$$\begin{bmatrix}\dot{x_1}\\ \dot{x_2}\end{bmatrix} = \begin{bmatrix}0 & \frac{-(1-\alpha)}{L_{PV}}\\ \frac{(1-\alpha)}{C_{PV}} & \frac{-1}{RC_{PV}}\end{bmatrix}.\begin{bmatrix}x_1\\ x_2\end{bmatrix} + \begin{bmatrix}\frac{1}{L_{PV}}\\ 0\end{bmatrix}V_{PV} \quad \text{(III-5)}$$

In this representation, the state variables are the current through the inductor and the output voltage across the capacitor C_{PV}.

III.4.5 Maximum power point tracking (MPPT) techniques for PV systems

The MPPT technique is essential for optimizing the energy output of PV cells, which can vary due to changes in sunlight intensity and temperature. MPPT continuously adjusts the operation of a power converter to ensure that the PV cells are producing their maximum possible power at any given moment. This is achieved using various control algorithms, such as "perturb and observe" and incremental conductance, as well as more advanced methods like fuzzy logic and artificial neural networks [62].

PV have non-linear characteristics, meaning their performance can change significantly based on external conditions like temperature and light levels, which can lead to energy losses and lower efficiency. To improve this efficiency, a DC-DC converter with a MPPT controller is often used, as it helps find the best operating point for maximizing power output. The complexity of the MPPT algorithm can vary depending on the desired performance and implementation, but all MPPT techniques must adjust the duty cycle of the associated converter to optimize energy capture.

A. Incremental conductance

The INC algorithm is a widely used method for MPPT in PV systems. This algorithm takes advantage of the fact that at the maximum power point, the slope of the power-voltage (PV) curve is zero, meaning that the change in power (ΔP) divided by the change in voltage (ΔV) equals zero. The system calculates the voltage changes by comparing the current and previous

voltage and current values ($V(k)$ and $V(k-1)$, $I(k)$ and $I(k-1)$ to determine how to adjust the operation for optimal power output, as illustrated in the accompanying flowchart (**Figure III.7**).

The effectiveness of the INC algorithm is demonstrated through the simulation results, which depict the dynamic behavior of current, voltage, and power under changing irradiance conditions (**Figure III.8**).

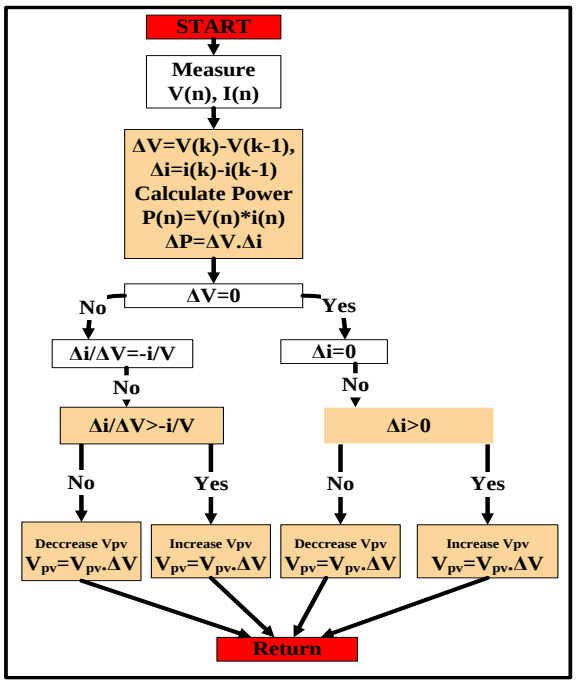

Figure III.7 Flowchart of the incremental conductance (INC) MPPT algorithm for photovoltaic systems

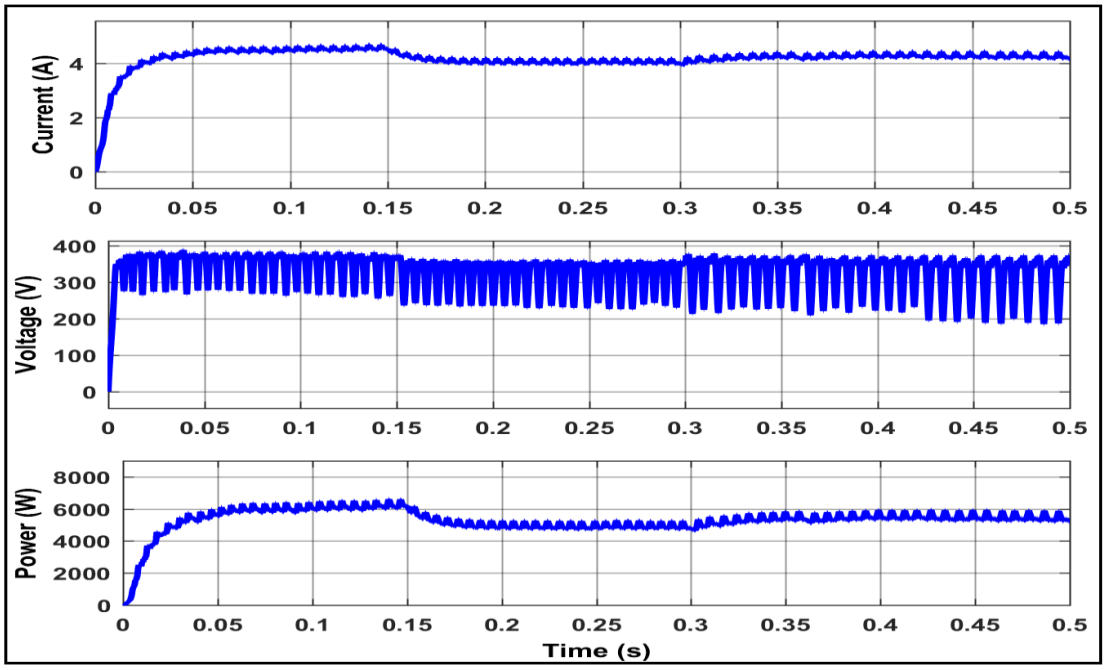

Figure III.8. Simulation of current, voltage, and power curves for PV system using Incremental Conductance (INC) MPPT

B. Perturb and Observe

The P&O algorithm is a widely used method for maximizing the power output from PV panels. It works by slightly changing the operating conditions, such as the reference voltage or duty cycle, and then observing how these changes affect the power output. If the power increases after a change, the algorithm shown in **Figure. III.9**, continues in that direction; if it decreases, it reverses the change, allowing the system to find the optimal operating point for maximum power generation. The performance of the P&O algorithm, including the dynamic response of current, voltage, and power under varying irradiance conditions, is demonstrated in **Figure III.10**.

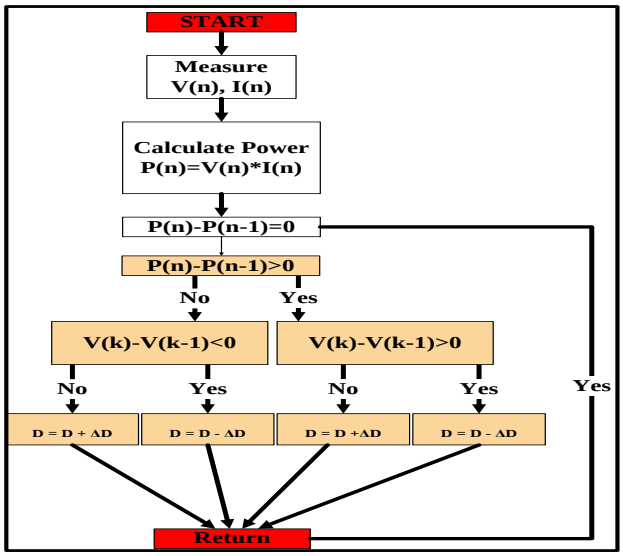

Figure III.9 Flowchart of the Perturb and Observe (P&O) MPPT algorithm for photovoltaic systems

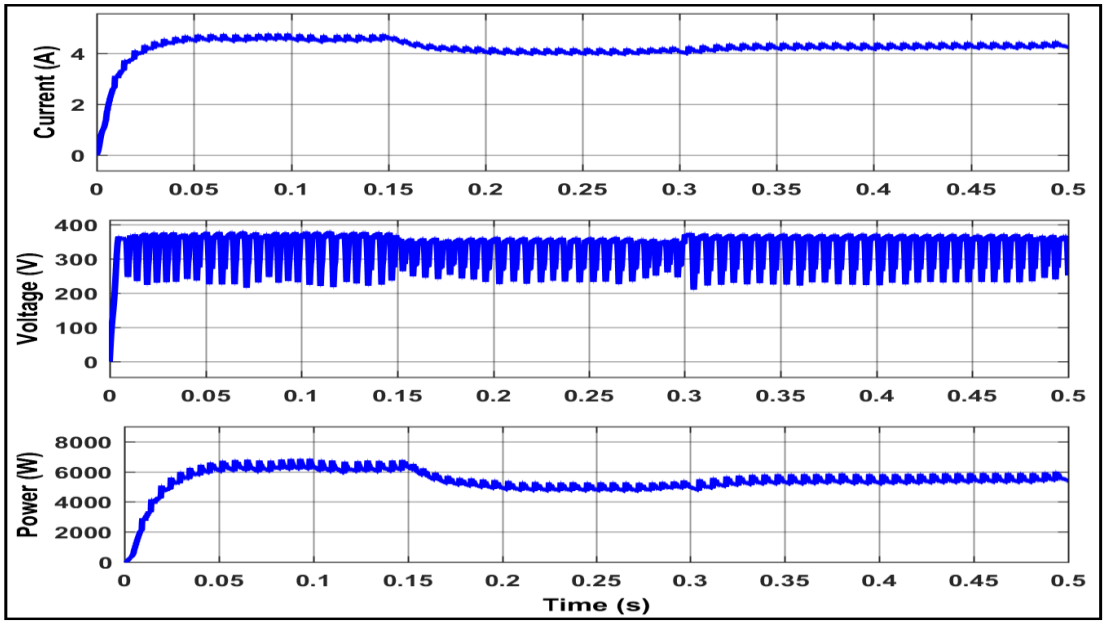

Figure III.10 Simulation of current, voltage, and power curves for PV system using P&O MPPT

C. III.3.3 Enhanced Perturb and Observe (E-P&O)

To achieve an optimal balance between fast dynamic response and minimal steady-state oscillations, the proposed (E-P&O) algorithm introduces an adaptive perturbation step size. This step size is automatically adjusted based on the absolute value of the variation in PV power (dP_{PV}), voltage (dV_{PV}), and current (dI_{PV}) as shown in Equation (III-6). These parameters are weighted by a manually tunable scaling factor N, which must be less than 1. This factor is crucial for achieving a desirable trade-off between rapid convergence and reduced steady-state fluctuations:

$$step = N.|dP_{PV} + dV_{PV}.dI_{PV}| \quad \text{(III-6)}$$

The dynamically adjusted step size allows the EP&O algorithm to modify the duty cycle of the DC-DC converter more effectively. When the operating point is far from the MPPT, a larger perturbation step is used to accelerate convergence. Conversely, when the system approaches the MPP, a smaller step is applied to minimize power oscillations and ensure stable operation.

The adjustment of the duty cycle $D(K)$ at time step K is expressed as:

$$D(K) = D(K-1) \pm step \quad \text{(III-7)}$$

This dynamic approach enhances the traditional P&O algorithm by improving both convergence speed and accuracy under varying irradiance and temperature conditions. The operational flow of the enhanced algorithm is illustrated in **Figure III.11**, while its performance is illustrated through simulation results in **Figure III.12**.

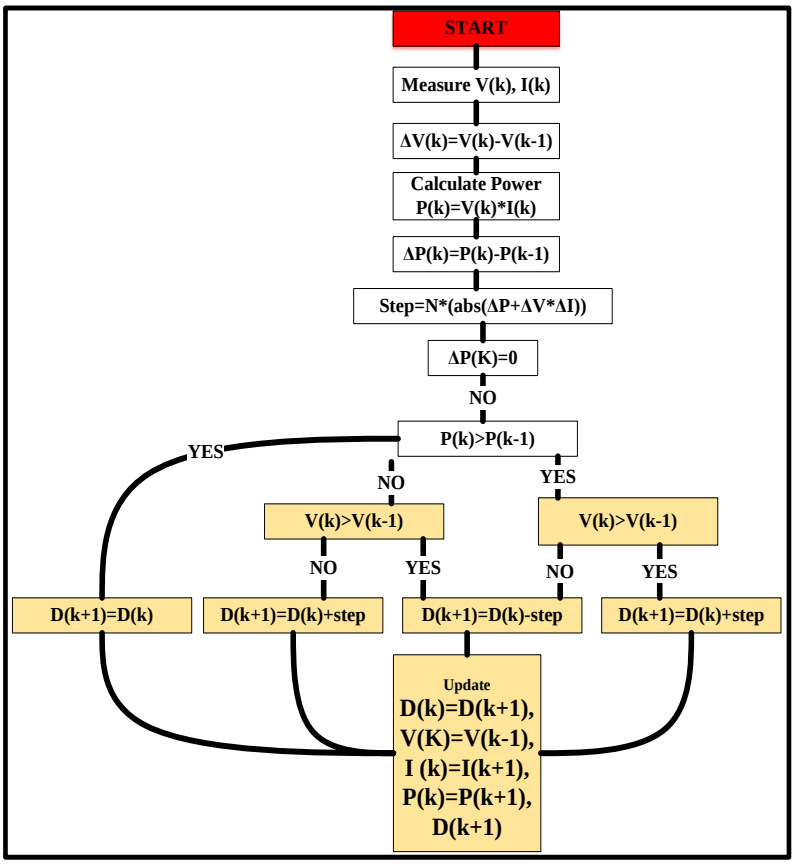

Figure III.11 E-P&O algorithm flowchart for PV MPPT

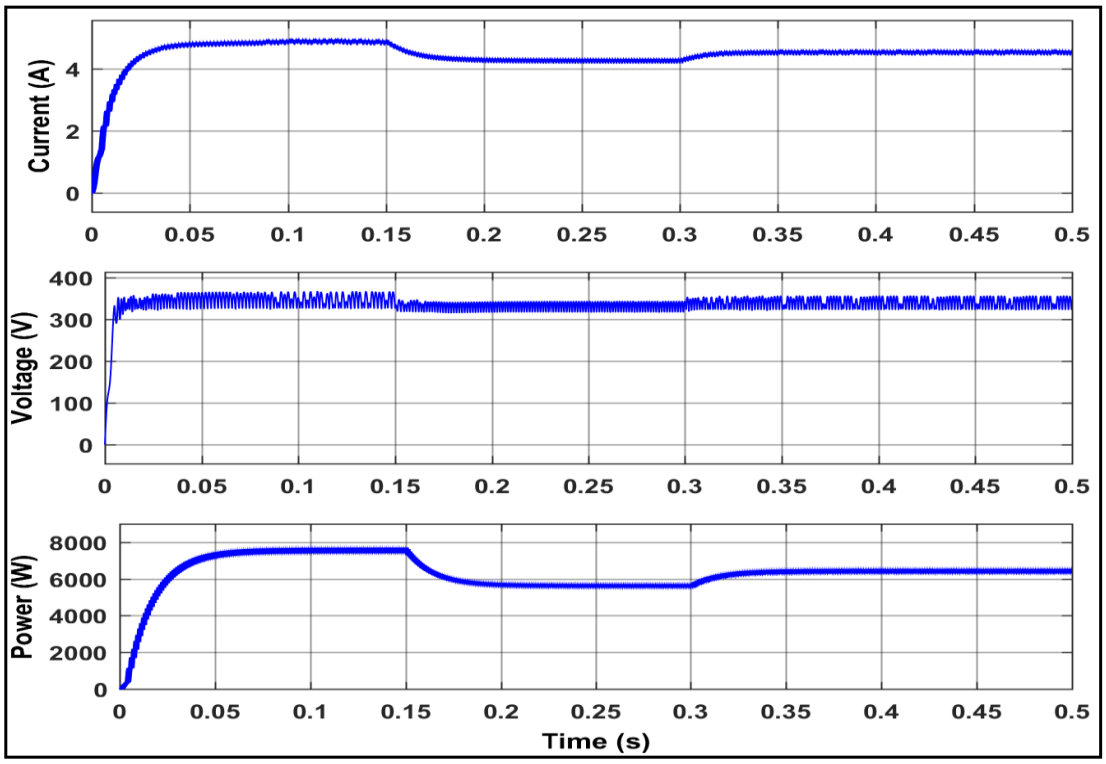

Figure III.12 Simulation of current, voltage, and power curves for PV system using EP&O MPPT

D. artificial neural networks

The use of artificial neural networks (ANN) for MPPT in PV systems. ANNs are advanced computational models that learn from data, and their effectiveness depends on factors like the type of network, the number of hidden layers, and the amount of training data. In this context, the ANN controller takes inputs such as voltage, current, and environmental conditions to optimize the power output of the PV system, and it can be implemented more easily by using MATLAB's ANN toolbox to manage the necessary data, as shown in **Figure. III.13**, which illustrates the feedforward neural network architecture for MPPT prediction.

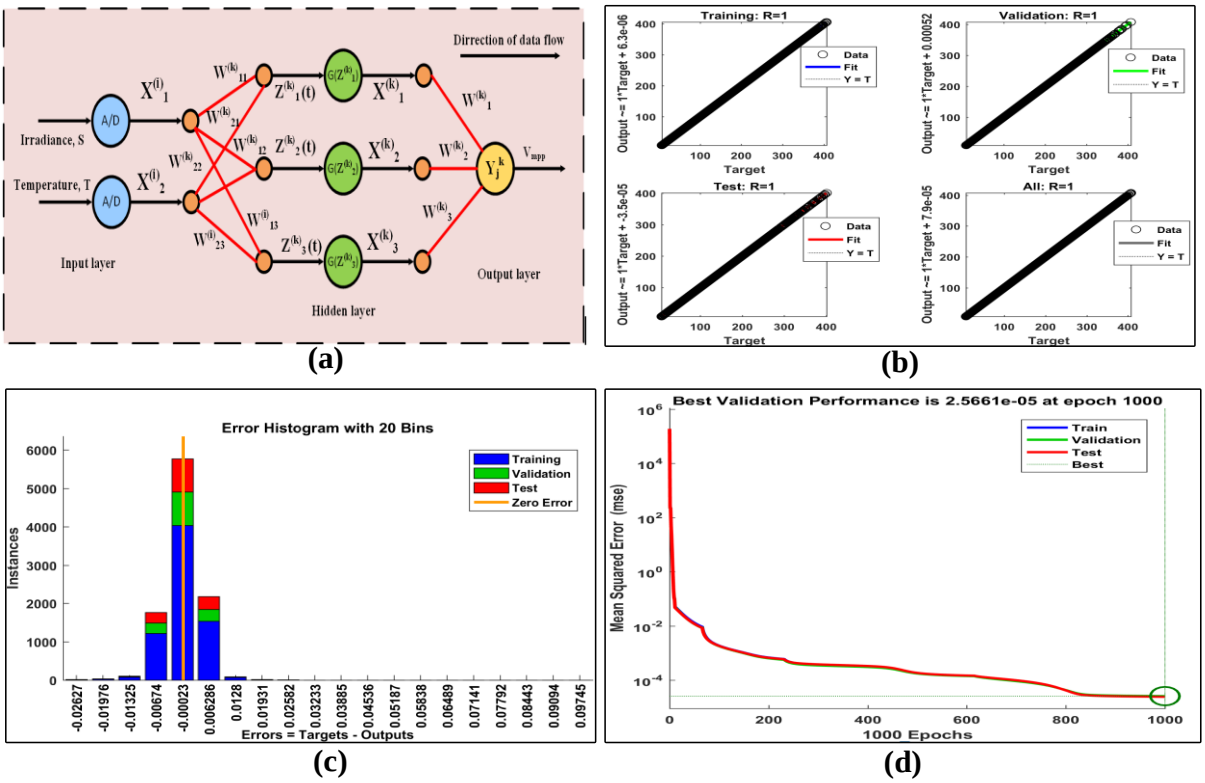

Figure III.13 (a) Structure of the proposed ANN-MPPT model. (b) Regression results for training, validation, and testing datasets. (c) Error histogram illustrating prediction accuracy. (d) Learning curves of training, validation, and test mean squared error (MSE) demonstrating stable convergence [79].

Figure III.14 illustrates the flowchart for the INC algorithm, which is integrated with the ANN-based MPPT technique. The duty ratio D, for the DC-DC boost converter is calculated using the INC technique using the acquired voltage V_{MPP}, and the PV current, I_{PV}. The power output P_{PV}, is evaluated first by this method, which then uses the data from earlier measurements to compute the changes in voltage (ΔV), power (ΔP), and current (Δi). The method optimizes the MPPT performance in real-time by adjusting (D) based on the signs of (Δi) and (ΔV) if the incremental power change (M), is below a predetermined threshold. The effectiveness of this hybrid ANN-based MPPT method is demonstrated in **Figure III.15**, which presents the simulated current, voltage, and power curves under varying irradiance and temperature conditions.

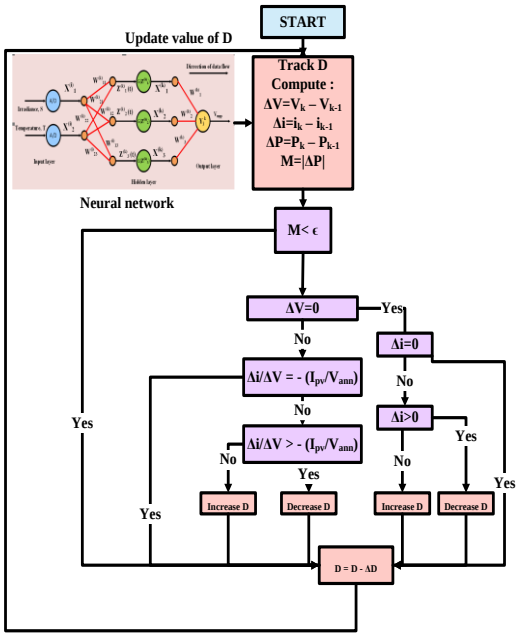

Figure III.14 ANN algorithm flowchart for PV MPPT

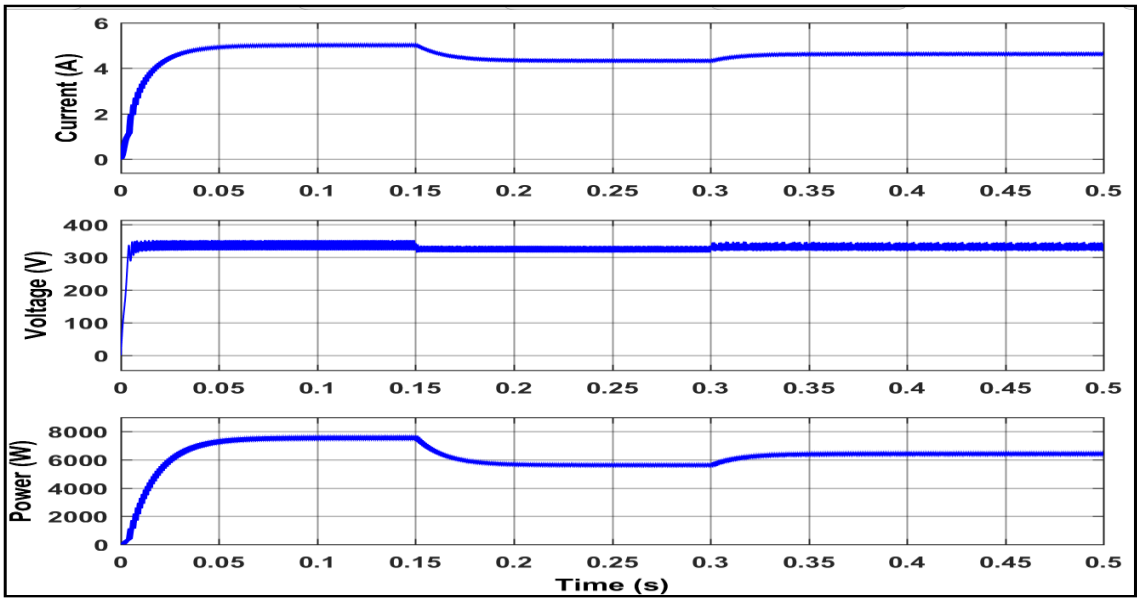

Figure III.15 Simulation of current, voltage, and power curves for PV system using ANN MPPT

E. Interpretation of results and performance comparison of MPPT techniques

The simulation aimed to evaluate the performance of four MPPT algorithms INC, P&O, E-P&O, and Artificial Neural Networks (ANN)—under dynamically changing irradiance and temperature conditions. The PV system used in this study comprises a configuration of 6 parallel and 7 series-connected solar modules, delivering a theoretical peak power of 8409 W at 1000 W/m² irradiance and 24°C.

The environmental profile was divided into three time intervals:

- 0 to 0.15 s: Irradiance = 1000 W/m², Temperature = 24°C
- 0.15 to 0.3 s: Irradiance = 750 W/m², Temperature = 30°C
- 0.3 to 0.5 s: Irradiance = 850 W/m², Temperature = 26°C

Figure III.16 illustrates the PV output power response using the different MPPT strategies.

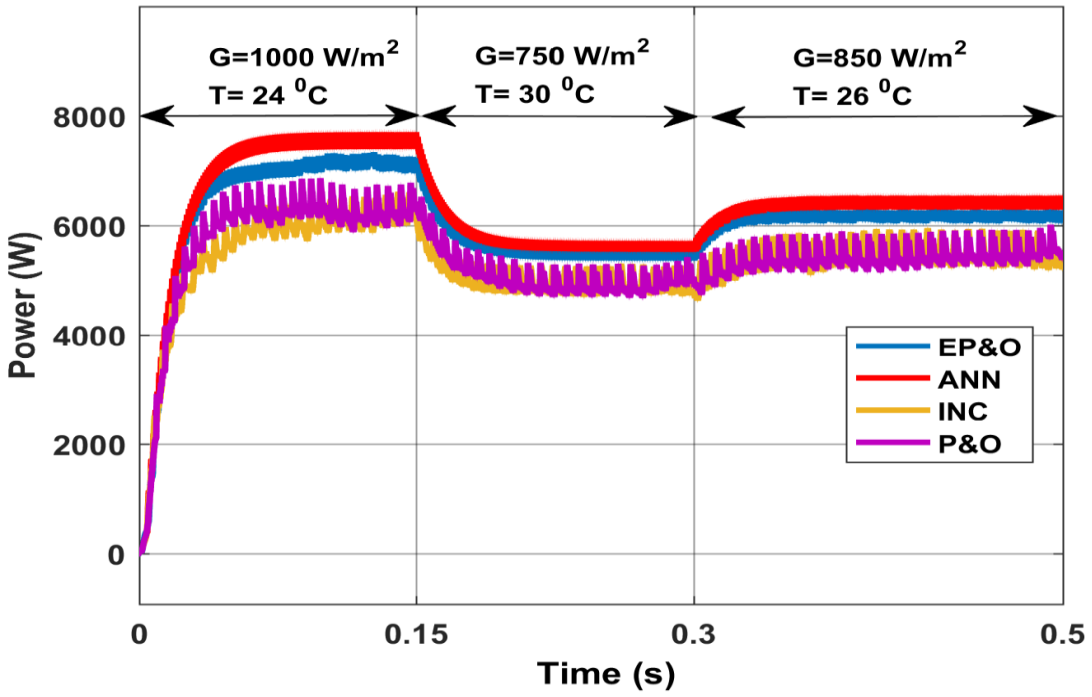

Figure III.16 PV Output power under varying irradiation levels using different MPPT techniques (INC, P&O, EP&O, and ANN)

The results clearly demonstrate the comparative effectiveness of each MPPT approach:

- INC and P&O algorithms exhibit noticeable instability and delayed convergence in response to changing environmental conditions. Both techniques display significant oscillations around the MPPT, particularly during transitions in irradiance. This reduces the overall tracking efficiency and power yield.
- EP&O, which incorporates an adaptive step size mechanism, performs noticeably better than the traditional methods. It responds more quickly to irradiance variations and maintains a more stable output with reduced oscillations. The algorithm successfully balances convergence speed and steady-state performance, improving upon the limitations of conventional P&O.
- ANN-based MPPT clearly outperforms all other techniques. It provides the most stable power output with minimal oscillations and exhibits superior adaptability to rapid environmental fluctuations. The neural network's ability to learn from data and generalize across operating conditions allows it to closely track the true MPP, even during dynamic irradiance changes.

The simulation results affirm that while traditional MPPT techniques (INC and P&O) are simple and widely used, they fall short in terms of dynamic response and stability. The Enhanced P&O method marks a significant improvement, but it is the ANN-based MPPT that

delivers the highest performance, achieving both fast convergence and stable power output across a range of irradiance and temperature conditions.

III.4.6 Control of the grid-side converter

A. Power Flow control strategy

The control strategy for a grid-connected PV system, which is designed to ensure that the energy produced by the solar panels is effectively transferred to the electrical grid and any connected loads. When the system operates at a unit power factor, it only injects active power into the grid. To maintain energy balance, the regular current (I_{ond}) is used to set the maximum reference current (I_{max}) for the inverter, which is synchronized with the grid frequency using a phase-locked loop (PLL) system, as shown in **Figure. III.17**. The reference current amplitude is determined by:

$$I_{max} = m\, I_{ond}$$ (III-8)

The dynamic behavior of the DC bus voltage is governed by the relationship:

$$dE_{dc} = C.V_{dcref}.dV_{dc} = \frac{3}{\sqrt{2}}V_s.I_{ond}.dt$$ (III-9)

leading to the transfer function:

$$\frac{V_{dc}}{I_{ond}} = \frac{3V_s}{\sqrt{2}\,C\,V_{dcref}\,s} = \frac{1}{k_s} \text{where: } k_s = \frac{\sqrt{2}\,C\,V_{dcref}\,s}{3V_s}$$ (III-10)

Hysteresis regulators are devices that compare reference currents, which are the desired current values, with the actual measured currents from the electrical grid. This comparison helps the regulator determine when to switch the inverter's switches (labeled as Sa, Sb, and Sc) on or off to maintain the desired performance of the PV energy system.

When there is an imbalance between the power generated by a PV (solar) system and the power sent out by the inverter, it causes changes in the energy stored in the capacitor of the DC bus, leading to noticeable variations in the DC voltage (V_{dc}). This voltage needs to be controlled and kept constant at a reference value, regardless of fluctuations in energy exchange between the solar system and the electrical grid. The simplified control loop for maintaining this DC bus voltage is represented in a diagram, which relates the output voltage to the input current through a specific mathematical equation.

To maintain Vdc at its reference value, a closed-loop control system is employed, with proportional and integral gains defined as:

$$k_p = 2\,\xi\,w_n\,k_s$$ (III-11)

$$k_i = k_s\,w_n^2$$ (III-12)

where ξ is the damping coefficient and ωn is the natural frequency, tuned to ensure a balance between dynamic response and stability. The PWM regulator compares the synchronized

reference currents with the measured grid-side currents to generate Inverter switching signals (Sa, Sb, and Sc), ensuring synchronized and optimal power injection into the grid.

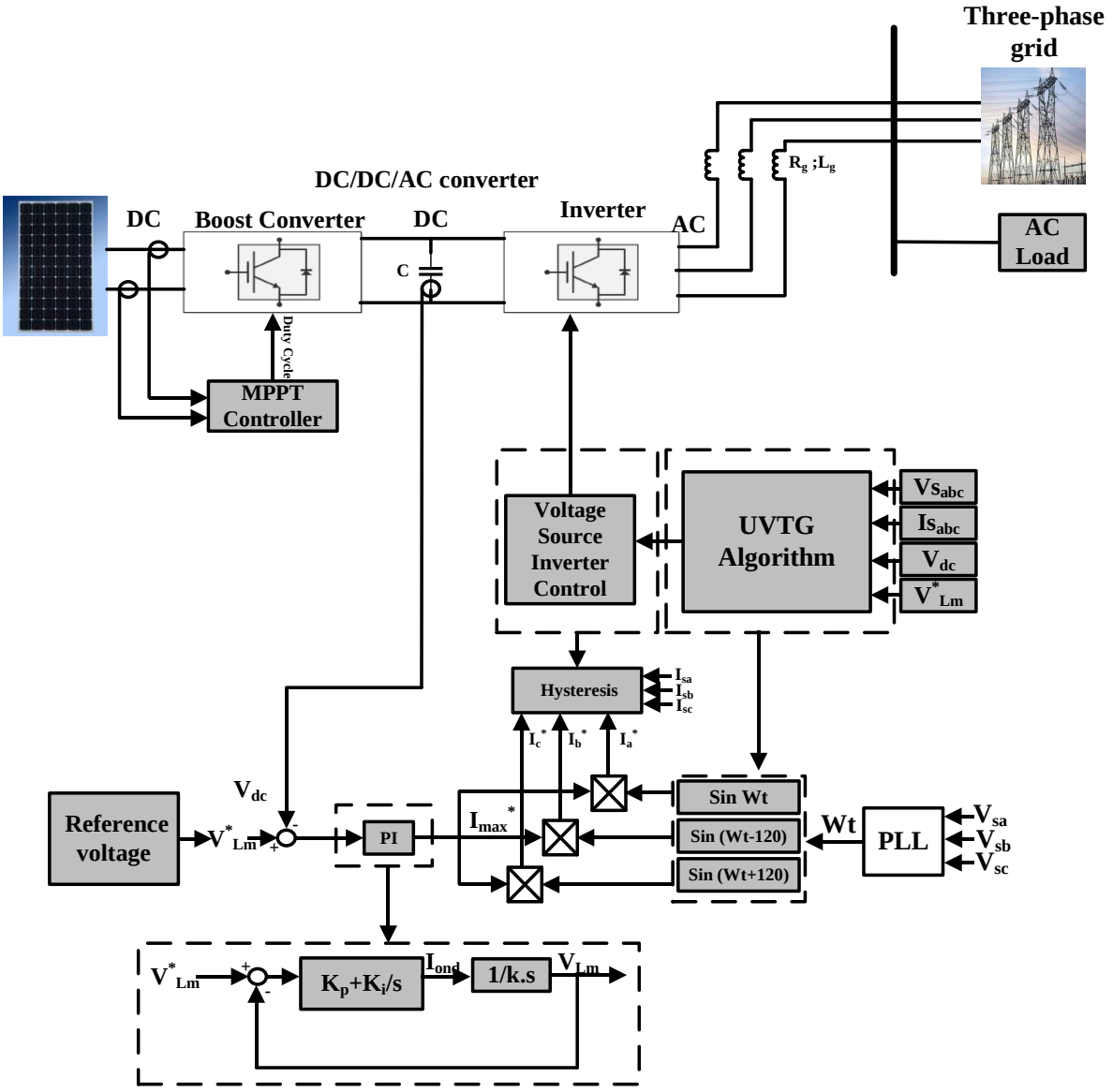

Figure III.17 Integration of PV power systems with converters into the grid

III.5 Simplified study on wind energy conversion

III.5.1 Principle of wind energy conversion

A WT, also known as an aerogenerator, transforms the kinetic energy of the wind into mechanical energy [80].

- **Step 1**: The rotor of the turbine captures the wind's energy and converts it into mechanical energy.
- **Step 2**: This mechanical energy is converted into electrical energy by an electric generator.
- The generated electricity can then be sent to the electrical grid for use.

III.5.2 Different designs of wind energy conversion chains

WTs can be classified based on several criteria, including their type, power output, the type of electrical machine used, and how they operate. For example:

- **Type**: Horizontal or vertical axis turbines.
- **Power Output**:
  - Small: Under 50 kW.
  - Medium: 50 kW to 1 MW.
  - Large: Over 1 MW.
- **Connectivity**: Standalone (isolated) or connected to the electrical grid.
- **Operational mode**: Fixed or variable speed operation depending on how they harness aerodynamic energy.

The power curves of a WT show that for each wind speed, there is a specific optimal rotational speed at which the turbine operates most efficiently. This means that if the turbine is connected directly to the electrical grid using synchronous or asynchronous generators, its rotational speed remains fairly constant. As a result, the aerodynamic efficiency of the turbine can only reach its maximum at one particular wind speed, known as the optimal tip speed ratio (λ_opt), as illustrated in **Figure III.18**, which shows the step variation in wind speed and its effect on WT output power at different wind speeds.

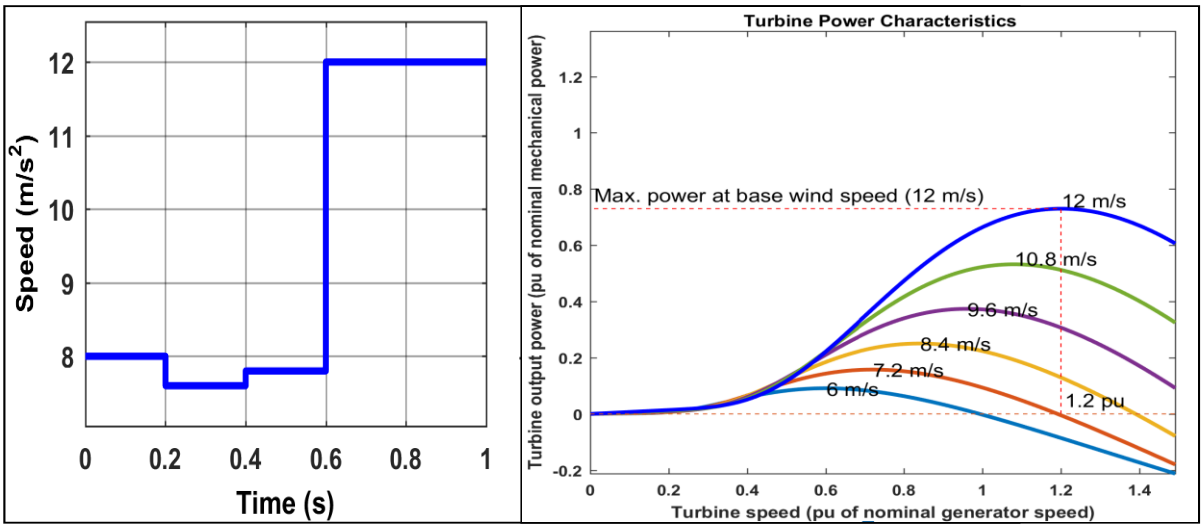

Figure III.18 Step variation in wind speed and its effect on wind turbine output power at different wind speeds

To illustrate the different configurations available for wind energy conversion systems and their respective trade-offs, **Table III.1** summarizes the types of WTs, outlining their advantages and disadvantages in terms of mechanical complexity, control requirements, and cost.

Table III.1 Types of wind turbines advantages and disadvantages [81]

Type	Advantages	Disadvantages
SCIG (Squirrel Cage Induction Generator) (Fixed Speed – MAS)	- Robust machine - Fixed speed operation - No need for power electronic converters - Low cost	- Extracted power not optimized - Gearbox maintenance required
WRIG (Wound Rotor Induction Generator) (Variable Speed – GADA)	- Variable speed operation - Optimized power extraction - Power electronics sized at ~30% of rated power - Power production outside synchronous speed - Rotor magnetized using capacitors	- Gearbox maintenance required - Complex control system - Issues with slip rings and brushes - High cost of power electronics
DFIG (Doubly-Fed Induction Generator) (Variable Speed – GSAP)	- Full variable speed range - No gearbox required - Optimized power extraction - Simple connection topology	- Large machine size - More or less complex control - High cost of power electronics - Power electronics rated to full machine capacity

III.5.3 Description of the studied wind energy conversion system

The wind energy conversion system described consists mainly of a turbine connected to a synchronous generator with permanent magnets (PMSG). The generator's stator is linked to a pulse-width modulation (PWM) rectifier, which helps control the turbine's rotation speed and optimize the power extracted from the wind. Additionally, an inverter is connected to the rectifier, allowing the system to supply energy to a three-phase load building and feed any excess power back into the electrical grid.

The system under consideration refers to a wind energy conversion system (WECS) designed for on-grid applications, which integrates a WT with a gearless Permanent Magnet Synchronous Generator (PMSG). This system employs a passive diode rectifier to convert the generated AC voltage into DC, and a DC/DC buck converter that not only steps down the rectified voltage to the desired level but also functions as a MPPT tracker to optimize energy extraction from varying wind conditions. The configuration aims to enhance efficiency, reduce complexity, and minimize component count while ensuring reliable operation in decentralized energy systems [82].

Different researchers have developed various models to predict how well WTs perform, and these models can be grouped into two main categories [83]. The first category includes models based on fundamental equations that describe the amount of power available in the wind. The second category consists of models that use the power curve of the WT, which shows how much power the turbine can generate at different wind speeds.

III.6 The wind system modelling

III.6.1 Turbine modeling

The kinetic energy of the wind is converted into rotational movement. This conversion from wind power to mechanical power is made possible by the interaction of WTs blades with the wind speed. A number of equations, referred to as Eq. (III-13), Eq.(III-14) and Eq.(III-15) in sources [82,83], outline the process of generating power from wind.

$$P_{mout} = \frac{1}{2}\pi\rho C_p R^2 V^3$$
(III-13)

$$C_p = \frac{1}{2}\left(\frac{116}{\lambda_1} - 0.4\beta - 5\right)e^{\frac{-165}{\lambda_1}}$$
(III-14)

$$\lambda_1 = \frac{1}{\frac{1}{\lambda+0.089} - \frac{0.035}{\beta^3+1}}$$ (III-15)

The equation set includes mechanical power P_{mout}, pitch angle β, blade radius R, and wind speed V. The tip-speed ratio λ is defined as $\lambda = \frac{WR}{V}$. C_p is a function of the tip-speed ratio (λ). C_p is the turbine's power coefficient, whereas λ_1 denotes any constant.

The turbine transforms kinetic energy into mechanical energy. This energy is then transferred to the generator via a shaft that connects the turbine and the generator's rotor. Inside the generator, the rotor winding, also known as the armature, spins within a fixed magnetic field. This process, which follows the basic principles of a generator, results in the production of electrical voltage [84,85].

After extracting the maximum mechanical power from the WT, this energy is utilized to drive a generator, converting mechanical energy into electrical energy. Permanent Magnet Synchronous Generator (PMSG)-based Wind Energy Systems (WESs) are particularly advantageous due to their high power density, efficiency, and direct drive design, making them a reliable and cost-effective option for energy generation [11,12]. To effectively manage the output power of the generator in low-power PMSG-based WESs, a configuration involving a passive rectifier followed by a DC-DC converter is identified as a more economical approach, facilitating efficient power conversion and regulation [86,88].

III.6.2 Modeling of the permanent magnet synchronous generator

The Permanent Magnet Synchronous Generator (PMSG) model, based on Park's transformation, utilizes a d-q coordinate system to simplify the analysis of three-phase systems

by decoupling the stator currents into direct (d) and quadrature (q) axes. The dynamic behavior of the stator currents is governed by the following state equations:

$$\frac{dI_{sd}}{dt} = -\frac{R_{sa}}{L_{sd}} I_{sd} + w_s \frac{L_{sq}}{L_{sd}} I_{sq} - \frac{1}{L_{sd}} V_{Sd} \quad \text{(III-16)}$$

$$\frac{dI_{sq}}{dt} = -\frac{R_{sa}}{L_{sq}} I_{sq} - w_s \frac{L_{sd}}{L_{sq}} I_{sd} + w_s \frac{1}{L_{sq}} \varphi_q - \frac{1}{L_{sq}} V_{Sq} \quad \text{(III-17)}$$

$$T_e = 1.5\ \frac{P}{2} [\varphi_q I_{sq} - I_{sd} I_{sq} (L_{sd} - L_{sq})] \quad \text{(III-18)}$$

The governing state equations describe the dynamics of the stator currents (isd and isq), stator resistances (R_{sa}), inductances (L_{sd} and L_{sq}), and voltages (V_{Sd} and V_{Sq}), allowing for the calculation of electromagnetic torque (T_e) based on the rotor's pole count (P) and the interaction between the stator currents and the permanent magnetic flux (φ). This framework facilitates the design and control of PMSG systems, particularly in applications such as wind energy conversion, by providing insights into their operational characteristics and performance under varying conditions [89].

III.6.3 Modeling of the passive rectifier and DC voltage conversion

The passive rectifier model described involves the use of a full-wave bridge rectifier to convert the AC output voltage from the generator into a rectified direct current (DC) voltage (V_r), which subsequently serves as the input voltage (V_i) for a buck converter stage. This conversion process is essential for enabling the efficient regulation and control of voltage in power electronics applications. The rectified DC voltage is calculated using Equation (III-19), which incorporates the effective line-to-line input voltage (V_{LL}) from the rectifier [91].

$$V_r = 1.5\ \frac{3\sqrt{2}}{\pi} V_{LL} \quad \text{(III-19)}$$

III.6.4 MPPT techniques for wind energy systems

The conventional MPPT converter in this system utilizes a buck DC/DC converter to reduce the output DC voltage from the rectifier to the desired level for the DC bus. The converter's switching is managed by a fixed-step P&O MPPT technique and enhanced PO, ANN, which optimally adjusts the duty cycle to maximize power extraction from the rectifier output.

After electricity is generated by the Permanent Magnet Synchronous Generator (PMSG), it is essential to design the boost converter (BC) effectively to ensure optimal performance in converting the generated voltage to a higher output voltage suitable for the load. In steady-state operation, the relationships between the output voltage (V_0), input voltage (V_{dc}), output current (I_L), and input current (I_{dc}) are given by the following equations [92]:

$$V_0 = 1.5\ \frac{V_{dc}}{(1-D)} \quad \text{(III-20)}$$

$$I_0 = I_{dc}(1 - D) \quad \text{(III-21)}$$

The design of a boost converter for wind energy conversion systems (WECS), three critical parameters must be determined: switching frequency (f_s), inductance (L_k), and capacitance (C). The inductance must exceed a certain threshold, denoted as L_k, to ensure the converter

operates in continuous-current mode, which is essential for maintaining stable performance and avoiding current ripple [90].

The capacitance (C) is calculated using the formula provided in equation (III-23), which incorporates the output voltage ripple (ΔV_0) as a critical parameter. The value of the inductance is chosen to guarantee operation in continuous conduction mode (CCM) and is calculated using:

$$L_k = \frac{DR_{Load}\,(1-D)^2}{2f_s} \quad \text{(III-22)}$$

$$C = \frac{D}{R_{Load}\,\Delta V_0\,2f_s} \quad \text{(III-23)}$$

To optimize the energy output of a wind power system, a MPPT controller is essential for regulating the chopper, ensuring that the system operates at its peak efficiency despite varying wind conditions. The study outlines various MPPT control techniques, which will be systematically summarized and analyzed, focusing on their internal architectural design and operational algorithmic steps [93].

Several control strategies have been developed in research to maximize the electrical power generated by variable-speed WTs [17,18].

A. Perturbation and observation

Perturbation and Observation (P&O) based MPPT algorithms are designed to optimize the power output of WTs by dynamically adjusting the operating point without requiring wind speed sensors or prior knowledge of the aerodynamic characteristics of the system. The algorithm operates by introducing disturbances to the system and observing the resulting changes in output power, allowing it to oscillate around the maximum power point. However, while P&O is effective in many scenarios, it becomes less reliable in medium- and high-power wind systems due to its inherent oscillatory behavior, which can lead to inefficiencies and instability in power tracking.

Once the MPP is identified, the algorithm tends to oscillate around the optimal output voltage, which can be visualized through a flowchart detailing its operational steps, similar to the flowchart shown for PV systems in **Figure III.9**.

This behavior is illustrated in the simulation shown in **Figure III.19**, which demonstrates the current, voltage, and power dynamics for a wind energy system using the P&O MPPT algorithm.

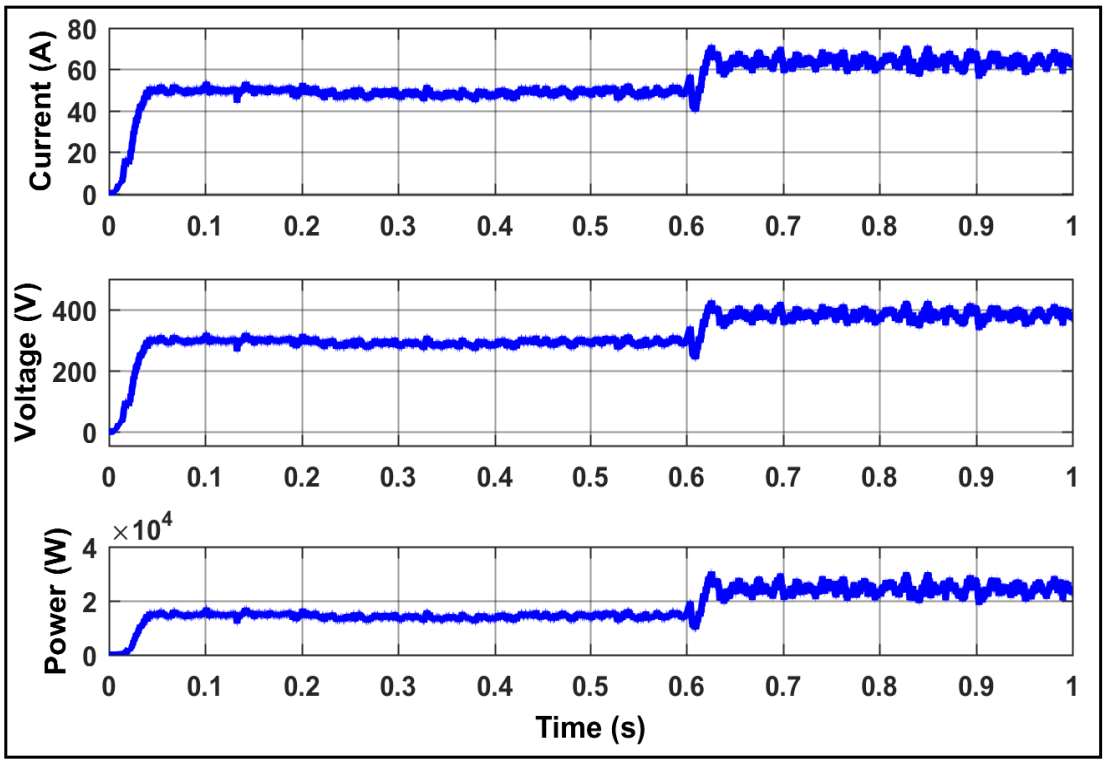

Figure III.19 Simulation of current, voltage, and power for wind energy system using Perturb and Observe (P&O) MPPT algorithm

B. E-P&O MPPT algorithm for WES

The flowchart in **Figure III.20** illustrates the operation of an E-P&O MPPT algorithm for WES. This enhanced algorithm operates by determining the location of the operating power point on the $P_m - w_m$ characteristic curve. To increase accuracy, a new curve, (v_{wind} * $\Delta P_{wind}/\Delta w_m$) is introduced and compared with the main characteristic curve. The algorithm then adjusts the step sizes based on the location of the operating point, optimizing the control strategy for MPPT. This approach ensures more precise and efficient tracking of the maximum power point, dynamically adapting to varying wind conditions. The simulation results of the current, voltage, and power characteristics for the wind energy system using the E-P&O MPPT algorithm are shown in **Figure III.21**.

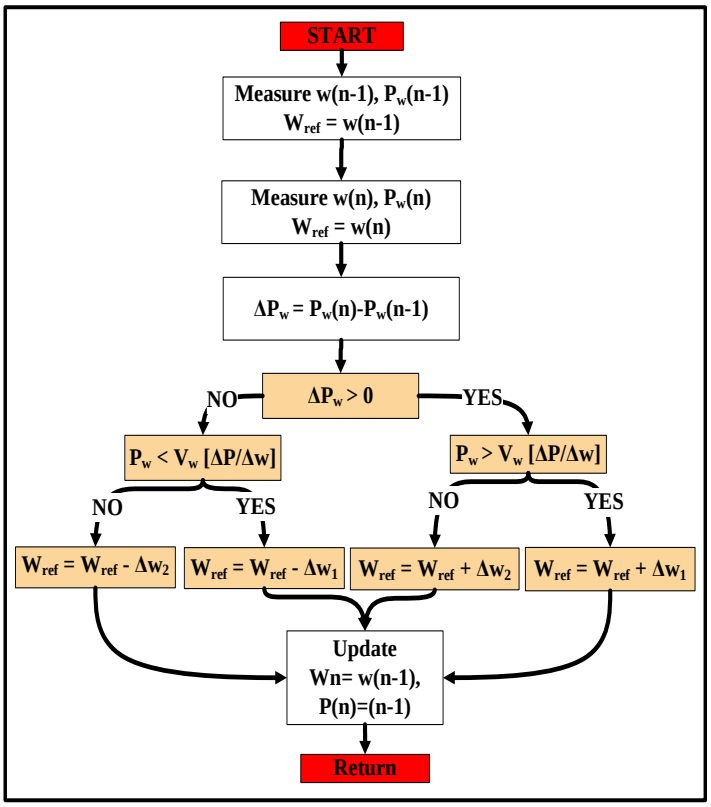

Figure III.20 E-P&O algorithm flowchart for wind MPPT

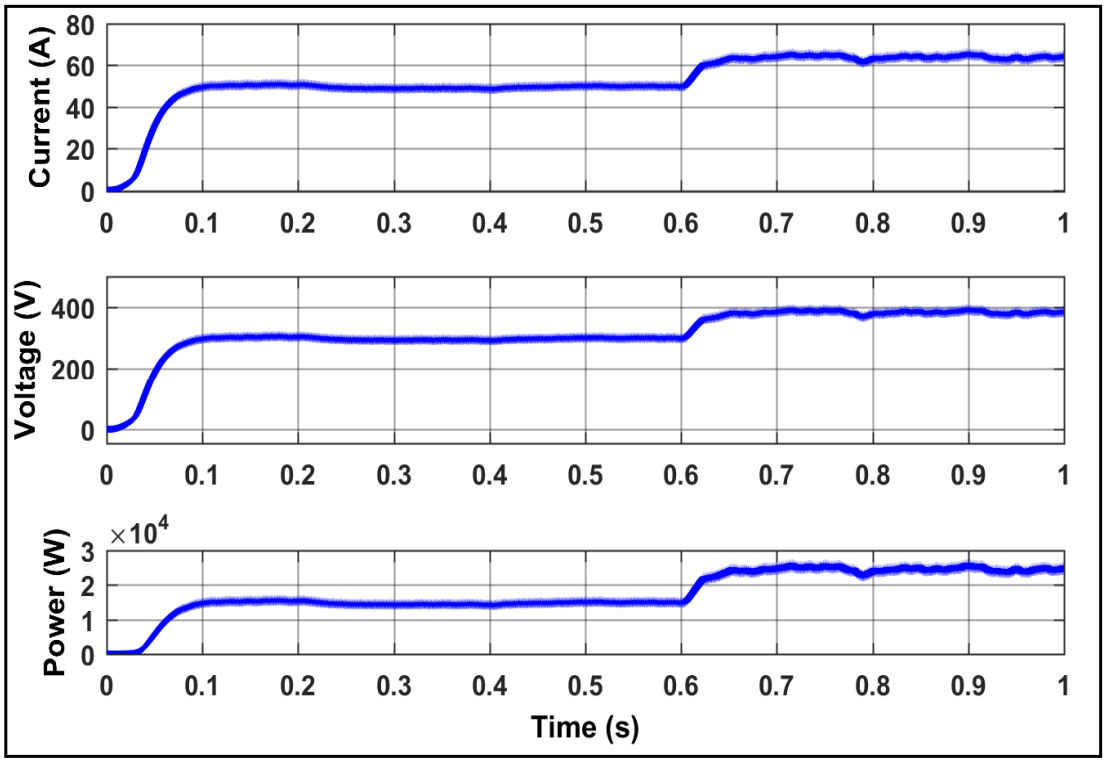

Figure III.21 Simulation of current, voltage, and power for wind energy system using EP&O MPPT algorithm

C. Neural Network ANN

The neural network (NN)-based MPPT algorithm leverages the architecture of neural networks, which comprises input, hidden, and output layers, to optimize the performance of WTs by processing various input parameters such as pitch angle, wind speed, and rotor speed. The NN outputs reference signals that guide the power electronic circuits to operate near the MPPT, with the convergence to this optimal operating point being influenced by the weights assigned during training, the specific algorithms employed in the hidden layer, and the diversity of input-output patterns encountered during the training phase. This approach, akin to fuzzy logic controllers, exemplifies the advancements in soft computing technologies that enhance the adaptability and efficiency of MPPT strategies in variable wind conditions. as illustrated in **Figure III.22**, which shows the ANN algorithm flowchart for wind MPPT.

Additionally, the simulation of current, voltage, and power for the wind energy system using the ANN-based MPPT algorithm is shown in **Figure III.23**.

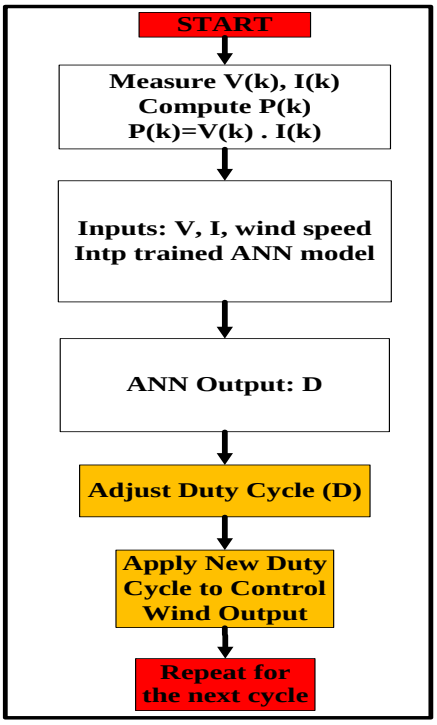

Figure III.22 ANN algorithm flowchart for wind MPPT

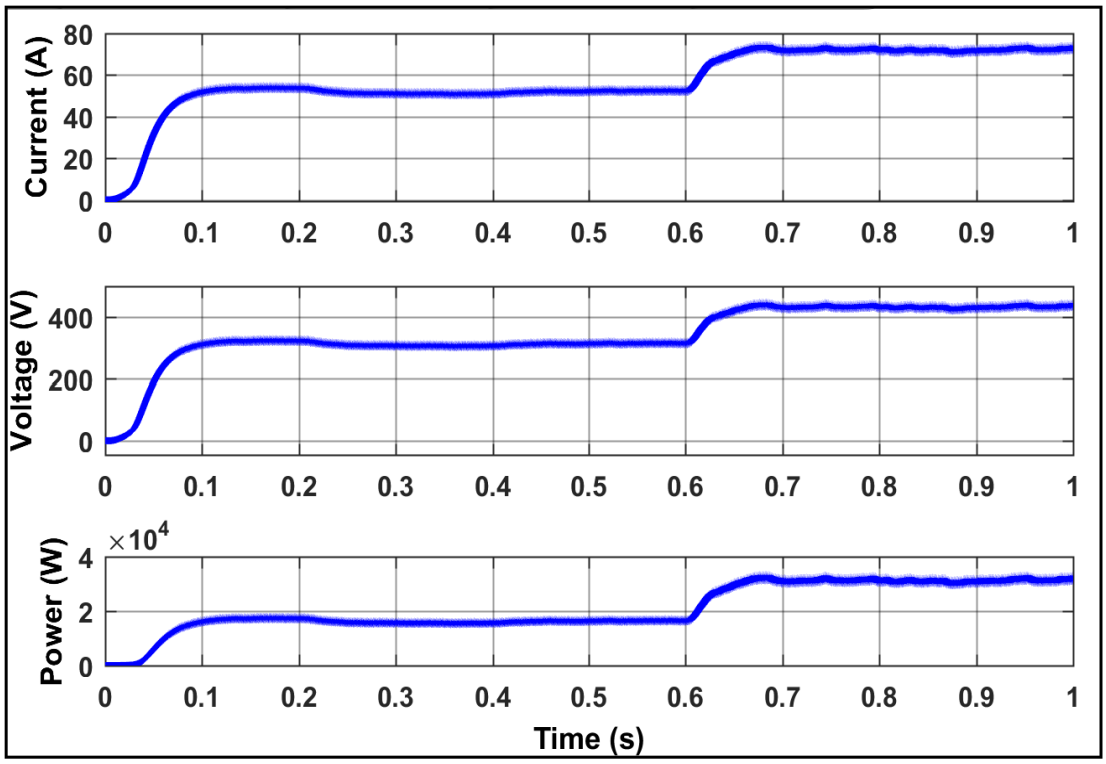

Figure III.23 Simulation of current, voltage, and power for wind energy system using ANN MPPT algorithm

D. Fuzzy logic

The fuzzy logic-based MPPT methodology is an advanced control strategy employed in wind energy systems to optimize power extraction by dynamically identifying and maintaining the operating point that yields maximum output, independent of varying wind speeds. This approach is characterized by its robustness compared to traditional control methods, as it does not necessitate a detailed mathematical model of the system; instead, it relies on three core components: fuzzification, an inference engine, and defuzzification. The effectiveness of a fuzzy controller hinges on the careful selection of input and output variables, the design of membership functions, and the formulation of fuzzy rules, which collectively influence the controller's performance in adapting to changing conditions.

The authors reference prior studies by [95] and [96] to substantiate their methodological choices regarding the selection of variables. These variables are specifically linked to three critical signals: the variation in rotor speed, the variation in electric power output, and the variation in the outputted DC power.

The selected inputs to the fuzzy MPPT controller are based on the temporal variation of key signals, defined as follows:

$$ew_r(k) = w_r(k) - w_r(k-1) \quad \text{(III-24)}$$

$$eP_e(k) = P_e(k) - P_e(k-1) \quad \text{(III-25)}$$

$$eV_{DC}(k) = V_{DC}(k) - V_{DC}(k-1) \quad \text{(III-26)}$$

These variables correspond respectively to the variation in rotor speed, the variation in electric power output, and the variation in DC-link voltage, as shown in the **Figure III.24**, which illustrates the FLC algorithm flowchart for wind MPPT.

Additionally, the simulation of current, voltage, and power for the wind energy system using the FLC MPPT algorithm is shown in **Figure III.25**.

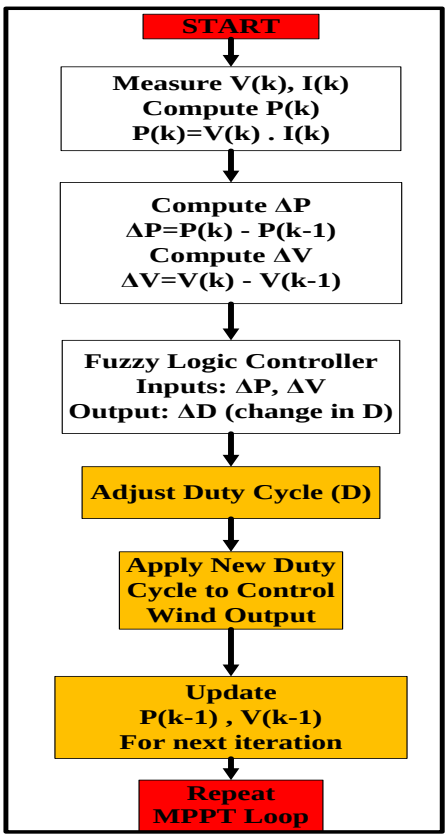

Figure III.24 FLC algorithm flowchart for wind MPPT

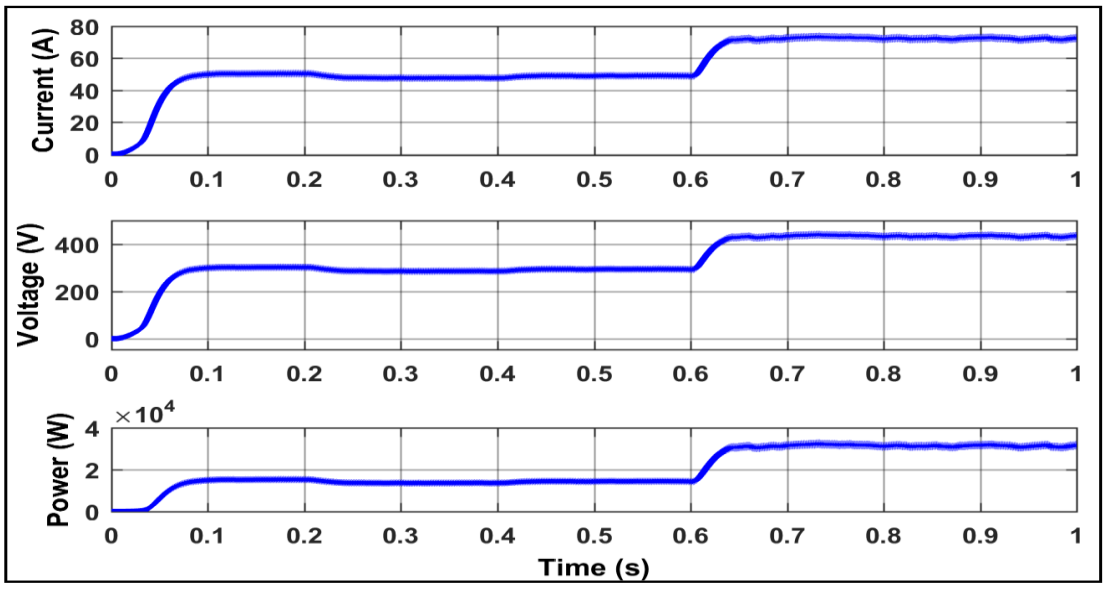

Figure III.25 Simulation of current, voltage, and power for wind energy system using FLC MPPT algorithm

E. Results for Wind MPPT algorithms under varying wind speeds

The comparative analysis of the three MPPT techniques E-P&O, Fuzzy Logic Control (FLC), and Artificial Neural Network (ANN)—under varying wind speed conditions is illustrated in **Figure III.26**. The wind speed variations are defined as follows:

- From 0 to 0.2 s, wind speed is 8 m/s.
- From 0.2 to 0.4 s, wind speed is 6 m/s.
- From 0.4 to 0.6 s, wind speed is 7 m/s.
- From 0.6 s to 1 s, wind speed is 12 m/s.

The simulation results reveal that the P&O algorithm struggles to maintain stable operation in these conditions, especially as the wind speed fluctuates. The algorithm fails to accurately follow the reference power due to large fluctuations in the power delta, leading to significant instability in tracking the MPPT. As a result, we did not include the P&O results for comparison in the figures.

In contrast, the Enhanced P&O (EP&O), ANN, and Fuzzy Logic (FLC) MPPT algorithms maintain stable performance and follow the reference power trajectory effectively throughout the varying wind speed conditions. Among these three, the ANN-based MPPT algorithm demonstrates superior performance, not only maintaining stability but also delivering higher power output than the EP&O and FLC algorithms. The ANN algorithm exhibits a smoother and more accurate power tracking response, making it both more stable and more efficient compared to the other two algorithms.

Figures displaying the performance of the EP&O, ANN, and FLC algorithms clearly illustrate their ability to follow the reference power trajectory under varying wind speeds. While all three algorithms remain stable, the ANN stands out for its improved stability and greater power output compared to EP&O and FLC.

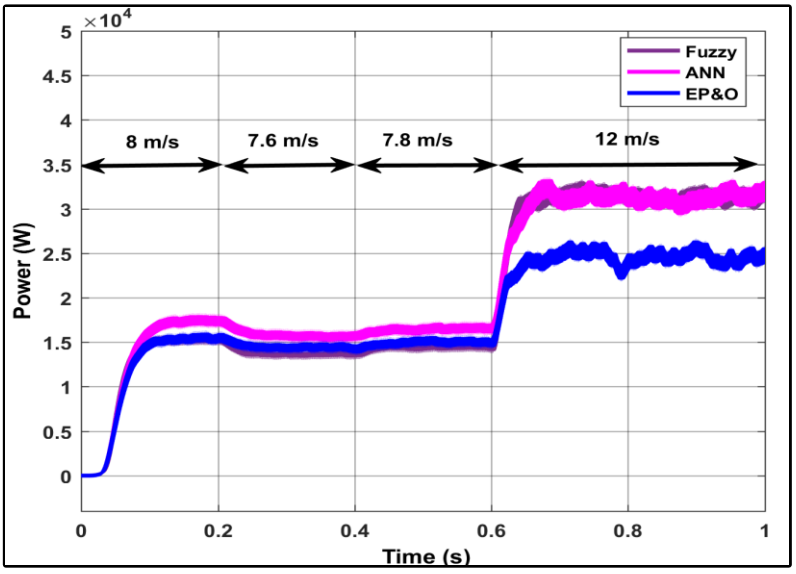

Figure III.26 Wind output power under varying speed levels using different MPPT techniques (EP&O, FLC and ANN)

III.7 Control of the converter for wind energy integration with the electrical grid

The control of a converter that connects a wind energy production system to a building and the electrical grid. The main goal of this control is to transfer all the active power generated by the WT to both the building's load and the grid while ensuring that the voltage of the direct current bus, which comes from the rectifier at the generator's output, remains at a constant reference value [97].

III.7.1 Control of injected active and reactive powers

The active and reactive powers transmitted to the load and the electrical grid through a two-level voltage inverter are expressed using specific equations in a SRF, known as the dq frame. These equations are derived at a point where a RL filter is installed, which helps to reduce high-frequency noise or harmonics that can interfere with the PQ. The active power P_{inv}, representing the real power transferred to the load or grid, and the reactive power Q_{inv} indicating the power exchanged to maintain voltage levels, are given by the following equations:

$$P_{inv} = V_{Sd}I_{sd} + V_{Sq}I_{sq} \quad \text{(III-27)}$$

$$Q_{inv} = V_{Sq}I_{sd} - V_{Sd}I_{sq} \quad \text{(III-28)}$$

(P_{inv}) and (Q_{inv}) represent the active and reactive power delivered at the output of the converter, which is part of a wind energy system. The terms (V_{invd}) and (V_{invq}) refer to the direct and quadrature components of voltage, while (I_{sd}) and (I_{sq}) refer to the corresponding current components at the output of a filter.

The active and reactive power in a wind energy conversion system depend on two components of current and voltage, which are linked through a coordinate system. To control these powers effectively, a method is used that aligns the rotating reference frame (dq) with the voltage vector of the grid, ensuring that the component related to reactive power is zero thereby eliminating the reactive component of the inverter voltage [94]:

$$V_{inv} = V_{invd} \text{ and } V_{invq} = 0 \quad \text{(III-29)}$$

As a result, the inverter voltage can be simplified to just its active component, making it easier to manage the system's performance are then determined by:

$$P_{inv} = V_{invd}I_{sd} \quad \text{(III-30)}$$

$$Q_{inv} = -V_{invd}I_{sq} \quad \text{(III-31)}$$

According to Equations (III-30), the active power (which is the useful power that does work) and reactive power (which supports the voltage levels necessary for energy transfer) can be controlled using two different components of current. The direct current component is responsible for managing the active power, while the quadrature current component is used to control the reactive power.

The dynamic model of the inverter voltages in the SRF (dq) describes how the voltages behave based on the currents and other electrical parameters. This model is represented by a set of

equations that relate the direct current (Id) and quadrature current (Iq) to the inverter's voltage outputs (V_{invd} and V_{invq}). These are expressed as [81]:

$$V_{invd} = R_f\, I_{sd} + L_f \frac{dI_{sd}}{dt} - w_s\, L_f\, I_{sq} + V_{Sd} \quad \text{(III-32)}$$

$$V_{invq} = R_f\, I_{sq} + L_f \frac{dI_{sq}}{dt} + w_s\, L_f\, I_{sd} + V_{Sq} \quad \text{(III-33)}$$

Two control loops need to be implemented in the wind energy conversion system to manage the currents effectively. These loops use proportional-integral (PI) controllers to generate reference voltages, which help control the switches in the inverter. The current on the quadrature axis is used to manage reactive power, keeping it at zero, while the current on the direct axis maintains a constant voltage, ensuring efficient transfer of active power [94].

The current on the quadrature axis is used to control reactive power, which is set to zero (Qc = 0) to ensure that the system operates at a unit power factor, meaning it uses power efficiently. Meanwhile, the current on the direct axis helps maintain a constant voltage in the DC bus, allowing for the full transfer of active power, which is the actual power used to perform work.

As illustrated in **Figure III.27**, this diagram shows the integration of wind power systems with converters into the grid.

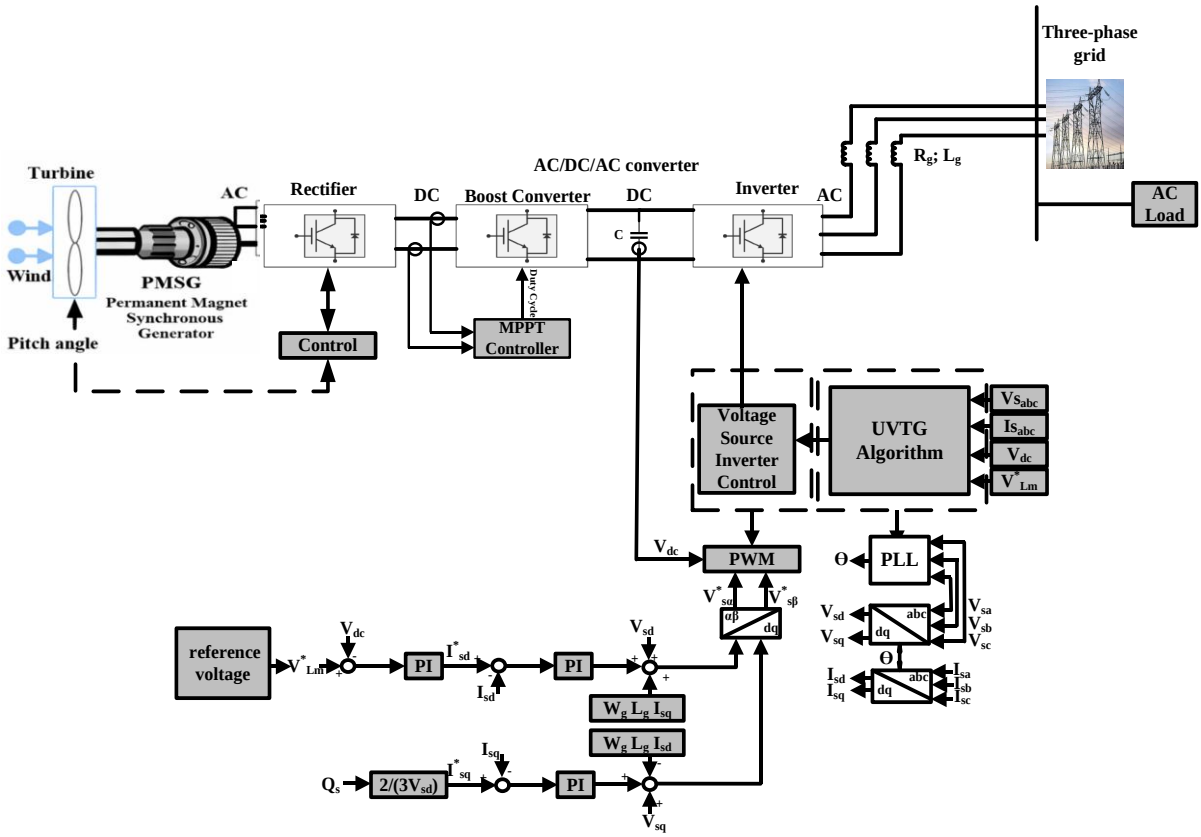

Figure III.27 Integration of wind power systems with converters into the grid

Similar to previous equations discussed in the document, the transfer equations for each component of the current need to be adjusted or "decoupled" using specific compensation terms. This adjustment helps ensure that the different components of the current can operate independently and effectively.

The decoupling terms are represented as:

$$e_d = -w_s\, L_f\, I_{sq} + V_{Sd} \tag{III-34}$$

$$e_q = +w_s\, L_f\, I_{sd} + V_{Sq} \tag{III-35}$$

The first-order transfer functions for two currents that have the same dynamic behavior in a wind energy conversion system. These transfer functions, represented as G1(s) and G2(s):

$$G_1(s) = \frac{I_{sd}}{V_{invd} - e_d} = \frac{1/\,R_f}{1+\,L_f\,\mathrm{s}/\,R_f} \tag{III-36}$$

$$G_2(s) = \frac{I_{sq}}{V_{invq} - e_q} = \frac{1/\,R_f}{1+\,L_f\,\mathrm{s}/\,R_f} \tag{III-37}$$

The regulation of the DC bus voltage (Vdc), which is an external control loop that works alongside the current regulation loop (I_{sd}). The reference current (I_{sdref}) is set based on the desired DC voltage (Vdc) to ensure that the power generated by the wind generator matches the power being sent to the load and the electrical grid. The method for calculating this regulator is similar to what was previously explained for PV systems, indicating a shared approach in managing energy conversion systems.

The estimation of the electrical angle (ω) using a Phase-Locked Loop (PLL) to ensure that the inverter, which converts wind energy into usable electricity, stays synchronized with the electrical grid. This synchronization is crucial for generating high-quality sinusoidal voltage and current that match the grid's frequency. The PLL uses measurements of the grid's voltage to adjust the phase angle, which helps the inverter produce the correct reference voltages for efficient energy transfer [98].

The measured voltages at the connection point of a wind energy system are represented in a two-phase coordinate system, known as the α-β frame:

$$\begin{bmatrix} V_{S\alpha} \\ V_{S\beta} \end{bmatrix} = \sqrt{2}\, V_{Seff} \begin{bmatrix} \sin\theta \\ \cos\theta \end{bmatrix} \tag{III-38}$$

Using the Park transformation based on an estimated electrical angle ($\hat{\theta}$), the measured voltages are expressed in a SRF:

$$\begin{bmatrix} V_{Sd} \\ V_{Sq} \end{bmatrix} = \sqrt{3}\, V_{Seff} \begin{bmatrix} \sin(\theta - \hat{\theta}) \\ -\cos(\theta - \hat{\theta}) \end{bmatrix} \tag{III-39}$$

A situation where the estimated angle of a system is very close to the actual physical angle. When this difference is small, a specific approximation can be used to simplify calculations:

$$V_{Sd} = \sqrt{3}\, V_{Seff}\, (\theta - \hat{\theta}) \tag{III-40}$$

And when the difference between the estimated angle ($\hat{\theta}$) and the actual angle (θ) is very small. When this difference is minimal, it can be assumed that the measured value of the direct voltage (Vgd) is approximately zero $V_{Sd} = 0$.

To control the angle (θ) in a wind energy conversion system by adjusting a specific electrical component, known as the direct component (V_{Sd}), to zero. This control is achieved through a method called Phase-Locked Loop (PLL), which helps synchronize the system's operation with the desired phase angle [99].

III.8 Battery Energy Storage System (BESS)

Energy storage systems (ESS) are essential components in the operation of microgrids, primarily facilitating the integration of RESs and addressing the imbalance between supply and demand. By providing continuous and flexible power, these systems enhance the stability of the electrical grid, allowing for excess energy generated during low-demand periods to be stored and utilized during peak demand times.

The energy storage system (ESS) is integrated into the electrical grid through a power electronics interface, which facilitates the bidirectional flow of energy, allowing for both injection into and extraction from the grid [25,26].

In this document, the Storage Energy Battery is described as an integrated system comprising a lithium-ion battery, a bidirectional AC/DC converter that facilitates energy transfer in both directions, and a voltage/current measurement device positioned at the PCC. This measurement equipment provides critical inputs to a control block, which generates switching signals for the semiconductor components of the converter, thereby enabling efficient energy management within the microgrid.

Eq. (III-41), the battery capacity is expressed as the total energy E_{Total} available for storage and distribution to the load during low generation hours [102].

$$E_{Total} = \frac{E_{Day}}{\eta_{inv}} \quad \text{(III-41)}$$

where η_{inv} represents the inverter efficiency

The formula in Eq. (III-42) for BES calculates the total energy stored in a battery E_{Bat} system based on various factors such as the total energy generated, battery efficiency, depth of discharge, and battery voltage. It provides a way to quantify the energy capacity of the battery bank and determine the number of batteries needed in series N_{Series} and parallel $N_{Parallel}$ configurations for efficient ESS and utilization in standalone hybrid RES Eq. (III-43) and Eq. (III-44).

$$E_{Bat} = \frac{E_{Total}\,\eta_a}{V_{Bat}\,\eta_{Bat} DOD} \quad \text{(III-42)}$$

$$N_{Series} = \frac{V_{Bus}}{V_{Bat}} \quad \text{(III-43)}$$

$$N_{Parallel} = \frac{E_{Bat}}{E_{Bat,rated}} \quad \text{(III-44)}$$

With η_a denoting the overall system efficiency, V_{Bat} the battery voltage, η_{Bat} the battery efficiency, the DOD depth of discharge and $E_{Bat,rated}$ is the rated battery energy.

The energy stored in batteries in a standalone hybrid RES is calculated in Eq. (III-45) based on energy production and absorption.

$$C_{Bat}(t) = C_{Bat}(t-1)(1-\sigma) + [P_{PV}(t) - \frac{P_{load}(t)}{\eta_{inv}}]\,\eta_{Bat} \quad \text{(III-45)}$$

$C_{Bat}(t)$ represents the battery bank's available power at a specific time t, while $C_{Bat}(t-1)$ indicates the power at the previous time. The symbol σ denotes the self-discharge rate, $P_{load}(t)$ represents the load requirement at time t, and the efficiencies of the battery and inverter are denoted as η_{Bat} and η_{inv}, respectively. The limits for $C_{Bat}(t)$ define in Eq. (III-46), the acceptable energy levels within a specified range between the minimum $C_{BatMin}$and maximum C_{BatMax} values.

$$C_{BatMin} \leq C_{Bat}(t) \leq C_{BatMax} \quad \text{(III-46)}$$

Managing battery performance in standalone RES, the maximum charging rate of the battery is determined by the product of the nominal battery capacity C_{Bat} and the total number of batteries N_{Bat} in Eq. (III-47). Additionally, the minimum number of batteries required is calculated in Eq. (III-48) based on the product of the power absorbed P_a , a factor related to the system's nominal capacity η_a, the battery efficiency η_{Bat}, and the DOD. The battery terminal voltage V_{Bat} is described in Eq. (III-49) as the difference between the output voltage V_{out} and various terms related to battery current i_{Bat}, internal resistance R_{Bat}, and charge/discharge characteristics, while the SOC of the battery is calculated in Eq. (III-50) and Eq. (III-51) based on the charging or discharging power, efficiency, and time [103].

$$SOC_{Max} = C_{Bat} N_{Bat} \quad \text{(III-47)}$$

$$N_{Bat} = \frac{P_a\ \eta_a}{C_{Bat}\ \eta_{Bat}\ DOD} \quad \text{(III-48)}$$

$$DOD\ V_{Bat=}\ V_{out} - i_{Bat}\ R_{Bat} - K\frac{Q}{Q - \int i_{Bat}dt} + Ae^{(-B\int i_B dt)} \quad \text{(III-49)}$$

$$SOC = 100(1 - \frac{\int i_{Bat}dt}{Q}) \quad \text{(III-50)}$$

The battery SOC is calculates as:

$$SOC(k) = \begin{cases} SOC(k-1) + [P_a(k) - P_l(k)]\ \eta_{Bat}\Delta T/C_{Bat}, for\ charging \\ SOC(k-1) - [P_l(k) - P_a(k)]\ \Delta T/\ \eta_{Bat}C_{Bat}, for\ discharging \end{cases} \quad \text{(III-51)}$$

The temperature dependence of battery performance can be modeled using the following equation:

$$T_{Bat} = T_{ambiant} + (R_{th}.I_{Bat}^2) \quad \text{(III-52)}$$

Where T_{Bat} represents the battery temperature, $T_{ambiant}$ is the ambient temperature, R_{th} is the thermal resistance of the battery, and I_{Bat} is the battery current.

The degradation of battery capacity over cycles is modeled by the equation:

$$C_{Cycle} = C_{nominale}.(1 - K_{deg}.n_{Cycle}) \quad \text{(III-53)}$$

where C_{Cycle} is the nominal capacity of the battery, K_{deg} is the degradation coefficient, and n_{Cycle}) represents the number of charge/discharge cycles.

The energy density of the battery, which is essential for system design, is calculated as:

$$E_{density} = Volume \,.\, C_{nominale} \quad \text{(III-54)}$$

where $C_{nominale}$ is the battery's nominal capacity, and Volume is the physical volume of the battery.

III.9 Structure and operation of Hybrid Renewable Energy Systems (HRES) with energy storage

The structure of a hybrid renewable energy system (HRES) involves combining multiple energy sources and storage units into one system to improve energy production and management [104].

A hybrid renewable energy system typically consists of multiple energy sources, with at least one being renewable, such as solar or wind power. This system may also include energy storage devices, like batteries, to help manage energy supply and demand [105].

Hybrid renewable energy systems (HRES) are designed to supply electricity to consumers in remote areas that lack access to traditional power grids. In these situations, the systems are sized according to the energy needs of the connected load, ensuring that RESs are prioritized over conventional energy sources.

This system helps balance the fluctuations in energy output from renewable sources, produces no greenhouse gas emissions, and can reduce peak energy consumption. Additionally, with energy storage devices like batteries, the system can continue to supply power even if the main energy source fails, making it especially useful for remote areas.

Hybrid energy systems with storage (HSHER) can be classified into two main categories based on their operation mode:

- The first category is "off-grid" systems, which operate completely independently from the public electricity grid, generating energy autonomously.
- The second category is "grid-connected" systems, which work alongside the electrical grid and can receive power from it if the hybrid system cannot meet energy demands, ensuring a reliable energy supply.

Various coupling modes for hybrid energy systems, which can be categorized into three primary groups: direct coupling to a direct current (DC) bus, coupling to an AC bus, and mixed DC-AC coupling. Each mode of coupling is designed to optimize the integration of different energy sources while addressing load requirements and minimizing installation costs. The accompanying flowchart in **Figure III.28** illustrates the most commonly used topologies, highlighting the structural configurations that facilitate efficient energy management in both isolated and grid-connected hybrid systems.

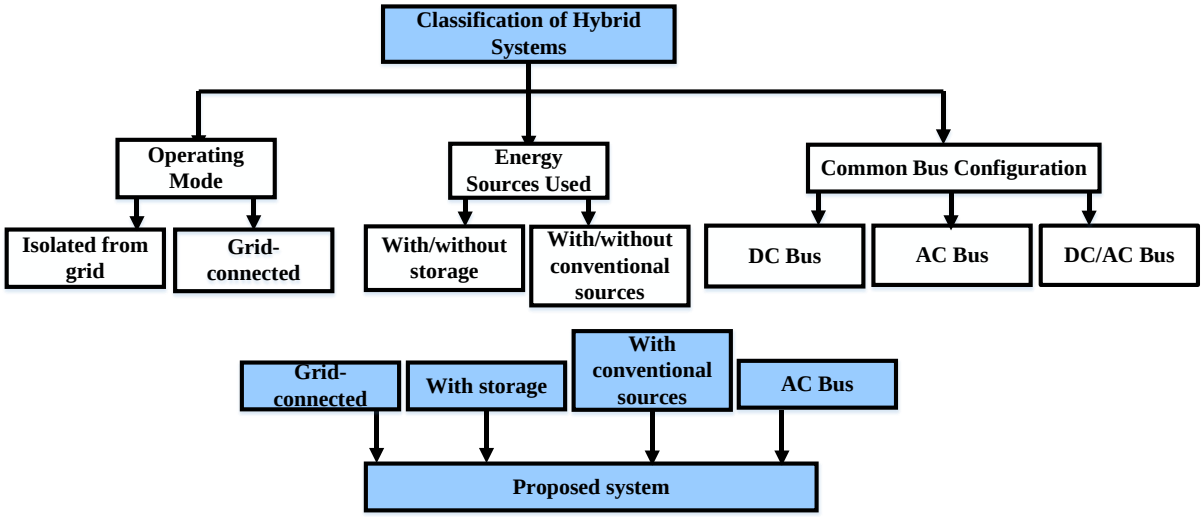

Figure III.28 Classification of hybrid systems

The AC coupling system in hybrid PV-wind energy systems (HSHERS) integrates each energy source to a common AC bus via its own static converter (DC/AC or AC/AC), facilitating direct connectivity to the public grid and alternative loads. This modular configuration enhances system flexibility and efficiency, allowing for seamless energy distribution and management [94]. As illustrated in **Figure III.29**, the AC hybrid system configuration promotes ease of energy dispatch, system expansion, and fault isolation, making it an attractive choice for modern hybrid renewable systems [20].

III.9.1 Simulation of the grid-connected HRES under linear and nonlinear loads

To assess the impact of power electronics and load type on the PQ of the proposed hybrid renewable energy system (HRES), simulations were carried out under both linear and nonlinear load conditions. The system includes PV, wind energy, and battery storage sources connected through power electronic converters (DC-DC, AC-DC, and DC-AC) to a common AC bus, as discussed in Section VI.

A. Linear load condition

Under linear loading, **Figure III.30** presents the simulation results:

- **Figure III.30 (a)** shows the source voltage and source current waveforms, where noticeable waveform deformation is observed, even though the load is linear. This distortion originates primarily from the switching operations of the power electronic converters used in interfacing the renewable sources with the AC grid.
- **Figure III.30 (b)** depicts the THD of the source voltage, measured at 9.80%.
- **Figure III.30 (c)** shows the THD of the source current, also at 9.78%.

These values highlight that even with linear loads, power electronic converters introduce significant harmonic distortion, degrading PQ at the PCC.

B. Nonlinear load condition

In the presence of nonlinear loads—such as diode-bridge rectifiers—the degradation of PQ becomes more pronounced. The simulation results under nonlinear loading are presented in **Figure III.31**:

- **Figure III.31 (a)** shows the source voltage and source current, which exhibit severe distortion, especially in the current waveform.
- **Figure III.31 (b)** presents the THD of the source voltage, recorded at 9.40%.
- **Figure III.31 (c)** reveals a dramatic increase in the THD of the source current, reaching 30.23%.

This stark contrast demonstrates the cumulative effects of both power electronic interfacing and nonlinear loading, which can cause unacceptable PQ levels if not mitigated.

These findings emphasize the necessity of implementing active power filtering techniques or advanced control strategies in HRES to maintain voltage and current quality within standard-compliant levels.

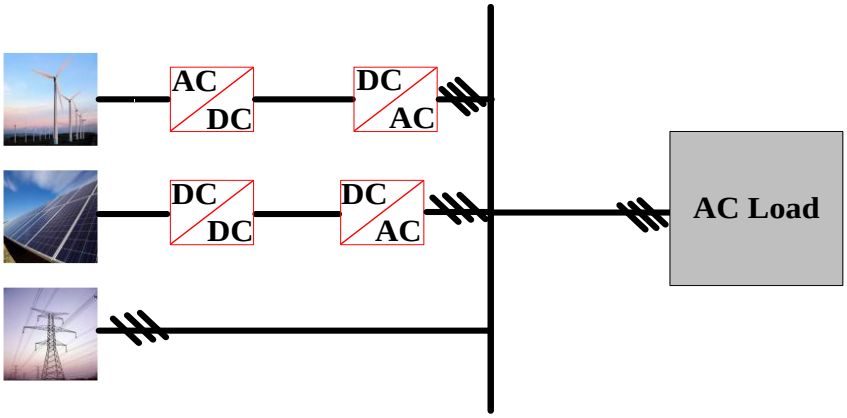

Figure III.29 AC hybrid systems

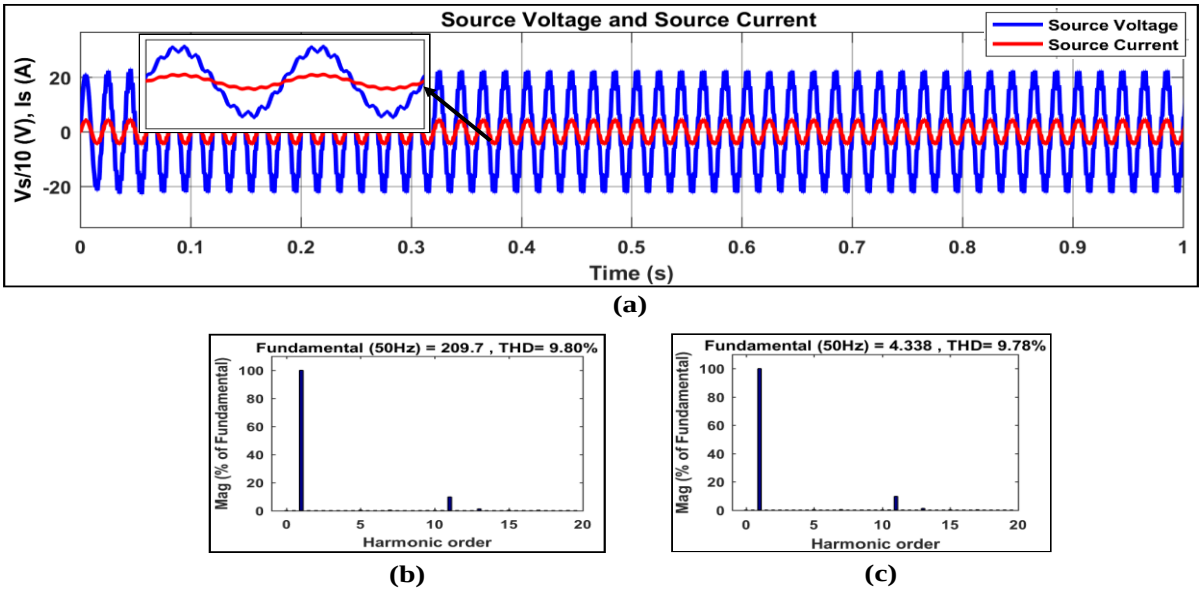

Figure III.30 Power quality analysis in a hybrid renewable energy system under Linear Load: (a) Source voltage and current, (b) THD of source voltage (9.80%), (c) THD of source current (9.78%)

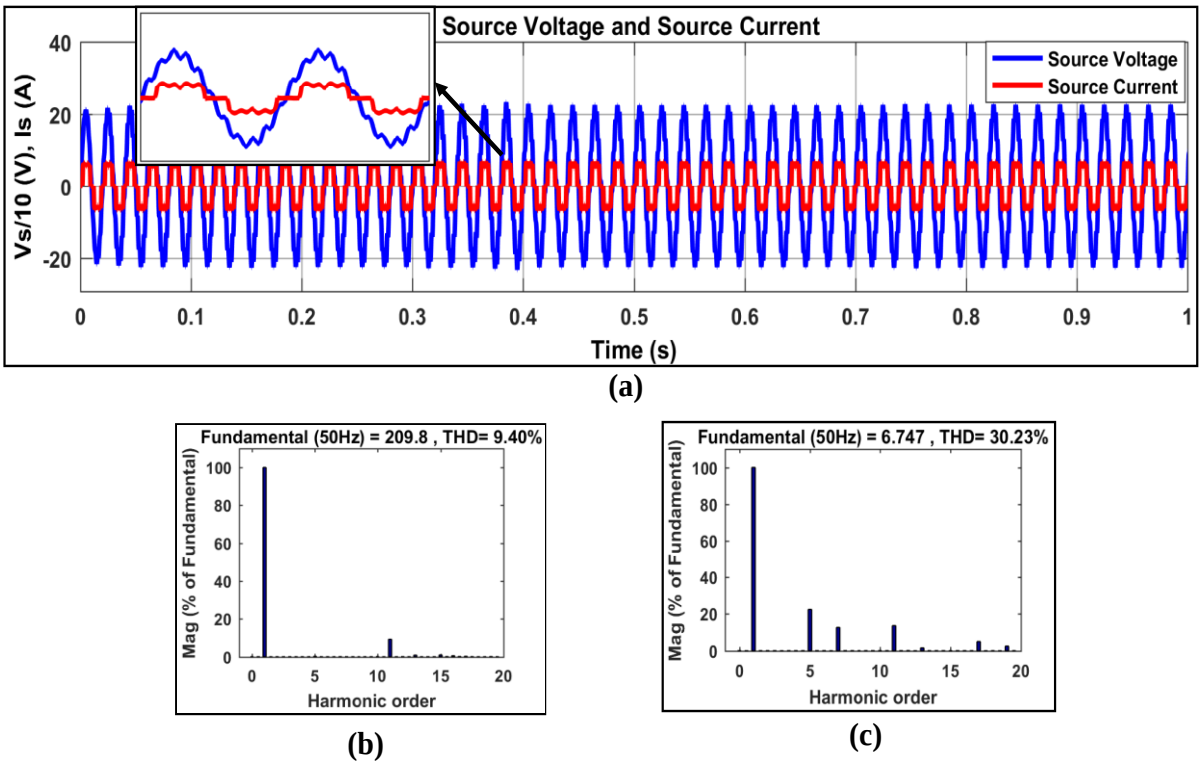

Figure III-31 Power quality analysis in a hybrid renewable energy system under nonlinear Load: (a) Source voltage and current, (b) THD of source voltage (9.40%), (c) THD of source current (30.23%)

III.10 Conclusion

This chapter presented the detailed modeling and simulation of a Hybrid Renewable Energy System (HRES) composed of PV, wind energy conversion systems (WECS), and BESS, all integrated into the electrical grid. Beginning with the PV subsystem, several MPPT algorithms INC, Perturb & Observe, Enhanced P&O, and Artificial Neural Networks—were implemented and compared under varying irradiance and temperature conditions. The results highlighted the strengths of AI-based techniques in providing faster and more stable tracking performance.

Subsequently, the wind energy system was modeled, including the WT, permanent magnet synchronous generator (PMSG), rectification stage, and associated MPPT controllers. MPPT strategies such as P&O, E-P&O, ANN, and fuzzy logic were also evaluated under fluctuating wind speeds, confirming again the superiority of intelligent control methods in tracking efficiency and system response.

The battery subsystem was integrated to support energy balance and improve system reliability, especially during intermittent RES output. The full hybrid system was then simulated under both linear and nonlinear load conditions.

Simulation results revealed that the source-side voltage was significantly distorted, due to the intermittent nature of RES and the impact of power electronic converters. Moreover, the inclusion of nonlinear loads introduced substantial harmonic distortion on the load side as well. These findings are consistent with the PQ disturbances previously identified in Chapter I and confirm that both the source and load sides of the HRES suffer from degradation in PQ.

These observations give rise to a critical need for comprehensive PQ conditioning, leading to the development of an integrated compensation solution. Therefore, the next chapter will introduce the UPQC, designed to mitigate both source-side and load-side disturbances. The UPQC will combine the most robust control strategies identified in Chapter II—UVTG for the series APF and SRF for the shunt APF—to ensure reliable and high-quality power delivery in grid-connected hybrid renewable energy systems.

Chapter IV:

Power Quality Enhancement in Grid-Connected Renewable Energy Systems Using Hybrid Active Filters

IV.1 Introduction

The growing penetration of renewable energy systems (RES), such as PV and wind energy systems (WES), into the electrical grid presents new challenges related to PQ. These challenges are primarily due to the nonlinear nature of power electronic interfaces and the variable behavior of renewable sources. While previous chapters addressed PQ issues individually—Chapter II focused on series and shunt APF, and Chapter III presented the structure and dynamics of hybrid RES—this chapter presents a holistic approach to PQ improvement in hybrid systems through integrated filtering solutions.

In this chapter, the integration of advanced filtering techniques is explored in the context of interconnected hybrid RES. Specifically, we investigate solutions that simultaneously mitigate disturbances at both the source and the load sides. This comprehensive strategy aims to ensure voltage stability, minimize harmonic distortion, and maintain system reliability under varying operating conditions.

The first part of this chapter focuses on mitigating source-side disturbances using a series APF. The Series APF is implemented in a hybrid PV-wind system, where it plays a crucial role in suppressing voltage harmonics caused by power electronic components interfacing the RES with the AC grid. The performance of the Series APF is validated through various case studies involving voltage dips, swells, and short circuits.

The second part expands the scope of the solution by integrating a UPQC, which combines the functionality of series and shunt filters. The UPQC is employed to mitigate disturbances originating both from the source side (e.g., harmonic voltage due to inverters) and the load side (e.g., nonlinear and unbalanced loads), thereby ensuring an enhanced level of PQ across the entire system.

This integrated approach reflects the real-world complexity of modern distributed energy systems and addresses the demand for smarter, more resilient power infrastructures.

IV.2 Modeling of the integrated PQ system using UVTG coordination

In this section, we develop the mathematical modeling of the integrated system composed of a Series APF, PV, and Wind Energy systems, all connected to a unified grid node. While the UVTG and VOC techniques were independently presented in Chapters II and III, here we focus on their coordinated control behavior under hybrid disturbances.

IV.2.1. System overview and power Flow architecture

The grid-connected hybrid system is modeled to enable simultaneous compensation for voltage sags/swells, harmonic distortions, and reactive power imbalance. The Series APF compensates voltage distortions, while the PV and Wind systems are controlled for DC link stability and grid current shaping. The novelty of this model lies in its unified control synchronization and the cooperative PQ enhancement.

IV.2.2. Coordinated UVTG-based reference generation

UVTG-based reference signal extraction has been applied to both Series APF (Chapter II) and PV/Wind systems (Chapter III). In this integrated model, these references are now synchronized via a common Phase-Locked Loop (PLL), ensuring that the Series APF and RES converters respond to grid disturbances with unified phase and frequency alignment.

IV.2.3 Mathematical modeling of the coordinated PV-Wind-Grid integration using series APF with UVTG

This section presents a detailed mathematical model of the integration of PV, wind energy systems (WES), and the electrical grid at a common coupling point (PCC), coordinated through a Series APF based on the Unit Vector Template Generator (UVTG) strategy. This setup ensures voltage stability, harmonic compensation, and power balance under dynamic operating conditions.

A. Power balance at the PCC

The total instantaneous active power injected at the PCC from the three sources (PV, Wind, Grid) must balance the power consumed by the load and system losses:

$$P_{PV}(t) + P_{Wind}(t) + P_{Grid}(t) = P_{Load}(t) + P_{Loss}(t) \quad \text{(IV-1)}$$

Assuming negligible losses:

$$\boldsymbol{P_{PV}(t) + P_{Wind}(t) + P_{Grid}(t) = P_{Load}(t)} \quad \text{(IV-2)}$$

Where:

$$\boldsymbol{P_{PV}(t) = V_{PCC}(t)\, i_{PV}(t)} \quad \text{(IV-3)}$$
$$\boldsymbol{P_{Wind}(t) = V_{PCC}(t)\, i_{Wind}(t)} \quad \text{(IV-4)}$$
$$\boldsymbol{P_{Grid}(t) = V_{PCC}(t)\, i_{Grid}(t)} \quad \text{(IV-5)}$$

Each of these sources is controlled to inject current at unity power factor.

B. UVTG-Based Voltage Reference Extraction

The UVTG control technique derives a unit voltage vector from the PCC voltages, which serves as the reference frame for synchronized control:

$$\boldsymbol{v_{abc}(t) = \frac{v_{abc}(t)}{\|v_{abc}(t)\|} = \frac{v_{abc}(t)}{V_m}(t)} \quad \text{(IV-6)}$$

Where:

$\boldsymbol{v_{abc}(t)}$: is the three-phase PCC voltage and $\boldsymbol{V_m}$ is the peak amplitude of the PCC voltage.

This unit vector is used in two ways:

- For synchronizing the phase and frequency of PV and Wind converters.

- For generating the reference voltage that the Series APF must inject to compensate distortions:

$$v_{ref}(t) = v_{desired}\,(t)\; v_{abc}(t) \quad \text{(IV-7)}$$

$$v_{inj}(t) \;=\; v_{ref}(t) \;-\; V_{PCC}(t) \quad \text{(IV-8)}$$

This injected voltage by the Series APF compensates harmonic distortion, voltage dips, swells, and imbalances.

C. dq Transformation and Reference Currents

To control each source efficiently in the SRF, we use Park's transformation:

$$\begin{bmatrix} i_d \\ i_q \end{bmatrix} = \frac{2}{3}\begin{bmatrix} cos(\theta) & cos(\theta - \frac{2\pi}{3}) & cos(\theta + \frac{2\pi}{3}) \\ sin(\theta) & sin(\theta - \frac{2\pi}{3}) & sin(\theta + \frac{2\pi}{3}) \end{bmatrix} \quad \text{(IV-9)}$$

Where θ is the grid voltage angle derived from a Phase-Locked Loop (PLL).

For both PV and Wind inverters, the control objective is to inject only active power, hence the reference dq currents are:

$$i_d^* = \frac{2}{3}\frac{P^*}{v_d},\; i_q^* = 0$$

These are compared with measured currents and controlled using PI controllers.

D. Series APF voltage injection modeling

The Series APF acts as a controlled voltage source in series with the PCC. Its operation is governed by:

$$v_{Series\ APF}(t) \;=\; v_{ref}(t) \;-\; V_{PCC}(t) \quad \text{(IV-10)}$$

This ensures that:

$$V_{PCC}(t) \;+\; v_{Series\ APF}(t) \;=\; v_{ref}(t) \quad \text{(IV-11)}$$

To maintain a sinusoidal voltage at the load terminals.

In the dq frame, the dynamics of Series APF injection are:

$$L_f\,\frac{di_d}{dt} = -\,R_f\; i_d + V_{d\_Series\ APF} - V_{d\_PCC} + w\; L_f i_q \quad \text{(IV-12)}$$

$$L_f\,\frac{di_q}{dt} = -\,R_f\; i_q + V_{q\_Series\ APF} - V_{q\_PCC} - w\; L_f i_d \quad \text{(IV-13)}$$

Where:

L_f, R_f are the Series APF filter inductance and resistance.

w is the grid angular frequency.

Decoupling and PI controllers are used to regulate i_d, i_q to follow the desired reference values.

E. PLL-based synchronization

All components (PV, Wind, Series APF) are synchronized through a shared PLL block that estimates the grid angle θ. The PLL operates on the αβ voltage components:

$$v_\alpha = v_\alpha,\ v_\beta = \frac{1}{\sqrt{3}}(v_b - v_c) \quad \text{(IV-14)}$$

$$\theta = \int w_{Grid}\, dt \quad \text{(IV-15)}$$

A PI controller adjusts w_{Grid} to align , $v_\beta \rightarrow 0$, locking the dq frame to the grid voltage vector.

F. Summary of control objectives

To achieve coordinated and reliable operation of the hybrid system, each subsystem is assigned a specific control objective, targeting either power regulation, voltage compensation, or synchronization. A detailed summary of these control objectives and their corresponding controlled variables is presented in **Table IV-1**.

Table IV-1 Control objectives and corresponding controlled variables for each subsystem in the proposed hybrid PQ system

Subsystem	Objective	Controlled variable
PV inverter	Inject active power	$i_d^*,\ i_q^* = 0$
Wind inverter	Inject active power	$i_d^*,\ i_q^* = 0$
Series APF	Compensate voltage distortions	v_{inj}
PLL	Ensure synchronism (θ, w)	$\theta(t), w(t)$
UVTG	Generate unified voltage reference	$v_{abc}(t)$

Figure IV-1 shows the proposed system configuration, where a hybrid PV–wind system is integrated with a three-phase, three-wire grid through a Series APF operating under a UVTG-based control algorithm. The Series APF improves the PQ at the PCC by compensating voltage disturbances such as swells, sags, dips, short circuits, and harmonic distortions. The grid voltage at the operating point is 254V (line-to-line) at 50 Hz.

The renewable system consists of two PV arrays, each rated at 4 kW, totaling 8 kW, and a wind energy system capable of producing up to 30 kW. Both PV and wind sources are connected to the AC grid via DC-DC boost converters followed by DC-AC inverters. The distorted source voltage (V_S) is corrected by the Series APF through the injection of compensating voltage (V_{inj}), resulting in a clean, balanced PCC voltage (V_{PCC}) for supplying sensitive loads.

The UVTG algorithm processes measured grid currents and voltages ($\boldsymbol{i_{G\_abc}}, \boldsymbol{V_{G\_abc}}$) to generate an appropriate reference voltage ($V^*_{ref\_abc}$) for the Series APF. Hysteresis control ensures dynamic tracking of the reference voltage, providing fast response and robust compensation under varying dynamic conditions.

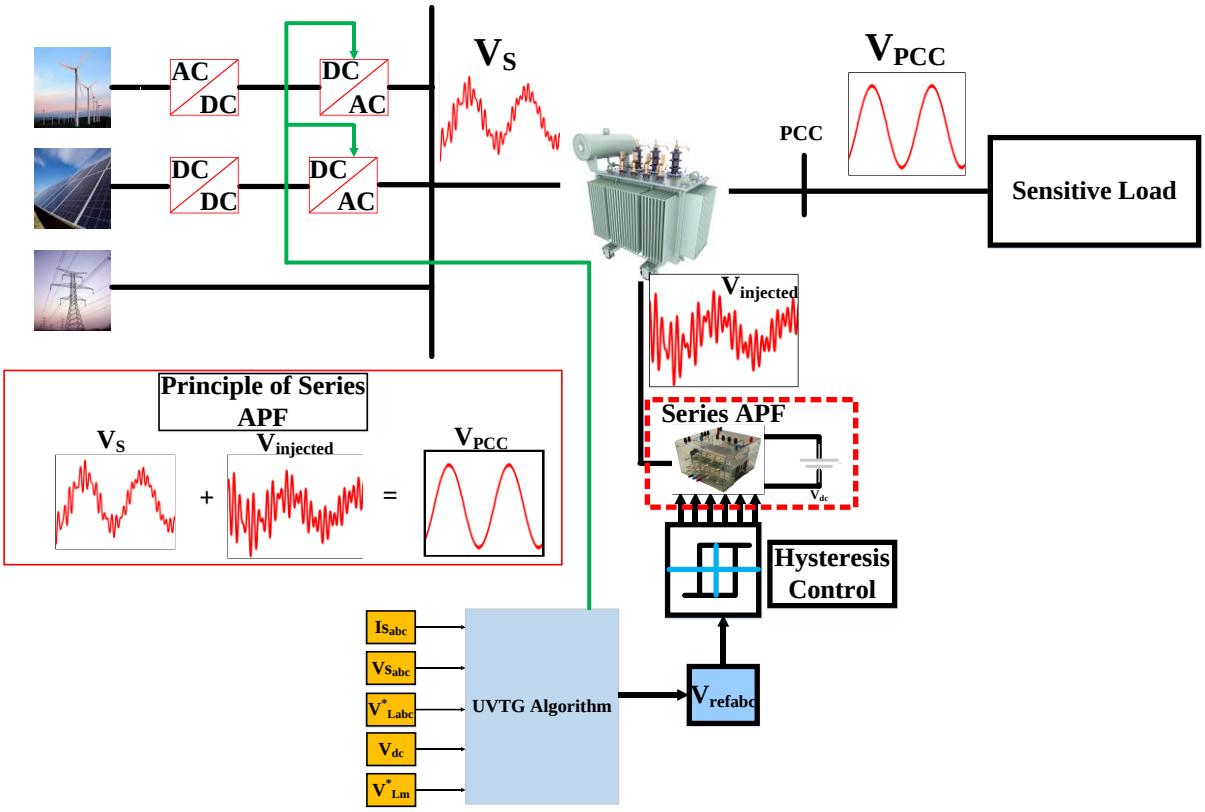

Figure IV.1. The suggested structure configuration: integrating solar PV panels with WE and connecting them to the grid using UVTG and the series APF ALSO using uvtg

IV.3 Simulation results and performance analysis of the PV–Wind–Grid integrated series APF system

IV.3.1 Voltage harmonic mitigation

This section presents the analysis of voltage harmonic distortion within the PV–Wind system integrated with the electrical grid. The primary focus is on the degradation of voltage quality due to the nonlinear characteristics of power electronic interfaces, notably the inverters associated with RESs.

Figure IV-2 illustrates the source voltage waveform during the time interval between 0.5 and 0.6 seconds. A clear deformation of the waveform is observed, leading to an increase in voltage distortion and a corresponding rise in THD levels. In the absence of the series APF, the load voltage THD reaches a value of 9.13%, as depicted in **Figure IV-3 (a)**. This elevated THD is primarily attributed to the integration of PV and wind systems, where the associated power electronic converters introduce significant harmonic components into the grid.

The implementation of the Series APF notably improves the voltage quality. As shown in **Figure IV-2**, following the activation of the Series APF, the THD value of the load voltage is drastically reduced to 0.12% during the interval from 0.5 to 0.7 seconds, as presented in **Figure IV-3 (b)**. This considerable reduction highlights the effectiveness of the Series APF in mitigating voltage harmonics and enhancing the PQ of the grid-connected hybrid system.

Furthermore, **Figure IV-2** demonstrates the overall improvement in the load voltage waveform throughout the specified time interval, confirming the Series APF's capacity to suppress distortions and maintain voltage stability. By minimizing harmonic distortions and reducing the THD, the Series APF significantly contributes to enhancing the quality and reliability of the delivered power.

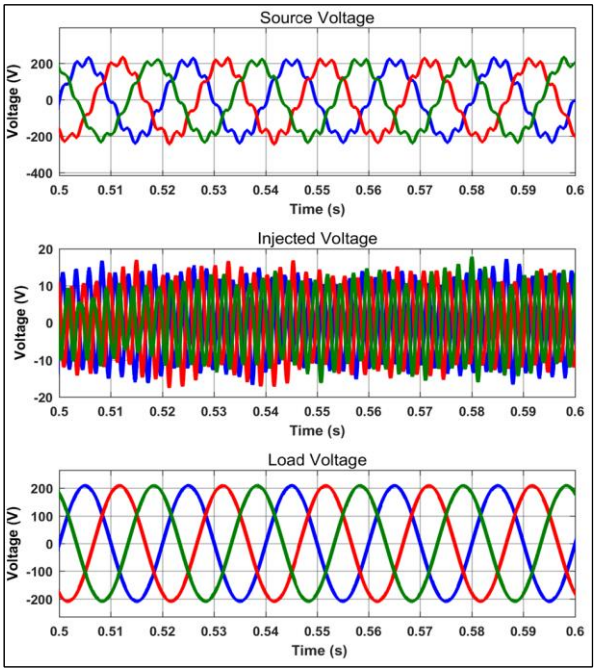

Figure IV.2. Source voltage, injected Series APF, and load terminals voltage

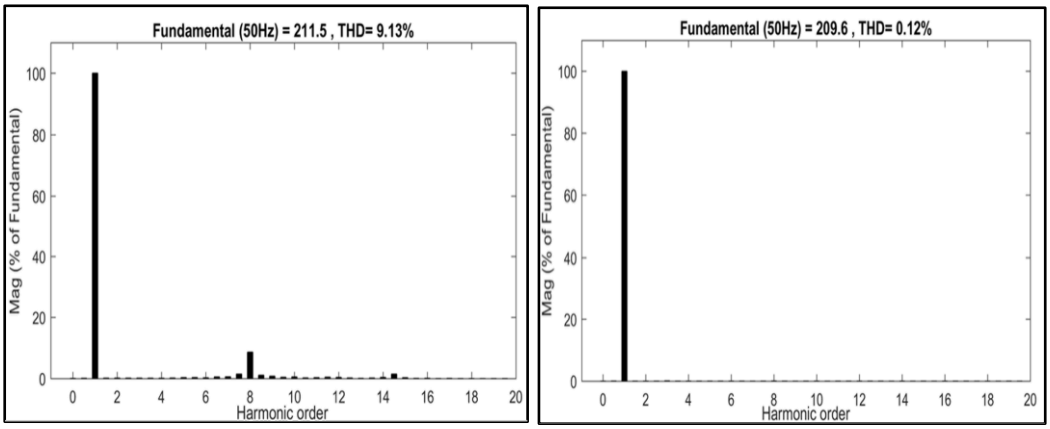

(a) (b)

Figure IV.3. THD analysis: (a) Load voltage before using Series APF and (b) Load voltage after using Series APF

IV.3.2 Compensation of voltage disturbances

In this section, the impact of voltage disruptions—including sags, swells, dips, and short circuits—is examined, along with an evaluation of the series APF performance in maintaining voltage quality under these adverse conditions.

Upon the integration of the Series APF, it is observed that the filter significantly enhances the voltage profile, mitigating the effects of disturbances and preventing voltage sag events. As illustrated in **Figure IV-4**, a voltage sag is applied between 0.1 and 0.2 seconds. Despite this disturbance, the Series APF maintains the voltage waveform with minimal deformation, effectively preserving voltage quality.

Similarly, a voltage swell scenario is introduced between 0.3 and 0.4 seconds, as shown in **Figure IV-6**. Again, the Series APF successfully regulates the voltage, ensuring that the load voltage remains stable and within acceptable limits, even under elevated voltage conditions. The behavior of the system during a voltage dip is depicted in **Figure IV-8**, further confirming the Series APF's ability to sustain voltage stability during various forms of disruptions.

Figures IV-5, **IV-7**, and **IV-9** provide detailed THD analyses for voltage signals under sag, swell, and dip conditions, respectively, both at the source and load sides. These results indicate that voltage disruptions not only alter voltage magnitudes but also increase harmonic distortion levels. However, the Series APF efficiently counteracts these adverse effects, improving the overall PQ by significantly reducing THD values.

Without Series APF intervention, the THD values at both the source and load sides exceed 5%, which is considered unacceptable for the operating voltage range. In contrast, with the Series APF active, the load-side voltage THD is consistently reduced to below 5% during sag, swell, and dip conditions, demonstrating the filter's effectiveness in minimizing harmonic distortions.

Moreover, when subjected to a three-phase short circuit with impedance, the Series APF injects compensating voltages to stabilize the load voltage at the PCC, as depicted in **Figure IV-10**. This response highlights the dynamic adaptability of the Series APF to sudden and severe faults within the system.

Overall, the simulation results affirm that the Series APF consistently provides superior THD reduction and voltage stabilization under a wide range of voltage disruption scenarios. However, it is noted that although the Series APF markedly improves PQ during disturbances, THD levels during sag, swell, and dip events remain slightly higher compared to those observed under normal, disturbance-free conditions.

These findings underscore the Series APF's vital role in enhancing grid-connected PV–Wind hybrid system performance, ensuring improved PQ and robust operation even under challenging grid conditions.

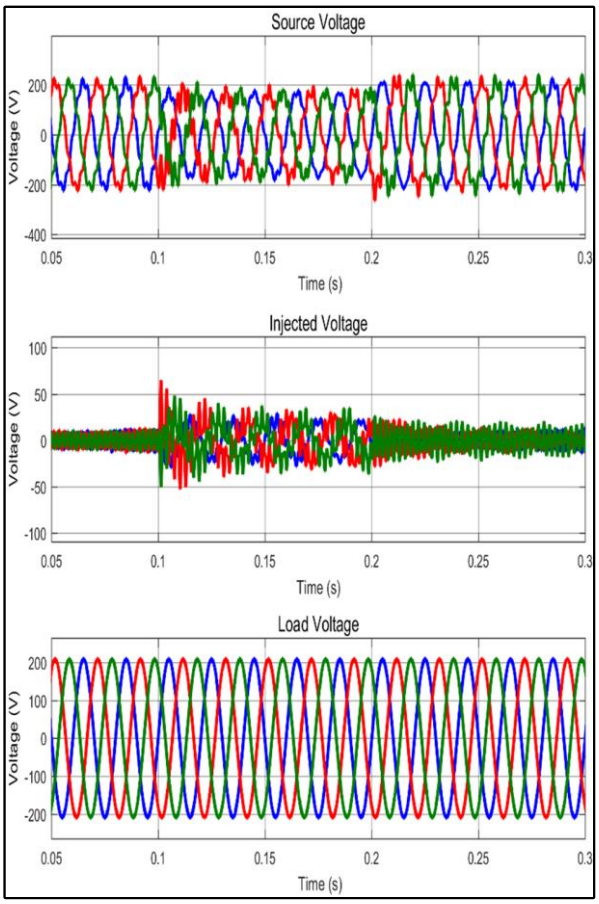

Figure IV.4. Voltage response during voltage sag: Source voltage, injected Series APF, and load terminals voltage

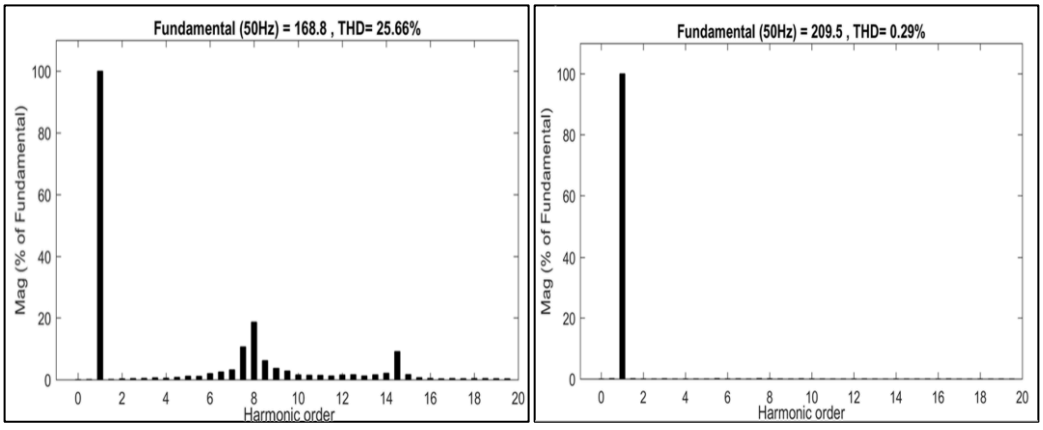

(a) (b)

Figure IV.5. THD Analysis: (a) Source voltage during voltage sag, (b) Load terminal voltage during voltage sag

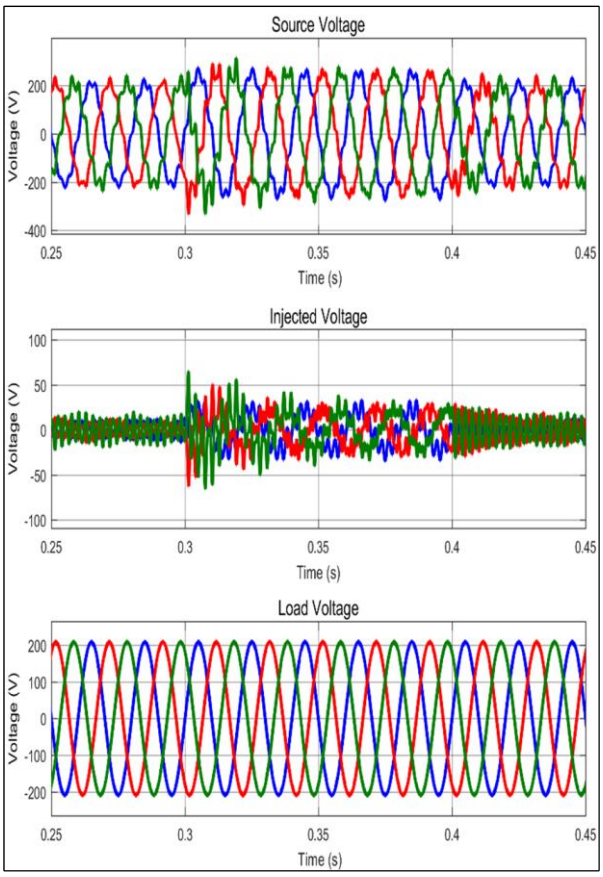

Figure IV.6. Voltage swell analysis: Source voltage, injected Series APF, and load terminals voltage

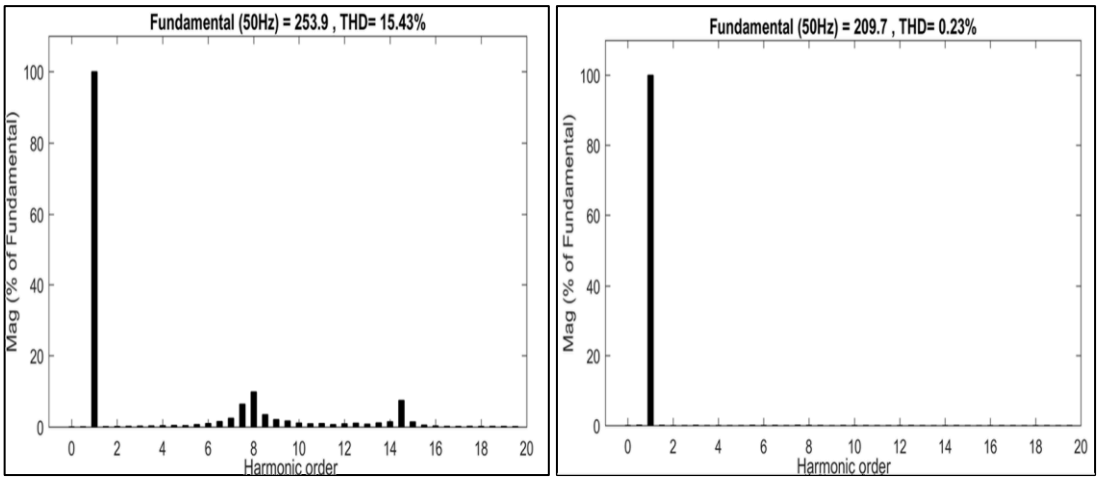

(a) (b)

Figure IV.7. THD analysis: (a) Source voltage during voltage swell, (b) Load terminal voltage during voltage swell

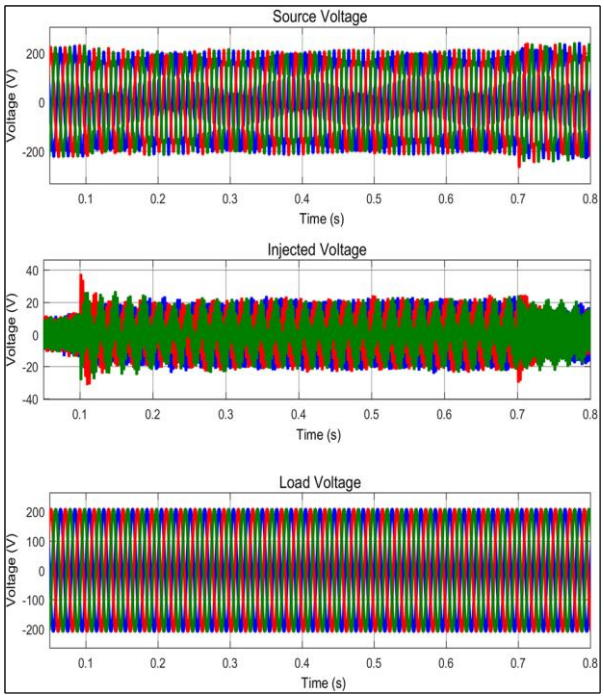

Figure IV.8. Voltage dips analysis: Source voltage, injected Series APF, and load terminals voltage

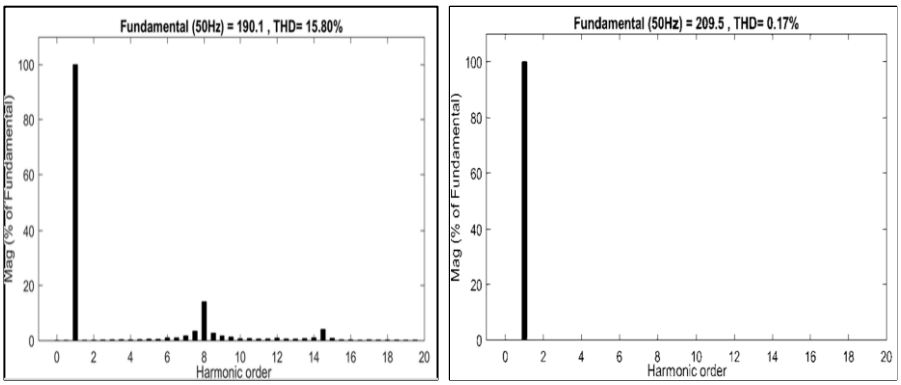

(a) (b)

Figure IV.9. THD Analysis: (a) Source voltage during voltage dips, (b) Load terminal voltage during voltage dips

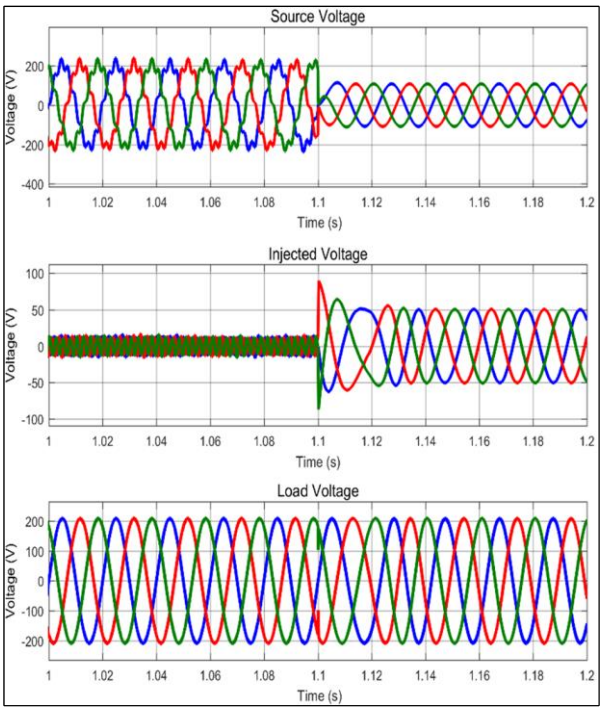

Fig. IV-10: Short circuit analysis: Source voltage, injected Series APF, and load terminals voltage

IV.4. Unified Power Quality Conditioner (UPQC) implementation for simultaneous source and load side compensation

After successfully mitigating voltage harmonic issues originating from the source side through the series APF, the next critical step involves addressing disturbances introduced by nonlinear loads (NL) at the load side. This necessity leads to the development of a more comprehensive solution: the deployment of the UPQC.

IV.4.1. System overview

Figure IV.11 presents the overall system architecture, illustrating the integration of the Grid–PV–Wind systems with nonlinear loads and the UPQC. In this configuration:

- The UVTG algorithm performs a dual role:
    1. It controls the converters to facilitate the seamless and stable integration of PV and Wind energy into the grid [6].
    2. It generates the voltage reference signals for the series part of the UPQC to actively mitigate voltage disturbances, including sags, swells, and voltage harmonics [6].

- Simultaneously, the SRF algorithm is employed for the shunt part of the UPQC to:
    1. Generate current reference signals for compensating load current harmonics and reactive power components, ensuring sinusoidal current injection into the grid.

This coordinated dual-control strategy (UVTG + SRF) ensures comprehensive mitigation of PQ issues, offering enhanced voltage regulation, current quality improvement, and increased stability for renewable energy-integrated systems.

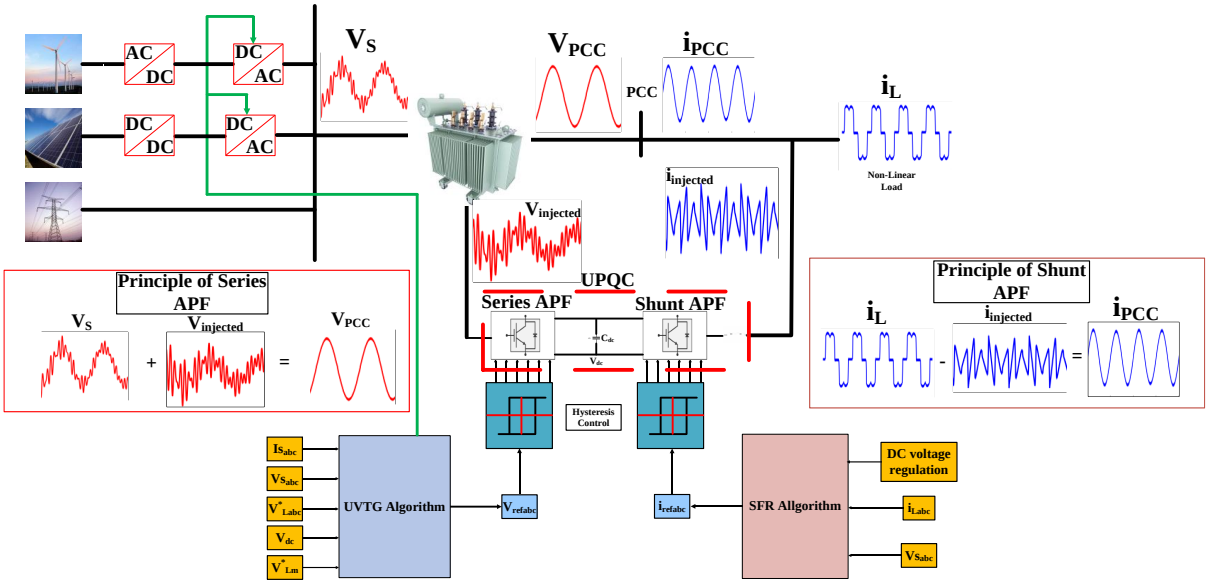

Figure IV.11. Integration of grid-PV-wind systems with NL and UPQC: System overview

A. Summary of series APF operation

As detailed in Chapter 2, the series APF is responsible for mitigating voltage-related disturbances such as voltage sags, swells, and harmonics from the source side. By injecting a compensating voltage in series with the supply, it ensures that the PCC voltage remains stable and within acceptable limits.

B. Summary of shunt APF operation

The Shunt APF, discussed previously, focuses on addressing current-related issues, particularly those introduced by nonlinear loads. It injects compensating currents into the system to cancel out load current harmonics and reactive power demands, ensuring sinusoidal current flow from the source.

C. Role of the UPQC in the integrated system

The UPQC combines the functionalities of both the series and shunt APFs, offering a holistic solution to PQ issues. In the proposed system (illustrated in **Figure IV.11**), the series APF manages voltage disturbances from the grid side, while the shunt APF compensates for current distortions caused by nonlinear loads [106].

By working in coordination, controlled respectively by the UVTG and SRF algorithms, the UPQC ensures:

- **Mitigation of voltage sags, swells, and harmonics.**
- **Compensation for load current harmonics and imbalances.**

- **Enhancement of overall power quality (PQ) and system stability in the presence of renewable energy sources.**

IV.5. UVTG-Controlled integration of PV and Wind systems with grid and UPQC coordination

The grid-connected PV system, shown in **Figure IV-12**, integrates a PV array with the utility grid through a DC-DC boost converter, a DC-AC inverter, and a control system based on the UVTG algorithm. The UVTG algorithm governs the inverter control to enable smooth power transfer, ensuring that the PV system synchronizes properly with the grid. Additionally, the UVTG provides critical voltage references that assist the series part of the UPQC to mitigate voltage disturbances, while the SRF-based controller manages the shunt part for current harmonics compensation.

Similarly, the wind power integration system, illustrated in **Figure IV-13**, utilizes a WT connected to a stator induction generator, followed by an AC-DC-AC converter. The UVTG algorithm plays a dual role here: it stabilizes the power injection from the wind system into the grid and simultaneously coordinates with the UPQC to manage both voltage and current quality at the PCC. Through the UVTG-driven inverter control and PLL synchronization, the system achieves stable operation despite fluctuations in wind energy.

Together**, Figures IV-12** and **IV-13** emphasize the critical function of the UVTG algorithm in facilitating the seamless integration of RESs (PV and wind) with the grid while enhancing PQ through effective coordination with the UPQC.

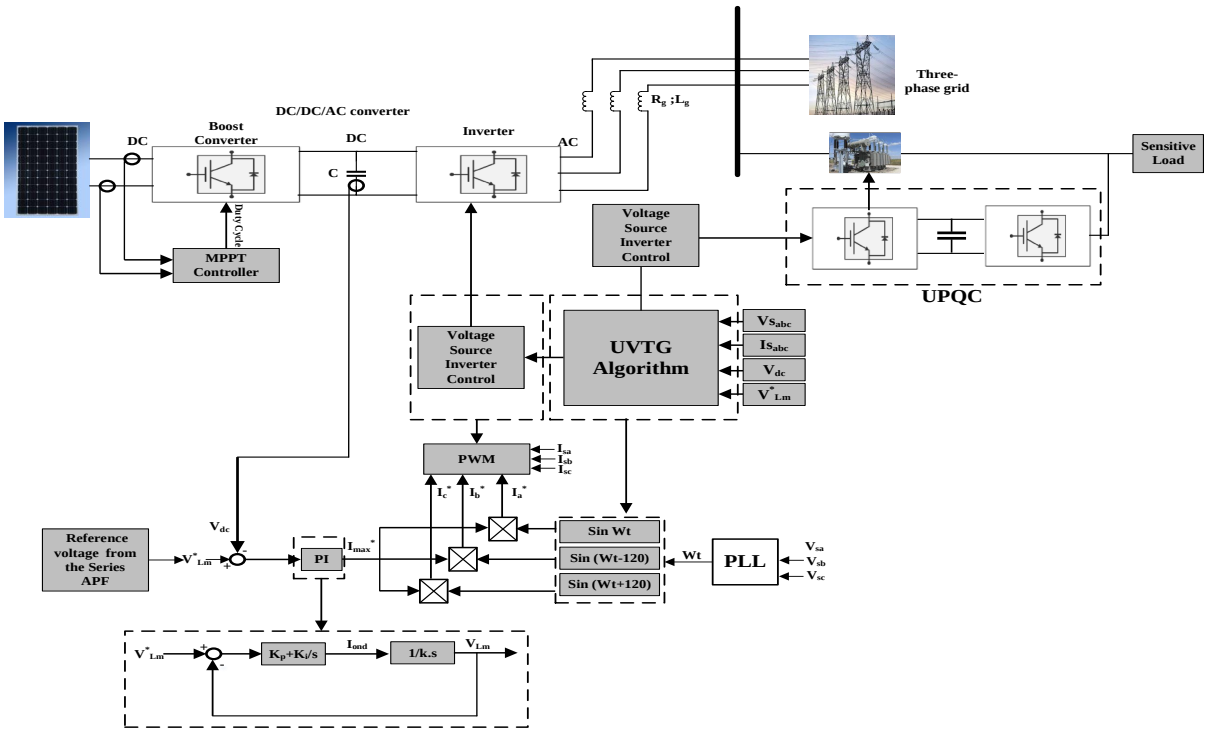

Figure IV.12. Integration of PV power systems with converters into the grid.

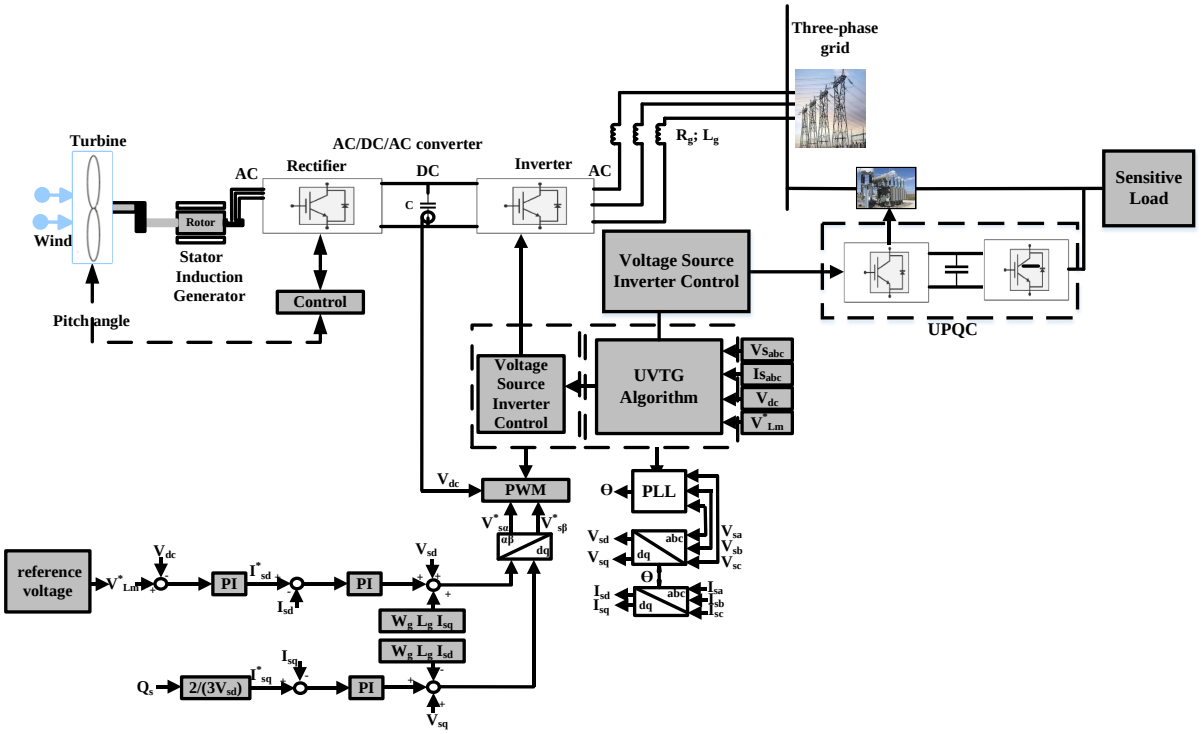

Figure IV.13. Integration of wind power systems with converters into the grid.

IV.6. Simulation results and performance analysis of the UPQC in grid-connected PV-Wind systems

After detailing the system integration and control strategies, this section presents the simulation results that validate the effectiveness of the proposed UPQC system.

The performance of the UPQC is assessed under different operating conditions, focusing on its ability to mitigate voltage disturbances from the source side and current harmonics introduced by nonlinear loads on the load side [50].

IV.6.1. Normal condition Test: Harmonic analysis under renewable integration and nonlinear load

The Normal Condition Test primarily focuses on analyzing the harmonic distortion of the grid-connected PV–Wind system with nonlinear loads (NL), under standard operating conditions without additional external disturbances.

The primary sources of voltage distortion in this scenario are the integration of RES via power electronics and the nonlinear current drawn by the NL. This test evaluates both current harmonics, originating from the NL, and voltage harmonics, resulting from the RES integration into the grid.

Figure IV.14 illustrates the source voltage waveform during the interval between 0.1 s and 0.2 s. It is observed that the voltage is noticeably distorted, contributing to elevated THD values.

In the absence of UPQC compensation, the load voltage exhibits a THD of 9.8%, as shown in **Figure IV.16 (a)**.

This high distortion level is attributed to the power electronic converters interfacing the RES with the grid, leading to deteriorated voltage quality.

The integration of the UPQC into the system significantly improves voltage quality. As demonstrated in **Figure IV.14**, the UPQC effectively mitigates voltage distortions, reducing the load voltage THD from 9.8% to 1.07%, as illustrated in **Figure IV.16 (b)**.

This substantial reduction highlights the UPQC's critical role in enhancing the PQ of grid-connected PV–Wind–Energy (PV-WE) systems by suppressing voltage harmonics induced by RES converters.

Similarly, the influence of the UPQC on current harmonics is depicted in **Figure IV.15**. Initially, the NL current exhibits a high THD value of 27.56%, indicating considerable harmonic content due to nonlinear loading. Upon UPQC activation at 0.1 s, the THD of the load current dramatically decreases to 1.91%, as presented in **Figure IV.17 (a)**.

This improvement demonstrates the UPQC's effectiveness in injecting compensating currents through its shunt part, thereby neutralizing the harmonic components and restoring a sinusoidal current profile.

Thus, the UPQC proves to be a vital element for achieving comprehensive PQ enhancement by addressing both voltage and current distortions, ensuring a cleaner, more reliable power supply in renewable energy-integrated grids.

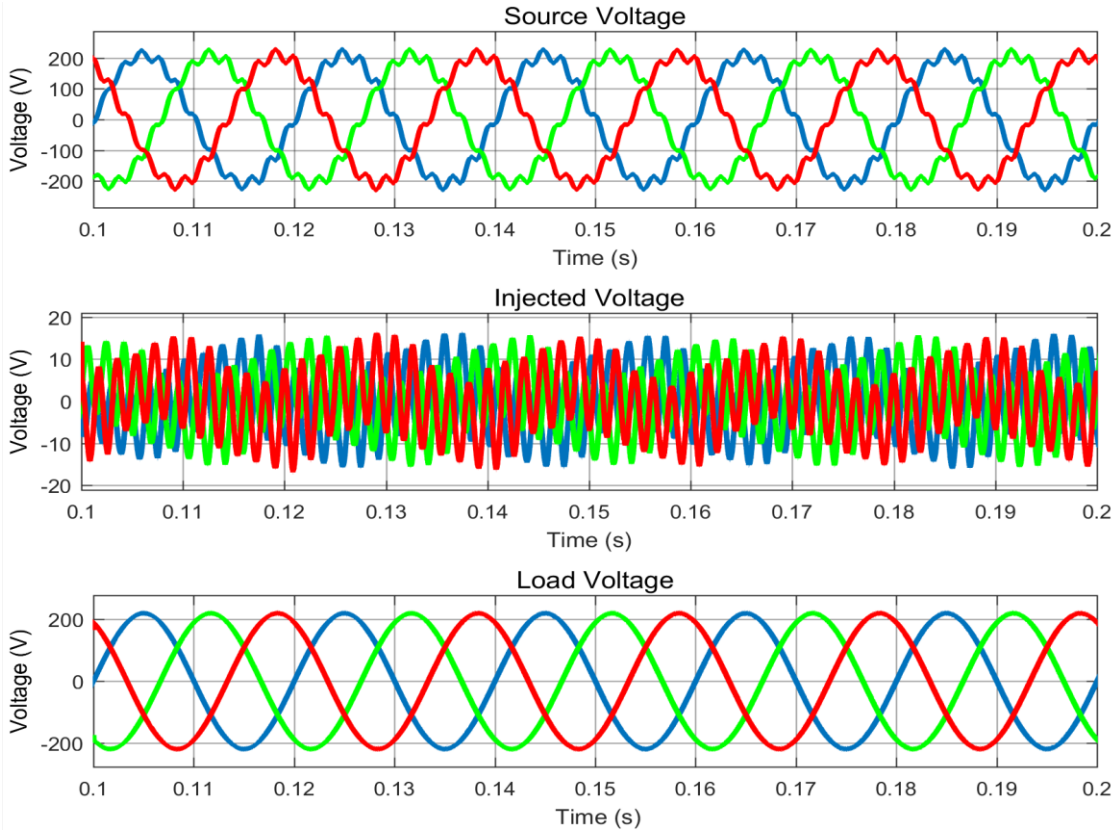

Figure IV.14. Voltage analysis: Source, Injected APF, and load terminals

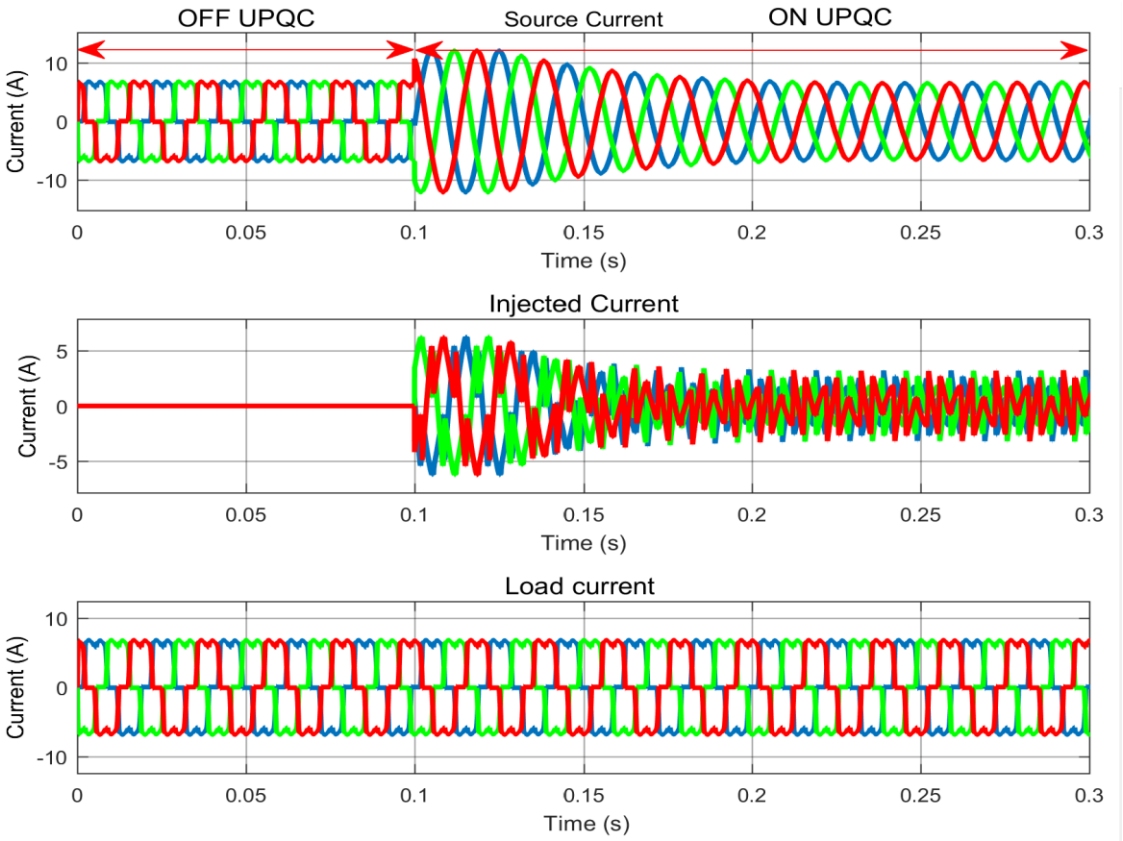

Figure IV.15. Current analysis: Source, Injected APF, and load terminals

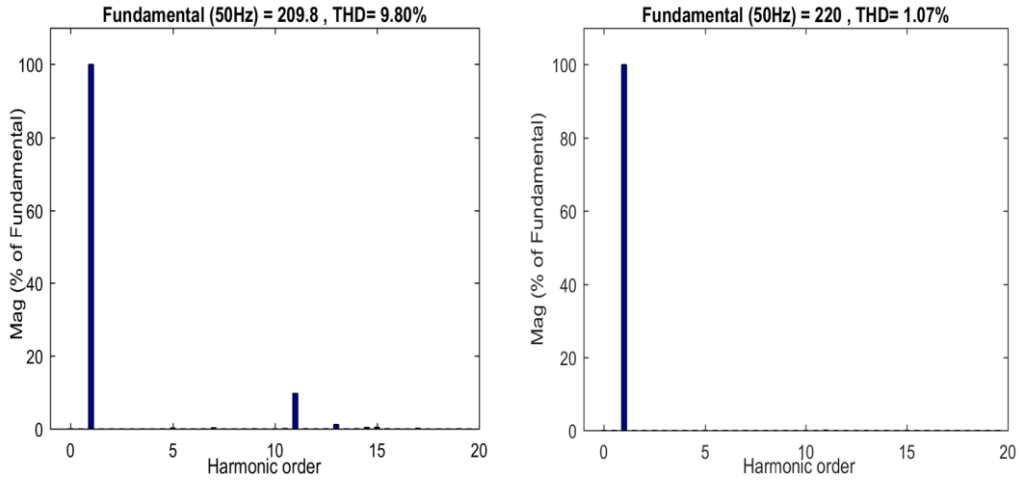

(a) **(b)**

Figure IV.16. THD voltage analysis: (a) Source voltage, (b) Load voltage

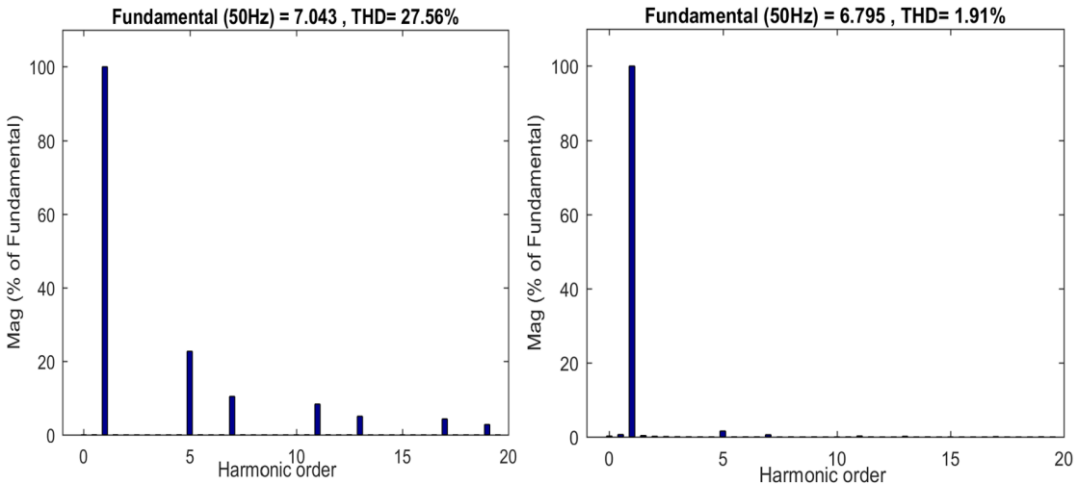

(a) **(b)**

Figure IV.17. THD current analysis: (a) Load current, (b) Source current

Furthermore, **Figure IV-18** illustrates the voltage at the DC bus, maintained steadily at 440 V, confirming effective regulation and control by the UPQC system. The waveforms of both the PCC voltage and PCC current are also shown to be sinusoidal and free from significant harmonic distortion.

This result highlights the UPQC's capability not only in harmonic mitigation but also in maintaining voltage and current stability at the PCC, ensuring a clean and reliable power supply to the grid.

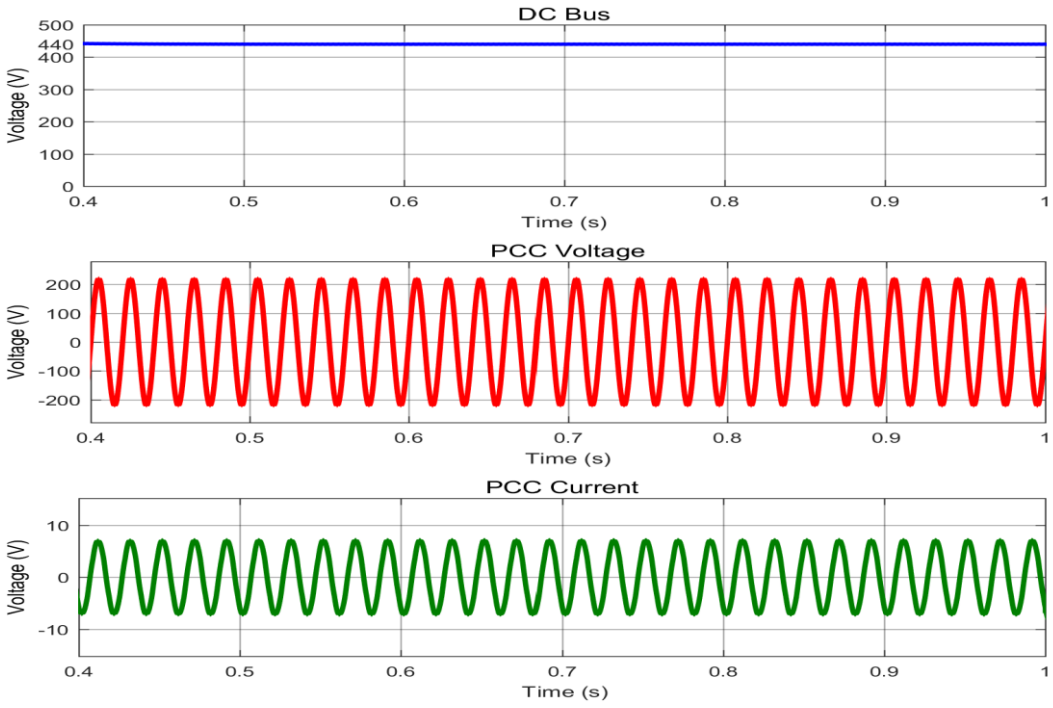

Figure IV.18. Voltage and current analysis: DC Bus, PCC voltage, and PCC current

IV.6.2. Fault analysis: Unbalanced voltage sag and swell

Figure IV.19 presents the source voltage, injected voltage, and load voltage waveforms over the time interval from 0.05 s to 0.45 s, under conditions of a 20% unbalanced voltage sag and swell.

During the period between 0.1 s and 0.2 s, the system experiences an unbalanced voltage sag. The series component of the UPQC, operating under the UVTG algorithm, accurately detects two simultaneous disturbances: harmonic distortions introduced by the integration of the PV–Wind system into the grid and the unbalanced voltage sag from the source.

In response, the UPQC injects the necessary compensating voltage, ensuring that the load voltage remains stable, sinusoidal, and unaffected by these disturbances.

Similarly, between 0.3 s and 0.4 s, when an unbalanced voltage swell occurs, the UPQC once again detects both the unbalanced swell and the accompanying harmonics. Through timely injection of compensatory voltage, it maintains a clean and stable load voltage, effectively mitigating the impact of the fault and preserving PQ at the load terminals.

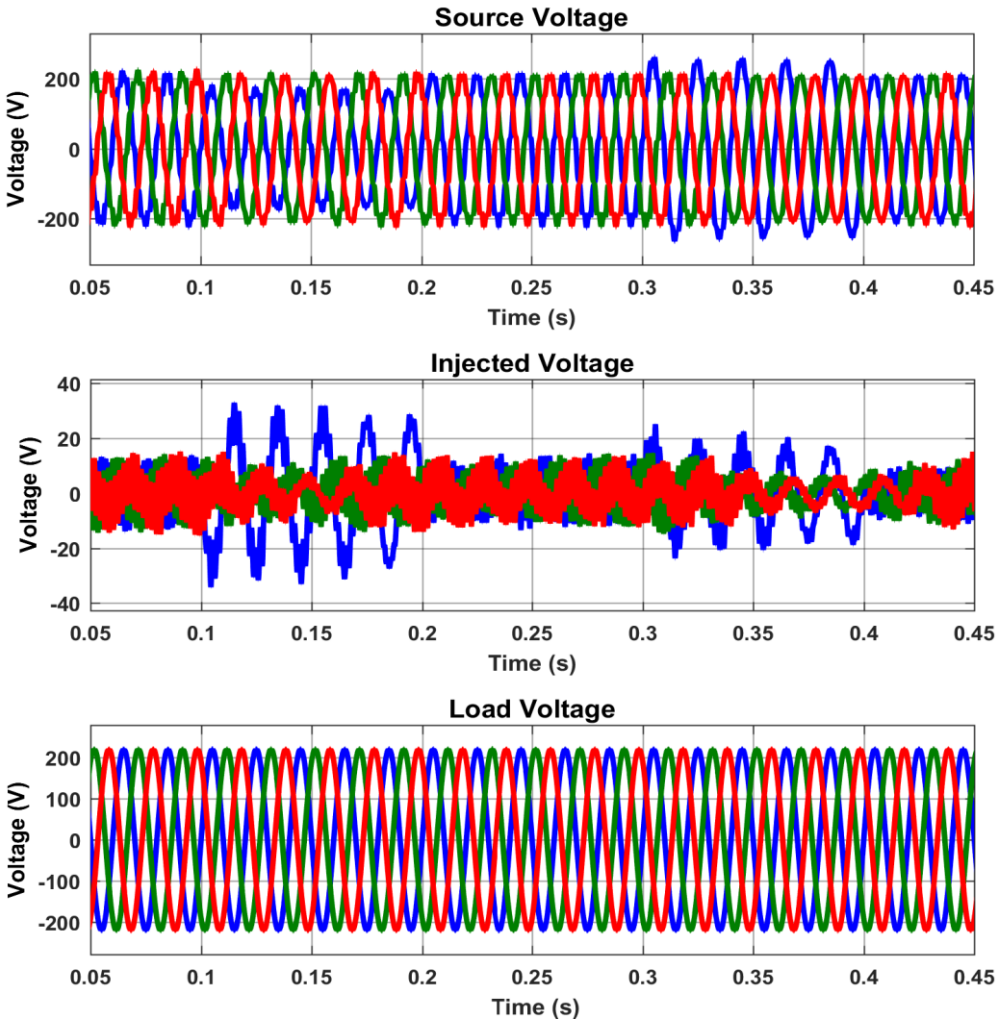

Figure IV.19. Source voltage, Injected voltage, and Load voltage under 20% unbalanced voltage sag and swell

IV.6.3. Robustness test: Nonlinear load (NL) variation

Figure IV.20 presents the system's current behavior during a nonlinear load (NL) variation event occurring at 1 second. The UPQC's rapid and dynamic response is clearly observed, as it swiftly adapts to the abrupt change in load conditions. This highlights the UPQC's strong capability to maintain harmonic mitigation and ensure power supply stability even under varying load scenarios.

As shown in **Figure IV-21**, prior to UPQC intervention, the THD of the second nonlinear load current is measured at 26.83%, indicating a significant presence of harmonic distortion. Following the activation of the UPQC, the THD dramatically decreases to 1.66%, clearly demonstrating the filter's high efficiency in suppressing harmonic content and improving overall PQ.

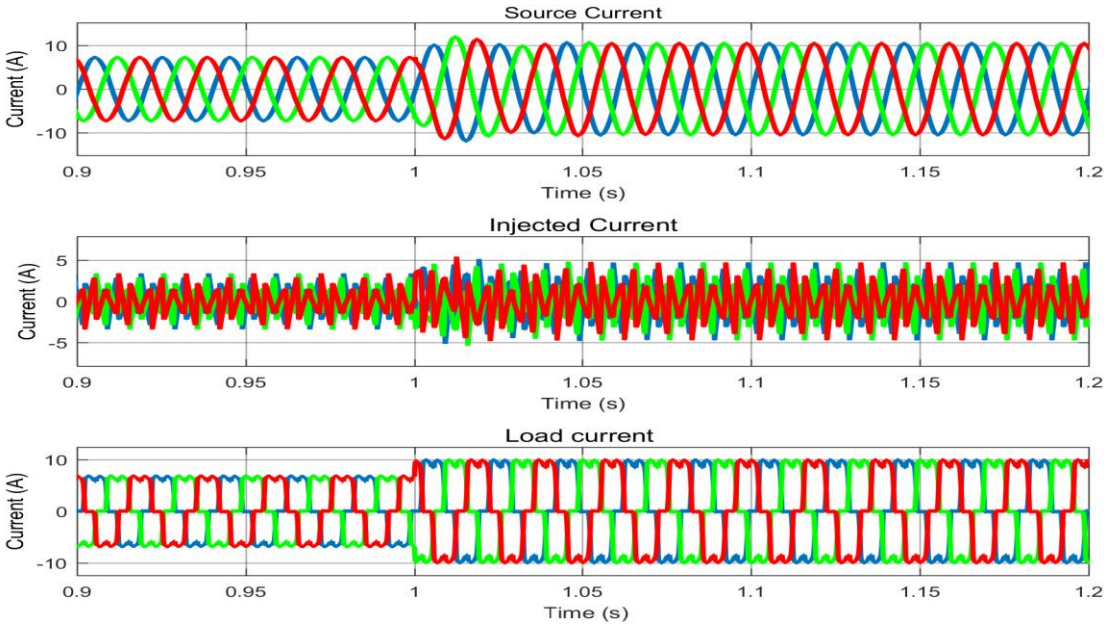

Figure IV-20. Current analysis during load variation: source, injected APF, and load terminals

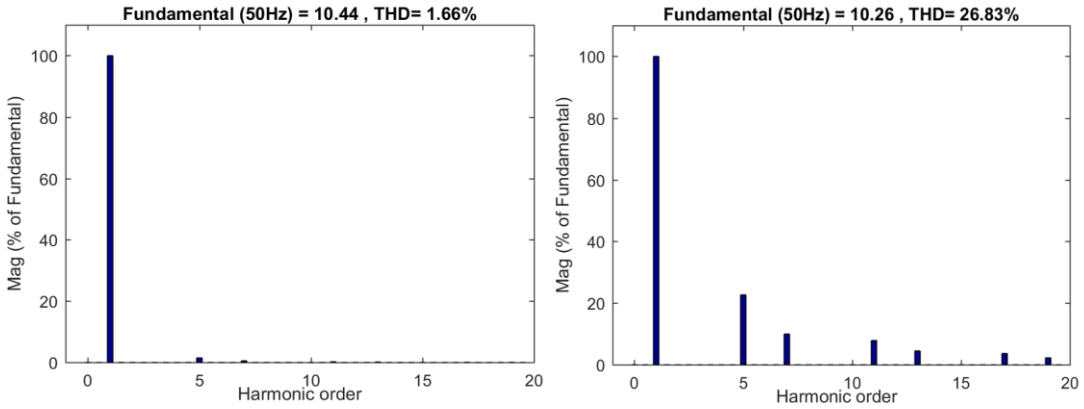

(a) **(b)**

Figure IV.21. THD current analysis for second load: (a) Source current, (b) Load current

In the robustness test, **Figure IV.22** illustrates the behavior of the DC bus voltage in conjunction with the source current and voltage at the PCC during nonlinear load variation. The DC bus voltage maintains a stable and consistent level, indicating effective regulation and control by the UPQC system. Additionally, the voltage and current waveforms at the PCC remain sinusoidal and exhibit minimal distortion, confirming the UPQC's capability to preserve PQ and system stability even under dynamic load conditions.

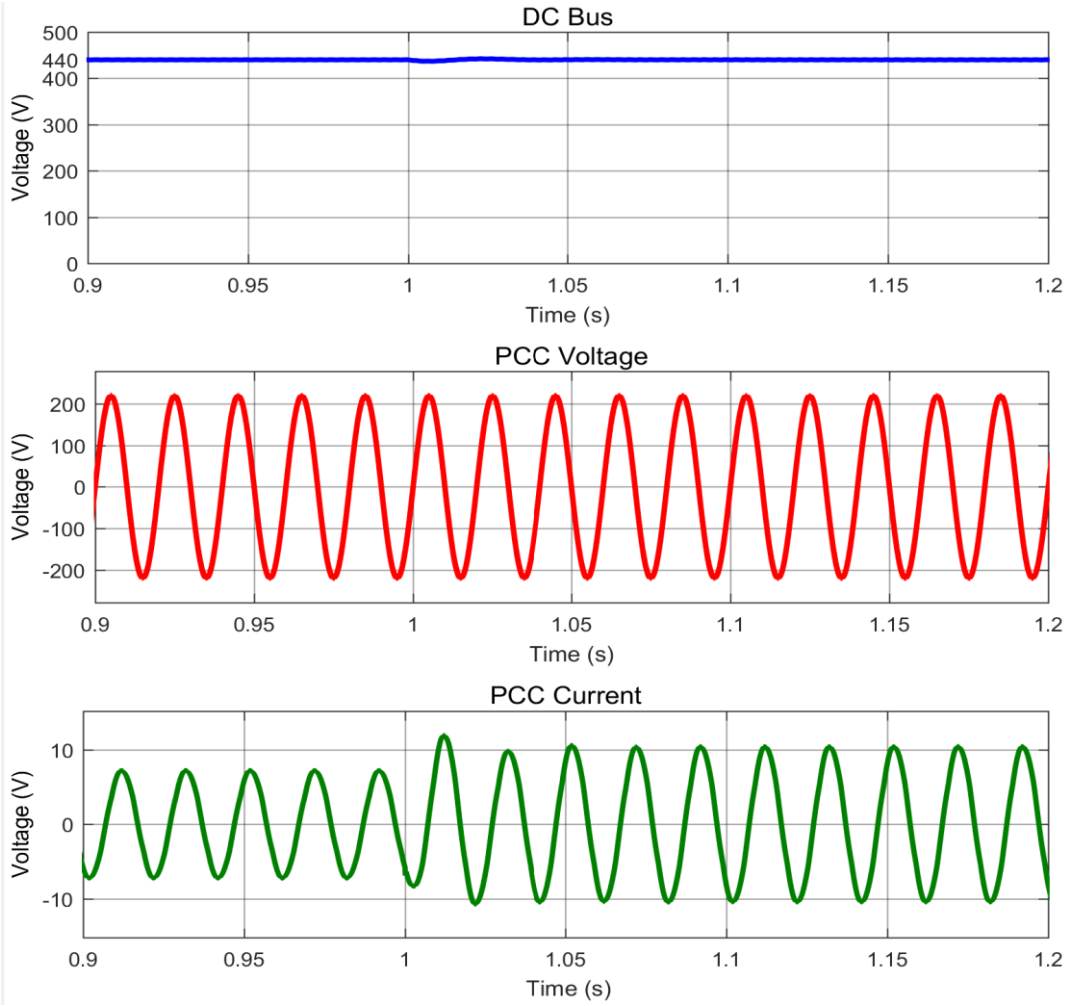

Figure IV.22. Voltage and current analysis during load variation: DC Bus, PCC voltage, and PCC current

IV.6.4. Unbalanced nonlinear load test

Figure IV.23 presents the current waveforms of the source, the injected current from the UPQC, and the load during the unbalanced nonlinear load test. THD of the unbalanced load current is measured at 28.37%, highlighting the significant harmonic content generated by the load. In contrast, the source current THD is significantly reduced to 2.23%, as illustrated in **Figure IV-24**. This substantial reduction demonstrates the effectiveness of the UPQC in mitigating harmonics and maintaining PQ at the source side, even under challenging unbalanced load conditions. The results affirm the UPQC's crucial role in ensuring a clean and stable power supply to the grid.

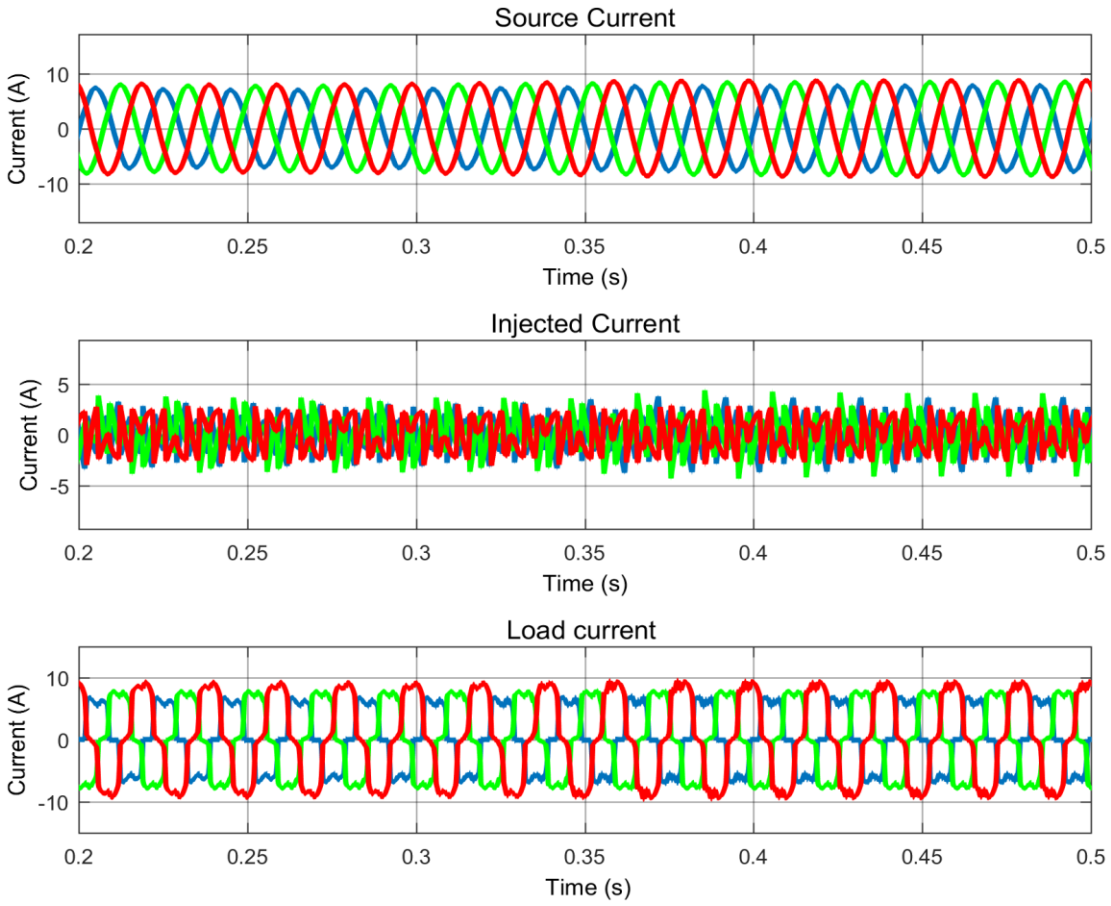

Figure IV.23. Current analysis during unbalanced load: source, injected APF, and load terminals

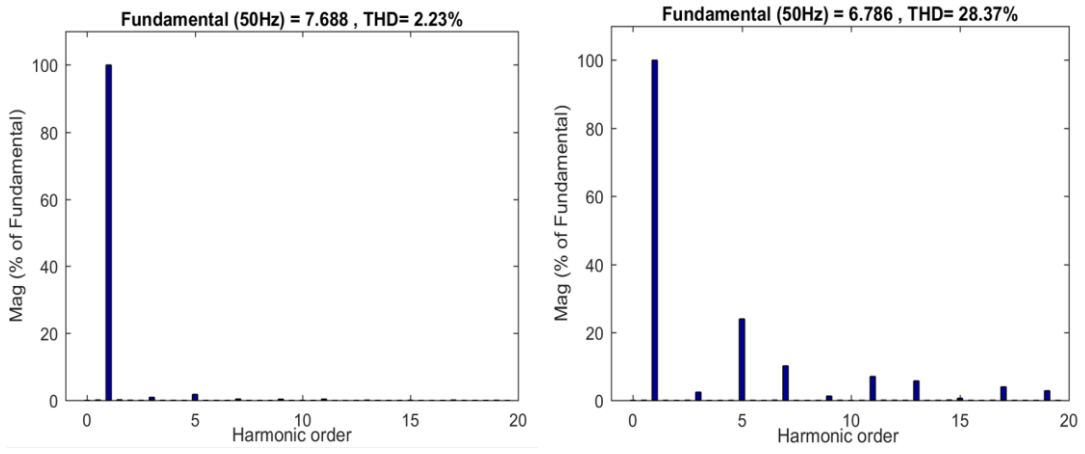

(a) **(b)**

Figure IV.24. THD current analysis for unbalanced load: (a) Source current, (b) Load current

IV.6.5 Unbalanced nonlinear load variation test

Figure IV.25 displays the current waveforms of the source, the injected current from the UPQC, and the load during the unbalanced nonlinear load variation event at 1 second. The

THD of the load current is recorded at 27.77%, indicating significant harmonic content. In contrast, the THD of the source current is effectively reduced to 2.10%, as presented in **Figure IV-26**.

The prompt response of the shunt component of the UPQC enables the immediate injection of compensating currents to correct load imbalances. This real-time injection allows the UPQC to dynamically counteract the adverse effects of unbalanced load conditions, effectively mitigating harmonic distortions. These results emphasize the UPQC's outstanding capability to maintain high PQ even under varying and challenging operating conditions.

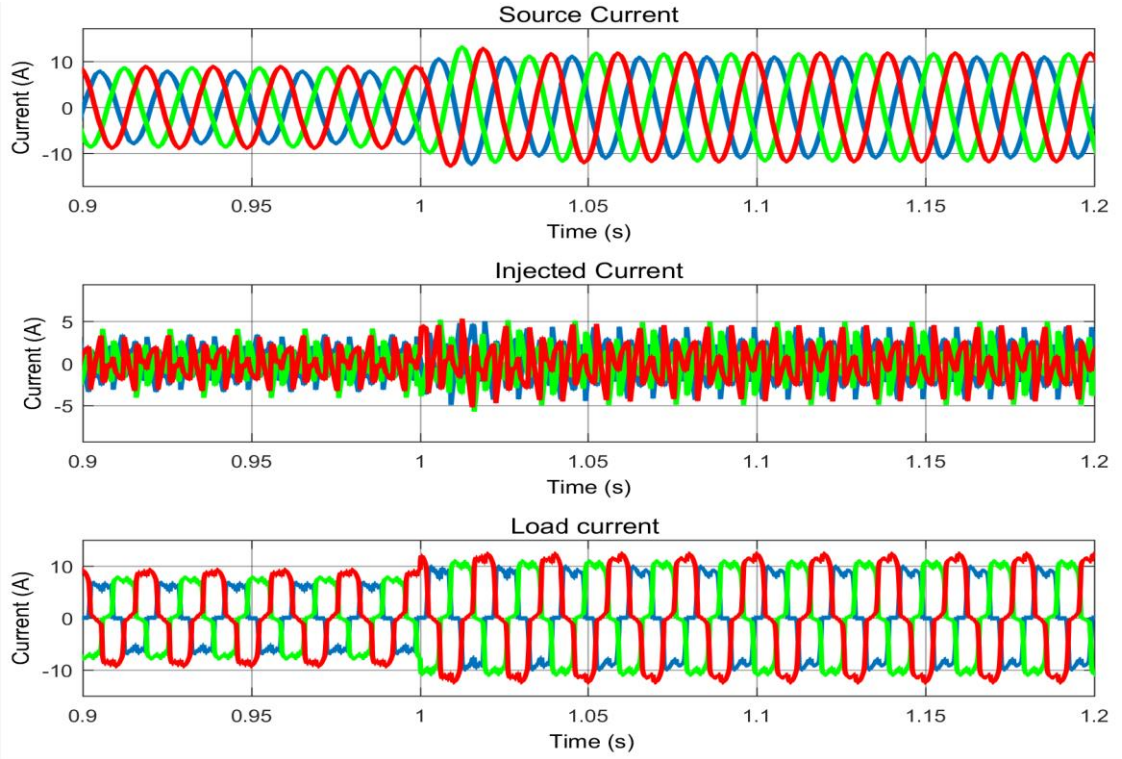

Figure IV.25. Current analysis during unbalanced load variation: Source, Injected APF, and load terminals

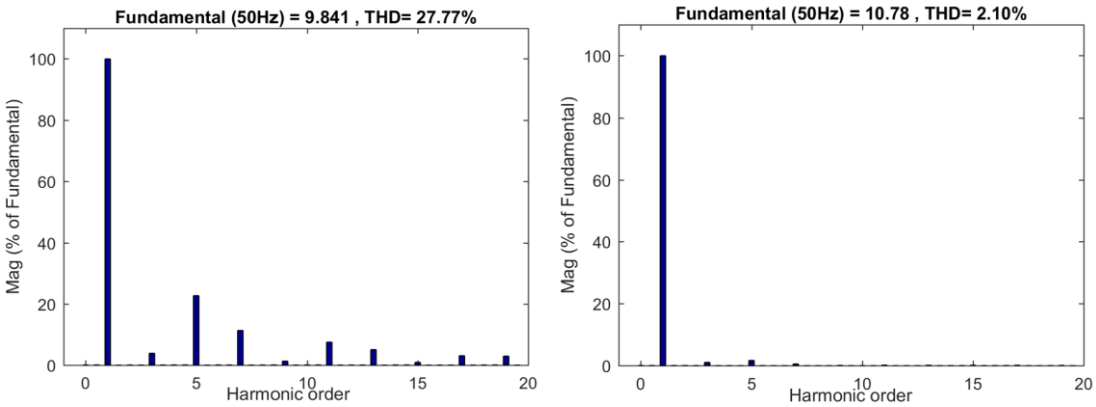

(a) **(b)**

Figure IV.26. THD current analysis for unbalanced load variation: (a) Load current, (b) Source current

IV.6.6. UPQC performance test at varying load percentages

The simulation results presented in **Figure IV-27** illustrate the performance of the UPQC in mitigating harmonic distortions under varying load conditions across a time span from 0.05 to 0.36 seconds.

Initially, during the period between 0.05 and 0.1 seconds, with a 100% nonlinear load (NL) condition, the THD of the source current is measured at 1.91%. When the load composition shifts to 50% linear load (LL) and 50% NL between 0.1 and 0.2 seconds, the THD decreases to 1.06%.

Further adjustment of the load to 75% LL and 25% NL from 0.2 to 0.3 seconds results in a THD of 0.93%, which reduces even further to 0.72% during the final interval (0.3 to 0.35 seconds) under the same load ratio.

These outcomes highlight the robustness and adaptability of the UPQC in maintaining the source current quality within IEEE 519 standards, effectively reducing harmonic content and enhancing overall PQ across various dynamic load scenarios.

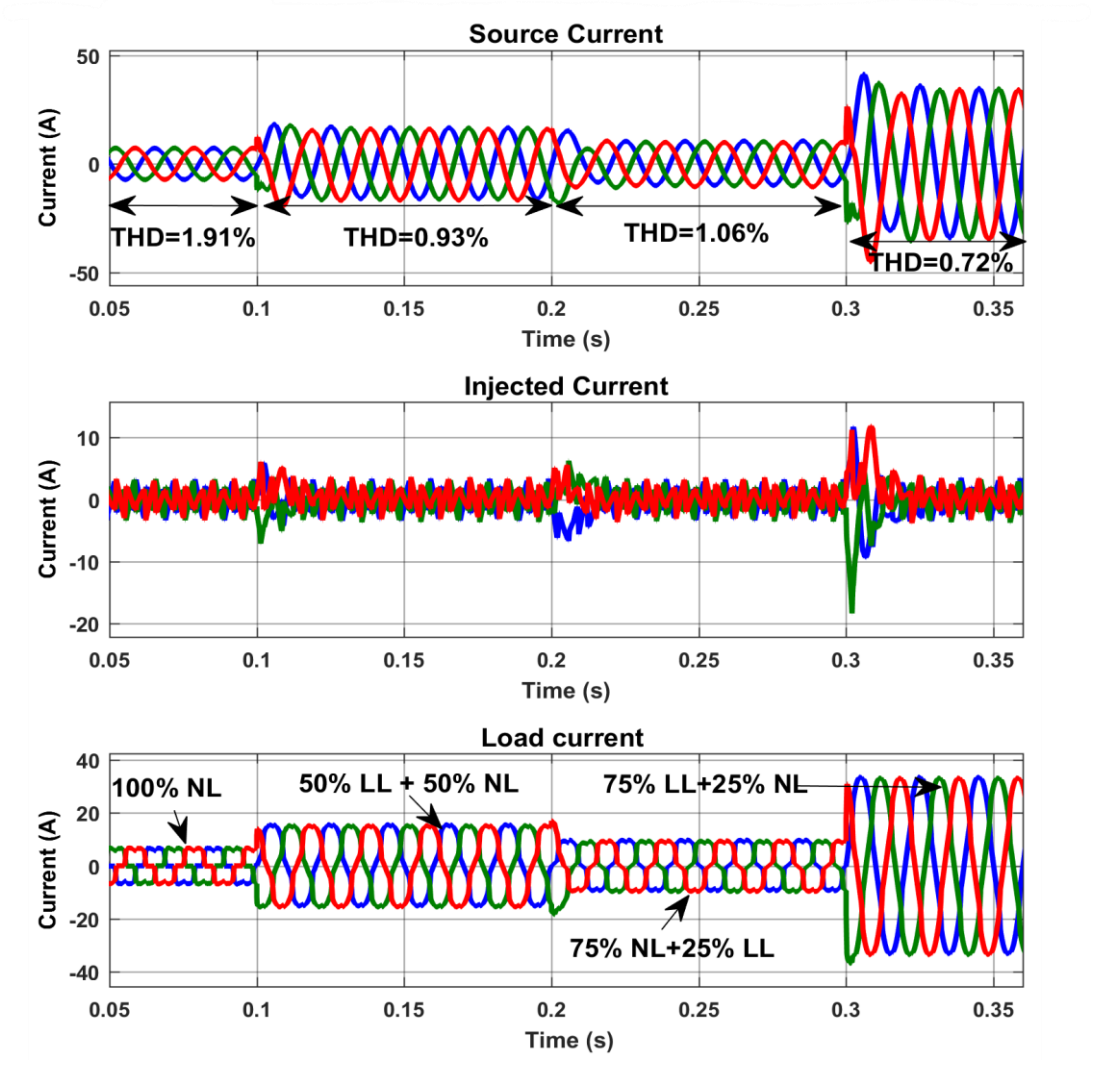

Figure IV-27. UPQC performance test at varying load percentages with linear and nonlinear load scenarios (LL and NL)

IV.6.7. UPQC Performance test under a highly nonlinear load with THD exceeding 55%

Figure IV.28 demonstrates the system's performance under the presence of a highly nonlinear load (NL), where the THD exceeds 55%.

Initially, the load current exhibits substantial distortion, with a THD measured at 55.13%, primarily caused by a diode bridge RLC load, as depicted in **Figure IV-29 (a)**. Following compensation by the UPQC, the THD of the source current is effectively reduced to 2.03%, as shown in **Figure IV-29 (b)**.

The shunt component of the UPQC successfully injects harmonic currents of equal magnitude and opposite phase, effectively canceling out the load-induced harmonics. This performance complies with IEEE International Harmonic Standards, demonstrating the robustness, adaptability, and high efficiency of the proposed control algorithm in mitigating extreme harmonic distortion scenarios.

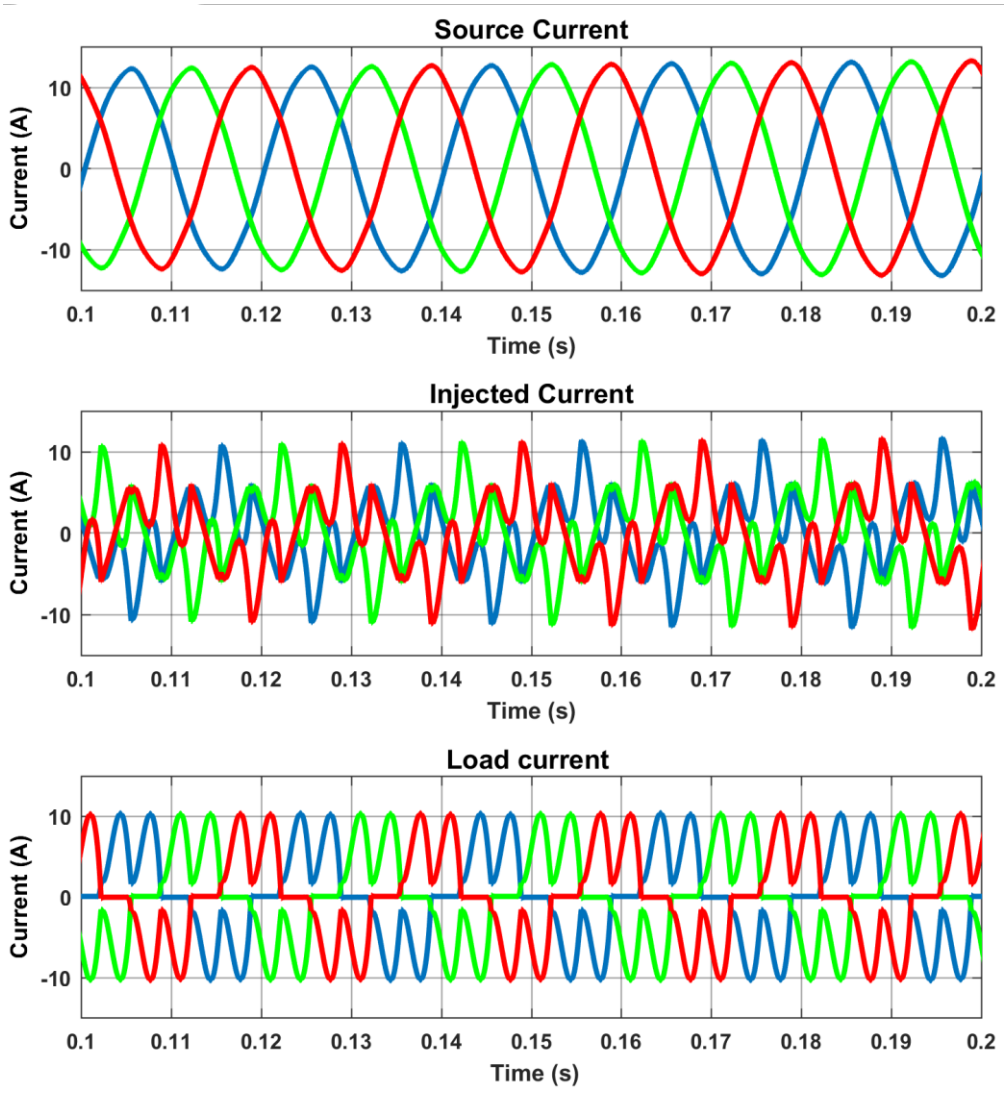

Figure IV.28. System performance under a highly nonlinear load

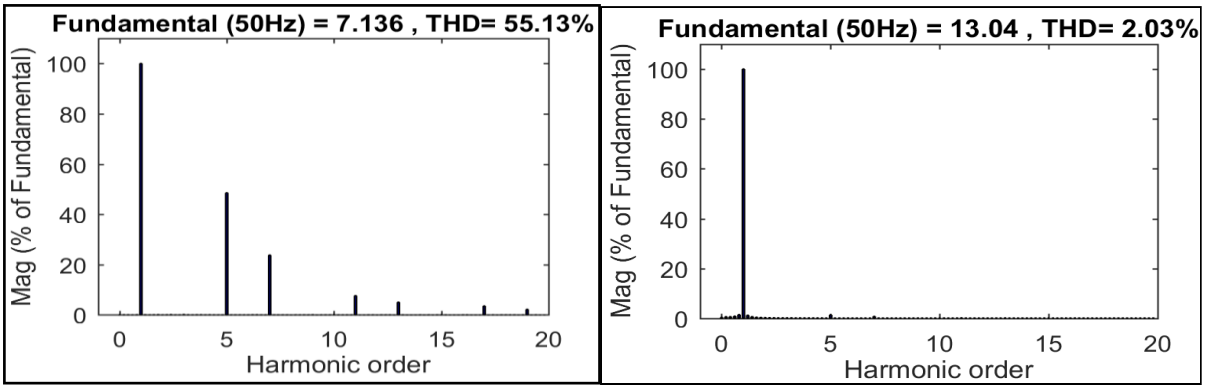

(a) **(b)**

Figure IV-29. THD of current: (a) Load current, (b) Source current

IV.7. Conclusion

In this chapter, we addressed the PQ challenges introduced by the integration of RESs specifically PV and wind systems—into the electrical grid, particularly in the presence of nonlinear loads (NLs). The fluctuating nature of renewable generation and the complex behavior of nonlinear loads contribute to significant voltage and current distortions that compromise system stability and reliability.

The first part of the chapter focused on the use of the Series APF to mitigate voltage-related disturbances such as harmonics, sags, swells, dips, and short-circuit effects. The Series APF demonstrated excellent performance in reducing voltage THD, stabilizing voltage profiles, and improving overall PQ in grid-connected PV-Wind systems.

In the second part, the application of the UPQC was explored to address both voltage and current distortions under various grid and load conditions. The UPQC effectively maintained stable voltage and current waveforms and reduced harmonic content to levels within IEEE 519 standards, even under highly nonlinear and unbalanced scenarios. These results confirmed the UPQC's effectiveness as a comprehensive solution for enhancing power performance in renewable energy-integrated systems.

While Series APF and UPQC play a critical role in improving PQ, ensuring the reliable and stable operation of hybrid renewable energy systems also requires effective energy management. As load demand varies with time and renewable generation fluctuates with weather conditions, balancing supply and demand becomes a major challenge. Therefore, the next chapter focuses on the development and implementation of energy management strategies, including the role of BESS, to ensure energy availability, optimize system performance, and enhance overall system efficiency.

Chapter V:

Intelligent Energy Management of a Hybrid Renewable Microgrid

V.1 Introduction

In this chapter, an advanced strategy for intelligent energy management is proposed for a hybrid energy system composed of PV panels, WT, a BESS, and the electrical grid. This multi-source microgrid is designed to effectively meet the load demand while ensuring optimal and reliable utilization of available renewable energy resources.

The intelligent energy management system is built upon two key components:

- The use of Artificial Neural Network (ANN)-based MPPT algorithms for both PV and wind sources, enabling dynamic and maximum power extraction under varying environmental conditions.
- The integration of a battery storage system, which is managed intelligently to store surplus energy when available and supply power to the load when renewable generation is insufficient, based on the battery's State of Charge (SoC).

An energy management system (EMS), implemented using a rule-based control approach, coordinates power distribution among the renewable sources, battery, load, and the grid. It considers renewable energy forecasts, load predictions, battery state, and operational priorities to achieve efficient and optimal energy flow control.

The proposed Energy Management System (EMS) for the grid-connected PV–Wind–Battery hybrid microgrid is designed to optimize energy flow between renewable generation, battery storage, and the utility grid. The flowchart in Figure V.2 illustrates the decision-making process of the EMS. It first senses real-time parameters including current PV and wind power, battery state-of-charge (SOC), and load demand. A forecasting module predicts the future PV and wind power generation, as well as future load demand, to compute the net expected power. The EMS then determines whether there will be a power surplus or deficit in the upcoming period and takes appropriate actions to maintain load supply, battery health, and efficient grid interaction.

Several operational scenarios are simulated over a typical day to evaluate the behavior and performance of the intelligent energy management system. The main objective is to demonstrate the system's ability to maximize self-consumption, reduce grid dependency, maintain stable power delivery, and enhance overall reliability in energy applications.

V.2. Optimal energy management for a hybrid microgrid

V.2.1 System configuration and description of the microgrid

The system studied in this work is designed as a grid-connected hybrid microgrid. The overall architecture of the microgrid is illustrated in **Figure V.1**.

The microgrid includes the following main components:

- A non-controllable variable load with a nominal power of 1-150 kW,
- A PV array with a peak generation capacity of 107.5 kW,
- A wind turbine (WT) system with a rated capacity of 18 kW,
- A battery energy storage system,
- And various load profiles representing typical residential consumption patterns.

The entire system is coordinated by an Energy Management System (EMS), which is responsible for regulating power exchange among the generation units, the battery, the load, and the grid. The EMS ensures that power balance is maintained while optimizing the use of renewable resources and battery storage, based on real-time operating conditions.

This microgrid architecture enables intelligent operation under various scenarios such as energy surplus, energy deficit, and peak load demand, while enhancing reliability, sustainability, and efficiency of the energy supply [107].

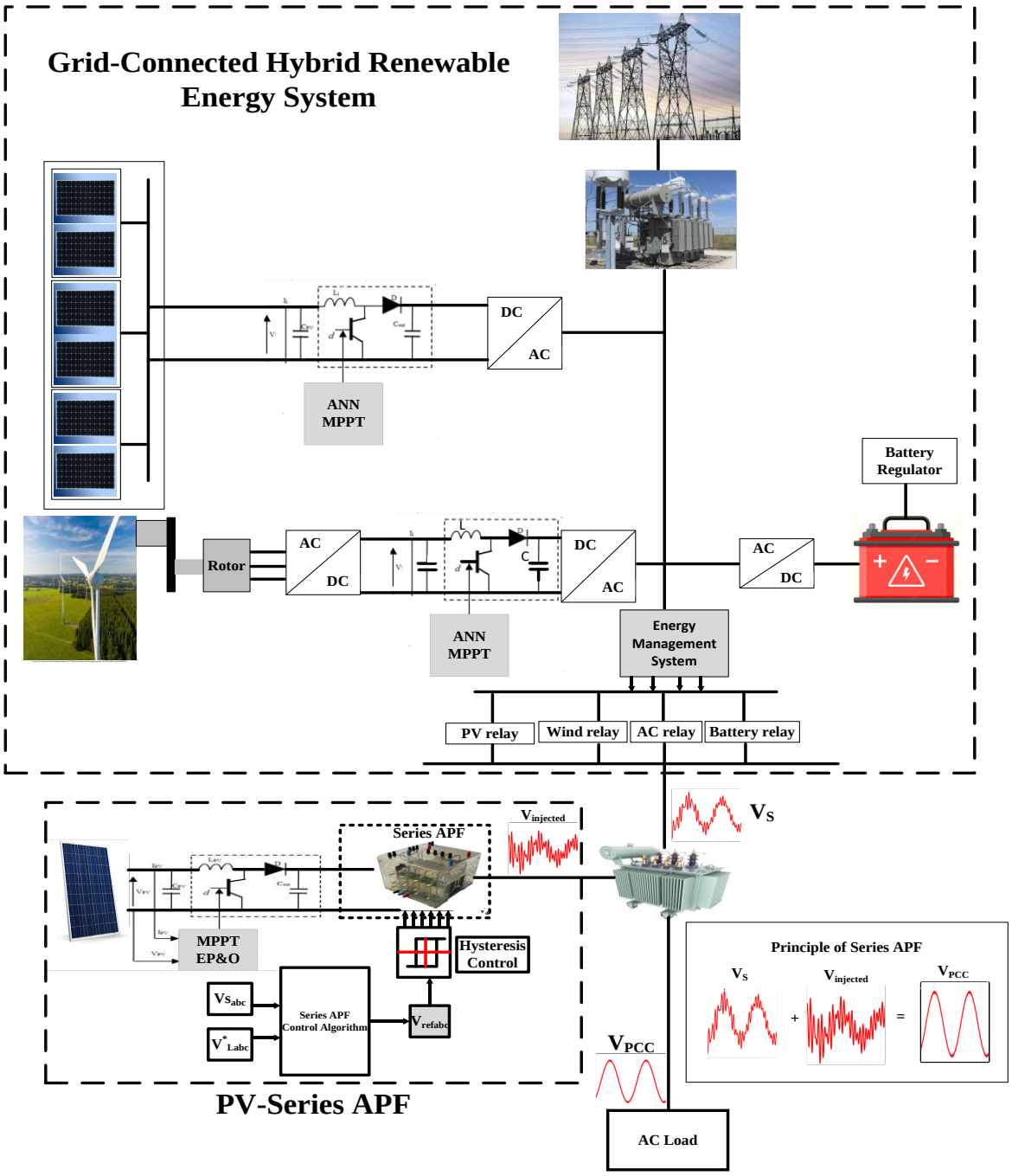

Figure V.1 General description of the PV-Wind-Battery microgrid with ANN algorithm and PV-series APF for PQ improvement (Constant parameters: PV Power (P_{PV}) = 107.5 kW, Wind Power (18kW), Load power (P_{Load}) = 1 to 150 kW, PV Power for series APF (P_{PV}) = 10 kW)

V.3. Energy management for a grid-connected microgrid

V.3.1. Rule-based energy management system (RB-EMS)

In this section, a Rule-Based Energy Management System (RB-EMS) is implemented to achieve optimal energy management in a grid-connected, multi-source hybrid microgrid.

The primary function of the RB-EMS is to optimally schedule and coordinate the operation of distributed energy resources (DERs) including PV, WT, BESS, and the grid connection—in order to meet the real-time energy demand of the load.

The control strategy is formulated using a set of predefined rules in the form of "if–then–else" decision logic. This logical structure enables real-time execution of decision-making processes that determine the power flow direction among the system components based on the following criteria:

- Availability of renewable generation (PV and wind),
- Load demand level,
- Battery State of Charge (SOC),
- Grid status (available/unavailable).

The RB-EMS operates by continuously monitoring system variables and dynamically managing the flow of energy between sources, storage, load, and the grid. It ensures that:

- Surplus energy from renewables is first used to supply the local load, and any excess is stored in the battery,
- If the battery is fully charged and there is still surplus energy, it is injected into the grid,
- In case of a deficit in renewable generation, the battery discharges to support the load if SOC permits,
- When both renewables and battery are insufficient, the grid supplies the remaining load demand.

This management approach ensures a balanced, efficient, and reliable operation of the hybrid system while promoting self-consumption and minimizing reliance on the utility grid.

V.3.2. Forecast-based decision strategy for intelligent energy scheduling

The Energy Management System (EMS) receives forecasted data related to the load demand, the distributed energy resources (DERs) namely PV and WT systems (including solar irradiance and wind speed) as well as the State of Charge (SOC) of the battery storage system.

Based on this information, the EMS schedules and imposes the optimal output power setpoints for the generation units, controls the import/export power exchange with the main grid, and ensures the balance between generation, storage, and demand.

The system's operational decisions are primarily determined by:

- The available PV and WT power,
- The real-time load demand,
- And the battery's SOC level.

This predictive and rule-based approach allows the EMS to dynamically adjust power flows, ensuring efficient utilization of renewable energy, optimized storage usage, and minimized grid dependency [100].

The operation of the system is primarily determined by the available PV and wind power, the State of Charge (SoC) of the battery storage system, and the real-time load demand [98,99].

The energy management strategy is governed by the following main rules:

- Renewable energy sources (PV and wind) are given priority to supply the load directly.
- The Battery Energy Storage System is charged using the surplus power from renewable sources when generation exceeds load demand.
- The BESS discharges to supply the load when PV and wind generation are insufficient.
- The main grid supplies the load only when PV, wind, and battery storage are all unable to meet the demand.

The constraints applied to the optimization process of the microgrid are described below.

The power balance within the microgrid must be maintained at all times, as expressed by Equation (V.1):

$$P_{Load}(t) = P_{PV}(t) + P_{Wind}(t) + P_{Grid}(t) + P_{Bat}(t) \quad \text{(V-1)}$$

Where:

- $P_{Load}(t)$ is the load demand at time *t*,
- $P_{PV}(t)$ is the power generated by the PV system,
- $P_{Wind}(t)$ is the power generated by the wind turbine,
- $P_{Bat}(t)$ is the power delivered (positive) or absorbed (negative) by the battery,
- $P_{Grid}(t)$ is the power imported from the utility grid,

In addition to the power balance constraint, two cases are considered to quantify power surplus and power deficit, as given in Equations (V-2) and (V-3):

- Surplus power (when generation exceeds demand):

$$P_{ex}(t) = [P_{PV}(t) + P_{Wind}(t)] - P_{Load}(t) \quad \text{(V-2)}$$

- Deficit power (when demand exceeds generation):

$$P_{Def}(t) = P_{Load}(t) - [P_{PV}(t) + P_{Wind}(t)] \quad \text{(V-3)}$$

Additionally, the power drawn from the grid is limited by the maximum import capacity, defined as:

$$P_{Grid}(t) < P_{Grid\_MAX} \quad \text{(V-4)}$$

The load must always be supplied by a combination of available energy sources: renewable generation (solar and wind), the static BESS, or the utility grid.

The battery power flow $P_{Bat}(t)$ is considered positive during discharging and power injection operations, and negative when charging.

It is also assumed that the initial and final State of Charge (SOC) of the battery system are not necessarily identical, allowing flexibility in energy scheduling over the optimization horizon.

In addition to the Rule-Based Energy Management System (RB-EMS), a forecast-based predictive strategy is incorporated to enhance the intelligent scheduling of energy in the grid-connected PV–Wind–Battery hybrid microgrid. The EMS receives short-term predictions of PV and wind power generation, load demand, and battery State of Charge (SOC) to calculate the expected net power for the upcoming period.

Based on this predictive information, the EMS makes proactive decisions to manage surplus or deficit conditions: if a surplus is expected, the battery is pre-charged or excess energy is exported to the grid; if a deficit is predicted, the battery is discharged or additional power is imported from the utility grid. This approach optimizes the use of renewable energy, ensures reliable load supply, and maintains the battery within safe SOC limits, while reducing dependency on the grid. Figure V.2 illustrates the operational flow of this predictive and rule-based EMS, integrating real-time measurements with forecasted data for intelligent decision-making.

V.3.3. Battery state of charge (SOC) constraint

The State of Charge (SOC) of the BESS is constrained within predefined operational limits to ensure safe and efficient operation. This constraint is expressed as follows:

$$SOC_{BatMin} \leq SOC_{Bat}(t) \leq SOC_{BatMax} \quad \text{(V-5)}$$

This condition ensures that the battery system (BESS) is neither charged nor discharged when the SOC falls outside the permissible range. Exceeding these limits could lead to battery degradation or unsafe operation.

Figure V.2 illustrates in detail the flow of the Rule-Based Algorithm (RBA), which governs the control logic based on SoC levels, renewable availability, and load demand.

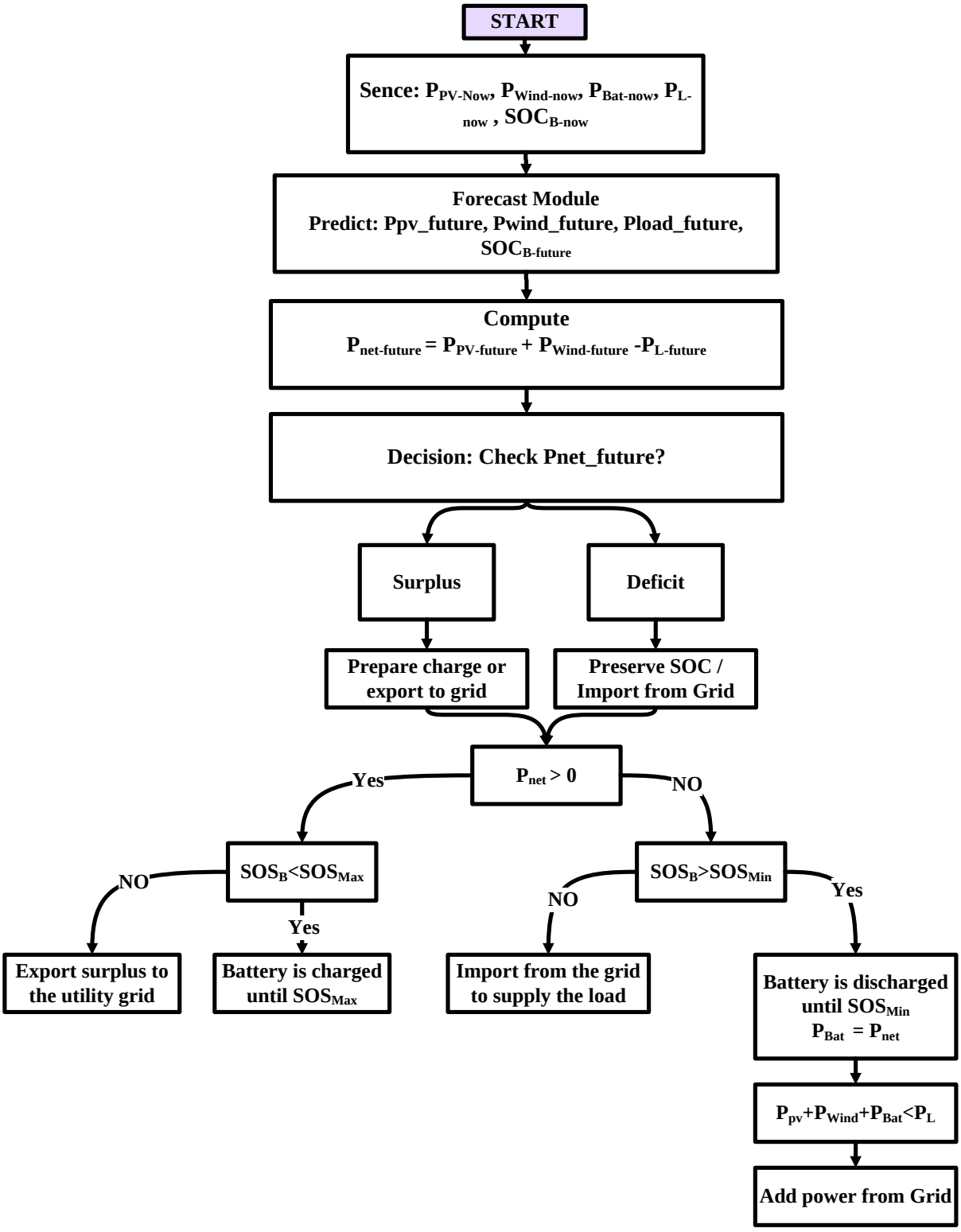

Figure V.2 Flowchart of the energy management system for a grid-connected PV–Wind–Battery hybrid microgrid

V.4. Simulation results and discussion

The simulation results under Matlab/Simulink of a microgrid operating in both grid-connected and islanded modes are presented to evaluate the efficiency of the proposed method.

Different operating scenarios are implemented to observe the behavior of the Energy Management System (EMS) in the optimal power sharing between the various sources, taking into account renewable energy production, the State of Charge (SOC) of the BESS, and the load demand.

The simulations were carried out over a period of 24 hours to visualize different operating conditions. The operation of the system is divided into three modes:

- Mode 1 – Normal operation: Different scenarios are executed for a sunny day.
- Mode 2 – Intermittent nature: Two scenarios are executed for a cloudy day and a disturbed irradiation profile.
- Mode 3 – Low SOC edge case (battery protection mode): Initial SOC < 20%.
- Mode 4 High SOC edge case (Grid export mode): Initial SOC > 80%

In the last operating mode, the EMS considers exporting the excess renewable energy not consumed locally to the utility grid.

The operation of the microgrid is highly influenced by two critical factors:

- The peak hours of the electrical grid, and
- The intermittency of renewable energy production.

On clear and sunny days, the PV system follows a typical bell-shaped solar irradiance profile, with maximum power output occurring around solar noon. This characteristic behavior is shown in **Figure V.3 (a)**, which depicts the irradiance curve under ideal solar conditions.

In contrast, wind energy production is subject to random and irregular fluctuations, as it depends directly on wind speed variability, which is inherently stochastic. To illustrate the variability in solar and wind resources, the following figures are provided:

- **Figure V.3 (b)**: Solar irradiance profile for a cloudy day,
- **Figure V.3 (c)**: Perturbed irradiance profile representing highly variable solar conditions,
- **Figure V.3 (d)**: Wind speed variation over a 24-hour period, directly influencing the output of the Wind Energy System (WES).

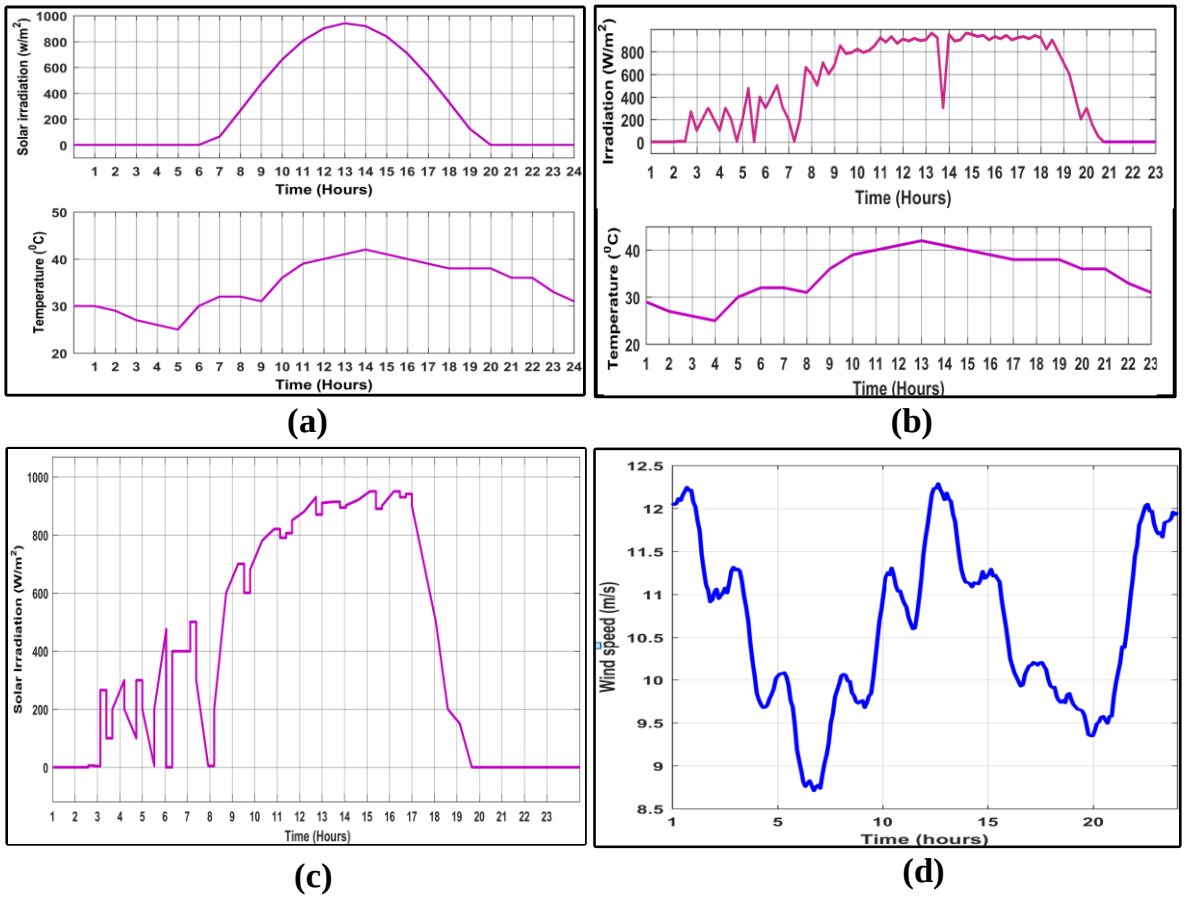

Figure V.3 Irradiance, temperature and Wind speed profiles: (a) Sunny day, (b) Sudden variation, (c) cloudy day, (d) wind speed

V.4.1. Mode 1 – Normal operation:

In this microgrid (MG) system, the primary sources of electricity generation are the PV and wind systems, which are designed to produce **107.5 kW** and 18 kW, respectively, under Standard Test Conditions (STC). **Figure V.4** illustrates the actual power output from both the PV system and the wind system over a 24-hour period, highlighting their role in supplying the MG.

Due to the variability in PV and wind energy availability, the MG relies on secondary sources, particularly the BESS, to ensure a continuous and reliable power supply.

The Energy Management System (EMS) plays a central role in the microgrid (MG) operation by efficiently managing and allocating power from multiple sources—including the PV system, wind energy system (WES), BESS, and the main grid—to meet the instantaneous load demand. The EMS algorithm strategically controls energy flows to maintain a continuous balance between supply and demand, optimizing the utilization of available resources. This approach not only enhances overall system efficiency but also contributes to reducing operational costs and environmental impact. The primary objective is to ensure a resilient, reliable, and sustainable energy supply within the MG, as illustrated in **Figure V.4**, which presents the power flow from PV (P_{PV}), wind (P_{Wind}), battery ($P_{Battery}$), grid (P_{Grid}), and load (P_{Load}).

The power requirement of the microgrid (MG) system fluctuates between 1 kW and 150 kW, as illustrated in **Figure V.4** (P_{Load}). This variability in load demand underscores the necessity for an effective Energy Management System (EMS). To maintain operational stability and ensure continuous power supply under varying conditions, the system integrates a BESS unit governed by advanced control strategies. The primary objective is to regulate power flow dynamics efficiently and manage fluctuations in both energy generation and consumption.

The variations in solar irradiation lead to corresponding changes in the power generation patterns of the PV array, as illustrated in **Figure V.4** (P_{PV}). These fluctuations directly affect the amount of electricity produced by the RES, emphasizing the importance of implementing an effective energy management strategy capable of adapting to dynamic environmental conditions. Such management is essential to ensure optimal power generation and reliable operation of the microgrid (MG) system.

The fluctuations observed in the battery power profile, as shown in **Figure V.4** ($P_{Battery}$), reflect periods where the available power exceeds the microgrid (MG) demand. These variations are represented by the battery's charging and discharging cycles, illustrating how the system regulates the balance between energy supply and load requirements. The BESS plays a vital role in storing excess energy during generation surpluses and delivering power during periods of elevated demand, thereby contributing significantly to the stability and operational efficiency of the MG.

Figure V.4 show that between 1:00 a.m. and 6:00 a.m., the available wind power exceeds the load demand, allowing the wind system to supply the load and simultaneously charge the battery. As the load demand increases after 6:00 a.m., wind power alone becomes insufficient, and the BESS begins to discharge in order to supplement the power supply. By approximately 8:00 a.m., the battery reaches its maximum discharge capacity of 15 kW, at which point the utility grid is engaged to maintain the balance between power generation and load demand.

At around 11:30 a.m., PV generation gradually begins, increasing steadily and reaching its peak output at 2:00 p.m. During this period, the combined output of PV and wind exceeds the load demand, allowing the battery to recharge.

After 3:00 p.m, the PV output begins to decline, while the load demand continues to increase, reaching its daily peak at 9:00 p.m. During this high-demand period, both the battery and the grid are utilized to meet the energy requirements and maintain system stability.

Figure V.5 illustrates the battery's charging and discharging behavior, along with its State of Charge (SOC) profile. The battery is observed to be in charging mode during the periods 01:00–06:00, 12:00–15:00, and after 23:00, which coincides with intervals where solar irradiation peaks or where wind generation exceeds load demand. During these periods, the excess energy generated by the PV and wind systems is efficiently stored in the battery.

Conversely, the battery undergoes discharging between 06:00–12:00 and again from 17:00–23:00, when the combined output from the PV and wind sources is insufficient to meet the load requirements—either due to low irradiation in the early morning or night-time conditions.

This strategic management of the Energy Storage System (ESS) ensures a continuous and stable power supply to the load, maximizes the utilization of available RES, and minimizes the dependency on the utility grid.

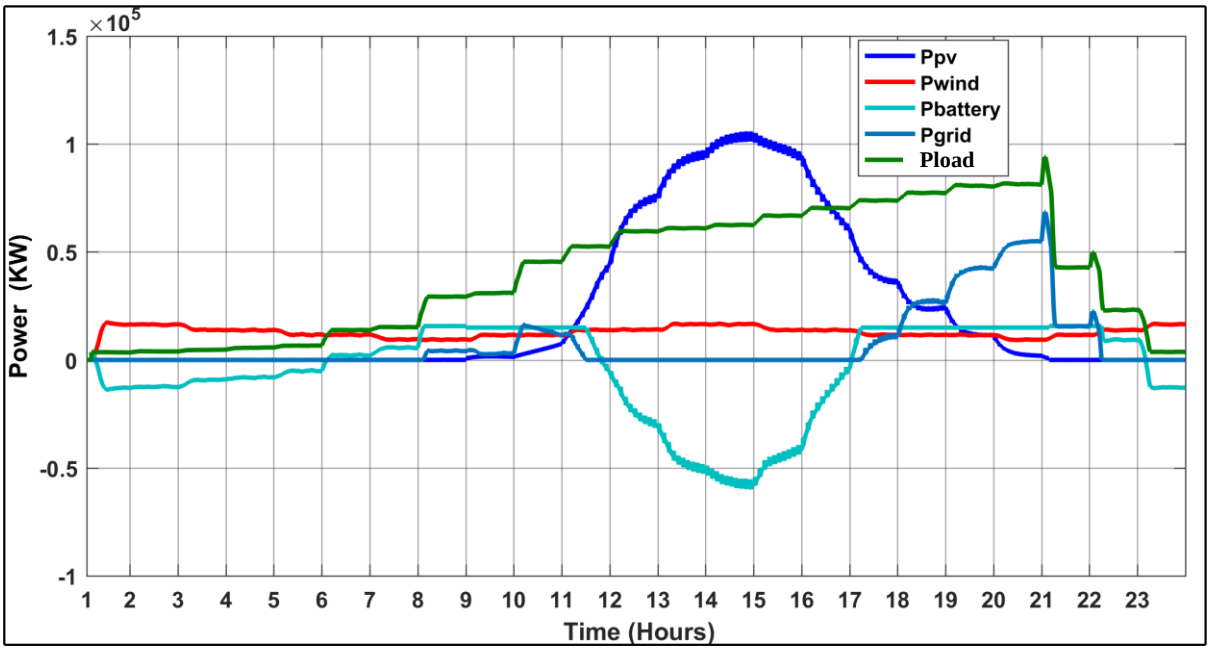

Figure V.4 Energy Management in the Microgrid: PV, Wind, Battery, Grid, and Load Power

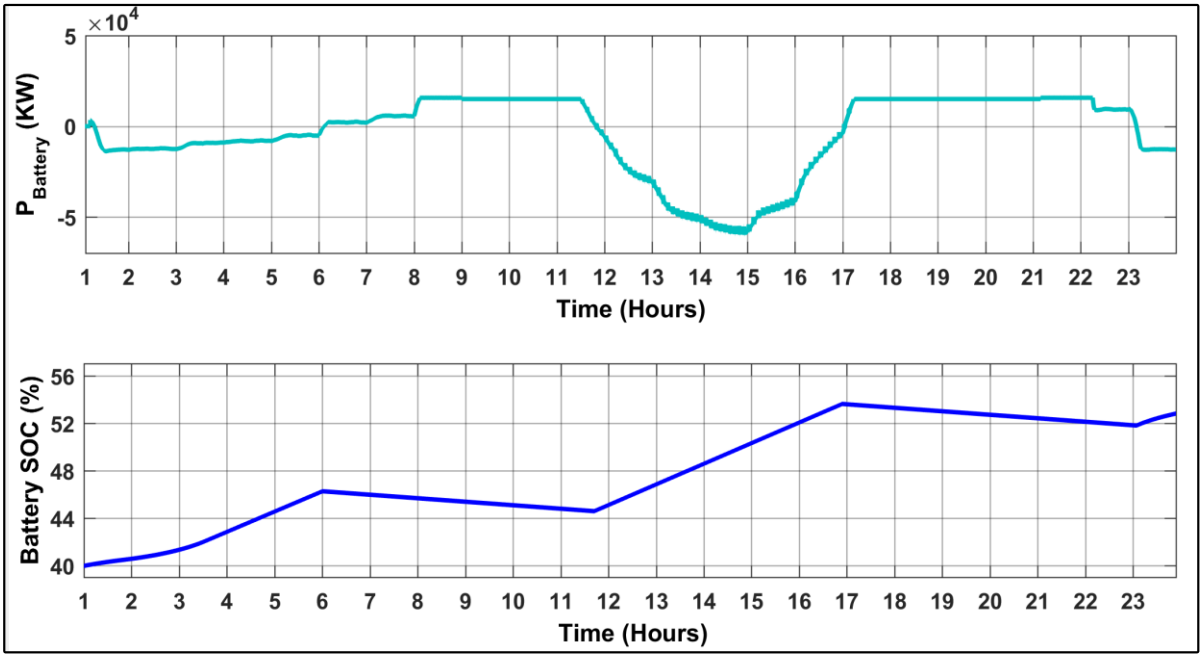

Figure V.5 Battery power and SOC during energy management

V.4.2. Mode 2 – Energy management under variable solar conditions:

Figure V.6 illustrates the energy management behavior of the microgrid during a cloudy day scenario, characterized by frequent and irregular solar irradiation fluctuations. These fluctuations lead to instability in PV power generation, which directly affects the ability of the

RES to meet the real-time load demand. The Energy Management System (EMS) plays a pivotal role in this context by dynamically coordinating the power contributions from the PV system, WT, BESS, and the utility grid.

During intervals when the combined output from the PV and wind sources exceeds the load demand, the excess power is utilized to charge the battery, thereby enhancing the system's self-sufficiency and reducing dependence on the grid. However, in periods when PV output drops due to cloud cover, and wind generation alone is insufficient, the EMS initiates the discharging process of the BESS to bridge the energy gap. This approach ensures that the load is continuously supplied without interruption. In the event that both RES and battery storage are inadequate to meet the demand, power is imported from the grid, thereby guaranteeing the reliability of the microgrid under variable environmental conditions.

Figure V.7 further illustrates the system's performance under a scenario with sudden and extreme fluctuations in solar irradiation—a condition that can occur due to transient cloud cover or abrupt weather changes. In such cases, the EMS must react swiftly to maintain power balance. The system first attempts to meet the load demand using the available PV and wind power. If the RES output exceeds the demand, the battery is charged to absorb the surplus energy. Conversely, if there is a deficit in power generation, the battery is discharged to compensate for the shortfall. Only when both RES and BESS fail to meet the load requirement does the EMS allow for grid power support to maintain operational continuity.

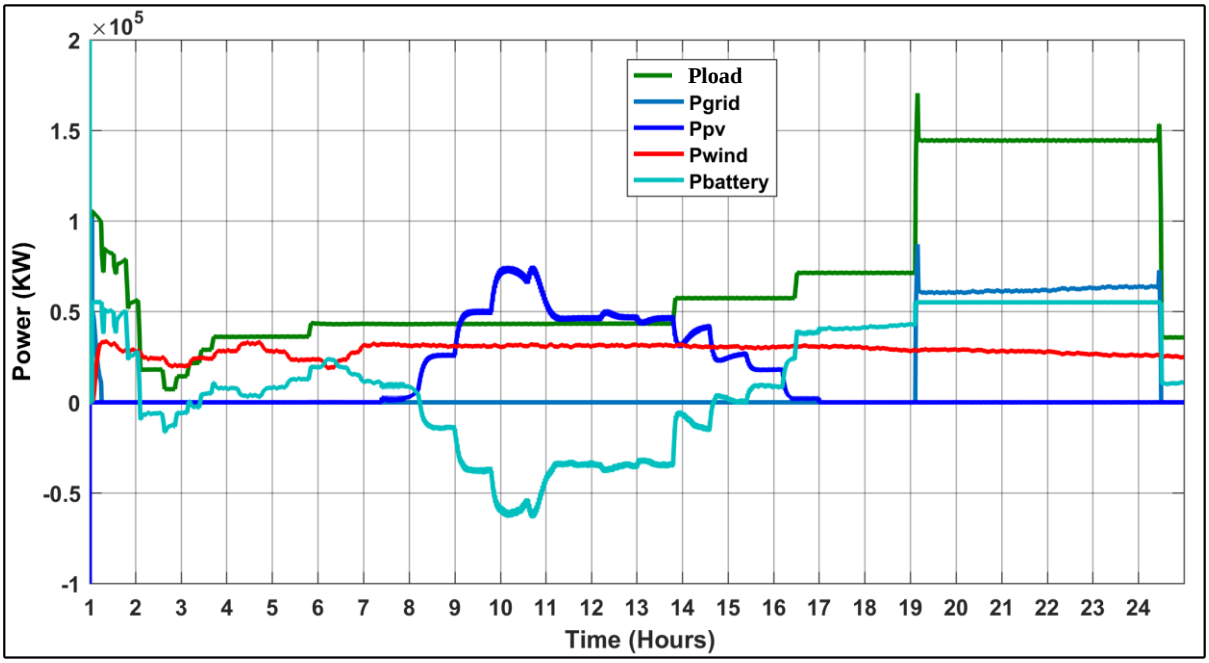

Figure V.6 Energy management in the microgrid during cloudy day: PV, wind, battery, grid, and load power

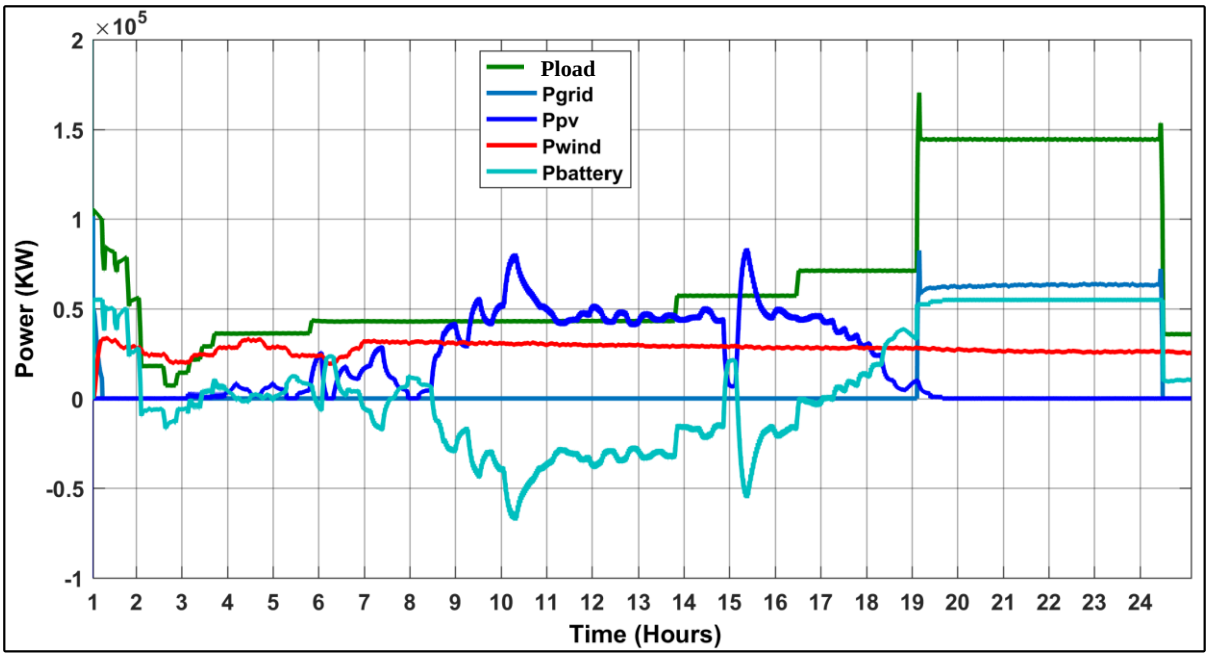

Figure V.7 Energy management in the microgrid during sudden irradiation change day: PV, wind, battery, grid, and load power

V.4.3. Mode 3: Battery protection mode under low SOC conditions:

In this operational mode, the microgrid operates under a critical battery condition, where the State of Charge (SOC) of the BESS falls below 20%. This threshold is considered a protective limit, below which discharging the battery would pose significant risks to its health, efficiency, and long-term lifespan. Deep discharges beyond this level are known to accelerate electrochemical degradation, reduce cycle life, and lead to capacity fading, as established in the literature on lithium-ion and other battery technologies.

To prevent such deterioration, the Energy Management System (EMS) is configured to completely prohibit battery discharge when the SOC is below 20%. As illustrated in **Figure V.8**, the EMS prioritizes the use of renewable energy sources (PV and wind) to meet the load demand. If the combined renewable power generation exceeds the load, the excess energy is directed towards recharging the battery, thereby supporting its recovery to a safe operational range.

However, during periods where renewable generation is insufficient, the EMS does not allow the BESS to discharge, regardless of the energy deficit. Instead, the system activates grid support to supplement the load demand. This strategy ensures system reliability while preserving the integrity and longevity of the battery.

This mode highlights the EMS's ability to prioritize asset protection over short-term energy balancing. It demonstrates the implementation of battery-aware energy management, where the state of health (SOH) and operational constraints of the BESS are factored into the real-time control decisions. This aligns with best practices in modern microgrid design, which increasingly incorporate battery degradation models into EMS algorithms for predictive maintenance, lifecycle optimization, and cost-effective operation.

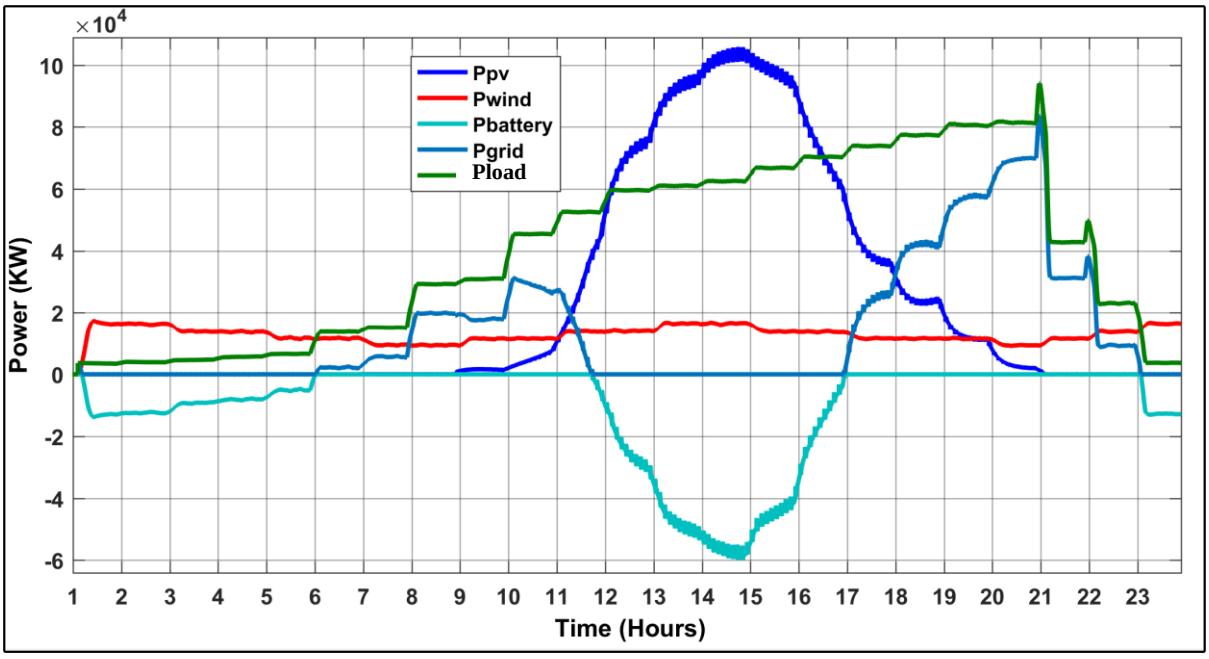

Figure V.8 Power Flow Management under Battery Protection Mode (SOC < 20%)

V.4.4. Mode 4: Grid export mode under high SOC conditions:

In this operational mode, the State of Charge (SOC) of the BESS exceeds 80%, representing a high-charge threshold. Under such conditions, the Energy Management System (EMS) is configured to prevent further charging of the battery. This decision is grounded in well-established battery management principles aimed at preserving the state of health (SOH) and extending the lifecycle of the battery.

Overcharging—especially when consistently operating near 100% SOC—has been shown to accelerate electrochemical degradation mechanisms, including lithium plating, increased internal resistance, and thermal stress, particularly in lithium-ion battery chemistries. These factors lead to premature capacity loss and reduced performance over time. Therefore, to maintain battery longevity and ensure safe operation, the EMS imposes an upper SOC limit, typically between 80%–90%, depending on the battery model and system requirements.

When renewable power generation (PV + wind) exceeds the load demand and the battery is near full capacity, the EMS redirects the surplus energy to the utility grid, as illustrated in **Figure V.9**. This approach not only prevents overcharging of the BESS but also offers several technical and economic advantages to both the microgrid and the main grid infrastructure.

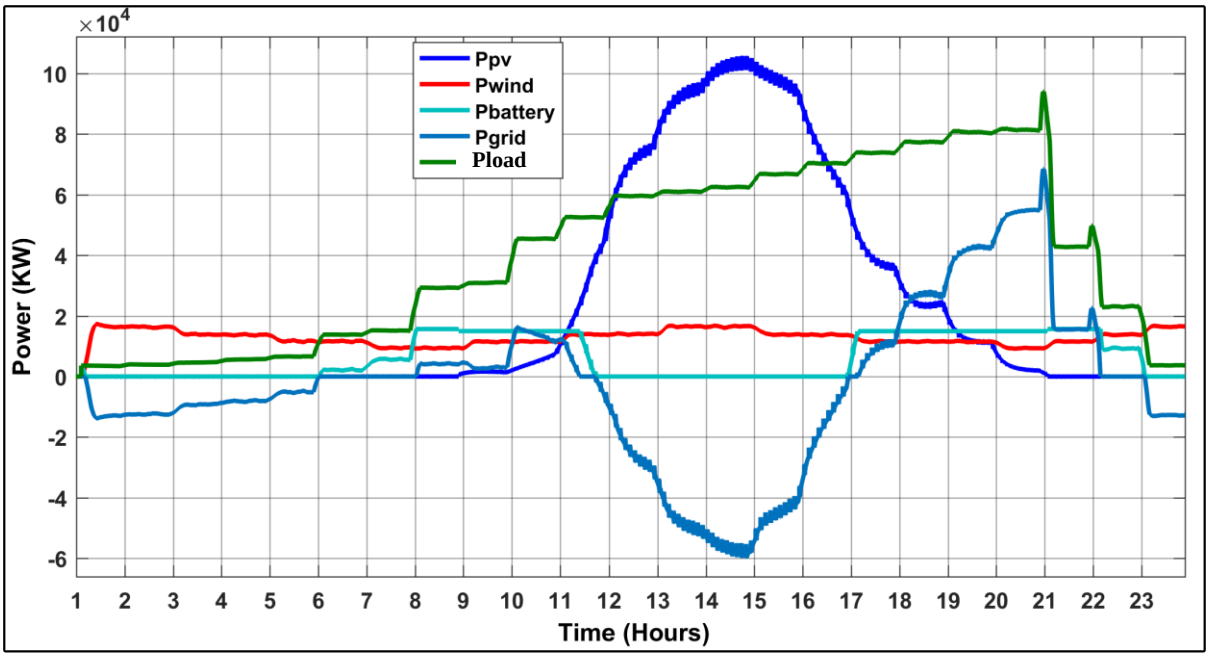

Figure V.9 Grid export mode under high SOC conditions (SOC > 80%)

Table V.1 presents the different operating modes defined in the simulation, along with the corresponding control strategies implemented by the Energy Management System (EMS). Each mode reflects a specific system condition based on renewable energy availability and battery State of Charge (SOC), guiding optimal energy management decisions across the PV, wind, battery, and utility grid components.

Table V.1. Summary of EMS operating modes and control strategies

Mode	Operating condition	EMS strategy	Battery behavior	Grid interaction	Objective
Mode 1	Normal operation – sunny day	Prioritize PV and wind to supply the load.	Charges when excess power is available	Grid used only if RES + battery are insufficient	Maximize use of RES and maintain supply–demand balance
Mode 2	Intermittent RES – cloudy/disturbed irradiation	Coordinate RES, battery, and grid based on generation variability	Charges/discharges as needed	Grid compensates when RES + battery cannot meet load	Ensure reliability during variable RES production
Mode 3	SOC < 20% – battery protection mode	Prevent battery discharge; supply load using RES or grid	Charging only (no discharge allowed)	Grid supplies deficit if RES is insufficient	Protect battery from degradation and ensure load supply

Mode 4	SOC > 80% – battery full	Prevent battery charging; supply load using RES	No further charging	Export surplus RES to the grid	Prevent overcharge, relieve grid, enable RES injection

V.5. Conclusion

This chapter presented the design and implementation of an intelligent energy management strategy for a hybrid microgrid composed of PV panels, WTs, a BESS, and grid connectivity. The proposed system leverages advanced control techniques, including ANN-based MPPT algorithms for optimal renewable energy harvesting and a rule-based EMS for real-time energy flow coordination.

The implemented EMS provides an intelligent and adaptive framework for energy management in a PV–Wind–Battery hybrid microgrid. Through predictive control and real-time decision-making, it ensures that the load demand is reliably met, the battery operates safely, and excess renewable energy is efficiently utilized either by charging the battery or exporting to the grid. The flowchart highlights the systematic coordination between energy sources and storage, demonstrating that the proposed EMS can optimize the hybrid microgrid operation under dynamic conditions, including variations in renewable generation and load demand.

The simulation results demonstrated the EMS's ability to dynamically adapt to changing environmental and load conditions through the implementation of four distinct operational modes:

- Mode 1 (Normal Operation): The microgrid effectively meets the load demand using PV and wind power, while charging the battery when excess renewable energy is available.
- Mode 2 (Intermittent Renewable Generation): The EMS coordinates between RES, battery, and grid to balance supply and demand during variable weather conditions, ensuring uninterrupted power delivery.
- Mode 3 (Low SOC Protection Mode): When the battery SOC falls below 20%, the EMS prevents further discharge to avoid degradation, relying on RES and grid support to meet the load.
- Mode 4 (High SOC Grid Export Mode): When the SOC exceeds 80%, the battery stops charging, and surplus renewable energy is exported to the grid, supporting grid stability and enhancing energy efficiency.

These modes collectively demonstrate the system’s capability to ensure battery longevity, maximize renewable energy utilization, minimize grid dependency, and maintain continuous power supply. The intelligent EMS thus represents a robust and practical solution for smart and sustainable energy management.

General Conclusion

This doctoral research has investigated a comprehensive approach to the integration, control, and energy management of hybrid renewable energy systems (HRES) based on PV, WT, and BESS, with a strong focus on PQ enhancement and intelligent energy management.

In Chapter I, a foundational analysis of PQ disturbances in renewable-based systems was conducted. It highlighted how both renewable sources and nonlinear loads introduce harmonics, voltage deviations, and waveform distortions that compromise system efficiency, grid stability, and equipment reliability. The limitations of traditional mitigation techniques further underscored the need for advanced filtering and intelligent control strategies.

Chapter II responded to these challenges by modeling and evaluating the performance of Series and Shunt APF. Among several control techniques tested, the UVTG method and the SRF strategy emerged as the most robust for voltage and current compensation, respectively. These methods laid the groundwork for the dual-filter architecture used in later chapters.

Chapter III detailed the modeling of a realistic HRES comprising PV, WT, and BESS. Various MPPT strategies—including artificial intelligence–based approaches—were compared, with ANN-based algorithms proving superior in tracking accuracy and dynamic response. However, simulations revealed that both source-side fluctuations (from RES variability) and load-side nonlinearities lead to significant PQ degradation, confirming the findings from Chapter I and reinforcing the need for integrated filtering and control.

In Chapter IV, a hybrid compensation framework using Series APF and UPQC was implemented. The UPQC, combining UVTG and SRF techniques, effectively mitigated both source and load-side disturbances, maintaining THD within IEEE 519 limits under variable and nonlinear operating conditions. This demonstrated the critical role of coordinated filtering in renewable-integrated microgrids.

Finally, Chapter V proposed and validated an intelligent energy management system (EMS) for a hybrid PV-WT microgrid. The system integrated ANN-based MPPT for optimal energy extraction and a rule-based EMS for adaptive energy flow coordination across four operating modes. These modes addressed various scenarios—normal operation, renewable intermittency, battery protection, and grid export—ensuring efficient resource utilization, battery longevity, and reliable load supply.

Contributions of the Study

This doctoral research offers several key innovations and methodological advancements aimed at enhancing the integration of RESs into modern power systems while ensuring high PQ and intelligent energy management. The main contributions of the study are summarized as follows:

- Novel Dual-Function Series Unit for Unified Power Quality Conditioning:

The study introduces an innovative series unit within the UPQC architecture, based on the Unified Voltage Template Generation (UVTG) technique. Unlike conventional designs, this series unit serves a dual function: (i) facilitating the integration of RESs (such as PV or wind systems) into the electrical grid, and (ii) generating real-time voltage reference signals to mitigate voltage-related disturbances—including sags, swells, and harmonics. This multifunctional approach offers a scalable solution to emerging PQ challenges in hybrid energy systems.

- Comprehensive Voltage and Current Compensation via UPQC

The proposed UPQC design achieves simultaneous compensation of voltage and current disturbances, through the coordinated operation of its series and shunt units. The series unit addresses voltage distortions, while the shunt unit compensates for current harmonics and imbalances. This comprehensive compensation strategy ensures an improved overall PQ performance compared to traditional systems, which typically target either voltage or current issues in isolation.

- High-Fidelity Harmonic Mitigation under Extreme Conditions

This research evaluates the UPQC performance under severely distorted conditions, including nonlinear loads with dominant 5th and 7th harmonic components contributing over 55% of the fundamental. Despite such harsh operating scenarios, the system achieves harmonic reduction rates of approximately 77.56% for voltage and 72.22% for current, demonstrating the proposed UPQC's robustness and superior filtering capability. These results surpass those reported in related literature, particularly for THD mitigation in highly nonlinear environments.

- Exploration of Unaddressed and Complex Case Studies

The study presents several novel case studies not previously explored in existing works. These include situations where both source and load inject harmonic distortions, hybrid configurations with significant nonlinear load presence, and the simultaneous occurrence of voltage sags and swells. The proposed system's effectiveness in these complex scenarios confirms its adaptability and reliability under diverse and challenging PQ conditions.

- Significant Power Quality Enhancement in Hybrid Renewable Systems

Through detailed simulation and analysis, the proposed system demonstrates substantial reductions in THD for both voltage and current, even under conditions involving rapidly fluctuating renewable generation and unbalanced nonlinear loads. The UPQC ensures waveform stability, fast dynamic response, and improved energy efficiency, thereby contributing to the reliability and robustness of hybrid microgrids.

- Integrated Energy Management Strategy (EMS) with AI-Based MPPT

In addition to PQ enhancement, the thesis proposes an intelligent energy management system (EMS) for microgrids integrating PV, wind, battery storage, and grid connections. Key EMS contributions include:

Implementation of artificial neural network (ANN)-based MPPT algorithms for dynamic and optimal power extraction from variable renewable energy resources.

Development of a rule-based EMS framework to manage energy flows between renewable sources, storage units, and the grid.

Real-time coordination that adapts to battery state-of-charge (SOC), load demand, and environmental conditions, thus promoting resilient and sustainable energy practices.

- Contribution to the State-of-the-Art

Overall, this research establishes a comprehensive framework that addresses both PQ enhancement and intelligent energy management in hybrid renewable energy systems. The

combined implementation of UPQC with advanced control strategies and intelligent EMS creates a robust and scalable model for future smart grid applications, contributing meaningfully to the field of sustainable power systems and setting a benchmark for integrated PQ and EMS performance.

Future Perspectives

Building upon the results and methodologies developed in this thesis, several promising research directions can be explored to further enhance the performance, practicality, and scalability of hybrid renewable microgrids:

- Intelligent Economic Dispatch Optimization:

While this work primarily focused on power quality and energy management, future studies can integrate dynamic pricing mechanisms and economic dispatch strategies into the control framework. By applying intelligent algorithms—such as genetic algorithms, particle swarm optimization, or reinforcement learning—it will be possible to optimize energy flow not only from a technical perspective but also from an economic standpoint, minimizing operational costs while maximizing renewable energy usage.

- Incorporation of Vehicle-to-Grid (V2G) Systems:

The growing adoption of electric vehicles (EVs) presents new challenges and opportunities for microgrid stability. Future research should consider EV integration as mobile energy storage units, accounting for bidirectional power flow and stochastic behavior of EV charging. This introduces further dynamic perturbations into the system but also provides additional flexibility and resilience if managed properly.

Scientific Production

The research work documented in this thesis has been materialized through several international publications and conference presentations, as listed below:

1. International Journal Publications (5 Articles)

1. **Zakaria Reguieg,** Ismail Bouyakoub, and Fayçal Mehedi, "Optimizing power quality in interconnected renewable energy systems: series active power filter integration for harmonic reduction and enhanced performance," Electrical Engineering, Springer, 2024. DOI:https://www.doi.org/10.1007/s00202-024-02489-3. (**Q2, Scopus-indexed**).
2. **Zakaria Reguieg,** Ismail Bouyakoub, and Fayçal Mehedi, and Fatiha Bouhadji, "Optimizing Power Quality: Simulation of UPQC Integrated PV with Comprehensive Reliability and Performance Analysis," International Journal of Smart Grid, vol. 8, no. 1, pp. 47–52, 2024. DOI: https://doi.org/10.20508/ijsmartgrid.v8i1.333.g338. (**Q2, Scopus-indexed**).
3. **Zakaria Reguieg,** Ismail Bouyakoub, and Fayçal Mehedi, and Fatiha Bouhadji, "Robust Harmonic Elimination Method for Various Load Conditions," J. Renew. Energies, vol. 1, no. 1, pp. 73 – 84, 2024, doi: https://doi.org/10.54966/jreen.v1i3.1295. (**Q4, Scopus-indexed**)
4. **Zakaria Reguieg,** Ismail Bouyakoub, and Fayçal Mehedi, "Harmonic mitigation in grid-integrated renewable energy systems with nonlinear loads," Energy, vol. 324, no. May 2024, p. 135882, 2025, DOI: https://doi.org/10.1016/j.energy.2025.135882. (**Q1, Scopus-indexed**)
5. **Zakaria Reguieg,** Ismail Bouyakoub, and Fayçal Mehedi, "Integrated optimization of power quality and energy management in a photovoltaic-battery microgrid," Renewable Energy, vol. 241, no. January, 2025, doi: https://doi.org/10.1016/j.renene.2025.122358. (**Q1, Scopus-indexed**)
6. **Reguieg, Z.**, F. Mehedi, I. Bouyakoub, W. M. Kacemi, F. Saidi, and S. Mekhilef, "ANN-based PV-integrated power conditioning system for MPPT optimization and power quality enhancement in hybrid microgrids," *Energy Reports*, 2026. doi: https://doi.org/10.1016/j.egyr.2026.109129. (**Q1, Scopus-indexed**)

2. International Conference Communications (6 Conferences)

1. Zakaria Reguieg, Ismail Bouyakoub, and Fayçal Mehedi, "Enhancing Power Quality: Integration of Series Active Power Filter And PV System for Optimal Performance," 1st

International Conference on Electrical Engineering and Renewable Energies Systems (ICEERES'23), 21-23 November 2023, Algeria, University TAHRI Mohamed of Bechar.

2. Zakaria Reguieg, Ismail Bouyakoub, Fayçal Mehedi, and Fatiha Bouhadji, "Optimizing Power Quality: Simulation of UPQC Integrated PV with Comprehensive Reliability and Performance Analysis," 4th International Conference on Advanced Engineering in Process Intelligent (ICAEPI'23), 28–30 November 2023, Algeria, Skikda University.

3. Zakaria Reguieg, Ismail Bouyakoub, Fayçal Mehedi, and Fatiha Bouhadji, "Enhancing Electrical Grid Stability through Power Quality Optimization via PV-PO-UPQC: An Integrat Approach," 2nd IEEE International Conference on Electrical Engineering and Automatic Control (IEEE ICEEAC 2024), 12–14 May 2024, Setif, Algeria, Setif 1 University.

4. Zakaria Reguieg, Ismail Bouyakoub, Fayçal Mehedi, and Fatiha Bouhadji, "Optimizing Power Quality: Voltage Compensation Strategies with PO-PV-Series Active Power Filters," 3rd International Conference on Energy, Materials and Environment (ICEME 2024), 6–7 May 2024, Djilali Bounaama University, Khemis Miliana, Algeria.

5. Zakaria Reguieg, Ismail Bouyakoub, and Fayçal Mehedi, "Adaptive Harmonic Mitigation and Power Quality Improvement in Grid-Connected PV Systems Using LMS-Controlled DSTATCOM," 4th International Conference on Electronics and Electrical Engineering (ICE3E'2024), 9–10 November 2024, University of Bouira, Algeria.

6. Zakaria Reguieg, Ismail Bouyakoub, and Fayçal Mehedi, "Enhancing Power Quality with Photovoltaic-Based Dynamic Voltage Restorer using Load Voltage Controller Algorithm," 4th International Conference on Electronics and Electrical Engineering (ICE3E'2024), 9–10 November 2024, University of Bouira, Algeria.

References

References

[1] P. K. Kesavan, U. Subramaniam, D. J. Almakhles, and S. Selvam, "Modelling and Coordinated Control of Grid Connected Photovoltaic, Wind Turbine Driven PMSG, and Energy Storage Device for a Hybrid DC/AC Microgrid," *Prot. Control Mod. Power Syst.*, vol. 9, no. 1, pp. 154–167, 2024, doi: 10.23919/pcmp.2023.000272.

[2] A. H. Elmetwaly *et al.*, "Improving Power Quality Problems of Isolated MG Based on ANN Under Different Operating Conditions Through PMS and ASSC Integration," *IEEE Access*, vol. 11, no. September, pp. 99822–99835, 2023, doi: 10.1109/ACCESS.2023.3311369.

[3] S. Rehman *et al.*, "Optimal Design and Model Predictive Control of Standalone HRES : A Real Case Study for Residential Demand Side Management," vol. 8, pp. 29767–29814, 2020, doi: 10.1109/ACCESS.2020.2972302.

[4] B. Tan, J. Zhao, M. Netto, V. Krishnan, V. Terzija, and Y. Zhang, "Power system inertia estimation: Review of methods and the impacts of converter-interfaced generations," *Int. J. Electr. Power Energy Syst.*, vol. 134, no. May 2021, p. 107362, 2022, doi: 10.1016/j.ijepes.2021.107362.

[5] W. M. Kacemi, "Contribution to the Control of Hybrid Excitation Synchronous Generators for Wind Energy Conversion," Université Hassiba Benbouali de Chlef, Algeria, 2025.

[6] Z. Reguieg, I. Bouyakoub, and F. Mehedi, "Harmonic mitigation in grid-integrated renewable energy systems with nonlinear loads," *Energy*, vol. 324, no. May 2024, p. 135882, 2025, doi: 10.1016/j.energy.2025.135882.

[7] M. N. Adu-Gyamfi *et al.*, "Moving towards renewable energy to mitigate carbon emissions from fossil fuel," *Am. J. Environ. Sci. Eng.*, vol. 6, no. 2, pp. 91–100, 2022, doi: 10.11648/j.ajese.20220602.12.

[8] S. Kumar, R. K. Saket, D. K. Dheer, J. B. Holm-Nielsen, and P. Sanjeevikumar, "Reliability enhancement of electrical power system including impacts of renewable energy sources: A comprehensive review," *IET Gener. Transm. Distrib.*, vol. 14, no. 10, pp. 1799–1815, 2020, doi: 10.1049/iet-gtd.2019.1402.

[9] M. Shafiul Alam, F. S. Al-Ismail, A. Salem, and M. A. Abido, "High-level penetration of renewable energy sources into grid utility: Challenges and solutions," *IEEE Access*, vol. 8, pp. 190277–190299, 2020, doi: 10.1109/ACCESS.2020.3031481.

[10] M. Bajaj and A. K. Singh, "Grid integrated renewable DG systems: A review of power quality challenges and state-of-the-art mitigation techniques," *Int. J. Energy Res.*, vol. 44, no. 1, pp. 26–69, 2020, doi: 10.1002/er.4847.

[11] N. F. Ibrahim, A. Alkuhayli, A. Beroual, U. Khaled, and M. M. Mahmoud, "Enhancing the Functionality of a Grid-Connected Photovoltaic System in a Distant Egyptian Region Using an Optimized Dynamic Voltage Restorer: Application of Artificial Rabbits Optimization," *Sensors*, vol. 23, no. 16, 2023, doi: 10.3390/s23167146.

[12] Z. Hu, Y. Han, A. S. Zalhaf, S. Zhou, E. Zhao, and P. Yang, "Harmonic Sources Modeling and Characterization in Modern Power Systems: A Comprehensive Overview," *Electr. Power Syst. Res.*, vol. 218, no. February, p. 109234, 2023, doi: 10.1016/j.epsr.2023.109234.

[13] S. Singh, P. Chauhan, M. A. Aftab, I. Ali, S. M. Suhail Hussain, and T. S. Ustun, "Cost optimization of a stand-alone hybrid energy system with fuel cell and PV," *Energies*, vol. 13, no. 5, pp. 1–23, 2020, doi: 10.3390/en13051295.

[14] A. Sajadi *et al.*, "Guest Editorial: Special Issue on recent advancements in electric power system planning with high-penetration of renewable energy resources and dynamic loads," *Int. J. Electr. Power Energy Syst.*, vol. 129, no. September 2020, p. 106597, 2021, doi: 10.1016/j.ijepes.2020.106597.

[15] S. R. Sinsel, R. L. Riemke, and V. H. Hoffmann, "Challenges and solution technologies for the integration of variable renewable energy sources—a review," *Renew. Energy*, vol. 145, pp. 2271–2285, 2020, doi: 10.1016/j.renene.2019.06.147.

[16] M. Abdelsattar, M. A. Ismeil, M. M. Aly, and S. Saber Abu-Elwfa, "Analysis of Renewable Energy Sources and Electrical Vehicles Integration into Microgrid," *IEEE Access*, vol. 12, no. March, pp. 66822–66832, 2024, doi: 10.1109/ACCESS.2024.3399124.

[17] L. Meegahapola, A. Sguarezi, J. S. Bryant, M. Gu, E. R. Conde D., and R. B. A. Cunha, "Power system stability with power-electronic converter interfaced renewable power generation: Present issues and future trends," *Energies*, vol. 13, no. 13, p. 3441, 2020, doi: 10.3390/en13133441.

[18] M. Shafiullah, S. D. Ahmed, and F. A. Al-Sulaiman, "Grid Integration Challenges and Solution Strategies for Solar PV Systems: A Review," *IEEE Access*, vol. 10, pp. 52233–52257, 2022, doi: 10.1109/ACCESS.2022.3174555.

[19] B. B. Adetokun, J. O. Ojo, and C. M. Muriithi, "Reactive Power-Voltage-Based Voltage Instability Sensitivity Indices for Power Grid with Increasing Renewable Energy Penetration," *IEEE Access*, vol. 8, pp. 85401–85410, 2020, doi: 10.1109/ACCESS.2020.2992194.

[20] A. B. Djilali, A. Yahdou, E. Bounadja, H. Benbouhenni, D. Zellouma, and I. Colak, "Energy management of the hybrid power system based on improved intelligent Perturb and Observe control using battery storage systems," *Energy Reports*, vol. 11, no. November 2023, pp. 1611–1626, 2024, doi: 10.1016/j.egyr.2024.01.010.

[21] E. Hernández-Mayoral *et al.*, "A Comprehensive Review on Power-Quality Issues, Optimization Techniques, and Control Strategies of Microgrid Based on Renewable Energy Sources," *Sustain.*, vol. 15, no. 12, p. 9847, 2023, doi: 10.3390/su15129847.

[22] B. Aljafari, S. Vasantharaj, V. Indragandhi, and R. Vaibhav, "Optimization of DC, AC, and Hybrid AC/DC Microgrid-Based IoT Systems: A Review," *Energies*, vol. 15, no. 18, p. 6813, 2022.

[23] G. Van den Broeck, J. Stuyts, and J. Driesen, "A critical review of power quality standards and definitions applied to DC microgrids," *Appl. Energy*, vol. 229, no. April, pp. 281–288, 2018, doi: 10.1016/j.apenergy.2018.07.058.

[24] X. Liang, "Emerging Power Quality Challenges Due to Integration of Renewable Energy Sources," *IEEE Trans. Ind. Appl.*, vol. 53, no. 2, pp. 855–866, 2017, doi: 10.1109/TIA.2016.2626253.

[25] M. Mishra, "Power quality disturbance detection and classification using signal processing and soft computing techniques: A comprehensive review," *Int. Trans. Electr. Energy Syst.*, vol. 29, no. 8, pp. 1–42, 2019, doi: 10.1002/2050-7038.12008.

[26] D. Zhang and T. Liu, "Effects of Voltage Sag on the Performance of Induction Motor Based on a New Transient Sequence Component Method," *CES Trans. Electr. Mach. Syst.*, vol. 3, no. 3, pp. 316–324, 2019, doi: 10.30941/CESTEMS.2019.00042.

[27] J. Prousalidis, "On improving the earthing quality in ship electric energy systems," *J. Mar. Eng. Technol.*, vol. 18, no. 1, pp. 46–55, 2019, doi: 10.1080/20464177.2018.1493024.

[28] P. Roy, J. He, T. Zhao, and Y. V. Singh, "Recent Advances of Wind-Solar Hybrid Renewable Energy Systems for Power Generation: A Review," *IEEE Open J. Ind. Electron. Soc.*, vol. 3, pp. 81–104, 2022, doi: 10.1109/OJIES.2022.3144093.

[29] M. E. T. Souza Junior and L. C. G. Freitas, "Power Electronics for Modern Sustainable Power Systems: Distributed Generation, Microgrids and Smart Grids—A Review," *Sustain.*, vol. 14, no. 6, p. 3597, 2022, doi: 10.3390/su14063597.

[30] D. Razmi, T. Lu, B. Papari, E. Akbari, G. Fathi, and M. Ghadamyari, "An Overview on Power Quality Issues and Control Strategies for Distribution Networks With the Presence of Distributed Generation Resources," *IEEE Access*, vol. 11, pp. 10308–10325, 2023, doi: 10.1109/ACCESS.2023.3238685.

[31] S. Sepasi, C. Talichet, and A. S. Pramanik, "Power Quality in Microgrids: A Critical Review of Fundamentals, Standards, and Case Studies," *IEEE Access*, vol. 11, no. September, pp. 108493–108531, 2023, doi: 10.1109/ACCESS.2023.3321301.

[32] M. Bajaj and A. K. Singh, “Increasing renewable energy penetration in harmonically polluted distribution grids using passive filtering: a comparative assessment of common filter types,” *Electr. Eng.*, vol. 104, no. 5, pp. 2979–3005, 2022, doi: 10.1007/s00202-022-01521-8.

[33] P. Khetarpal and M. M. Tripathi, “A critical and comprehensive review on power quality disturbance detection and classification,” *Sustain. Comput. Informatics Syst.*, vol. 28, p. 100417, 2020, doi: 10.1016/j.suscom.2020.100417.

[34] G. S. Chawda *et al.*, “Comprehensive Review on Detection and Classification of Power Quality Disturbances in Utility Grid with Renewable Energy Penetration,” *IEEE Access*, vol. 8, pp. 146807–146830, 2020, doi: 10.1109/ACCESS.2020.3014732.

[35] S. Choudhury and G. K. Sahoo, “A critical analysis of different power quality improvement techniques in microgrid,” *e-Prime - Adv. Electr. Eng. Electron. Energy*, vol. 8, no. February, p. 100520, 2024, doi: 10.1016/j.prime.2024.100520.

[36] S. S. NC, S. S. Reddy, and P. Sujatha, “Power Quality Issues on Grid Due To Integration of Renewable Energy System: a Review,” *Power*, vol. 52, no. 3, pp. 231–243, 2023, [Online]. Available: http://www.journal-iiie-india.com/1_mar_23/23_online.pdf

[37] L. Chen, X. Xie, J. He, T. Xu, D. Xu, and N. Ma, “Wideband oscillation monitoring in power systems with high-penetration of renewable energy sources and power electronics: A review,” *Renew. Sustain. Energy Rev.*, vol. 175, p. 113148, 2023, doi: 10.1016/j.rser.2023.113148.

[38] Z. Y. and X. Y. Muhammad Yasir Ali Khan, Haoming Liu *, “A Comprehensive Review on Grid Connected Photovoltaic Inverters, Their Modulation Techniques, and Control Strategies,” *Energies*, vol. 13, no. 6, 2020.

[39] X. Peng, Z. Liu, and D. Jiang, “A review of multiphase energy conversion in wind power generation,” *Renew. Sustain. Energy Rev.*, vol. 147, no. April, p. 111172, 2021, doi: 10.1016/j.rser.2021.111172.

[40] A. Raouf, K. B. Tawfiq, E. T. Eldin, H. Youssef, and E. E. El-Kholy, “Wind Energy Conversion Systems Based on a Synchronous Generator: Comparative Review of Control Methods and Performance,” *Energies*, vol. 16, no. 5, 2023, doi: 10.3390/en16052147.

[41] A. Owosuhi, Y. Hamam, and J. Munda, “Maximizing the Integration of a Battery Energy Storage System–Photovoltaic Distributed Generation for Power System Harmonic Reduction: An Overview,” *Energies*, vol. 16, no. 6, 2023, doi: 10.3390/en16062549.

[42] F. Blaabjerg, Y. Yang, K. A. Kim, and J. Rodriguez, “Power Electronics Technology for Large-Scale Renewable Energy Generation,” *Proc. IEEE*, vol. 111, no. 4, pp. 335–355, 2023, doi: 10.1109/JPROC.2023.3253165.

[43] A. Bouhouta, S. Moulahoum, and N. Kabache, “Harmonic Mitigation in Utility Grid with Highly Unbalanced Non- linear Load Using Intelligent Controller: an Experimental Study,” *PRZEGLĄD ELEKTROTECHNICZNY*, vol. 98, no. 4, pp. 1–6, 2022.

[44] K. S. Gadgil, P. Khampariya, and S. M. Bakre, “An Overview on the Investigation of Power Quality Problems and Harmonic Exclusion in the Power System using Frequency Estimation Techniques,” *Int. J. Intell. Syst. Appl. Eng.*, vol. 11, no. 3s, pp. 49–62, 2023, doi: 10.14704/nq.2022.20.5.NQ22147.

[45] Abdelkader MORSLI, “Réduction de la pollution des réseaux électriques basses tensions fondée sur les compensateurs actifs : Théorie et réalisation,” 2018.

[46] KHELIL CHERFI Mohamed, “Commande d’un system photovoltaïque alimentant un filtre actif de puissance connecté au réseau,” 2023.

[47] S. G. Reddy, S. Ganapathy, and M. Manikandan, “Three Phase Four Switch Inverter Based DVR for Power Quality Improvement with Optimized CSA Approach,” *IEEE Access*, vol. 10, no. July, pp. 72263–72278, 2022, doi: 10.1109/ACCESS.2022.3188629.

[48] V. Ansal, “ALO-optimized artificial neural network-controlled dynamic voltage restorer for

compensation of voltage issues in distribution system," *Soft Comput.*, vol. 24, no. 2, pp. 1171–1184, 2020, doi: 10.1007/s00500-019-03952-1.

[49] X. Liang, H. Chai, and J. Ravishankar, "Analytical Methods of Voltage Stability in Renewable Dominated Power Systems: A Review," *Electricity*, vol. 3, no. 1, pp. 75–107, 2022, doi: 10.3390/electricity3010006.

[50] Z. Reguieg, I. Bouyakoub, and F. Mehedi, "Enhancing Power Quality : Integration of Series Active Power Filter And PV System for Optimal Performance," *Int. J. Electron. Electr. Eng. Syst.*, vol. 7, no. 2, pp. 21–27, 2024.

[51] A. H. Soomro, A. S. Larik, M. A. Mahar, A. A. Sahito, A. M. Soomro, and G. S. Kaloi, "Dynamic Voltage Restorer—A comprehensive review," *Energy Reports*, vol. 7, pp. 6786–6805, 2021, doi: 10.1016/j.egyr.2021.09.004.

[52] Z. Reguieg, I. Bouyakoub, F. Mehedi, and F. Bouhadji, "Optimizing Power Quality : Simulation of UPQC Integrated PV with Comprehensive Reliability and Performance Analysis," *Int. J. SMART GRID*, vol. 8, no. 1, pp. 47–52, 2024.

[53] M. Rawa, H. N. Mohamed, Y. Al-Turki, K. Sedraoui, and A. M. Ibrahim, "Dynamic voltage restorer under different grid operating conditions for power quality enhancement with the deployment of a PI controller using gorilla troops algorithm," *Ain Shams Eng. J.*, vol. 14, no. 10, p. 102172, 2023, doi: 10.1016/j.asej.2023.102172.

[54] A. Mohamed Eltamaly, Y. Sayed Mohamed, A. H. Mustafa El-Sayed, and A. N. Abd Elghaffar, "Enhancement of Power System Quality Using PI Control Technique with DVR for Mitigation Voltage Sag," *2018 20th Int. Middle East Power Syst. Conf. MEPCON 2018 - Proc.*, pp. 116–121, 2018, doi: 10.1109/MEPCON.2018.8635221.

[55] Z. Reguieg, I. Bouyakoub, and F. Mehedi, "Optimizing power quality in interconnected renewable energy systems: series active power filter integration for harmonic reduction and enhanced performance," *Electr. Eng.*, 2024.

[56] I. Bouyakoub, A. Djahbar, B. Mazari, and O. Maarouf, "Simulation of Shunt Active Power Filter Controlled by SVPWM Connected to a Photovoltaic Generator," *Int. J. Adv. Comput. Sci. Appl.*, vol. 7, no. 8, pp. 65–71, 2016, doi: 10.14569/ijacsa.2016.070810.

[57] J. Gong, D. Li, T. Wang, W. Pan, and X. Ding, "A comprehensive review of improving power quality using active power filters," *Electr. Power Syst. Res.*, vol. 199, no. April, p. 107389, 2021, doi: 10.1016/j.epsr.2021.107389.

[58] I. Bouyakoub, R. Taleb, H. Mellah, and A. Zerglaine, "Implementation of space vector modulation for two level Three-phase inverter using dSPACE DS1104," *Indones. J. Electr. Eng. Comput. Sci.*, vol. 20, no. 2, pp. 744–751, 2020, doi: 10.11591/ijeecs.v20.i2.pp744-751.

[59] Abdelmadjid Chaoui, "FILTRAGE ACTIF TRIPHASE POUR CHARGES NON LINEAIRES," Poitiers, 2010.

[60] I. Bouyakoub, "Identification des courants harmoniques par la statégie neuromimétique: applications au filtre actif parallèlle," PhD thesis, Université des Sciences et de la Technologie d'Oran, Algeria, 2016-2017.

[61] X. Du, L. Zhou, H. Lu, and H. M. Tai, "DC link active power filter for three-phase diode rectifier," *IEEE Trans. Ind. Electron.*, vol. 59, no. 3, pp. 1430–1442, 2012, doi: 10.1109/TIE.2011.2167112.

[62] M. T. Benchouia, I. Ghadbane, A. Golea, K. Srairi, and M. E. H. Benbouzid, "Implementation of adaptive fuzzy logic and PI controllers to regulate the DC bus voltage of shunt active power filter," *Appl. Soft Comput. J.*, vol. 28, pp. 125–131, 2015, doi: 10.1016/j.asoc.2014.10.043.

[63] Z. Reguieg, I. Bouyakoub, F. Mehedi, and F. Bouhadji, "Robust Harmonic Elimination Method for Various Load Conditions," *J. Renew. Energies*, vol. 1, no. 1, pp. 73 – 84, 2024, doi: https://doi.org/10.54966/jreen.v1i1.1295.

[64] S. R. Das, P. K. Ray, A. K. Sahoo, K. K. Singh, G. Dhiman, and A. Singh, "Artificial intelligence based grid connected inverters for power quality improvement in smart grid applications," *Comput. Electr. Eng.*, vol. 93, no. September 2020, p. 107208, 2021, doi: 10.1016/j.compeleceng.2021.107208.

[65] I. GHADBANE, "Etude Et Réalisation D'un Filtre Actif Parallèle En Utilisant Différentes Stratégies De Contrôle," Biskra, 2016.

[66] S. S. Wamane, J. R. Baviskar, and S. R. Wagh, "A Comparative Study on Compensating Current Generation Algorithms for Shunt Active Filter under Non-linear Load Conditions," *Int. J. Sci. Res. Publ.*, vol. 3, no. 6, pp. 2–7, 2013, [Online]. Available: www.ijsrp.org

[67] M. Popescu, A. Bitoleanu, C. V. Suru, M. Linca, and L. Alboteanu, "Shunt Active Power Filters in Three-Phase, Three-Wire Systems: A Topical Review," *Energies*, vol. 17, no. 12, p. 2867, 2024, doi: 10.3390/en17122867.

[68] A. Govind, K. Jayaswal, V. K. Tayal, and P. Kumar, "Simulation and real time implementation of shunt active power filter for power quality enhancement using adaptive neural network topology," *Electr. Power Syst. Res.*, vol. 228, no. January 2023, p. 110042, 2024, doi: 10.1016/j.epsr.2023.110042.

[69] M. Popescu, A. Bitoleanu, C. V. Suru, M. Linca, and G. E. Subtirelu, "Adaptive Control of DC Voltage in Three-Phase Three-Wire Shunt Active Power Filters Systems," *Energies*, vol. 13, p. 3147, 2020, doi: 10.3390/en13123147.

[70] J. Baros *et al.*, "Review of Fundamental Active Current Extraction Techniques for SAPF," *Sensors*, vol. 22, no. 20, pp. 1–41, 2022, doi: 10.3390/s22207985.

[71] F. Bouhadji, I. Bouyakoub, F. Mehedi, W. M. Kacemi, and Z. Reguieg, "Optimization of grid power quality using third order sliding mode controller in PV systems with multilevel inverter," *Energy Reports*, vol. 12, no. November, pp. 5177–5193, 2024, doi: 10.1016/j.egyr.2024.10.064.

[72] A. Szromba, "Improving the Efficiency of the Shunt Active Power Filter Acting with the Use of the Hysteresis Current Control Technique," *Energies*, vol. 16, no. 10, p. 4080, 2023, doi: 10.3390/en16104080.

[73] A. BOUHOUTA, "Amélioration de la Qualité de l'Énergie Électrique Par des Convertisseurs Statiques Associés Aux Générateurs Photovoltaïques," Université Yahia Farés de Médéa, 2023.

[74] V. Dumbrava, G. C. Lazaroui, S. Leva, G. Balaban, M. Teliceanu, and M. TÎRŞU, "Photovoltaic production management in stochastic optimized microgrids," *UPB Sci. Bull. Ser. C Electr. Eng.*, vol. 79, no. 1, pp. 225–244, 2017.

[75] M. M. Refaat, Y. Atia, M. M. F. Sayed, and H. Abdel, "Adaptive fuzzy logic controller as MPPT optimization technique applied to grid-connected PV systems," *A. Mod. Maximum Power Point Track. Tech. Photovolt. Energy Syst. Green Energy Technol. Springer, Cham*, no. July, pp. 247–281, 2020, doi: 10.1007/978-3-030-05578-3_9.

[76] H. KANCHEV, "'Gestion des flux énergétiques dans un système hybride de sources d'énergie renouvelable : Optimisation de la planification opérationnelle et ajustement d'un micro réseau électrique urbain,'" Ecole centrale de Lille, 2014.

[77] D. Sera, L. Mathe, T. Kerekes, S. V. Spataru, and R. Teodorescu, "On the perturb-and-observe and incremental conductance mppt methods for PV systems," *IEEE J. Photovoltaics*, vol. 3, no. 3, pp. 1070–1078, 2013, doi: 10.1109/JPHOTOV.2013.2261118.

[78] A. S. Al-Ezzi and M. N. M. Ansari, "Photovoltaic Solar Cells: A Review," *Appl. Syst. Innov.*, vol. 5, no. 4, pp. 1–17, 2022, doi: 10.3390/asi5040067.

[79] Z. Reguieg, F. Mehedi, I. Bouyakoub, W. Mohammed, F. Saidi, and S. Mekhilef, "ANN-based PV-integrated power conditioning system for MPPT optimization and power quality enhancement in hybrid microgrids," *Energy Reports*, vol. 15, no. February, p. 109129, 2026, doi: 10.1016/j.egyr.2026.109129.

[80] M. SMAILI, “Modélisation et commande d’un aérogénérateur à machine asynchrone à double alimentation en vue de simulation des problèmes de cogénération,” Université du Québec en Abitibi-Témiscamingue, 2013.

[81] A. Abdelaali, “Modélisation, commande et optimisation énergétique d’un système à base de sources renouvelables : application aux bâtiments à basse consommation,” Université de Batna 2, 2023.

[82] N. E. Zakzouk, “Continuous input current buck DC/DC converter for small-size wind energy systems featuring current sensorless MPPT control,” *Sci. Rep.*, vol. 14, no. 1, pp. 1–24, 2024, doi: 10.1038/s41598-023-50692-2.

[83] M. M. M. Al Anfaf, “Contribution à la modélisation et à l’optimisation de systèmes énergétiques multi-sources et multi-charges Mohamed,” Université de Lorraine, 2016.

[84] A. Chaudhuri, R. Datta, M. P. Kumar, J. P. Davim, and S. Pramanik, “Energy Conversion Strategies for Wind Energy System: Electrical, Mechanical and Material Aspects,” *Materials (Basel).*, vol. 15, no. 3, pp. 1–34, 2022, doi: 10.3390/ma15031232.

[85] R. Roul and A. Kumar, “Fluid-structure interaction of wind turbine blade using four different materials: Numerical investigation,” *Symmetry (Basel).*, vol. 12, no. 9, 2020, doi: 10.3390/sym12091467.

[86] R. Akbari and A. Izadian, “Modeling and Control of Flywheel-Integrated Generators in Split-Shaft Wind Turbines,” *J. Sol. Energy Eng. Trans. ASME*, vol. 144, no. 1, 2022, doi: 10.1115/1.4052056.

[87] A. Bensalah, G. Barakat, and Y. Amara, “Electrical Generators for Large Wind Turbine: Trends and Challenges,” *Energies*, vol. 15, no. 18, 2022, doi: 10.3390/en15186700.

[88] J. Carroll, A. McDonald, and D. McMillan, “Reliability Comparison of Wind Turbines With DFIG and PMG Drive Trains,” *IEEE Trans. Energy Convers.*, vol. 30, no. 2, pp. 663–670, 2015, doi: 10.1109/TEC.2014.2367243.

[89] A. R. Nejad *et al.*, “Wind turbine drivetrains: State-of-the-art technologies and future development trends,” *Wind Energy Sci.*, vol. 7, no. 1, pp. 387–411, 2022, doi: 10.5194/wes-7-387-2022.

[90] O. Cornea, D. Hulea, N. Muntean, and G. D. Andreescu, “Step-Down Switched-Inductor Hybrid DC-DC Converter for Small Power Wind Energy Conversion Systems with Hybrid Storage,” *IEEE Access*, vol. 8, no. July, pp. 136092–136107, 2020, doi: 10.1109/ACCESS.2020.3012029.

[91] R. W. & Erickson and D. Maksimovic, “Fundamentals of Power Electronics,” in *Springer*, 2020. doi: 10.1201/9780203913468.ch2.

[92] İ. Yazıcı, E. K. Yaylacı, and F. Yalçın, “Modified golden section search based MPPT algorithm for the WECS,” *Eng. Sci. Technol. an Int. J.*, vol. 24, no. 5, pp. 1123–1133, 2021, doi: 10.1016/j.jestch.2021.02.006.

[93] H. Gaied *et al.*, “Comparative analysis of MPPT techniques for enhancing a wind energy conversion system,” *Front. Energy Res.*, vol. 10, no. August, pp. 1–15, 2022, doi: 10.3389/fenrg.2022.975134.

[94] Y. TRIKI, “Contribution à l’optimisation des systèmes hybrides de production d’énergies renouvelables,” Université de Haute Alsace – Mulhouse ; Université Mouloud Mammeri (Tizi-Ouzou, Algérie), 2020.

[95] M. Zerouali, M. Boutouba, A. El Ougli, and B. Tidhaf, “Control of variable speed wind energy conversion systems by fuzzy logic and conventional PO,” in *Proceedings - 2019 International Conference on Intelligent Systems and Advanced Computing Sciences, ISACS 2019*, 2019, pp. 8–12. doi: 10.1109/ISACS48493.2019.9068866.

[96] H. Elaissaoui, M. Zerouali, A. El Ougli, and B. Tidhaf, “MPPT algorithm based on fuzzy logic and artificial neural network (ANN) for a hybrid solar/wind power generation system,” in *4th*

Int. Conf. Intell. Comput. Data Sci. ICDS 2020, 2020.

[97] H. GALLAS, "Contribution à la Commande d'un Générateur de type Synchrone à Double Excitation dans le cas d'une Application Éolienne et Comparaison avec d'autres Architectures," CY Cergy Paris Université ; Ecole Nationale d'Ingénieurs de Sfax, 2021.

[98] A. CHAOUI, "Filtrage Actif Triphase Pour Charges Non Lineaires," Université Farhat Abbas-Setif, 2010.

[99] A. Alibi, L. Chrifi-Alaoui, S. Labdai, and S. Drid, "Fuzzy control and optimization of a photovoltaic system for smart building with low energy consumption," *UPB Sci. Bull. Ser. C Electr. Eng. Comput. Sci.*, vol. 83, no. 4, pp. 265–282, 2021.

[100] N. Attou, S. A. Zidi, M. Khatir, and S. Hadjeri, "Energy management system for hybrid microgrids," *EEA - Electroteh. Electron. Autom.*, vol. 69, no. 2, pp. 21–30, 2021, doi: 10.46904/EEA.21.69.2.1108003.

[101] N. A. Luu, "Control and management strategies for a microgrid," Université de Grenoble France, 2015. [Online]. Available: https://hal.science/tel-01144941v2/document

[102] C. Ndukwe and T. Iqbal, "Sizing and dynamic modelling and simulation of a standalone PV based DC microgrid with battery storage system for a remote community in Nigeria," *J. Energy Syst.*, vol. 3, no. 2, pp. 67–85, 2019, doi: 10.30521/jes.544710.

[103] J. Lu, W. Wang, Y. Zhang, and S. Cheng, "Multi-objective optimal design of stand-alone hybrid energy system using entropy weight method based on HOMER," *Energies*, vol. 10, no. 10, 2017, doi: 10.3390/en10101664.

[104] L. Croci, "Gestion de l'énergie dans un système multi-sources photovoltaïque et éolien avec stockage hybride batteries / supercondensateurs," Université de Poitiers, 2013.

[105] L. Stoyanov, "Etude de différentes structures de systèmes hybrides à sources d' énergie renouvelables," Université Pascal Paoli, 2011.

[106] Z. Reguieg, I. Bouyakoub, F. Mehedi, and F. Bouhadji, "Enhancing Electrical Grid Stability Through Power Quality Optimization via PV-PO-UPQC: An Integrated Approach," in *2024 2nd International Conference on Electrical Engineering and Automatic Control (ICEEAC)*, 2024, pp. 1–7.

[107] Z. Reguieg, I. Bouyakoub, and F. Mehedi, "Integrated optimization of power quality and energy management in a photovoltaic-battery microgrid," *Renew. Energy*, vol. 241, no. January, 2025, doi: 10.1016/j.renene.2025.122358.

Appendix

Table 1. Summary of System Parameters

Parameter	Value
Grid Parameter	
Source voltage	360 V
Frequency	50 Hz
Rg	95e-5 Ω
Lg	30.3 e-5 H
Series APF Parameter	
DC bus voltage Vdc	440 V
Injection transformer	140/280 V, 1.7e6 VA
Filter element	1.5 mH
UPQC Parameter	
dc-bus capacitors Cdc	1.22 e-3 F
Coupling impedance Lf	3.5 e-3 H
Load Parameter	
Nonlinear Load	R1 =56Ω, L1 =2e-3 H and R2 =120Ω, L2 =2e-3 H
Unbalance Nonlinear Load	3-phase: R1 =56Ω, L1 =2e-3 H, R2 =120Ω, L2 =2e-3 H 2-phase diode rectifier: R =200Ω, L =2e-3 H 3-phase diode rectifier: R =300Ω, L =2e-3 H
PV Panel	
Model	Solthec 1-STH215-P
Open-Circuit Voltage (Voc)	36.3 V
Short-Circuit Current (Isc)	7.84 A
Voltage at Maximum Power (Vmp)	29 V
Configuration	25 panels in parallel, 20 in series
PMSG	
Number of pole pairs	3
Stator resistance (Rs)	0.36 Ω
Inductance	1.67 mH
Direct-axis inductance (Ld) in the (d,q) reference frame	0.0211 H
Quadrature-axis inductance (Lq) in the (d,q) reference frame	0.012 H
Magnetic flux produced by the magnet (Φ)	0.6194 Weber
Moment of inertia	0.00141 kg·m²
Friction coefficient (f)	0.001
Battery	
Battery Type	Li-ion
Capacity	1160 Ah
Nominal Voltage	220 V
PV Series APF	

Configuration	3 parallel, 10 series
Injection transformer	140/280 V, 1.7e6 VA
Nominal Voltage	220 V

Table 2. PI Controller Parameters for DC Bus Voltage Regulation in PV and Wind Systems

Parameter	Value
System Gain $\frac{3V_s}{\sqrt{2}\,C\,V_{dcref}\,s} = \frac{1}{k_s}$	$k_s = 0.6936$
Damping Ratio ζ	0.707
Proportional Gain $k_p = 2\,\xi\,w_n\,k_s$	306.1
Integral Gain $k_i = k_s w_n^2$	68510

Table 3. Configuration of the mppt proposed ann-based controller for PV system

parameter	**description / value**
ann type	feedforward multilayer perceptron (mlp)
application	maximum power point tracking (mppt)
input variables	solar irradiance (ir), temperature (t)
number of input neurons	2
number of hidden layers	1
number of hidden neurons	3
output variable	maximum power point voltage (v_mpp)
number of output neurons	1
training algorithm	levenberg-marquardt (lm)
performance function	mean squared error (mse)
dataset size	10,000 samples
training data ratio	70%
validation data ratio	15%
testing data ratio	15%
temperature range	temp_min to temp_max
irradiance range	ir_min to ir_max
activation function (hidden layer)	tan-sigmoid (tansig)
activation function (output layer)	linear (purelin)
software tool	matlab neural network toolbox
training objective	minimize error between v_mpp and v_est
evaluation metrics	mse, correlation coefficient (r)

Detailed design of the fuzzy logic MPPT controller for the wind energy conversion system

Table 4. Input and output variables of the fuzzy controller

Variable	**Description**	**Normalized range**	**Number of membership functions**
ΔP	power variation	[-1, 1]	7

ΔV	voltage/speed variation	[-1, 1]	7
ΔD	duty cycle variation	[-1, 1]	7

Table 5. Linguistic labels used in the fuzzy controller

Abbreviation	Meaning
NB	negative big
NM	negative medium
NS	negative small
ZE	zero
PS	positive small
PM	positive medium
PB	positive big

Table 6. Triangular membership function parameters

Label	Type	Parameters (a, b, c)
NB	trapezoidal/triangular	(-1, -1, -0.66)
NM	triangular	(-1, -0.66, -0.33)
NS	triangular	(-0.66, -0.33, 0)
ZE	triangular	(-0.33, 0, 0.33)
PS	triangular	(0, 0.33, 0.66)
PM	triangular	(0.33, 0.66, 1)
PB	trapezoidal/triangular	(0.66, 1, 1)

Table 7. Fuzzy rule base of the MPPT controller

ΔP \ ΔV	NB	NM	NS	ZE	PS	PM	PB
NB	ΔD= PB	ΔD= PB	ΔD= PM	ΔD= PM	ΔD=PM	ΔD= ZE	ΔD= ZE
NM	ΔD= PB	ΔD= PM	ΔD= PM	ΔD= PS	ΔD= ZE	ΔD=NS	ΔD=NS
NS	ΔD= PM	ΔD= PM	ΔD= PS	ΔD= ZE	ΔD=NS	ΔD=NM	ΔD=NM
ZE	ΔD= PM	ΔD= PS	ΔD= ZE	ΔD= ZE	ΔD= ZE	ΔD=NS	ΔD=NM
PS	ΔD= PS	ΔD= ZE	ΔD= NS	ΔD=NS	ΔD=NM	ΔD=NM	ΔD=NB
PM	ΔD= ZE	ΔD= NS	ΔD= NM	ΔD=NM	ΔD=NB	ΔD=NB	ΔD=NB
PB	ΔD= ZE	ΔD= NS	ΔD= NM	ΔD=NB	ΔD=NB	ΔD=NB	ΔD=NB

Table 8. Fuzzy inference configuration

Parameter	Selected method
fuzzification	mamdani
operator	min
aggregation	max
defuzzification	centroid